JOURNAL OF FLUID MECHANICS

VOLUME 11 PART 1

AUGUST 1961

PUBLISHED BY

CAMBRIDGE UNIVERSITY PRESS

BENTLEY HOUSE, 200 EUSTON ROAD, LONDON, N.W.1

AMERICAN BRANCH: 32 EAST 57TH STREET, NEW YORK 22, N.Y.

Price 30*s.* (*U.S.A.* $5.00)

The JOURNAL OF FLUID MECHANICS exists for the publication of theoretical and experimental investigations of all aspects of the mechanics of fluids, and is issued in four parts per volume.

EDITORS

DR G. K. BATCHELOR, DR T. BROOKE BENJAMIN

Department of Applied Mathematics and Theoretical Physics, University of Cambridge, Free School Lane, Cambridge, England

ASSISTANT EDITORS

DR J. R. A. PEARSON, DR O. M. PHILLIPS

ASSOCIATE EDITORS

PROF. G. F. CARRIER

Pierce Hall, Harvard University, Cambridge 38, *Massachusetts, U.S.A.*

DR W. C. GRIFFITH

Lockheed Missiles and Space Division, Palo Alto, California, U.S.A.

M. J. LIGHTHILL

Royal Aircraft Establishment, Farnborough, Hampshire, England

PROF. R. R. LONG

School of Engineering, The Johns Hopkins University, Baltimore 18, *Maryland, U.S.A.*

DR P. G. SAFFMAN

Department of Mathematics, King's College, London, W.C. 2, *England*

Authors wishing to have papers published in the JOURNAL should communicate them to any one of the persons named above, choosing one in their own country where possible.

Authors are urged to ensure that their papers are written clearly and attractively, in order that their work will be readily accessible to readers.

Manuscripts should be typed in double spacing on one side of the paper only, with references listed at the end in alphabetical order of authors. Drawings should be done on a large scale in Indian ink on tracing cloth or drawing paper, the lettering being shown clearly in pencil for reproduction by the printer; the list of captions should be typed at the end of the manuscript. Proofs of papers from overseas will usually be despatched to authors by airmail. There is no charge for publication. Authors are entitled to receive 50 offprints of a paper in the JOURNAL free of charge, and additional offprints can be purchased if ordered in advance.

SUBSCRIPTIONS

The subscription price for a volume of four parts is £5. 10*s*. net, post free, payable in advance; separate parts 30*s*. net, plus postage. Subscriptions may be sent to any bookseller, or to the Cambridge University Press, Bentley House, 200 Euston Road, London, N.W.1.

Subscribers in the United States should send their orders to the Cambridge University Press, American Branch, 32 East 57th Street, New York 22, N.Y. The subscription price per volume is $18.50, post free, payable in advance; separate parts $5.00, plus postage.

Quotations for available back volumes and parts may be obtained on application to the Cambridge University Press.

A simplified analysis of spherical and cylindrical blast waves

By MANFRED P. FRIEDMAN

Aerophysics Laboratory, Massachusetts Institute of Technology, Cambridge, Massachusetts

(Received 6 January 1961)

Investigations into the behaviour of the gas flow behind spherical or cylindrical blasts have shown that secondary shocks arise within the original detonation gases. The secondary shock, at first weak, is carried outward with the expanding gases. Subsequently it strengthens and bends back toward the origin, arriving there with high intensity.

By using some recently developed techniques in shock dynamics and extending them where necessary, a theory is developed by which the motion of the main shock wave, as well as the formation and subsequent motion of the secondary shock, are given by explicit formulae. In addition, a method for determining, also by explicit formulae, the location of the contact surface between the detonation gases and the outside atmosphere is given. The results of a specific problem, which has been solved by numerically integrating the total equations of motion, and has also been checked experimentally, are compared with the results of the present theory.

1. Introduction

Recent theoretical and experimental studies of spherical and cylindrical blast waves (Boyer 1960; Brode 1957, 1959; Shardin 1954; Wecken 1950) enable us to give the following qualitative description of these processes. Assume that at time $t = 0$ a gas sphere (or cylinder) of radius $x = x_0$ under high internal pressure, $p = p_4$, is in a still air atmosphere at pressure $p = p_0$ ($p_4 \gg p_0$). The names 'gas' and 'air', respectively, will henceforth be used to describe the fluids initially within and outside this sphere. For $t > 0$, an equalization (explosion) process takes place. At the initial point $t = 0$, $x = x_0$, the region $x \geqslant 0$, $t > 0$ can be separated into five domains (figure 1): (0) undisturbed air; (1) air which has been overtaken by the main blast wave; (2) nearly uniform region outside the main expansion; (3) gas in the main expansion region; (4) gas not yet disturbed by the expansion. The gas in region (2) and the air in region (1) are separated by a contact front. Also, a secondary shock develops and separates regions (3) and (2).

The interesting phenomenon of a secondary shock appears only in spherical (and cylindrical) flows and does not arise in one-dimensional shock-tube studies. For the latter the main shock and the expansion come into an instantaneous equilibrium, being separated by a region of uniform pressure and velocity. The physical reason for the secondary shock formation is that the high-pressure gas,

upon passing through a spherical rarefaction wave, must expand to lower pressures than those reached through an equivalent one-dimensional expansion. This is due to the increase of volume. Because of this 'over-expansion', the pressures at the tail of the rarefaction wave are lower than the pressures transmitted back by the main shock, and a compression, or second shock, must be inserted to connect the two phases. By mathematical reasoning the situation is further clarified: the centred expansion is accomplished through the negative characteristics (of slope $dx/dt = u - a$, where u is particle velocity and a is sound speed). The characteristics at the head of the wave point in the decreasing x-direction (subsonic flow), and they then fan around to the increasing x-direction as the velocity increases. Negative characteristics are also reflected from the main shock, but as the shock expands it becomes weaker and these character-

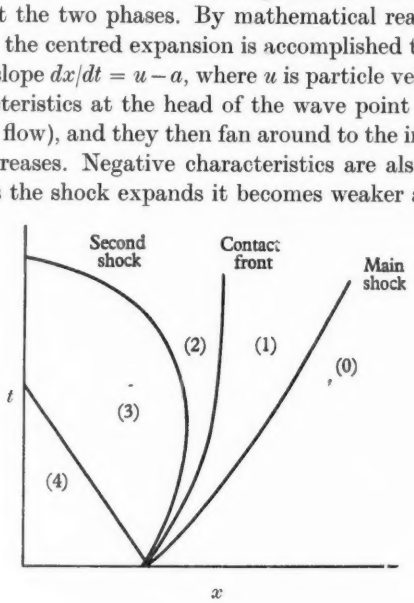

FIGURE 1. Explosion flow diagram. The indicated regions are: (0) undisturbed air; (1) air overtaken by main blast wave; (2) gas which has passed through secondary shock; (3) expanding gas; (4) undisturbed gas.

istics incline more and more toward the decreasing x-direction. Hence, characteristics of the same family, but arising from two different sources, will tend to intersect. This is prevented by the secondary shock. A similar situation arises in one-dimensional flows when a shock moving down a uniform tube meets an area change (Friedman 1960). The shock strength is attenuated, and characteristics reflected from the shock will be bent. They will meet the characteristics of the same family which originated in the uniform section of the tube unless a secondary shock is inserted.

This reasoning in terms of characteristics leads directly to a method for determining explicitly the path of the secondary shock. It is easily shown (Courant & Friedrichs 1948, p. 159) that the slope of a weak shock, at each point, is nearly equal to the average of the slopes of the incoming characteristics at that point. Using this fact, Whitham (1952) developed a technique for obtaining a differential equation for the shock path. This technique is used with the present problem to get the initial motion of the secondary shock.

As the secondary shock moves outward it strengthens, and the above 'weak shock' theory is no longer applicable. In order to follow further shock develop-

ment, a relation obtained by Chisnell (1957) and amplified by Whitham (1958) is introduced. Chisnell considered a shock wave moving in a channel with varying cross-sectional area and derived an analytic expression which gives the relation between the channel area and shock strength. For the present analysis the channel area is identified with the shock surface area, and hence is related to the shock radius. Whitham simplified and extended Chisnell's analysis by showing that the 'shock-area' relation can be obtained by the following method: the differential relation which is to be satisfied by the flow quantities along a characteristic coming into a shock is applied to the flow quantities just behind the shock; then, if they are expressed in terms of the shock strength, a differential equation is obtained relating changes in shock strength and radius. This differential equation can be integrated, if the flow ahead of the shock is uniform, to give Chisnell's result. The inward-facing secondary shock of the present problem, however, has ahead of it the non-uniform expanding gas. Here the shock motion depends not only on its radius but also on the flow conditions immediately ahead of it. Whitham's derivation of the 'shock-area' relation is extended to include this situation. The secondary shock is therefore obtained in two segments which take into account its changing nature from very weak, initially, to quite strong when it finally implodes at the origin. When it is weak, the average slope technique will be used to describe its motion until the shock strength becomes too large. From this point on, the extended shock-area rule is used.

The determination of the main shock wave separating regions (0) and (1) is much simpler than that of the secondary shock. This is because the flow ahead of the main shock in region (0) is uniform, and direct application of the integrated form of the shock-area relation suffices to give the shock strength and location. It should be emphasized that the shock-area relation is expected to be a good approximation in this problem because the shock weakens primarily due to its increased surface area; in the one-dimensional case its strength would remain constant. This is in contrast to the Taylor blast-wave problem, for example, where the weakening effect of disturbances from behind is equally important.

Flow properties arising at the main shock are propagated back into the interior along the negative characteristics. These cross the contact front and are altered upon entering the gas. In order to determine the flow changes at the contact front it is necessary to determine the path of the front. Toward this end a differential equation, obtained in a similar manner to the one describing the weak shock path, has been derived, i.e., the motion of the contact front is prescribed by known flow properties on characteristics meeting it.

At some places in the present analysis the additional entropy changes above those in the one-dimensional problem will be neglected. This will not affect the calculations in the expansion region (3) since the expansion is isentropic, nor in the initial portions of region (2) since the flow here has passed through the weak section of the secondary shock. For determination of the shocks by application of the shock-area rule, entropy effects are correctly included in the shock conditions. It is seen then that the only place where neglect of entropy changes could seriously affect the calculations is in following the flow properties from the main shock through region (1) to the contact front.

The slope of the secondary shock, when it initially forms and moves outward, is determined by the slopes of the negative characteristics of regions (3) and (2) which meet it. In § 2 an approximate solution for the flow in the expansion region (3) is determined. Since the flow near the initial point can be accurately described by one-dimensional shock-tube theory, a solution in region (3) which includes three-dimensional effects is obtained by perturbing about the known one-dimensional solution. This improved solution is used to give negative characteristics in region (3), and these are in turn used for the determination of the initial motion of the secondary shock. In addition, this solution gives information about the incoming flow which is required for use with the shock-area rule when the secondary shock strengthens. The negative characteristics for region (2) originate at the main shock, move through region (1) and have a discontinuity in slope upon crossing the contact front. For determination of these characteristics, the main shock and negative characteristics reflected from it must first be found; this is accomplished in § 3. The contact front and its affect on characteristics crossing it is discussed in § 4. Here a differential equation is determined by which the path of the contact front is given in terms of known flow quantities. In § 5 the results of the previous sections are utilized to give the motion of the secondary shock. Here both the weak-shock theory and the extended shock-area rule are presented. A specific problem involving a spherical blast is treated in § 6, and the results are compared with other solutions to this problem.

As a consequence of the form of the shock-area relation, the x and t co-ordinates of the main shock are determined parametrically as functions of shock Mach number. Similarly, since the contact front and secondary shock are determined by extrapolation of the known flow conditions at the main shock, their co-ordinates are also determined as parametric functions of the main shock Mach number. Therefore, starting at the initial point with the known main shock Mach number, small incremental steps in this Mach number are made. Corresponding to each increment, a point on the main shock, contact front and secondary shock are determined. The present analysis will describe the motion of the secondary shock as it initially moves outward and until it finally implodes at the origin. Beyond that time, its motion cannot be given by this theory. Similarly, this time will roughly delineate the region of validity for the main-shock and contact-front approximations.

2. Expansion region

Immediately after detonation, the high-pressure gas in region (4) of figure 1 is penetrated by a centred expansion fan and moves rapidly outward. This expansion, region (3), is isentropic and satisfies the following flow equations written in characteristic form:

$$\left(\frac{1}{\gamma-1}a_t+\tfrac{1}{2}u_t\right)+(u+a)\left(\frac{1}{\gamma-1}a_x+\tfrac{1}{2}u_x\right)+\frac{nua}{2x}=0, \tag{1}$$

$$\left(\frac{1}{\gamma-1}a_t-\tfrac{1}{2}u_t\right)+(u-a)\left(\frac{1}{\gamma-1}a_x-\tfrac{1}{2}u_x\right)+\frac{nua}{2x}=0, \tag{2}$$

where $n = 1, 2$ for cylindrically symmetric flows and spherically symetricm flows, respectively, and where γ is the ratio of specific heats. The flow variables a and u, the sound speed and particle velocity, and also the independent variables x and t, the radial distance and time, are all assumed to have been made dimensionless as follows:

$$a = \bar{a}/a_0, \quad u = \bar{u}/a_0, \quad x = \bar{x}/x_0, \quad t = \bar{t}a_0/x_0.$$

Barred quantities are true physical variables, a_0 is the sound speed outside the blast wave in region (0) of figure 1, and x_0 is the initial blast radius.

An approximate solution to equations (1) and (2) is obtained by perturbing about a one-dimensional centred expansion wave, whose solution can be given explicitly (Courant & Friedrichs 1948, p. 104). This approximation holds exactly as the initial point $x = 1, t = 0$ is approached. We first define

$$\left.\begin{aligned} u &= u_1 + u_2, \quad a = a_1 + a_2, \\ r &= \frac{1}{\gamma - 1} a_1 + \tfrac{1}{2} u_1, \quad s = \frac{1}{\gamma - 1} a_1 - \tfrac{1}{2} u_1, \\ R &= \frac{1}{\gamma - 1} a_2 + \tfrac{1}{2} u_2, \quad S = \frac{1}{\gamma - 1} a_2 - \tfrac{1}{2} u_2, \end{aligned}\right\} \tag{3}$$

where the variables with subscript 1 are solutions to the one-dimensional centred expansion problem (equations (1) and (2) with $n = 0$); that is,

$$\left.\begin{aligned} u_1 &= 2\mu r + (1-\mu)\frac{x-1}{t}, \\ a_1 &= \mu\left(2r - \frac{x-1}{t}\right), \quad \mu = \frac{\gamma - 1}{\gamma + 1}, \quad r = \text{const.}, \\ s &= (1-2\mu)\, r - (1-\mu)\frac{x-1}{t}. \end{aligned}\right\} \tag{4}$$

Substituting (3) and (4) into (1) and retaining first-order terms, we obtain, as an equation for R,

$$R_t + (u_1 + a_1) R_x + \frac{n u_1 a_1}{2x} = 0,$$

or

$$\frac{dt}{t} = \frac{dx}{4\mu r t + (1-2\mu)(x-1)} = -\frac{2x\, dR}{n t u_1 a_1}. \tag{5}$$

The first relation in (5) gives, for the curvilinear positive characteristics,

$$\frac{x-1}{t} - 2r = -K t^{-2\mu}, \quad \text{or} \quad a_1 t^{2\mu} = K\mu, \tag{6}$$

where K is a constant for each characteristic.

Using (6) to eliminate x, we obtain the differential equation for R along the positive characteristics

$$\frac{dR}{dt} = -\frac{n\mu K[2r - (1-\mu) K t^{-2\mu}] t^{-2\mu}}{2[1 + t(2r - K t^{-2\mu})]}. \tag{7}$$

It does not seem possible to integrate this equation for arbitrary μ. However, for certain specific values an integral in closed form is possible. The integration for $\mu = \frac{1}{6}$ and $\frac{1}{4}$, corresponding to $\gamma = \frac{7}{5}$ and $\frac{5}{3}$, can be carried out, but with the

present approximate theory the added complexity of the exact integral does not seem justified. The expression on the right-hand side of (7) is therefore simplified by assuming the bracketed term in the denominator equal to 1. This implies that the characteristic remains close to the line $x = 1$, which is roughly correct except for very high intensity blast waves. On this assumption we have

$$\frac{dR}{dt} = -\frac{n\mu K}{2}[2r-(1-\mu)Kt^{-2\mu}]t^{-2\mu},$$

which can be integrated to give

$$R = -\frac{nK\mu t}{2}\left[\frac{2r}{1-2\mu}t^{-2\mu} - \frac{(1-\mu)K}{1-4\mu}t^{-4\mu}\right] + f(a_1 t^{2\mu}).$$

Eliminating K by means of (6), we get

$$R = \frac{nt}{2}\left[\frac{(1-\mu)}{\mu(1-4\mu)}a_1^2 - \frac{2r}{1-2\mu}a_1\right] + f(a_1 t^{2\mu}). \tag{8}$$

The arbitrary function $f(a_1 t^{2\mu})$, constant along each positive characteristic, and the constant r are determined by continuously connecting $(\gamma-1)^{-1}a + \frac{1}{2}u$ across the boundary characteristic between regions (3) and (4). Since we shall assume (4) to be a region of uniform flow with $u_4 = 0$ and a_4 constant, the boundary characteristic is

$$x - 1 = -a_4 t. \tag{9}$$

For this case we would have

$$\left.\begin{aligned} r &= \frac{1}{\gamma-1}a_4, \\ f(a_1 t^{2\mu}) &= -\frac{tn}{2}\left(\frac{a_1}{a_4}\right)^{1/2\mu}\left[\frac{1-\mu}{\mu(1-4\mu)}a_4^2 - \frac{2r}{1-2\mu}a_4\right]. \end{aligned}\right\} \tag{10}$$

The second equation in (10) is obtained by requiring R to vanish at the boundary between regions (3) and (4). It is clear that by properly choosing the arbitrary characteristic function $f(a_1 t^{2\mu})$ appearing in equation (8), a more general boundary condition could be satisfied. Combining (8) and (10) we have, for region (3),

$$\frac{1}{\gamma-1}a_3 + \tfrac{1}{2}u_3 = \frac{1}{\gamma-1}a_4 + tH(a_1), \tag{11}$$

with
$$H(a_1) = \frac{n}{2}\left\{\frac{1-\mu}{\mu(1-4\mu)}\left[a_1^2 - \left(\frac{a_1}{a_4}\right)^{1/2\mu}a_4^2\right] - \frac{2r}{1-2\mu}\left[a_1 - \left(\frac{a_1}{a_4}\right)^{1/2\mu}a_4\right]\right\},$$

$$a_1 = \mu\left(2r - \frac{x-1}{t}\right).$$

The second-order terms in the negative characteristic approximation are obtained by substituting the relations (3) and (4) into the negative characteristic equation (2), the equation obtained for S being

$$tS_t + (x-1)S_x + [(2\mu-1)R + S] + \frac{nu_1 a_1 t}{2x} = 0, \tag{12}$$

where $R = tH(a_1)$ and H is defined in (11). Writing (12) in characteristic form, we have

$$\frac{dt}{t} = \frac{dx}{x-1} = \frac{dS}{-[(2\mu-1)R+S] - \dfrac{nu_1 a_1 t}{2x}}. \tag{13}$$

The first of equations (13) gives, for the characteristics, the lines $x-1=Lt$, with L constant along each characteristic. Along the characteristics, (13) also gives

$$\frac{d}{dt}(tS) = (1-2\mu)R - \frac{nu_1a_1t}{2(1+Lt)} = (1-2\mu)tH(a_1) - \frac{nu_1a_1t}{2(1+Lt)}. \tag{14}$$

Since u_1 and a_1 are constant along the characteristic lines, (14) can be integrated immediately to give

$$S = (1-2\mu)\frac{t}{2}H(a_1) - \frac{nu_1a_1}{2L}\left[1 - \frac{\log(1+Lt)}{Lt}\right].$$

Letting $L=(x-1)/t$ and using equation (4), we have

$$\frac{1}{\gamma-1}a_3 - \tfrac{1}{2}u_3 = (1-2\mu)r - (1-\mu)\frac{x-1}{t} + \frac{(1-2\mu)}{2}tH(a_1) - \frac{nu_1a_1t}{2(x-1)^2}[x-1-\log x]. \tag{15}$$

The equation for the negative characteristics can now be determined. The lowest-order approximation for this is $x=1+Lt$; however, by use of the above results, a more exact solution is obtained. Taking a proper linear combination of (11) and (15), we get, for the negative characteristic slope,

$$u_3 - a_3 = \frac{x-1}{t} + \frac{1-2\mu}{2-2\mu}tH(a_1) + \frac{nu_1a_1t}{2(1-\mu)(x-1)^2}[x-1-\log x]. \tag{16}$$

To facilitate integration, the right-hand side of (16) is simplified by assuming that $x=1+Lt$ and that u_1, a_1 and L are constant along the negative characteristics. This gives

$$\frac{dx}{dt} = L + \frac{1-2\mu}{2-2\mu}tH(a_1) + \frac{nu_1a_1t}{2(1-\mu)L}\left[1 - \frac{\log(1+Lt)}{Lt}\right],$$

$$x \simeq 1 + Lt + \frac{(1-2\mu)t^2}{4(1-\mu)}H(a_1) + \frac{nu_1a_1}{2(1-\mu)L}\left[1 - \frac{\log(1+Lt)}{Lt}\right]\frac{t}{2},$$

or, if we let $L=(x-1)/t$ in the last term,

$$x \simeq 1 + Lt + \frac{(1-2\mu)t^2}{4(1-\mu)}H(a_1) + \frac{nu_1a_1t^2}{4(1-\mu)(x-1)}\left[1 - \frac{\log x}{x-1}\right], \tag{17}$$

where $H(a_1)$ is given in equation (11). Since the logarithmic term in (16) does not vary much, an approximate integration was used to obtain (17).

Equations (11), (15), (16) and (17) will be used for describing the flow in region (3).

3. Main shock and region (1)

The characteristic equations (1) and (2), written with pressure and velocity as dependent variables, are

$$p_t + \rho a u_t + (u+a)(p_x + \rho a u_x) + \frac{\rho a^2 u n}{x} = 0, \tag{18}$$

$$p_t - \rho a u_t + (u-a)(p_x - \rho a u_x) + \frac{\rho a^2 u n}{x} = 0. \tag{19}$$

When written in this form, the equations are valid whether or not the flow is isentropic.

Since the positive characteristics are the ones coming into the main shock, equation (18) is used in an application of Whitham's rule (given in § 1) for the determination of the shock motion. We write (18) in the form

$$dp+\rho a\,du=-\frac{\rho a^2 un}{u+a}\frac{dx}{x}. \tag{20}$$

At the shock the Hugoniot relations are

$$\left.\begin{aligned} u&=\frac{2a_0}{\gamma+1}(M-M^{-1}), \quad p=\frac{p_0}{\gamma+1}(2\gamma M^2-\gamma+1),\\ \rho&=\frac{\rho_0(\gamma+1)M^2}{(\gamma-1)M^2+2}, \quad a^2=\frac{a_0^2(2\gamma M^2-\gamma+1)\{M^2(\gamma-1)+2\}}{(\gamma+1)^2M^2}, \end{aligned}\right\} \tag{21}$$

where $M=U/a_0$, U is the shock velocity, and subscript 0 refers to values ahead of the shock (region (0) in figure 1). Substituting these relations into (20) we obtain a differential relation between the shock Mach number and its radius x_m:

$$-n\frac{dx_m}{x_m}=dM\left\{\frac{4M}{2\gamma M^2-\gamma+1}+\frac{2(M^2+1)}{M\sqrt{\{[2\gamma M^2-\gamma+1][M^2(\gamma-1)+2]\}}}\right.$$
$$\left.+\frac{2M}{M^2-1}\sqrt{\left\{\frac{(\gamma-1)M^2+2}{2\gamma M^2-\gamma+1}\right\}}+\frac{M^2+1}{M(M^2-1)}\right\}. \tag{22}$$

This can be integrated to give

$$(x_m)^n\left[\frac{\{2\gamma M^2-\gamma+1\}^{\frac{1}{2}}-\{(\gamma-1)M^2+2\}^{\frac{1}{2}}}{M}\right]^2[\{(\gamma-1)(2\gamma M^2-\gamma+1)\}^{\frac{1}{2}}$$
$$-\{2\gamma[(\gamma-1)M^2+2]\}^{\frac{1}{2}}]^{\sqrt{\{2\gamma/(\gamma-1)\}}}(2\gamma M^2-\gamma+1)^{1/\gamma}$$
$$\times\exp\left[\frac{1}{\{2(\gamma-1)\}^{\frac{1}{2}}}\sin^{-1}\left\{\frac{2(2\gamma M^2-\gamma+1)-(\gamma-1)[(\gamma-1)M^2+2]}{M^2(\gamma+1)^2}\right\}\right]=\text{const.} \tag{23}$$

Using the dimensionless co-ordinates introduced in (3), we relate t_m and M, along the shock, by

$$M\,dt_m=dx_m, \tag{24}$$

with dx_m defined in equation (22).

The motion of the main shock as a function of its Mach number is given by equations (23) and (24) in conjunction with an initial condition specifying its position and Mach number at a certain time, ordinarily the instant of detonation. For both spherical and cylindrical blast waves, the initial motion is insensitive to the geometrical situation, and the initial shock Mach number can be determined by use of one-dimensional shock-tube theory. Specifically, if the gas inside the sphere (or cylinder) were steady with pressure p_4 and sound speed a_4, and the outside atmosphere were steady at p_0 and a_0, the one-dimensional

theory would give the following relation, which the initial shock Mach number must satisfy:

$$\frac{p_4}{p_0}\left\{1-\frac{\mu a_0}{a_4}(M-M^{-1})\right\}^{(\mu+1)/\mu} = (1+\mu)\,M^2-\mu. \tag{25}$$

It will be seen that the only flow property required in region (1) is the position of the negative characteristics, reflected from the main shock. Since the contact front follows closely behind the main shock, region (1) is small, and it suffices to approximate the negative characteristics there by straight lines. Essentially, this approximation neglects entropy and three-dimensionality. Effects of the changing shock strength, due to expansion, are propagated into region (1) by adjustments of the slope of each characteristic to be that value of $u-a$ where the characteristic meets the shock. The characteristics are therefore

$$x = x_m + w_1(M)\,(t-t_m), \tag{26}$$

with $w_1(M) = u-a$ evaluated at the point (x_m, t_m) on the main shock.

Equations (23), (24) and (26) define the main shock and negative characteristics behind the shock as functions of the shock Mach number M.

4. Contact front

The negative characteristics arising at the main shock propagate through region (1) and meet the contact front separating the gas in region (2) from the air in region (1). At this front the characteristic suffers an abrupt change in slope and continues into region (2). In order to determine this slope discontinuity, the location of the contact front and its point of intersection with the characteristic must be known. A technique for obtaining these is now developed.

Since the contact front moves with the local particle velocity u, it will be met by positive characteristics, with slope $u+a$, from region (2) and negative characteristics, with slope $u-a$, from region (1). The positive characteristic values are obtained from equation (11). Although this equation was derived to give $(\gamma-1)^{-1}a+\frac{1}{2}u$ in region (3), we shall assume it to be applicable in region (2), since the secondary shock which separates regions (2) and (3) is weak where this approximation is made. Let Q_2, Q_1 and w_2, w_1 denote $(\gamma-1)^{-1}a+\frac{1}{2}u$ and $u-a$ in regions (2) and (1) respectively. We have, due to continuity of velocity across the contact front,

$$\left.\begin{aligned} Q_2+\frac{1}{\gamma-1}w_2 &= Q_1+\frac{1}{\gamma-1}w_1, \\ \text{or}\qquad w_2-w_1 &= -(\gamma-1)\,(Q_2-Q_1). \end{aligned}\right\} \tag{27}$$

On a particle path, we have the relation between pressure and sound speed

$$\frac{p}{p_i} = \left(\frac{a}{a_i}\right)^{2\gamma/(\gamma-1)},$$

where subscript i stands for the initial state. Consequently, due to continuity of pressure across the contact front,

$$\left.\begin{aligned} \left(\frac{a}{a_i}\right)_2 &= \left(\frac{a}{a_i}\right)_1 \\ \text{or}\qquad 2Q_2-w_2 &= \frac{a_{i2}}{a_{i1}}(2Q_1-w_1). \end{aligned}\right\} \tag{28}$$

(It should be noted that in the derivation of equations (27) and (28) the assumption has been made that γ, the ratio of specific heats, has the same magnitude in both regions (1) and (2). The extension to the case of different γ is direct but not very simple.) We obtain the negative characteristic slopes for region (2) in terms of known quantities by eliminating Q_1 from equations (27) and (28): thus,

$$w_2 = \frac{\left(\frac{\gamma+1}{\gamma-1}\right)\frac{a_{i2}}{a_{i1}}w_1 + 2\left(1-\frac{a_{i2}}{a_{i1}}\right)Q_2}{1+\left(\frac{2}{\gamma-1}\right)\frac{a_{i2}}{a_{i1}}}. \tag{29}$$

Evaluation of (29) is not direct, since w_1 is known only as a function of main shock Mach number (equation (26)) and Q_2 is known only as a point function of x and t (equation (11)). We must determine, therefore, the (x,t)-co-ordinates of the contact front in terms of the parameter M.

First, a is expressed in terms of w_1 and Q_2. Since velocity is continuous across the contact front, we can write

$$2Q_2 - w_1 = \frac{2}{\gamma-1}a_2 + a_1,$$

and, combining this with the first of equations (28),

$$a_1 = \frac{2Q_2 - w_1}{1+\left(\frac{2}{\gamma-1}\right)\frac{a_{i2}}{a_{i1}}}. \tag{30}$$

Next, let $x_c = C(t_c)$ be the equation of the contact front. The negative characteristic given in equation (26) meets the contact front at the point (x_c, t_c). Hence, at this point,

$$C(t_c) = x_m + w_1(M)\,(t_c - t_m).$$

Differentiating with respect to t_c, we get

$$\frac{dC}{dt_c} = w_1 + \frac{dM}{dt_c}\{x'_m + w'_1(t_c - t_m) - w_1 t'_m\}.$$

Here primes indicate differentiation with respect to M. As the contact front moves with local particle velocity, it follows that

$$\frac{dC}{dt_c} = \frac{dx_c}{dt_c} = u.$$

Combining the two above equations, using $w = u - a$, we have

$$a_1 = \frac{dM}{dt_c}\{x'_m + w'_1(t_c - t_m) - w_1 t'_m\}. \tag{31}$$

Eliminating a_1 from (30) and (31), we obtain a differential equation relating t_c and M:

$$\frac{dt_c}{dM} = \frac{\left\{1+\left(\frac{2}{\gamma-1}\right)\frac{a_{i2}}{a_{i1}}\right\}\{x'_m + w'_1(t_c - t_m) - w_1 t'_m\}}{2Q_2 - w_1}. \tag{32}$$

Equation (32), together with

$$x_c = x_m + w_1(M)\,(t_c - t_m), \tag{33}$$

define the co-ordinates of the contact front (x_c, t_c) as functions of the parameter M. With this result we have directly, for the negative characteristics in region (2),

$$x = x_c + (t - t_c)\,w_2, \tag{34}$$

where t_c and x_c are given by (32) and (33), and w_2 is given by (29).

5. Secondary shock

We now have enough information about the flow to fit the secondary shock between regions (3) and (2). The negative characteristics arising in the expansion region (3) fan into the increasing x-direction, while those arising at the main shock tend to point more and more toward the decreasing x-direction. The latter is due to the fact that the main shock weakens as it expands, causing the characteristic slope $u_1 - a_1$ to decrease.

The secondary shock must be inserted so that the shock relations are satisfied; these are approximated, for a weak shock, by requiring its slope at each point to equal the average of the slopes of the characteristics meeting it. Since we have the equations, (17) and (34), describing the characteristics which meet the shock, we can, using a technique developed by Whitham (1952), obtain the shock motion.

The characteristics which arise in the expansion fan and at the main shock are respectively

$$\left.\begin{aligned} x &= 1 + Lt + f(x,t), \\ x &= x_c + w_2(t - t_c), \end{aligned}\right\} \tag{35}$$

where $f(x,t)$ represents terms appearing in equation (17), and x_c, t_c, and w_2 are functions of main shock Mach number M as given in equations (33), (32) and (29). Assuming the secondary shock path to be given by

$$x_s = 1 + S(t_s),$$

we have along the shock path

$$\left.\begin{aligned} S(t_s) &= w_2(t_s - t_c) + x_c - 1 \\ &= Lt_s + f\{x_c + (t_s - t_c)\,w_2, t_s\}. \end{aligned}\right\} \tag{36}$$

Expressing the shock slope as the average of the characteristic slopes as obtained from (35), we obtain

$$\frac{dS}{dt_s} = \frac{1}{2}\left(w_2 + \frac{L + f_t}{1 - f_x}\right). \tag{37}$$

Letting the parameters M and L and the variable x_s all be dependent on t_s, we can obtain another representation for dS/dt_s, using (35) and (36); with primes representing differentiation with respect to M, this is

$$\frac{dS}{dt_s} = \frac{1}{2}\left(w_2 + \frac{dM}{dt_s}\,[x_c' + w_2'(t_s - t_c) - w_2 t_c'] + \frac{L + f_t}{1 - f_x} + \frac{t(dL/dt)}{1 - f_x}\right).$$

When combined with (37), this equation yields

$$t\,\frac{dL}{dM} = -(1 - f_x)\{x_c' + w_2'(t_s - t_c) - w_2 t_c'\}. \tag{38}$$

Eliminating L from (38) by use of (36), we obtain, after working through some algebra and integrating with respect to M, a relation between t_s and M:

$$[x_c - 1 - t_c w_2]^2 = t_s \int_{M_i}^{M} [x_c - 1 - t_c w_2] \left[-2w_2' + \frac{d}{dM}\left(\frac{f}{t_s}\right) + \frac{f_x}{t_s}\{x_c' + w_2'(t_s - t_c) - w_2 t_c'\} \right] dM. \tag{39}$$

Here, $f(x,t)$ and $f_x(x,t)$ are evaluated at $x = x_c + (t_s - t_c)\, w_2$, $t = t_s$; M_i is the initial Mach number of the main shock wave. Equation (39) is solved by an iterative numerical technique; since for a fixed M the right-hand side of (39) increases monotonically with t_s and the left-hand side is a function of M alone, it is possible, for each increment in M, to solve for the corresponding t_s. Once t_s is determined, x_s is given by

$$x_s = x_c + w_2(t_s - t_c). \tag{40}$$

It should be noted that the secondary shock does not form at the initial point of the fluid flow field, $t = 0$, $x = 1$. By taking the limit $M \to M_i$ in (39), the time of shock formation t_i is obtained; its position is given by (40). If one neglects the expansion-region correction term f in (39), the initial time can be given explicitly as $t_i = (w_2 t_c' - x_c')/w_2'$; otherwise an iterative procedure must be used. For the problem given in the next section, the explosion of a sphere of gas at ambient temperature and a pressure ratio of 22, the point of shock formation was found to be $x_i = 1{\cdot}43$, $t_i = 1{\cdot}40$ when the correction term f was neglected; and $x_i = 1{\cdot}14$, $t_i = 0{\cdot}41$ for the full equations.

The technique described above, while useful to describe the initial motion of the secondary shock, is valid only when this shock is still weak. In the present situation, however, this shock strengthens as it is carried outward by the expanding gases and another method must be used to describe its subsequent motion. (The change-over point for a specific problem was arbitrarily chosen to be either when the shock begins to turn back toward the origin or when the shock strength becomes of magnitude unity, whichever comes first. Shock strength is defined in this case as $\bar{M} - 1$, where $\bar{M}$ is the secondary-shock Mach number.)

The method used in § 3, when altered to account for the non-uniform flow ahead of the secondary shock, is applicable for describing the later motion of this shock. In order to extend the formulation of § 3, we start with the characteristic differential relation corresponding to (20). Since the negative characteristics are the ones coming into the shock, we use

$$dp - \rho a\, du = -\frac{\rho a^2 un}{u - a}\frac{dx}{x}. \tag{41}$$

The Hugoniot relations given in (21) are used with the variables a_0, p_0, ρ_0 replaced by a_3, p_3, ρ_3. Also, the velocity relation is altered to account for the fact that the shock is backward facing and the flow in region (3) is non-stationary, giving

$$u = u_3 - \frac{2a_3}{\gamma + 1}(\bar{M} - \bar{M}^{-1}),$$

where $\bar{M} = (u_3 - U_s)/a_3$, and U_s is the secondary shock velocity. Substituting these relations into (41), we obtain equations which hold along the secondary shock:

$$\left.\begin{aligned}\frac{dM}{dx} = \Bigg\{&\frac{(\gamma+1)}{2}\frac{\bar{M}}{R}\left[\frac{u_{3t}/U_s + u_{3x}}{a_3}\right] - \left[\frac{\bar{M}^2-1}{R} + \frac{1}{\gamma-1}\right]\left[\frac{a_{3t}/U_s + a_{3x}}{a_3}\right] \\ &+ \left[\frac{2a_3(\bar{M}^2-1) - (\gamma+1)\bar{M}u_3}{(\gamma+1)\bar{M}u_3 - 2a_3(\bar{M}^2-1) - R}\right]\frac{n}{2x}\Bigg\} \Bigg/ \left\{\frac{2\bar{M}}{2\gamma\bar{M} - \gamma + 1} + \frac{\bar{M}^2+1}{\bar{M}R}\right\}, \\ \frac{dt}{dx} &= U_s^{-1}, \quad U_s = u_3 - \bar{M}a_3; \\ \text{with} \qquad R &= \sqrt{\{(2\gamma\bar{M}^2 - \gamma + 1)(\bar{M}^2(\gamma-1)+2)\}}.\end{aligned}\right\} \tag{42}$$

The quantities u_3, a_3 and their derivatives are obtained from equations (11) and (16). Equations (42) are solved stepwise from a given point where x, t, and U_s or $\bar{M}$ are prescribed.

6. Application to a specific problem

We shall describe here the application of the present theory to a specific problem which has been solved theoretically by Brode (1957), and investigated experimentally by Boyer (1960). A sphere of radius 1, containing a gas at 22 atm. and at a temperature of 299° K, is assumed to be surrounded by air at 1 atm. and the same temperature. The compressed gas is also air, and the ratio of specific heats γ is assumed to equal 1·4 everywhere. The initial Mach number of the main shock, as determined by one-dimensional shock tube theory, is 1·846. With this, the constant on the right-hand side of the main shock equation (23) is 26·1. For this case the sound speed and particle velocity, made dimensionless with respect to the flow in region (0), are as follows at the initial point $x = 1, t = 0$:

$$\begin{aligned} u_0 &= 0, & a_0 &= 1, \\ u_1 &= 1{\cdot}087, & a_1 &= 1{\cdot}252, \\ u_2 &= 1{\cdot}087, & a_2 &= 0{\cdot}729, \\ u_3 &= \frac{5}{6}\left(1 + \frac{x-1}{t}\right), & a_3 &= \frac{1}{6}\left(5 - \frac{x-1}{t}\right), \\ u_4 &= 0, & a_4 &= 1. \end{aligned}$$

The leading characteristic of the expansion fan in region (3) is $(x-1)/t = -1$.

For region (3) we have, corresponding to equations (11), (16) and (17),

$$2{\cdot}5a_3 + 0{\cdot}5u_3 = 2{\cdot}5 - \frac{t}{28{\cdot}8}\left(5 - \frac{x-1}{t}\right)\left(1 + \frac{x-1}{t}\right)^2, \tag{6.11}$$

$$u_3 - a_3 = \frac{x-1}{t} - \frac{1}{72}\left[\left(5 - \frac{x-1}{t}\right)\left(1 + \frac{x-1}{t}\right)t\right]\left[\left(1 + \frac{x-1}{t}\right) - \frac{12}{x-1}\left(1 - \frac{\log x}{x-1}\right)\right], \tag{6.16}$$

$$x = 1 + Lt - \frac{1}{144}\left[\left(5 - \frac{x-1}{t}\right)\left(1 + \frac{x-1}{t}\right)t^2\right]\left[\left(1 + \frac{x-1}{t}\right) - \frac{12}{x-1}\left(1 - \frac{\log x}{x-1}\right)\right]. \tag{6.17}$$

The contact front is given by

$$\frac{dt_c}{dM} = \frac{4{\cdot}127\{x'_m + w'_1(t_c - t_m) - w_1 t'_m\}}{5a_3 + u_3 - w_1}, \tag{6.32}$$

$$x_c = x_m + w_1(M)\,(t_c - t_m). \tag{6.33}$$

Here $w_1(M)$ is the negative characteristic slope $u - a$ in region (1); it is evaluated, as a function of the main shock Mach number M, by using the Hugoniot relations in equation (21). In region (2) the negative characteristic slope w_2 is

$$w_2 = 0{\cdot}909w_1 + 0{\cdot}182(2{\cdot}5a_3 + 0{\cdot}5u_3). \tag{6.29}$$

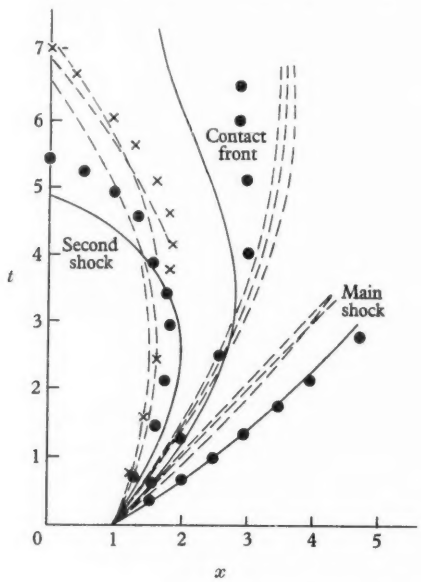

FIGURE 2. Experimental and theoretical spherical-blast results: ----, experiment (Boyer); ——, numerical integration (Brode); ●, present theory; ×, simplified second-shock approximation.

In figure 2 the present theory is compared with that of Boyer and Brode. The results of several experimental explosions carried out by Boyer are indicated by dashed lines. Brode's results, obtained by numerical integration of the Lagrangian equations of motion, are indicated by solid lines. The present theory is given by the curves composed of heavy dots. The time taken to compute the two shocks and the contact front on an IBM 704 was about 3 min.

Since Boyer's experimental work involved the bursting of a glass sphere, the differences between his result and Brode's may be due to the presence of glass particles in the flow field. As the present model, a hypothetical sudden expansion of a gas sphere, is the same as Brode's, it is expected that the results be comparable with his. The initial motion of the main shock and contact front as obtained by Brode compares quite favourably with that obtained with the present theory. It must be stated, however, that the present determination of

the main shock is based entirely on Chisnell's work. Brode shows the secondary shock expanding slightly more, and imploding sooner, than both the present theory and Boyer's experiments. The differences in the initial motion could be due simply to the difficulty in interpreting data when the shock is weak. Brode, using the von Neumann–Richtmyer pseudo-viscosity technique, which spreads out the shock, might have difficulty in determining the true locations of a weak shock. Boyer's experimental technique, which used the schlieren shadowgraph to determine the secondary shock, would have difficulty in locating weak shocks which give correspondingly weak shadows. As to the determination of the time of implosion, Lagrangian mass co-ordinates, as used by Brode, may have lead to inaccuracies near the flow centre because the density there is quite low. Most of the mass is located near the contact front and main shock. However, since the present theory neglects certain entropy changes and in addition becomes less valid as the distance to the initial point ($x = 1$, $t = 0$) increases, it is rather difficult to determine precisely the causes of the small discrepancies in the different results. Over-all, however, the agreement is quite good.

A simplified determination of the secondary shock is indicated by the curve composed of $\times$'s in figure 2. For this, the one-dimensional solution was used to describe the flow in region (3). This is given by omitting the last term in equations (6.11), (6.16) and (6.17), and also setting f and f_x equal to zero in the secondary shock equation (39). This approximation for the secondary shock motion agrees remarkably well with Boyer's experimental work, and it may be useful for giving a qualitative description of the flow as it affords a marked simplification of some of the equations.

This research was carried out at New York University, and was sponsored by AEC Contract No. AT (30-1)–1480 and Air Force Office of Scientific Research, Contract No. AF 49 (638)–446.

REFERENCES

Boyer, D. W. 1960 *J. Fluid Mech.* **9**, 401.

Brode, H. L. 1957 *Rand Corporation, Rep.* RM-1974.

Brode, H. L. 1959 *Phys. Fluids*, **2**, 217.

Chisnell, R. F. 1957 *J. Fluid Mech.* **2**, 286.

Courant, R. & Friedrichs, K. O. 1948 *Supersonic Flow and Shock Waves.* New York: Interscience.

Friedman, M. P. 1960 *J. Fluid Mech.* **8**, 193.

Shardin, H. 1954 *Comm. Pure Appl. Math.* **7**, 223.

Wecken, F. 1950 *Z. angew. Math. Mech.* **30**, 271.

Whitham, G. B. 1952 *Comm. Pure Appl. Math.* **5**, 301.

Whitham, G. B. 1958 *J. Fluid Mech.* **4**, 337.

Propagation of a solitary wave along a magnetic field in a cold collision-free plasma

By P. G. SAFFMAN
King's College, London

(Received 10 February 1961)

It is shown that solitary hydromagnetic waves can propagate parallel to a uniform magnetic field in a cold collision-free plasma. These waves are exact solutions of the non-linear equations of motion except for the quasi-neutral approximation. The velocity of propagation lies in a range of values somewhat larger than the Alfvén velocity, and is of the order of 25 times the Alfvén velocity for hydrogen, the precise value depending upon the strength of the wave. Simple expressions exist for the velocities of the ions and electrons and the magnetic field inside the wave. The lines of force are spirals about the direction of propagation. The waves are symmetrical about their middle. The order of magnitude of their width is the geometric mean of the gyro-radii of the ions and electrons when moving with the Alfvén velocity. The maximum value of the magnetic field can be somewhat larger than the value away from the wave.

1. Introduction

The propagation of finite-amplitude waves across a magnetic field in a cold collision-free plasma has been investigated by Adlam & Allen (1958) and Davis, Lüst & Schlüter (1958). One-dimensional solutions were obtained which describe the motion of a pulse or solitary wave in a direction perpendicular to a magnetic field, all quantities being uniform in planes perpendicular to the direction of propagation. The motion is steady relative to an observer moving with the wave. Davis *et al.* also obtained solutions describing periodic waves comprising an infinite wave train. The particular interest of the solitary wave solutions lies in the belief that they may provide zero-order approximations to collision-free shocks which propagate transversely to a magnetic field.

The similar problem of the propagation of finite-amplitude one-dimensional waves parallel to a magnetic field (as opposed to across) has been studied by Ferraro (1956) and Montgomery (1959). Their solutions, however, all described periodic waves of infinite extent. In the present note, it will be shown that solutions of the equations exist which represent solitary waves, which are perhaps of more intrinsic interest as being possibly relevant to collision-free shocks which propagate along a magnetic field.

In all this work, it is assumed that the plasma is approximately electrically neutral. That is, the number density of ions and electron are assumed equal, except in the Maxwell equation for the electric displacement. This assumption is valid provided all velocities are non-relativistic and any frequency is small

compared with the plasma frequency. In fact, it is easy to show that the approximation is exact if the ion and electron masses are equal; and in the general case the waves are modified very slightly by the deviations from strict neutrality which actually occur.

2. The equations of motion

We consider now the existence of solitary waves in a cold collision-free plasma which propagate steadily with velocity U along a magnetic field. We suppose that at infinity ahead of the wave conditions are uniform, the magnetic field is of strength H_0, and the number density of ions and electrons is N. Then, in a frame of reference moving with the wave, the motion is steady, all quantities are functions of x, the co-ordinate parallel to the magnetic field at infinity, and the velocity of ions and electrons at infinity is U parallel to the x-axis.

We employ Gaussian units. Then all quantities can be made non-dimensional by the use of a characteristic velocity U, a characteristic number density N, a characteristic magnetic intensity H_0, and a characteristic length

$$l = \frac{ac\sqrt{(m_i m_e)}}{eH_0}, \tag{2.1}$$

where e is the electronic charge, m_i and m_e are the masses of ions and electrons respectively, c is the velocity of light, and

$$a = \sqrt{\left[\frac{H_0^2}{4\pi N(m_i+m_e)}\right]} \tag{2.2}$$

is the Alfvén velocity in the undisturbed plasma. The length l is the geometric mean of the gyro-radii of the ions and electrons when moving with the Alfvén velocity.

Let n denote the dimensionless number density of the ions and electrons (assumed equal by the quasi-neutral approximation). Then the equations of continuity show that the x-components of the velocity of the ions and electrons are equal; and denoting this (dimensionless) velocity by u, we have from the equations of continuity

$$nu = 1. \tag{2.3}$$

The conditions at infinity require that $n \to 1$ and $u \to 1$ as $x \to -\infty$.

It follows from Maxwell's equations with the particular geometry of this problem that only the x-component of the electric field is non-zero and that the x-component of the magnetic field is constant. Then the components of the (dimensionless) magnetic field can be written $(1, h_2, h_3)$, and those of the electric field $(E, 0, 0)$, the actual electric field being EUH_0/c. We denote the (dimensionless) velocity of the ions by (u, v_i, w_i) and that of the electrons by (u, v_e, w_e). Then the equations of motion and Maxwell's equations (Montgomery 1959) reduce to

$$\frac{M}{\gamma}u\frac{du}{dx} = E - w_i h_2 + v_i h_3, \qquad M\gamma u\frac{du}{dx} = -E + w_e h_2 - v_e h_3; \tag{2.4a,b}$$

$$\frac{M}{\gamma}u\frac{dv_i}{dx} = -uh_3 + w_i, \qquad M\gamma u\frac{dv_e}{dx} = uh_3 - w_e; \tag{2.5a,b}$$

$$\frac{M}{\gamma}u\frac{dw_i}{dx} = uh_2 - v_i, \qquad M\gamma u\frac{dw_e}{dx} = -uh_2 + v_e; \tag{2.6a,b}$$

$$\frac{dh_2}{dx} = \frac{Mn}{\gamma+\gamma^{-1}}(w_i - w_e), \qquad \frac{dh_3}{dx} = -\frac{Mn}{\gamma+\gamma^{-1}}(v_i - v_e). \tag{2.7a,b}$$

Here, $M = U/a$ can be called the Alfvén Mach number, and $\gamma^2 = m_e/m_i$ is the ratio of the particle masses. Altogether, we have nine equations for nine unknowns, and we are interested in solutions for which all variables except u and n tend to zero as $x \to -\infty$.

These equations are valid provided u never changes sign, that is, provided the particle trajectories are not looped.

3. Reduction of the equations of motion

Simple integrals of these equations can easily be obtained. From (2.6) and (2.7), and the conditions at infinity, it follows that

$$h_3 = \frac{M^2}{\gamma+\gamma^{-1}}\left(\frac{w_i}{\gamma} + \gamma w_e\right), \tag{3.1}$$

and similarly

$$h_2 = \frac{M^2}{\gamma+\gamma^{-1}}\left(\frac{v_i}{\gamma} + \gamma v_e\right). \tag{3.2}$$

Eliminating E from (2.4) and substituting for h_2 and h_3, we obtain

$$(\gamma+\gamma^{-1})u\frac{du}{dx} = M(v_i w_e - v_e w_i). \tag{3.3}$$

Now, from (2.5a) and (2.6a),

$$\frac{M}{\gamma}\left(v_i\frac{dv_i}{dx} + w_i\frac{dw_i}{dx}\right) = w_i h_2 - v_i h_3$$

$$= \frac{M^2\gamma}{\gamma+\gamma^{-1}}(w_i v_e - w_e v_i) = -M\gamma u\frac{du}{dx}.$$

Hence

$$v_i^2 + w_i^2 = \gamma^2(1-u^2), \tag{3.4}$$

and similarly

$$v_e^2 + w_e^2 = \gamma^{-2}(1-u^2). \tag{3.5}$$

These equations show that in a real solution u must be less than one.

Equation (3.3) can also be written

$$M^2\frac{du}{dx} + h_2\frac{dh_2}{dx} + h_3\frac{dh_3}{dx} = 0.$$

Hence

$$M^2u + \tfrac{1}{2}h_2^2 + \tfrac{1}{2}h_3^2 = M^2, \tag{3.6}$$

by virtue of the conditions at infinity. This last integral may be interpreted physically as the conservation of momentum flux.

We can now obtain an equation for u. Substitute (3.1) and (3.2) for h_2 and h_3 in (3.6), and use (3.3), (3.4), (3.5) and the identity

$$(v_i w_e - v_e w_i)^2 + (v_i v_e + w_i w_e)^2 \equiv (v_i^2 + w_i^2)(v_e^2 + w_e^2),$$

to obtain

$$\left(u\frac{du}{dx}\right)^2 = (1-u)^2\left\{2(1+u) - \frac{(\gamma+\gamma^{-1})^2}{M^2}\right\}. \tag{3.7}$$

When this equation is solved for u, the magnitudes of the transverse velocities of the ions and electrons and the transverse magnetic field follow immediately from (3.4), (3.5) and (3.6).

The orientation of the transverse components can be found without difficulty. If we write

$$\tan\theta = h_3/h_2, \quad \tan\theta_i = w_i/v_i, \quad \tan\theta_e = w_e/v_e,$$

then combination of equations (2.7) with the equations of this section gives

$$u\frac{d\theta}{dx} = \frac{1}{2M}(\gamma^{-1}-\gamma), \tag{3.8}$$

and moreover

$$\theta = \tfrac{1}{2}(\theta_i+\theta_e), \quad \cos\tfrac{1}{2}(\theta_i-\theta_e) = \frac{\gamma+\gamma^{-1}}{M[2(1+u)]^{\frac{1}{2}}}. \tag{3.9}$$

4. Structure of the solitary wave

Equation (3.7) is symmetrical in x, so the solution can only be a solitary wave, with conditions the same ahead of and behind the wave, and not a shock. The condition that it represents a real wave is that the expression in curly brackets in (3.7) is positive for $u = 1$ and vanishes for some value of u between 0 and 1. This condition requires

$$\frac{\gamma+\gamma^{-1}}{\sqrt{2}} > M > \frac{\gamma+\gamma^{-1}}{2}, \tag{4.1a}$$

or, in terms of dimensional quantities,

$$\frac{H_0^2(m_i+m_e)}{8\pi N m_i m_e} > U^2 > \frac{H_0^2(m_i+m_e)}{16\pi N m_i m_e}, \tag{4.1b}$$

where U is the velocity of propagation of the waves referred to a frame in which the plasma is at rest at infinity. The upper limit on U expresses the condition that the trajectories are not looped.

Simple expressions for the wave structure can be obtained by introducing a new independent variable t by the relation

$$dx/dt = u. \tag{4.2}$$

Here t is the time for a particle to go a distance x. Then (3.7) can be integrated immediately to give

$$u = 1-2\lambda^2\operatorname{sech}^2\lambda t \tag{4.3}$$

and

$$x = t-2\lambda\tanh\lambda t, \tag{4.4}$$

where

$$\lambda^2 = 1-\frac{(\gamma+\gamma^{-1})^2}{4M^2}.$$

The values of all the other variables follow immediately. In particular,

$$h_2^2+h_3^2 = 4M^2\lambda^2\operatorname{sech}^2\lambda t, \tag{4.5}$$

and

$$\theta = \frac{1}{2M}(\gamma^{-1}-\gamma)t. \tag{4.6}$$

Thus the component of the magnetic field in the plane of the wave rotates at a constant rate following a particle.

The dimensional thickness of the waves is of the order of the characteristic length l, as is the case for solitary waves moving across a magnetic field. It is to be noted that since the value of $\gamma \simeq \frac{1}{4\theta}$, the waves move much faster than linearized Alfvén waves in the plasma. This is very different from the case for transverse waves, whose velocity of propagation lies between a and $2a$.

These solitary waves are the only non-trivial solutions of the equations of motion for the case in which the plasma and magnetic field are uniform ahead of the wave and the magnetic field is parallel to the direction of propagation. They do not in themselves provide a collision-free shock, since conditions behind the wave are identical with those ahead. However, it is intended to investigate in a subsequent paper the case in which the magnetic field is inclined at an angle to the direction of propagation. It is hoped to show that in this case there may be more than one type of solution, and moreover that there are solutions with shock-like properties for which conditions at downstream infinity differ from those at upstream infinity.

I am grateful to Dr J. A. Shercliff for a suggestion which led to the present work.

REFERENCES

Adlam, J. H. & Allen, J. E. 1958 *Phil. Mag.* **3**, 448.
Davis, L., Lüst, R. & Schlüter, A. 1958 *Z. Naturforsch.* **13***a*, 916.
Ferraro, V. C. A. 1955 *Proc. Roy. Soc.* A, **233**, 310.
Montgomery, D. 1959 *Phys. Fluids*, **2**, 585.

Measurements of entrainment by axisymmetrical turbulent jets

By F. P. RICOU† AND D. B. SPALDING

Mechanical Engineering Department, Imperial College of Science and Technology, London, S.W.7

(Received 23 November 1960)

A new technique is described for measuring the axial mass flow rate in the turbulent jet formed when a gas is injected into a reservoir of stagnant air at uniform pressure. The jet is surrounded by a porous-walled cylindrical chamber, and air is injected through the wall until the pressure in the chamber is uniform and atmospheric, a condition which is taken to signify that the 'entrainment appetite' of the jet is satisfied.

Measurements made with the apparatus have allowed the deduction of an entrainment law relating mass flow rate, jet momentum, axial distance and air density, regardless of the density of the injected gas, and including the effects of buoyancy. When the injected gas burns in the jet the entrainment rate is up to 30 % lower than when it does not.

1. Introduction

The problem

Several accounts are available (e.g. Schlichting 1955; Pai 1954) of the turbulent jet which results from the injection of a fluid through a nozzle into a large reservoir in which a second fluid is at rest. In the present paper, attention is concentrated on one property of the jet: the mass flow rate across a section at right angles to the jet axis. This quantity will be denoted by the symbol m; it may be related to the fluid velocity u in the axial direction, the fluid density ρ, and the radial distance y by

$$m = \int_0^\infty 2\pi \overline{\rho u} y \, dy, \tag{1}$$

where the over bar denotes a time-mean.

The mass flow rate m is known to increase with distance x from the nozzle. As a consequence, fluid from the surrounding reservoir is drawn radially inwards towards the jet across its conical surface; this process is known as entrainment. Entrainment is also important in many more practical situations; for example, it controls the flow patterns in combustion chambers and furnaces; it causes 'fire-storms' around large conflagrations; and many mixing devices of the chemical industry rely on entrainment for their effectiveness. If such processes are to be understood and controlled, the quantitative laws which govern the rate of entrainment, i.e. the quantity dm/dx, must be discovered.

† Now at the Laboratoires de Mécanique des Fluides, Université de Grenoble.

Dimensional analysis may be employed to show that, when the fluid density is uniform, when the Reynolds number is high and when the distance x is much larger than the diameter of the orifice, m is proportional to x. More precisely, it may be demonstrated that

$$\frac{m}{xM^{\frac{1}{2}}\rho_1^{\frac{1}{2}}} = K_1, \tag{2}$$

where M stands for the excess momentum flux of the jet, ρ_1 is the density of the surrounding fluid,† and K_1 is a numerical constant. Consideration of Newton's Second Law of Motion shows that, since the static pressure of the flow is uniform, M must have a value which is independent of x; it is most easily evaluated at the orifice, where the fluid has the uniform velocity u_0, from

$$M = M_0 \equiv \tfrac{1}{4}\pi d_0^2 \rho_0 u_0^2. \tag{3}$$

Here d_0 is the orifice diameter and ρ_0 the density of the injected fluid.

The numerical magnitude of K_1 can only be determined, in the present state of turbulence theory, by experimental means. Similarly, only experiment can show how equation (2) must be modified when the jet density is rendered non-uniform by a chemical reaction in the jet, or by the existence of a difference of value between ρ_0 and the density of the surrounding fluid, ρ_1.

Previous work

Numerous measurements have been made of the axial-velocity profiles, $u(y)$, in isothermal air jets (see, for example, the bibliography compiled by Krzywoblocki 1956). These data may be inserted in equation (1), from which the mass flow rate m can then be evaluated by numerical quadrature; this has been done by Grimmett (1948), Polomik (1948) and Voorheis & Howe (1939).

Many authors have avoided the numerical quadrature by assuming that the $u(y)$ profile has one of the forms which permit analytical integration; the velocity and radius scales appropriate to a given section are then determined from, say, the measured velocity on the axis, and the radius at which the measured velocity has half this value. The resulting values for m then depend to some extent on the profile-shape assumed.

Values for K_1 obtained in this way for isothermal air jets range from about 0·22 up to 0·404, according to the investigator. The highest value, due to Schlichting (1955), is obtained by fitting to the experimental data of Reichardt (1942) a particularly full-skirted 'theoretical' curve.

The reasons for the present uncertainty about the value of K_1 are of several kinds. They include the following:

(i) It is difficult to measure $\overline{\rho u}$ at large values of y where the velocities are small and the flow may be intermittent; the presence of y as a multiplier of u in equation (1) augments the influence of inaccuracies in this region.

(ii) The above difficulty is avoided if an analytical form is chosen for the velocity profile. This choice, on the other hand, entails uncertainty as to what is

† The subscripts to ρ in equations (2) and (3) are not needed in the present discussion, which presumes that ρ is uniform throughout; they are nevertheless inserted for use later in the paper.

the 'best' profile. Small differences in profile height at large y can greatly affect the value of m which is deduced.

(iii) Whichever of the above procedures is used, it is desirable that x should be many times greater than d_0. Since the dynamic head at a Pitot tube in the jet is proportional to $(d_0/x)^2$, limitations on manometer sensitivity make it difficult to work at axial distances much greater than five times the length of the potential core.

Outline of the present contribution

The above remarks show that a new method of measuring m is required, even for uniform-density flows. When jets with non-uniform density are to be studied, the case for a new method is stronger still; for a recourse to equation (1) would now necessitate measurement of a density profile as well as one of velocity, and would raise questions as to the relation of $\overline{\rho u}$ to the measured $\overline{\rho}$ and $\overline{\rho u^2}$.

The present paper reports a new experimental method which is not open to the objections mentioned above: m is measured more directly and simply; no integration is required. This technique is described in § 2 below.

The results of the study are presented in § 3 and figures 4, 5 and 7. Summarized briefly, they are: that K_1 is equal to 0·282; that equation (2) holds for non-uniform density without modification provided that buoyancy effects are negligible; and that the presence of combustion reduces K_1. The role of buoyancy is not so easily summarized; it is discussed in § 4.

2. Apparatus

The principle of the method

In the ideal free jet which is under consideration, the surrounding reservoir is large and, except in the vicinity of the jet axis, at uniform pressure; the entrained fluid flows radially inward towards the jet axis. If, however, a turbulent jet is partially enclosed by cylindrical walls, the radial inflow is impeded; the fluid entrained by the enclosed part of the jet has to flow axially in the annular space between the cylindrical wall and the conical 'boundary' of jet; the corresponding axial pressure gradients can be measured.

Now let us suppose that the cylindrical wall is made porous, and that a controlled and measured amount of fluid can be caused to flow through it in a radially inward direction. Then, if this flow is equal in quantity to that which would have passed through the area occupied by the wall if the wall had been absent, the axial pressure gradients referred to in the last paragraph will disappear.

This recognition underlies the experimental method which has been used: the flow rate through the porous wall is varied until no axial pressure gradients can be detected; this flow rate is then measured and presumed to be equal to that which would be entrained if the jet were unenclosed.

Details of the apparatus

Figure 1 shows the porous-walled chambers which were used. The axis of the jet is coincident with the axis of the cylindrical porous wall. The base of the cylinder was completely closed, apart from the orifice from which the jet origin-

ated, and the upper end of the resulting chamber was partially closed; these measures had the effect of augmenting the axial pressure gradients which prevailed when the flow through the porous wall was not 'right', while in no way interfering with the radially inward flow to the jet when it was entraining under free-jet conditions.

The porous cylinders were built up of fine-grade filter cloth on a rigid framework. A Roots-type blower was used to supply the entrainable air; this permitted the use of an appreciable pressure drop (up to 5 in. of water) across the porous cylinder and helped to ensure uniformity of inflow. Calibrated orifice plates were

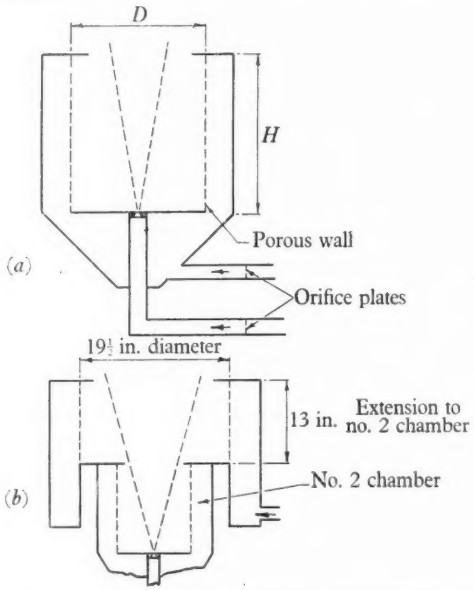

FIGURE 1. (*a*) Leading dimensions of three chambers.
(*b*) Dimensions of extension to no. 2 chamber.

	Entrainment chamber		
No.	1	2	3
H in.	8·7	13	3
D in.	5·8	8·9	8·9

used to measure the rate of supply of this air. The orifices used were of rounded profile, designed according to B.S. 1042. Their diameters (d_0) ranged from 0·0625 in. to 1·25 in. The corresponding range of dimensionless axial distances (x/d_0) over which measurements could be made was from 418 to 2·4.

The axial pressure difference which was measured was that across the outlet aperture; since the pressure variations within the chamber were small, this difference can be thought of as that between the pressure in the chamber and the pressure of the atmosphere. The micromanometer used was of the direct-reading type developed by Spalding (1950).

Preliminary tests: the choice of aperture size

The size of the aperture in the mask at the upper end of the 'entrainment chamber' had to be chosen with care. On the one hand, it was desired that the hole should be small, since this led to an easily detected pressure difference, when the flow through the porous wall was not properly matched to the free-jet requirements; however, if the hole were made too small, the mask would interfere with the axial flow in the jet itself.

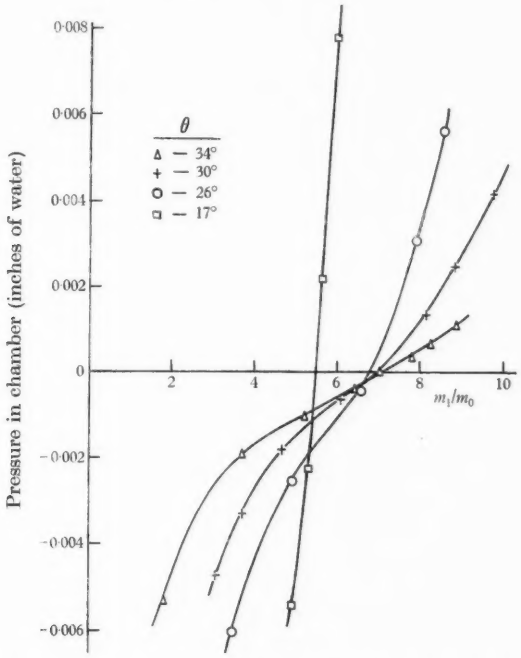

FIGURE 2. Variation of chamber pressure with flow rate through porous wall, for various apertures. Nozzle, 0·5 in. diameter; $x/d_0 = 25{\cdot}6$; $u_0 = 112$ ft./sec. (No. 2 chamber.)

Figure 2 shows the results of preliminary tests leading to the choice of aperture size, the latter being expressed in terms of the angle θ subtended by a diameter of the aperture at the centre of the base of the chamber. The ordinate is the excess pressure in the chamber; the abscissa is the ratio of the mass of air flowing through the porous wall, m_1, to the mass of gas (air) injected through the orifice, m_0; m_0, and the orifice diameter, d_0, have the same values throughout; each curve is drawn for a different value of aperture angle θ.

Inspection of figure 2 confirms that the smaller θ is the more steeply the excess pressure varies with variations of m_1; it also confirms that the aperture size influences the value of m_1/m_0 which gives zero excess pressure, if θ is too small. The latter influence is slight if θ is 30° or more; thus figure 2 shows that the value

of m_1/m_0 corresponding to free-jet conditions for the situation in question can be taken as 7·0. These tests led to the choice of 30° for the aperture angle in all the tests reported below.

Preliminary tests: the effect of the Reynolds number

Tests were carried out, using air as the injected fluid, to establish the value of the Reynolds number above which equation (2) was valid. Some of the data are recorded in figure 3 in the form of plots of m_1/m_0 versus the Reynolds number. The latter quantity is defined by

$$R \equiv \rho_0 u_0 d_0/\mu_0, \tag{4}$$

where μ_0 is the viscosity of the injected gas. From now onwards, m_1 will be used as signifying that value of the air flow rate through the porous wall which causes

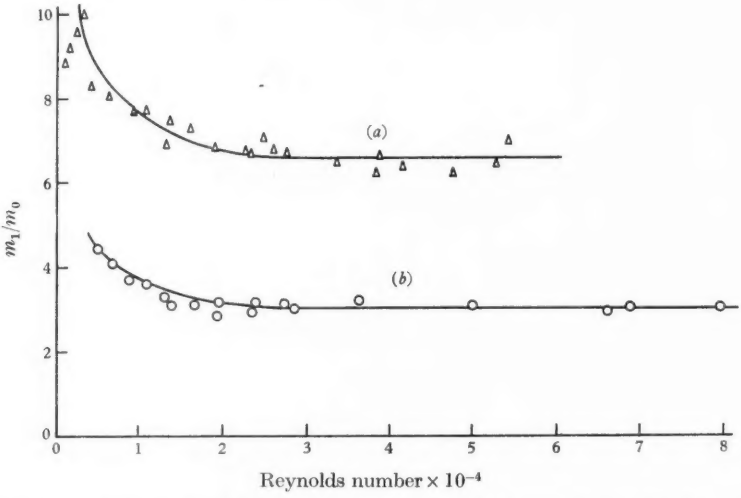

FIGURE 3. Variation of entrainment rate with the Reynolds number. (*a*) No. 2 chamber. Nozzle, 0·5 in. diameter; $x/d_0 = 25{\cdot}6$. (*b*) No. 1 chamber. Nozzle, 0·625 in. diameter; $x/d_0 = 13{\cdot}7$.

axial pressure gradients to disappear; m_1 is therefore connected with m, the mass flow rate in a free jet of length equal to the length of the entrainment chamber, by

$$m = m_1 + m_0. \tag{5}$$

The tests of figure 3 were carried out by varying the injection flow rate, and so the Reynolds number, and then measuring the corresponding m_1. Evidently, the ratio m_1/m_0 was approximately constant for Reynolds numbers in excess of $2{\cdot}5 \times 10^4$. All test data appearing in the remainder of the paper can be taken as pertaining to Reynolds numbers greater than this value, except for those in which the injected fluid is hydrogen.

3. Experimental results

Air into air: isothermal

Experiments were made with various combinations of chamber length x and nozzle diameter d_0, when the injected gas was air at the same temperature as the air supplied through the porous wall. The results are represented by the points in figure 4 clustered near the straight line marked (a); this line may be represented by the formula

$$\frac{m}{m_0} = 0{\cdot}32\frac{x}{d_0}. \tag{6}$$

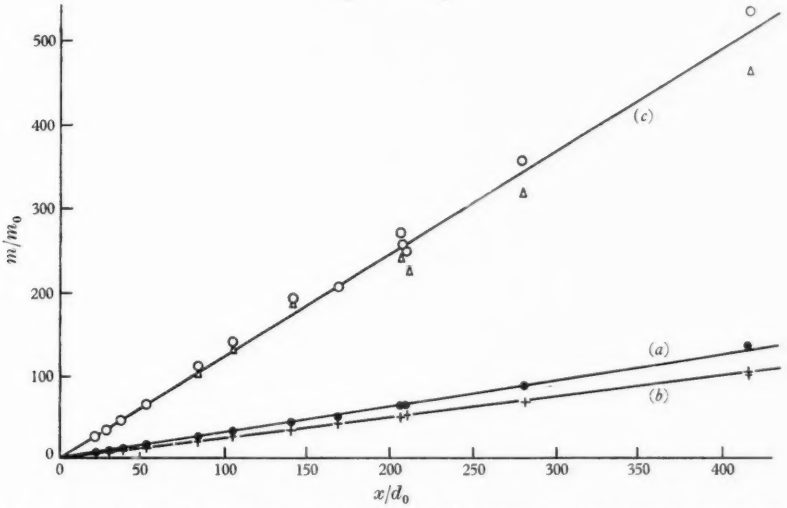

FIGURE 4. Variation of entrainment rate with axial distance for isothermal jets. Experimental results: (a) ●, air into air; (b) +, propane and carbon dioxide into air; (c) ○, hydrogen into air; (△, entrainment chamber inverted).

Heavy gas into air: isothermal

Corresponding measurements were made when the injected fluid was carbon dioxide or propane, two gases with equal densities, the temperatures being equal to that of the air supplied through the porous cylinder. The results are shown in figure 4 as a series of points clustered near the straight line marked (b): this line can be represented by the formula

$$\frac{m}{m_0} = 0{\cdot}26\frac{x}{d_0}. \tag{7}$$

Although flammable, the propane was not ignited in the experiments referred to here.

Light gas into air: isothermal

Figure 4 also contains results obtained by similar experiments in which hydrogen was the injected gas; the hydrogen jet was not ignited. The results are represented by the points near the straight line (c), the formula for which is

$$\frac{m}{m_0} = 1{\cdot}2\frac{x}{d_0}. \tag{8}$$

Since buoyancy was thought to affect the hydrogen jets, some experiments were carried out with the entrainment chamber inverted; it is seen that this inversion had an effect.

The high viscosity of hydrogen, and other limitations, prevented the performance of tests at Reynolds numbers in excess of 17,500.

Fuels into gas: combustion

Measurements were also made of the entrainment rate which prevailed when the fuel gases in the jet (propane and hydrogen) were ignited; in some cases both air and fuel were injected through the orifice simultaneously. The results of these tests, which showed a considerable effect of buoyancy, will be introduced in figure 7 below.

4. Discussion of results

Jets of uniform density

The equations (6), (7) and (8) may be cast in the form of equation (2) by introduction of equation (3) for the excess momentum flux and of a corresponding equation for the injected mass flux, m_0, namely

$$m_0 = \tfrac{1}{4}\pi d_0^2 \rho_0 u_0. \tag{9}$$

Equations (6), (7) and (8) then lead respectively to

$$\frac{m}{xM^{\frac{1}{2}}\rho_1^{\frac{1}{2}}} = 0{\cdot}32(\tfrac{1}{4}\pi)^{\frac{1}{2}} = 0{\cdot}283, \tag{10}$$

$$\frac{m}{xM^{\frac{1}{2}}\rho_1^{\frac{1}{2}}} = 0{\cdot}26(\tfrac{1}{4}\pi)^{\frac{1}{2}}(\tfrac{44}{29})^{\frac{1}{2}} = 0{\cdot}284, \tag{11}$$

$$\frac{m}{xM^{\frac{1}{2}}\rho_1^{\frac{1}{2}}} = 1{\cdot}2(\tfrac{1}{4}\pi)^{\frac{1}{2}}(\tfrac{2}{29})^{\frac{1}{2}} = 0{\cdot}279, \tag{12}$$

wherein $(\frac{44}{29})$ and $(\frac{2}{29})$ represent the density ratio ρ_0/ρ_1 for the respective cases of propane or carbon dioxide, and hydrogen.

Comparison of equations (10), (11) and (12) leads to the conclusion that equation (2) is valid, within the experimental error, for all the experimental results cited so far, if K_1 is given the value 0·282.

The same conclusion can be expressed differently by noting that all the data can be held to obey the relation

$$\frac{m}{m_0} = 0{\cdot}32\frac{x}{d_0}\left(\frac{\rho_1}{\rho_0}\right)^{\frac{1}{2}}. \tag{13}$$

This is illustrated by figure 5, which contains the data of figure 4 replotted in the manner indicated by equation (13).

The effect of buoyancy: theory

When the density of the fluid in the jet differs from that of the surrounding air, hydrostatic forces cause the excess momentum flux to increase with x (assuming that the jet fluid is the lighter and that the flow direction is upward). Consequently equation (2) no longer correctly expresses the variation of m with x.

Dimensional analysis indicates that, when x becomes very large, m is proportional to $x^{\frac{2}{3}}$ (Batchelor 1954); for this to hold, however, the excess momentum flux of the jet, M, must greatly exceed the value of M_0 defined by equation (3). How should m vary with x when M and M_0 are of the same order?

A tentative answer to this question may be obtained by supposing that the local rate of entrainment is uniquely related to the local excess momentum flux in accordance with the differential equation

$$\frac{1}{(M\rho_1)^{\frac{1}{2}}}\frac{dm}{dx} = 0{\cdot}282. \tag{14}$$

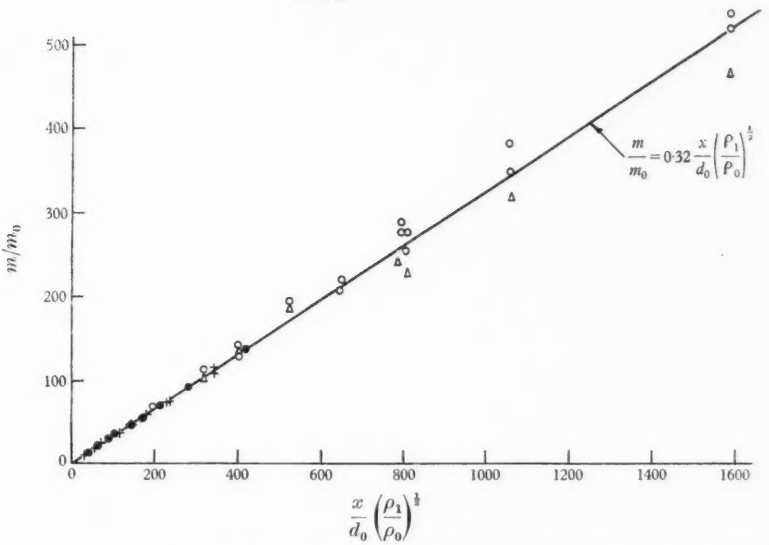

FIGURE 5. Entrainment rate for isothermal jets. Experimental results: (*a*) ●, air into air; (*b*) +, propane and carbon dioxide into air; (*c*), ○, hydrogen into air; (△, entrainment chamber inverted).

An assumption of this character has been made by Morton, Taylor & Turner (1950), and other authors, in connexion with the rise of turbulent plumes in the atmosphere.

In an unpublished study, one of the present authors has investigated the implications of equation (14), when combined with the assumptions: (i) that the velocity and temperature profiles are Gaussian, (ii) that the ratio of the widths of the temperature and velocity profiles is equal to 1·17 for all x, (iii) that chemical reaction is confined to regions of the jet which are much closer to the orifice than is the section x. The results of this study are represented by the curve of figure 6; the ordinate and abscissa quantities of this graph are self-explanatory apart from the Froude number, F, which is defined by:

in the absence of chemical reaction,

$$F \equiv \frac{c_1 T_1}{(h_0 - h_1)}\frac{u_0^2}{g d_0}\left(\frac{\rho_1}{\rho_0}\right)^{\frac{1}{2}}, \tag{15}$$

or, when chemical reaction occurs,

$$F \equiv \frac{c_1 T_1}{m_{fu} H + c_0 (T_0 - T_1)} \frac{u_0^2}{g d_0} \left(\frac{\rho_1}{\rho_0}\right)^{\frac{1}{2}}. \tag{16}$$

Here the symbols signify:

c	specific heat of gas at constant pressure,
T	absolute temperature of air,
h	enthalpy,
g	gravitational acceleration,
m_{fu}	mass fraction of fuel in injected gas,
H	heat of combustion of fuel,

and subscripts 0 and 1 refer, as before, to the injected fluid and to the surrounding air respectively.

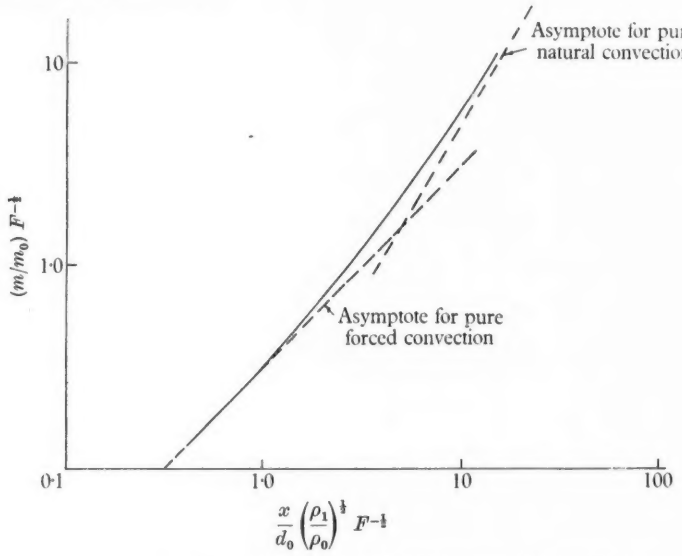

FIGURE 6. Theoretical prediction of entrainment in buoyant jets.

The effect of buoyancy: experiment

Figure 7 presents the data of figure 4 (upward flow only) together with the results of measurements made with burning jets. Also drawn for comparison is the curve of figure 6. The following features are evident.

(i) The data points lie close to the curve in the forced-convection régime; this, of course, is to be expected from figure 5, for example.

(ii) The influence of increasing buoyancy predicted by the theoretical curve, viz. an increased slope in the upper right corner, is exhibited by the experimental data. It is chiefly the hydrogen diffusion-flame data which are in question here.

(iii) Some of the data points, particularly those for pre-mixed hydrogen-air jets, lie well below both the curve and its forced-convection asymptote.

(iv) The scatter is considerable.

Comparison with previous work

It has already been stated that, in the absence of buoyancy, K_1 has been found by previous authors to lie between 0·22 and 0·404; the value obtained from the present work, viz. 0·282, can therefore be said to lie near the middle of the range of earlier values. The ease with which the measurements were made, in the present

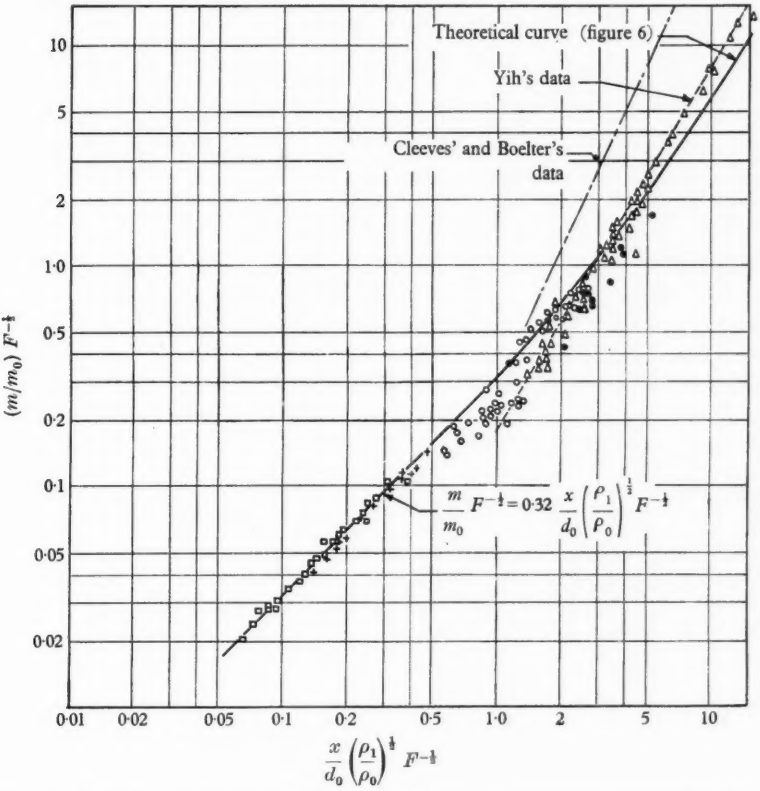

FIGURE 7. Entrainment by buoyant jets and flames. +, Unburnt propane jet; □, unburnt hydrogen jet; ○, pre-mixed air–hydrogen flame; △, hydrogen diffusion flame; ●, propane diffusion flame.

investigation, together with the straightforwardness of their interpretation, leads us to believe that the present value of K_1 is the most reliable established so far.

The finding that equation (2) holds, in the absence of buoyancy effects, for jets of non-uniform density was expected; it accords with the surmise of Squire & Trouncer (1944), and with the suggestion of Thring & Newby (1953), that the characteristic length of a turbulent jet is not d_0 but $d_0(\rho_0/\rho_1)^{\frac{1}{2}}$.

Other authors who have presented experimental data for the natural convection régime include Yih (1951), and Cleeves & Boelter (1947); the data of these authors are represented on figure 7 by broken straight lines which have been

plotted by ignoring experimental scatter and assuming Gaussian velocity and temperature profiles.

The data of Yih agree fairly well with the present hydrogen diffusion-flame data; both sets lie appreciably above the theoretical curve, indicating that the entrainment rate is greater in a buoyant jet than a non-buoyant one of the same excess momentum. The data of Cleeves & Boelter show the same tendency to an even more marked degree; they are, however, probably the least reliable of the data on figure 7, being appreciably influenced by potential-core effects.

5. Conclusions

(*a*) The new experimental technique for measuring the rate of entrainment by a turbulent jet was found to be easy to use, and to be applicable to jets of non-uniform density and to larger values of x/d_0 than had previously been investigated.

(*b*) The constant K_1 of equation (2) was found to have the value 0·282, irrespective of the density ratio.

(*c*) The curve of figure 6, based on the entrainment assumption expressed by equation (14), represents approximately the influence of buoyancy on the entrainment. However, it must be noted that: (i) there is a tendency for the curve to predict too low an entrainment rate in the natural-convection régime; (ii) the curve predicts too high an entrainment rate for some flames; (iii) the experimental scatter of the results of the present and earlier work in the natural-convection régime precludes the drawing of firm conclusions at present.

One of the authors (F. P. R.) acknowledges the financial support of the States of Jersey Committee of Education, and of Thomas Hedley and Company, Ltd.

This research was supported by a contract between Imperial College and the National Engineering Laboratory; the Director of the N.E.L. has given his permission for publication.

REFERENCES

Batchelor, G. K. 1954 *Quart. J. Roy. Met. Soc.* **80**, 339.

Cleeves, V. & Boelter, L. M. K. 1947 *Chem. Engng Progr.* **43**, 123.

Grimmett, H. L. 1948 M.S. Thesis, University of Illinois.

Krzywoblocki, M. Z. 1956 *Jet Prop.* **26**, 760.

Morton, B. R., Taylor, G. I. & Turner, J. S. 1950 *Proc. Roy. Soc.* A, **234**, 1.

Pai, S. I. 1954 *Fluid Dynamics of Jets.* New York: Van Nostrand.

Polomik, E. E. 1948 M.S. Thesis, University of Illinois.

Reichardt, H. 1942 *V.D.I.-Forschungsheft.* p. 414. (2nd ed. 1951).

Schlichting, H. 1955 *Boundary Layer Theory.* London: Pergamon Press.

Spalding, D. B. 1950 *J. Sci. Instrum.* **27**, 310.

Squire, H. B. & Trouncer, J. 1944 Round jets in a general stream. *Aero. Res. Counc. Tech. Rep.* R. &. M. no. 1974.

Thring, M. W. & Newby, M. P. 1953 *Fourth Symposium on Combustion*, p. 789. Baltimore: Williams and Wilkins.

Voorheis, T. S. & Howe, E. D. 1939 *Proc. Pac. Coast Gas Ass.* **30**, 198.

Yih, C. S. 1951 *Proc. First U.S. Nat. Congr. Appl. Mech.* p. 941.

The flow of thin liquid films between rollers

By E. PITTS AND J. GREILLER

Research Laboratories, Kodak Ltd, Wealdstone, Harrow, Middlesex

(Received 7 February 1961)

When rollers, placed horizontally and side by side so that each is half immersed in a tank of liquid, rotate in opposite directions, liquid is carried through the gap between them and divides to form a sheet over each roller. At low speeds the sheets are of uniform thickness across the width of the rollers, but at higher speeds they are regularly ridged owing to alternate increase and decrease in thickness. Preliminary observations led to the development of an approximate theoretical treatment of the even-flow régime and the critical conditions when the ribbed flow is about to begin. Results of this work are in full agreement with detailed experimental results.

1. Introduction

The production of uniform thin films of liquid as a coating is a frequent industrial requirement, and various methods are used for the purpose. It is a common observation that many of the methods which involve spreading or rolling of the liquid often give rise to very uneven or ribbed layers. It appeared that in spite of the widespread occurrence of the phenomenon, little work had been published relating to it, and no adequate explanation had been given. Accordingly, extensive experimental and theoretical work was carried out in these laboratories on a model consisting of two cylinders placed with their axes parallel and level with the surface of liquid in a tank. Each roller is thus half immersed in liquid. On rotation of the rollers in contrary motion, liquid is drawn up through the narrow gap separating them, and divides to form a sheet over each, returning to the bulk of the liquid. Using this apparatus it has been possible to make many determinations of the position of the meniscus where the liquid divides as a function of the physical and geometrical variables, and to observe the conditions in which the even film of liquid over each roller changes into a regularly rippled sheet. A description of these and other more detailed observations are presented in this paper together with an approximate theoretical treatment of the problem which satisfactorily accounts for all the observed phenomena.

At a late stage in our work we were informed of a similar problem being studied by Dr J. R. A. Pearson, which we discussed with him. The work has recently appeared in an interesting paper (Pearson 1960) in which the spreading of liquid over a plane surface by means of a wedge-shaped spreader is discussed. Pearson was able to account for the appearance of regularly spaced crests and troughs in the emergent thin film running parallel to the direction of motion of the spreader. The observed and calculated periodicities of the ripple were in fair agreement.

His discussion of the problem is, however, in some respects incomplete, since it does not permit the quantitative prediction of the conditions in which the uniform flow, stable for sufficiently low speeds of spreading, changes to the rippled form. Other approximations are made which obscure certain important features of the flow in the region of the meniscus.

We have been able to account for all the main features of the flow in our experiments, together with the quantitative prediction of the critical conditions. The treatment of the problem divides naturally into two parts: the even flow régime before the appearance of ripples, and the critical conditions in which ripples first appear.

2. The even flow régime

2.1. *Experimental methods*

The arrangement of the rollers in the tank of liquid and their direction of rotation are shown in figure 1. The tank was made of Perspex to allow observations to be made through the sides. Two sizes of roller were used, with known diameters, nominally 1 in. and 2 in. The gap separating the rollers at their closest approach (the nip) could be set from zero to 1 mm with an accuracy and uniformity within

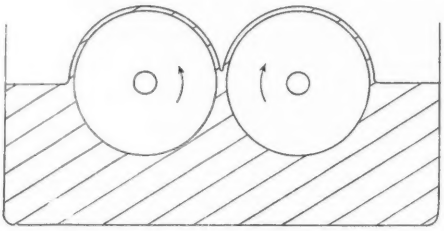

FIGURE 1. Arrangement of rollers in the liquid.

0·015 mm. Because these gaps were so narrow, great care had to be taken in making the rollers to ensure that each was a true cylinder accurately concentric with its spindle. Variation in the width of the gap along its length was about $\pm 5\,\%$ in the smallest gaps but much less in the larger gaps. Each roller rotated at the same speed, the maximum rate of rotation being about 75 r.p.m. The viscosity of the liquids used was in the range 0·25–6 poise. During the course of an experiment temperature changes occurred and allowance was made for the consequent change in viscosity when calculating results. When glycerin was used, changes in viscosity also occurred owing to the absorption of moisture from the air. These were known and kept as small as possible.

It became apparent that surface tension could not be changed in a controlled way by using surface-active agents, owing to the rapid rate of expansion of the liquid surface in the region under examination. It was therefore necessary to use liquids having intrinsically different surface tensions.

The basic flow pattern was obtained from photographs taken through the transparent walls of the tank along a direction parallel to the axes of the rollers. Streamlines were made more distinct by the introduction of very small air

bubbles. Other photographs were taken showing the profile of the meniscus at various speeds, together with its position between the rollers. In addition many determinations of meniscus position were made with a travelling microscope.

Sufficiently accurate measurements of the volume of liquid carried through the gap presented great difficulties. The method finally adopted was to collect and weigh the liquid carried by one roller using a tray with a rubber scraper blade. Edge effects were eliminated by using trays of different widths. The scraper could not be made to remove all the liquid from the roller surface and the amount left under different conditions was obtained by absorbing it on filter paper and weighing.

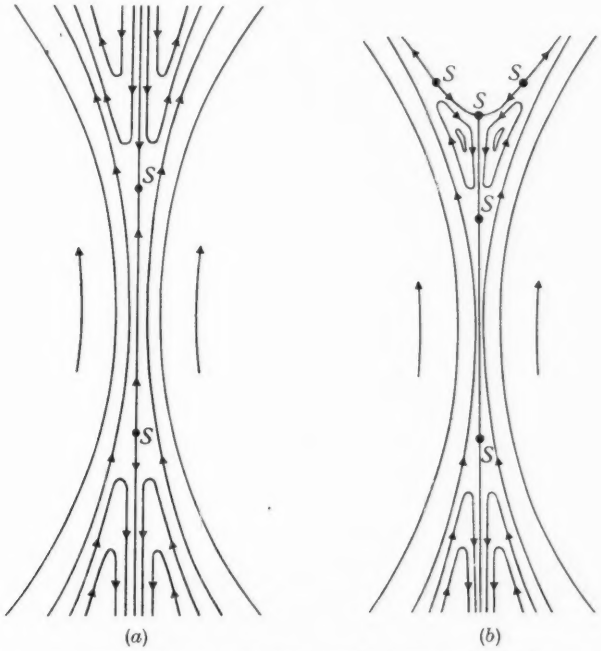

FIGURE 2. (*a*) Streamlines when rollers are totally immersed. (*b*) Streamlines when rollers are partially immersed.

2.2. *Experimental observations*

It is of interest to compare the flow pattern when the rollers are completely immersed in the liquid with that when they are half immersed. The streamlines are indicated in figures 2*a* and *b*, in which *S* indicates a stagnation point (where the fluid velocity is zero). It will be seen that the flow patterns on the ingoing side are alike, but on the outgoing side the presence of the meniscus causes two areas of circulatory flow, and three extra stagnation points in addition to the centres of the vortices.

By measurement of the many photographs taken, it has been established that, to a very close approximation, the meniscus is parabolic over a large part of its profile.

For a given gap between the rollers the position of the meniscus may be specified by measuring the ratio, σ_0, of the width of the channel at the lowest point of the meniscus to the gap width. In figure 3 the crosses show the value of σ_0 for a gap width of 0·020 cm as a function of $\log(\mu U/T)$, where μ and T are the viscosity and surface tension of the liquid, and U is the surface speed of the rollers. Two liquids were used, having surface tensions of 47 and 65 dynes/cm and viscosities were in the range 0·4–5·5 poise. In each experiment the speed was varied by a factor of nearly five, viscosity and surface tension remaining constant. It will be seen that as the speed is increased, σ_0 decreases, i.e. the meniscus moves in towards the nip. Similar results are found for other gap widths.

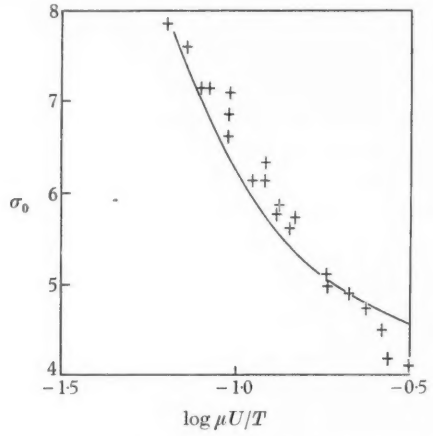

FIGURE 3. The position of the meniscus: + experimental observations; − theoretical curve.

Elementary considerations suggest that if $2h$ is the width of the nip, the quantity of liquid carried through per second per unit length of the roller will be $2\lambda Uh$, where λ is a number of order of magnitude unity. As has already been mentioned, the experimental measurement of the quantity carried through, and hence the determination of λ in given flow conditions, was difficult to achieve with sufficient accuracy. Liquid escaped collection, and the accuracy with which the smallest gaps could be set was probably not better than $\pm 10\,\%$. For a range of flow conditions the mean of the observed values of λ was 1·33, individual readings ranging from 1·38 to 1·26. A slight decrease in λ with increasing speed is indicated by the results.

In the next section we shall give an approximate theoretical account of this type of flow, and in §2·4 compare theory with the experimental results just described.

2.3. *Theory*

The flow pattern in the region of the meniscus, as revealed by experiment, is complicated and an exact theoretical treatment of the problem appears extremely difficult. Accordingly, we shall present a treatment which although approximate,

nevertheless reveals the most important of the relationships and accounts for the main experimental results.

The motion of the liquid in the region where the channel is narrow is predominantly determined by the drag due to the moving rollers and the variation in the width of the channel. It may be shown that inertia terms in the hydrodynamic equations can be neglected without serious error. Terms representing the effect of gravity were included in the original treatment but are here omitted for simplicity, since their influence is small except at the lowest speeds of rotation and for the largest gap widths. Pearson has outlined in his paper the arguments justifying these approximations.

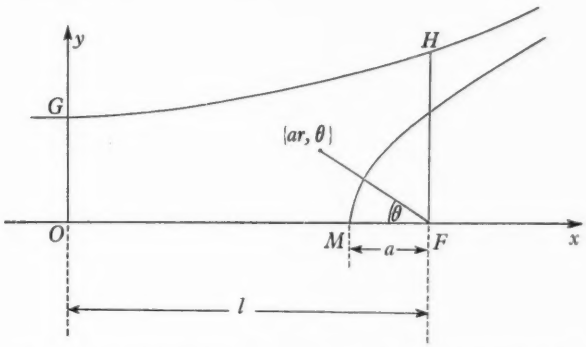

FIGURE 4. Co-ordinate system used to describe flow in the vicinity of the meniscus.

In principle, it should be possible to deduce both the form and the position of the free liquid surface from purely theoretical considerations. This degree of generality will not be attempted here. Instead, we shall make use of the experimental observations that the meniscus has a parabolic profile, and find theoretically its size and position along the axis of symmetry.

First, we shall ignore the presence of the meniscus and calculate the flow in the narrow part of the channel. It will be convenient to use the co-ordinate system shown in figure 4. The x-axis is along the axis of symmetry, the y-axis is in the plane through the axes of the rollers which are parallel to the z-axis. There is no component of fluid velocity in the z-direction. Let OG equal h (half the gap width) and let the radius of the rollers be R. A brief preliminary investigation suggests that new variables ξ and η, defined by the equations

$$x = \xi(Rh)^{\frac{1}{2}}, \quad y = \eta h \tag{2.1}$$

are suited to this problem. We can then use the ratio

$$\delta = h/R \tag{2.2}$$

as a small parameter (of the order 5×10^{-3}) in the development of the solution. If the surface of the roller is defined by the equation

$$\eta = \sigma(\xi), \tag{2.3}$$

elementary geometry shows that

$$\sigma = 1 + \tfrac{1}{2}\xi^2 + O(\delta). \tag{2.4}$$

If the component of velocity in the x-direction is written Uu, that in the y-direction $\delta^{\frac{1}{2}}Uv$, where U is the velocity of the surface of the roller, and

$$P = ph^{\frac{3}{2}}/\mu UR^{\frac{1}{2}}, \tag{2.5}$$

where p is the pressure and μ the viscosity of the liquid, the hydrodynamic equations become (neglecting inertia terms and the force due to gravity)

$$\frac{\partial P}{\partial \xi} = \frac{\partial^2 u}{\partial \eta^2} + O(\delta), \tag{2.6}$$

$$\frac{\partial P}{\partial \eta} = O(\delta). \tag{2.7}$$

The continuity equation is

$$\frac{\partial u}{\partial \xi} + \frac{\partial v}{\partial \eta} = 0. \tag{2.8}$$

At the roller surface the liquid velocity must equal that of the roller. Hence when $\eta = \sigma$

$$u = 1 + O(\delta). \tag{2.9}$$

Also the quantity of liquid per second per unit length crossing a plane perpendicular to the x-axis and extending to the surfaces of the rollers must be constant. If this quantity is $2\lambda Uh$, then we must have

$$\lambda = \int_0^\sigma u \, d\eta. \tag{2.10}$$

If we neglect terms $O(\delta)$ we find that

$$u = 1 + \tfrac{3}{2}(\sigma - \lambda)(\eta^2 - \sigma^2)/\sigma^3 \tag{2.11}$$

and

$$P = 3\int^\xi \left(\frac{\sigma - \lambda}{\sigma^3}\right) d\xi. \tag{2.12}$$

We notice that the position of the stagnation point on the axis is given by

$$\sigma = 3\lambda. \tag{2.13}$$

Equivalent results have also been given by other workers (for example, Banks & Mill 1954 and Hopkins 1957). If the rollers are completely immersed, it is easily shown that λ must be $\frac{4}{3}$, to this degree of approximation.

We shall now attempt to describe conditions in the neighbourhood of the meniscus by adding to the above solution terms which are important only near the meniscus, and which decrease rapidly elsewhere.

It is convenient to use cylindrical co-ordinates centred on the focus F of the parabolic meniscus, whose latus rectum is $4a$ (see figure 4). The distance from the nip to the focus is l. (Both l and a will be evaluated theoretically.) The radius vector has length ar, where r is dimensionless. If we introduce a stream function ψ, such that the component velocities divided by U are respectively

$$v_r = -\frac{1}{r}\frac{\partial \psi}{\partial \theta}, \quad v_\theta = \frac{\partial \psi}{\partial r}, \tag{2.14}$$

the Stokes equations are

$$\frac{a}{\mu U}\frac{\partial p}{\partial r} = -\frac{1}{r}\frac{\partial}{\partial \theta}\nabla^2\psi, \quad \frac{a}{\mu U}\frac{1}{r}\frac{\partial p}{\partial \theta} = \frac{\partial}{\partial r}\nabla^2\psi, \tag{2.15}$$

and ψ must satisfy the relation

$$\nabla^4\psi = 0. \tag{2.16}$$

The equation of the parabolic surface of the meniscus is

$$r(1+\cos\theta) = 2. \tag{2.17}$$

The boundary conditions are as follows. The velocity normal to this surface must be zero, i.e., on the surface, ψ is a constant, which may be put equal to zero

$$\psi = 0. \tag{2.18}$$

Also, the tangential stress in the liquid must be zero on the surface. If σ_r, σ_θ and $\tau_{r\theta}$ are the stresses defined in the usual way for cylindrical co-ordinates, and ϕ is the angle between the tangent to the surface at a point and the normal to the radius vector at the point, then the vanishing of the tangential stress may be written

$$(\sigma_r - \sigma_\theta)\sin\phi\cos\phi + \tau_{r\theta}(\cos^2\phi - \sin^2\phi) = 0. \tag{2.19}$$

From the equation for the parabola, it follows that

$$\phi = \tfrac{1}{2}\theta, \tag{2.20}$$

and, from this relation and the definitions of the stresses, the condition for zero tangential stress becomes

$$2\frac{\partial v_r}{\partial r}\sin\theta + \left(\frac{\partial v_\theta}{\partial r} - \frac{v_\theta}{r} + \frac{1}{r}\frac{\partial v_r}{\partial \theta}\right)\cos\theta = 0. \tag{2.21}$$

The outward normal component of stress S_N is given by

$$S_N = \sigma_r\cos^2\phi + \sigma_\theta\sin^2\phi - 2\tau_{r\theta}\sin\phi\cos\phi. \tag{2.22}$$

Using the above definitions together with the condition (2.19), we find

$$S_N = -p + \frac{2\mu U}{a\cos\theta}\frac{\partial v_r}{\partial r}. \tag{2.23}$$

S_N must equal the normal stress on the surface due to atmospheric pressure and the effect of surface tension T. When the radius of curvature at a point on the surface is calculated, and measuring pressure in excess of atmospheric pressure, the condition expressing continuity of normal stress becomes

$$\frac{T}{\mu U}\frac{(1+\cos\theta)^{\frac{3}{2}}}{2^{\frac{3}{2}}} = -\frac{ap}{\mu U} + \frac{2}{\cos\theta}\frac{\partial v_r}{\partial r}. \tag{2.24}$$

In addition, the resultant velocity at the surface of the rollers must equal U, and to ensure the constancy of net flux, ψ must be constant there.

We shall suppose that the solution of equation (2.16) relevant to this problem may be written

$$\psi = \sum_1^\infty \sin m\theta\,(A_m r^m + C_m r^{m+2} + B_m r^{-m} + D_m r^{2-m}), \tag{2.25}$$

where the coefficients A_m and C_m are those corresponding to the solution (2.11). The remaining terms express the influence of the meniscus. The pressure is then given by

$$p = -4\mu \sum_{1}^{\infty} \cos m\theta \,[(m+1)\, C_m r^m + (m-1)\, D_m r^{-m}] + c, \tag{2.26}$$

where c is a constant, and equation (2.21) gives

$$0 = \sum_{1}^{\infty} \sin (m+1)\theta \,[m(m+1)\, B_m r^{-m-2} + m(m-1)\, D_m r^{-m}] + \sum_{1}^{\infty} \sin (m-1)\theta \,[m(m-1)\, A_m r^{m-2} + m(m+1)\, C_m r^m], \tag{2.27}$$

where r is defined by equation (2.17).

If σ_1 is the ratio of the lengths FH to OG, by straightforward methods we find the following expressions for the A and C coefficients:

$$\left.\begin{aligned} A_1 &= \tfrac{1}{2}(3\kappa - 1), & C_1 &= \tfrac{3}{8}\alpha(1-\kappa), \\ A_2 &= \tfrac{3}{4}\kappa\beta, & C_2 &= \tfrac{1}{4}\alpha\beta(1-\tfrac{3}{2}\kappa), \\ A_3 &= -\tfrac{1}{3}C_1, & C_3 &= 0, \\ A_4 &= -\tfrac{1}{2}C_2, & C_4 &= 0, \end{aligned}\right\} \tag{2.28}$$

where we have defined

$$\left.\begin{aligned} \kappa &= \lambda/\sigma_1, & \beta &= la/\sigma_1 Rh, \\ \alpha &= (a/\sigma_1 h)^2, & \sigma &= \sigma_1(1-\beta r\cos\theta) + O(\delta), \end{aligned}\right\} \tag{2.29}$$

and neglected all terms $O(\beta^2)$ and $O(\delta)$. (Development of the theory confirms the experimental result that in cases of interest β is less than 0·09.)

We have now to determine the B and D coefficients so that the boundary conditions are satisfied. This problem is made particularly difficult by the complicated geometry of the surfaces in the neighbourhood of the meniscus. Instead of attempting to satisfy conditions exactly at both boundaries we shall take three terms which decrease as r increases, and choose the coefficients so that over the meniscus the boundary conditions are satisfied for terms of order θ and θ^3 in the expansion of equations (2.18), (2.21) and (2.24). Since D_1 may without loss of generality be assumed to be zero, we have retained B_1, D_2 and D_3, i.e. terms in the velocities of order r^{-1} and r^{-2}. The outcome of other choices has been investigated, and it appears that the general result is not greatly affected. In making this approximation the boundary conditions at the surface of the roller are violated. However, very interesting and useful results can be obtained in spite of this defect.

Equations (2.18), (2.21) and (2.24) each give two equations corresponding to the coefficients of θ and θ^3. These six equations may be solved and after lengthy algebra give A_1, C_1, B_1, D_2 and D_3 in terms of $T/\mu U$, A_2, and C_2. Finally, there is an expression which in effect relates p and $T/\mu U$, A_2 and C_2. The expressions for A_1, C_1 and that involving p may be written after some rearrangement

$$3\kappa = 1 - T/29{\cdot}3\mu U - 2{\cdot}44\kappa\beta + 3{\cdot}28\alpha\beta(1-\tfrac{3}{2}\kappa), \tag{2.30}$$

$$\alpha = (T/56{\cdot}4\mu U + 0{\cdot}59\kappa\beta)/[1-\kappa + 3{\cdot}20\beta(1-\tfrac{3}{2}\kappa)] \tag{2.31}$$

and $$\sigma_1 q(\sigma_1, \lambda) = (2h/\alpha R)^{\frac{1}{2}} [0{\cdot}148T/\mu U + 0{\cdot}30\kappa\beta + 1{\cdot}65\alpha\beta(1-\tfrac{3}{2}\kappa)], \quad (2.32)$$

where $$q(\sigma_1, \lambda) = -2\int_{-\infty}^{\xi_0} \left(\frac{\sigma-\lambda}{\sigma^3}\right) d\xi \quad (2.33)$$

and $$1 + \tfrac{1}{2}\xi_0^2 = \sigma_1(1-\beta). \quad (2.34)$$

Use of the relation (2.4) in evaluating the infinite integral in (2.33) introduces only negligible error.

From these equations we wish to find κ, α and λ for a given value of $T/\mu U$. It will be seen that the expression for κ involves κ on the right-hand side, but since these terms are small a first approximation to κ is immediately obtained. Using this and assuming λ to be $\frac{4}{3}$, a rough value of σ_1 is obtained. From equation (2.31),

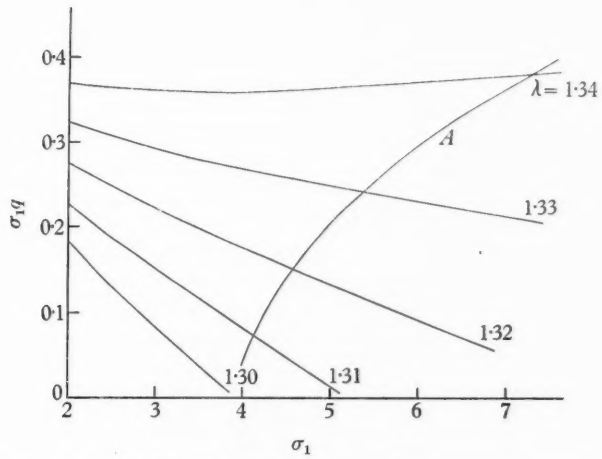

FIGURE 5. Values of $\sigma_1 q$ as a function of σ_1 and the appropriate value of λ.

by ignoring terms involving β, we next obtain a rough value of α. From our knowledge of σ_1 we can derive a rough value for l by geometry, and hence find β approximately. This enables a new derivation of κ to be made from equation (2.30). The process can be repeated to obtain better approximations. When these are obtained, we can calculate the right-hand side of equation (2.32). The left-hand side of this equation is independent of $T/\mu U$, and may be calculated as a function of σ_1, λ and β. These values are shown in figure 5. Since we know the value of the right-hand side of equation (2.32), i.e. the numerical value of $\sigma_1 q$, and also the value of σ_1 we can therefore obtain a new value of λ. This can then be used to improve the values of κ and α.

From curve A of figure 5 we can find how the value of λ changes as σ_1 changes (due to changes in $T/\mu U$). These calculations also enable us to find the value of σ_0 corresponding to the cross-section at M.

2.4. *Comparison with experiment*

From these results the value of σ_0 as a function of log $(\mu U/T)$ is known and has been indicated by the smooth curve in figure 3. It will be seen that the extent of the agreement is very satisfactory.

Similar agreement is found for other gap widths. The region where the discrepancy is largest is at small values of σ_0, i.e. high speeds of rotation. This may perhaps be because at low speeds the roller surfaces (where boundary conditions are violated) are relatively more distant from the region of the meniscus near the axis of symmetry, than when the speed is large. We might then expect that incorrect boundary conditions at the rollers would have most effect at high speeds.

Reference to figure 5 shows that as σ_1 decreases, λ also decreases. The substantiation of this theoretical change from about 1·34 when $\sigma_1 = 7$, to 1·30 when $\sigma_1 = 4$ would require experimental accuracy which could not be achieved without completely redesigning the apparatus. Nevertheless, the predicted change is in the same direction as the experimental trend.

3. Critical conditions

3.1. *Experimental observations*

As has already been described in §2.2, an increase in speed of rotation of the rollers causes the meniscus to recede towards the nip. When the meniscus is close to the stagnation point S_0 (see figure 2*b*), the circulatory regions are too small to be seen clearly. Any further increase in speed causes a change to take place in the flow pattern. In the region of the meniscus the velocity now has a component parallel to the axes of the rollers. The previously smooth sheet of liquid over each roller becomes regularly rippled across its width, with a consequent regular disturbance of the evenness of the liquid sheets. When first clearly visible, this ripple is of low wave-number (3 or 4 crests/in.) and is constant across the whole width of the rollers. With all conditions fixed, the surface remains steady, the cross-section of each line being of the same form and wavelength. The crests on one roller are directly opposite those on the other. A schematic diagram of the appearance of the liquid is shown in figure 6.

A further steady increase in speed results at first in an increase in amplitude only, then, after a slight wandering and merging of the lines, in an increase in their wave-number. This new state is again stable over a range of speeds, only changing in amplitude. Another transition follows and this cycle is repeated until eventually the ripples are very numerous (about 25/in.).

It is of interest to measure conditions under which the ripple first appears. This has been done for varying speed, viscosity and gap width, and with different liquids to investigate the effect of surface tension. It is difficult to judge when ripples of very small amplitude are first present, and so, to obtain more consistent results, a criterion was chosen in which the ripples were of sufficient amplitude to be unmistakable.

The results of these observations are shown in figure 7. The product μUR is shown as a function of Th in conditions under which ripples first appear. The

values of viscosity range between 0·4 and 5·4 poise and the gap varies between 0·005 cm (0·002 in.) and 0·05 cm (0·02 in.). Two sets of rollers were used, with radii nominally of 0·5 and 1 in. Two liquids were used, a glycerin–water mixture

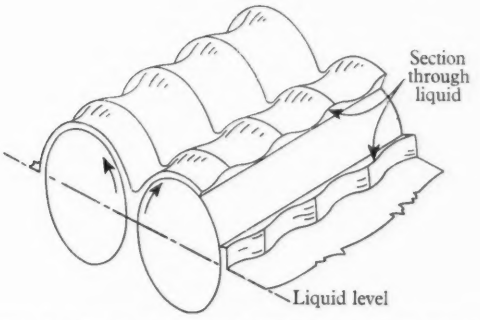

FIGURE 6. The appearance of ripples (not drawn to scale).

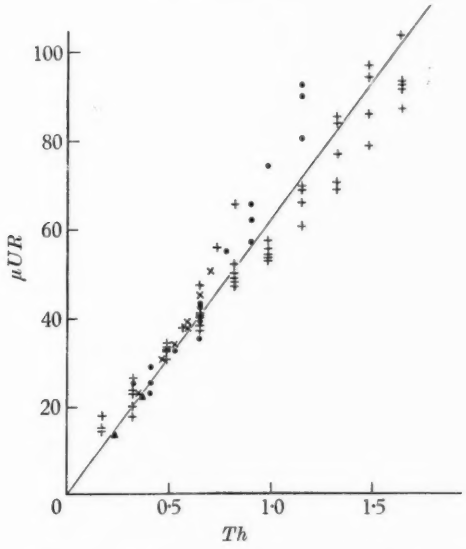

FIGURE 7. Critical conditions as determined by experiment. + Glycerin, 2 in. roller. ● Glycerin, 1 in. roller. × Lactic acid, 2 in. roller. ▲ Lactic acid, 1 in. roller.

with a surface tension of 65, and pure lactic acid with a surface tension of 47. It will be seen from the figure that when conditions are critical and ripples are first recognisably present $\mu UR/Th \simeq 62$. In §3.3 we shall discuss the reliability of this result more fully. Having regard to the experimental difficulties, especially the difficulty of deciding on the presence or absence of a ripple, the scatter of the experimental results is not excessive.

From this result it will be seen that the smaller the surface tension of the liquid or the smaller the gap, the lower the velocity at which ribbing occurs. Increasing

the viscosity of the liquid or the radius of the rollers likewise causes ribbing to appear at lower velocities. The effect of surface tension may be strikingly demonstrated by allowing ether vapour to collect near the meniscus when ripples are absent. Adsorption of ether causes a large reduction in surface tension which is usually sufficient to give rise to the appearance of ripples, because (at fixed speed) the critical value of the above ratio has been exceeded.

3.2. *Theory*

The experimental results just described demonstrate the importance of the dimensionless ratio $\mu UR/Th$ in determining the flow conditions. Before giving a detailed theoretical explanation, it will be helpful to give an outline of the main physical considerations to show qualitatively how this result arises.

Owing to the curvature of the meniscus, there is a drop in pressure on crossing the boundary equal to $T/2a$. The gradient of the pressure (equation (2.12)) near the meniscus is given approximately by the equation

$$dp/dx = 3\mu U(\sigma-\lambda)/\sigma^3 h^2.$$

Now imagine that at two different positions across the width of the roller, owing to a small perturbation, the menisci cut the axis at different distances x and $x+dx$ from the nip. At the meniscus farthest from the nip, the pressure drop will be less than that at the other site because a has increased. The pressure drop behind this meniscus but at a distance x from the nip will therefore be

$$\frac{T}{2a}+\left[\frac{d}{dx}\left(\frac{T}{2a}\right)+\frac{dp}{dx}\right]dx.$$

Thus, compared with the pressure at the other meniscus, there is a pressure difference of

$$\left(-\frac{T}{2a^2}\frac{da}{dx}+\frac{dp}{dx}\right)dx$$

tending to produce sideways motion of the liquid. If this difference is positive, there will be a tendency for liquid to flow towards the point where the meniscus is farther out, so that the perturbation may be increased, and hence instability arise. We might therefore expect our stability criterion to be

$$\frac{dp}{dx} < \frac{T}{2a^2}\frac{da}{dx}.$$

From equation (2.31) it will be seen that we may write $\alpha = kT/\mu U$. The quantity k is approximately constant in the conditions of interest. Assuming k is strictly constant, we may evaluate da/dx using (2.29), and the above criterion for instability becomes

$$\frac{3(\sigma-\lambda)}{\sigma} < \left(\frac{Th}{\mu UR}\right)^{\frac{1}{2}}\left(\frac{\sigma-1}{2k}\right)^{\frac{1}{2}}$$

after cancellation of common factors. This result shows that $\mu UR/Th$ depends on σ and since this quantity only varies slowly with $T/\mu U$, we have an indication that, at least approximately, $\mu UR/Th$ is a constant when conditions are critical. Evaluation of the constants gives the result that, when conditions are critical,

$\mu UR/Th$ has a value about 10, which is the order of magnitude of the experimental result. This suggests that the above argument is a sound basis for a more thorough analysis.

It will be seen that a vital step in this argument is the use of equation (2.31). The plausible hypothesis that the radius of curvature of the surface may approximately be put simply proportional to the channel width alone leads by a similar argument to the appearance of the group $\mu UR^{\frac{1}{2}}/Th^{\frac{1}{2}}$, which is not in accord with experiment. This assumption was however used successfully by Pearson (1960) in his discussion of another problem, but it evidently cannot be used here.

Two important factors have been entirely omitted in the above, viz. the effect of curvature of the meniscus in the other plane, and the variation in the amount of liquid carried away as a function of meniscus position. In the following we shall consider these additional factors.

It will be convenient to follow the analysis and notation used by Pearson, making use of equation (2.31) at a later stage, so that comparison with Pearson's work is easier. We need to know the effect of small changes in the shape of the meniscus on the flow pattern. Using the Cartesian co-ordinate system shown in figure 4, we shall suppose that the meniscus cuts the (x, z)-plane in the curve

$$x = x_0 + \epsilon \cos nz, \tag{3.1}$$

where ϵ is a small length whose square can be neglected. Since the meniscus cuts the (x, y)-plane in a parabola (latus rectum $4a$) the expression for the pressure reduction due to surface tension is found from the sum of the principal curvatures of the surface, and is

$$T\left(\frac{1}{2a} - \epsilon n^2 \cos nz\right). \tag{3.2}$$

We may find $\partial p/\partial z$ by the same argument as that used earlier, but using the expression (3.2) for the pressure drop. After a little manipulation, we find that

$$\frac{\partial p}{\partial z} = \epsilon n\left[\frac{3\mu U(\sigma_0 - \lambda)}{h^2\sigma_0^3} - T\left(\frac{1}{2a^2}\frac{da}{dx} + n^2\right)\right]\sin nz. \tag{3.3}$$

The effect of this small pressure on the flow pattern may be found by conventional perturbation methods. Suppose that the velocities of the liquid in the x- and z-directions are increased by the quantities u' and w', where

$$\frac{u'}{U} = \epsilon F(x)\left(\frac{\eta^2}{\sigma^2} - 1\right)\cos nz, \tag{3.4}$$

$$\frac{w'}{U} = \epsilon G(x)\left(\frac{\eta^2}{\sigma^2} - 1\right)\sin nz. \tag{3.5}$$

Both these additional velocities vanish at the surfaces of the rollers. If p' is the perturbation of the pressure, the perturbed parts of the equations of motion are approximately

$$\frac{\partial p'}{\partial x} = \frac{\mu}{h^2}\frac{\partial^2 u'}{\partial \eta^2}, \tag{3.6}$$

$$\frac{\partial p'}{\partial z} = \frac{\mu}{h^2}\frac{\partial^2 w'}{\partial \eta^2}. \tag{3.7}$$

The continuity of cross-sectional flow implies that

$$\frac{\partial}{\partial x}\int_0^\sigma u'\,d\eta+\frac{\partial}{\partial z}\int_0^\sigma w'\,d\eta=0. \tag{3.8}$$

By differentiating equations (3.6) and (3.7) and eliminating p', we find after substitution that

$$\frac{d}{dx}\left(\frac{G}{\sigma^2}\right)+\frac{nF}{\sigma^2}=0, \tag{3.9}$$

and from equation (3.8)

$$\frac{d}{dx}(\sigma F)+n\sigma G=0. \tag{3.10}$$

Eliminating F from these equations gives

$$G''-\frac{\sigma'G'}{\sigma}-\left(n^2+\frac{2\sigma''}{\sigma}\right)G=0, \tag{3.11}$$

where primes denote differentiation with respect to x (cf. Pearson).

From equations (3.7) and (3.3) we find that

$$\frac{3}{\sigma_0^2}\left(1-\frac{\lambda}{\sigma_0}\right)-\frac{h^2T}{\mu U}\left(\frac{a'}{2a^2}+n^2\right)=\frac{2G_0}{n\sigma_0^2}, \tag{3.12}$$

where G_0 is the value of $G(l-a)$. If we write

$$\alpha=kT/\mu U \tag{3.13}$$

then k is defined by equation (2.31) and varies only very slowly with $T/\mu U$. Using equation (3.13) and the definition of σ_1 (equation (2.4)) to find a', equation (3.12) may be written

$$\frac{3}{\sigma_0^2}\left(1-\frac{\lambda}{\sigma_0}\right)-\left(\frac{\sigma_1-1}{2k}\right)^{\frac{1}{2}}\Big/\sigma_1^2\Theta-N\Theta^{-2}=\frac{2G_0}{n\sigma_0^2}, \tag{3.14}$$

where

$$\Theta=(\mu UR/Th)^{\frac{1}{2}},\quad N=Rhn^2, \tag{3.15}$$

and $\sigma_1 h$ and $\sigma_0 h$ are half the width of the channel at the focus and nose of the meniscus, respectively. It will be noted that Θ is the parameter whose value was found from experiment to be constant when conditions are critical.

The amount of liquid flowing in the x-direction due to the perturbation is

$$h\int_0^\sigma u'\,d\eta=-\tfrac{2}{3}Uh\sigma F\epsilon\cos nz. \tag{3.16}$$

If the system were in equilibrium, the change in λ corresponding to the changed position of the meniscus would be $\epsilon\cos nz\,d\lambda/dx$ so that the amount of liquid removed would be increased by an amount $Uh\epsilon\cos nz\,d\lambda/dx$. If the latter is less than the expression (3.16) we should expect the perturbation to be increased. Hence the condition for instability is

$$d\lambda/dx<-\tfrac{2}{3}\sigma F. \tag{3.17}$$

Replacing F in terms of G, the condition may be written

$$\frac{d\lambda}{dx}<-\frac{2\sigma}{3n}\left(G_0'-\frac{2\sigma'}{\sigma}G_0\right). \tag{3.18}$$

To obtain numerical results, we must solve equation (3.11), using the condition (3.14), and substitute for G_0 in the inequality (3.18). The value of $d\lambda/dx$ may be

derived from the graph shown in figure 5. The outline of this work is indicated in the Appendix. The final result is

$$4{\cdot}24(1+\beta)^4\frac{(\sigma_0-1)^{\frac{1}{2}}}{\sigma_1}\frac{d\lambda}{d\sigma_1} < \left[3\left(\frac{\sigma_1}{\sigma_0}\right)^2\left(1-\frac{\lambda}{\sigma_0}\right)-\left(\frac{\sigma_1-1}{2k}\right)^{\frac{1}{2}}\Theta^{-1}-\sigma_1^2\Theta^{-2}N\right]\left[\rho-\frac{3(\sigma_0-1)^{\frac{1}{2}}}{2^{\frac{1}{2}}\sigma_0}\right], \quad (3.19)$$

where

$$\rho^2 = N+3\left(\frac{1}{\sigma_0}-\frac{1}{2\sigma_0^2}\right). \quad (3.20)$$

For convenience in the discussion of the condition for instability we write (3.19) in the form

$$(A) < (B)\,(C).$$

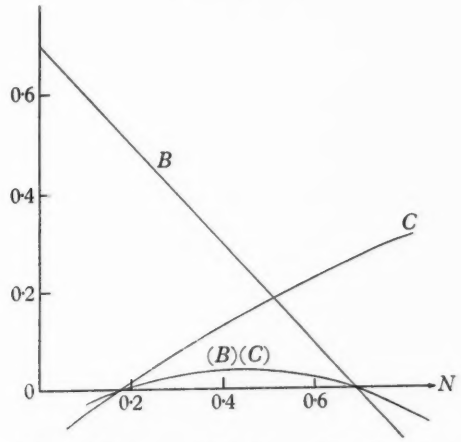

FIGURE 8. Values of the terms (B), (C), and $(B)\,(C)$ as functions of N.

3.3. *Comparison with experiment*

Numerical results are obtained from equation (3.19) in the following way. For a given value of Θ we may find the values of σ_1 and σ_0 and hence the value of (A). The value of (B) is a function which decreases linearly with increasing N, a measure of the ripple wave-number. The quantity (C) increases as N increases. In figure 8 values of (B), (C) and the product $(B)\,(C)$ are shown as functions of N, for the case $T/\mu U = 8$ and $h/R = 0{\cdot}004$. For given Θ as N varies there is a particular value of N which makes $(B)\,(C)$ a maximum. We must find the value of Θ such that the maximum value of the product just equals (A).

The results of these calculations are shown in figure 9, where curve M shows the maximum value of $(B)\,(C)$ and curve A the value of (A). For values of Θ less than 5·3 the maxima are all less than (A), i.e. conditions are always stable. For values of Θ greater than 5·3, conditions are unstable, i.e. for $(\mu UR/Th)$ greater than 28. The experimental value for this ratio is 62, which is known to be too high owing to difficulties in detecting the onset of ribbing (see next section).

The value of n at the critical point is 3·48, which means that the distance between ridges is 1·8 cm. Experimental observations showed that across the

5 in. roller there were approximately 17 crests, so that the observed distance was 0·75 cm.

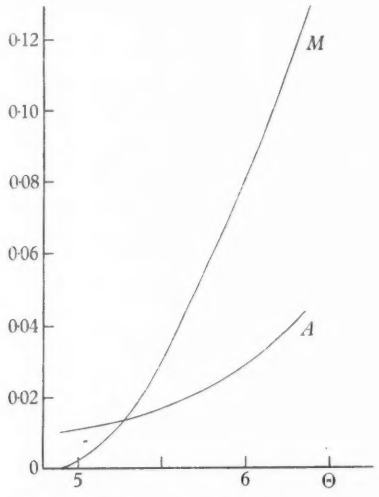

FIGURE 9. Theoretical determination of the critical value of Θ.

4. Discussion

The general agreement between theory and experiment for the even flow régime and also for the critical conditions at the transition shows that all the most important features have been satisfactorily explained. In view of the complexity of the problem and the approximations in the theoretical treatment the extent of the numerical agreement is also very satisfactory. A closer examination of the comparison between theory and experiment will show in more detail the extent of the agreement and what shortcomings still remain.

Reference to figure 3 shows that the theory is moderately successful in predicting the position of the meniscus, but the curvature of the theoretical line is not in complete agreement with the experimental points. In particular, in conditions in which the meniscus approaches most closely to the nip the theory is less satisfactory. Figure 5 shows that λ depends on the position of the meniscus and this result is in qualitative agreement with experiment, although as already explained the experiments were of only sufficient accuracy to enable a semi-quantitative comparison to be made. The dependence of α on $(T/\mu U)$ given by equation (2.31) is a result of great importance, which receives its confirmation in the theory of the critical conditions.

All these results have been obtained from a treatment that involves many approximations. It will be remembered that boundary conditions have only been satisfied at the meniscus, and even then only approximately and in a region close to the axis of symmetry. The fluid velocity at the surfaces of the rollers does not have the correct value. Nevertheless, in spite of these shortcomings, important results have been obtained which account for the main features

of the even flow régime, and are essential for the explanation of the transition to the ribbed flow pattern.

The explanation of the physical basis of the change in flow conditions given in §3.2 gives results which are qualitatively in complete agreement with the experiment. In this explanation the proportionality between α and $(T/\mu U)$ established by the theory of the even flow régime is of decisive importance. Without these results, the role played by the ratio $(\mu UR/Th)$ cannot be explained. The quantitative prediction of critical conditions is obviously a much more exacting requirement but here again the theory is fairly successful. In this case it must be remembered that experimental difficulties in recognizing reliably the first appearance of uneven flow are considerable. There is no doubt that, with more elaborate methods of viewing the surfaces of the liquid sheets over the rollers, it would have been possible to detect uneven flow for a value of $(\mu UR/Th)$ substantially lower than 62. A factor as large as 2 could possibly arise from this cause alone. Without any added refinements of viewing, it was always possible to observe uneven flow at speeds lower than those finally recorded in our experiments. In this region the unevenness was of such small amplitude that an observer could not consistently judge its true onset, but selected values of the speed varied by almost a factor of 2. A particular small amplitude was therefore adopted as a standard, the use of which made consistent results possible.

For this reason, the difference between Θ^2 from experiment (62) and from theory (28) is in the expected direction and is no doubt largely to be attributed to this experimental difficulty.

On the other hand it is likely that the theory is in error owing to several approximations. During the course of the numerical calculations it was obvious that comparatively small changes in certain terms could have a large effect on the value of the product (B) (C). The expression for $\partial p/\partial x$ near the meniscus is probably incorrect and the change in λ for the perturbed meniscus is derived from the variation of λ with position when conditions are in equilibrium. These may both be important sources of error.

With these facts in mind, it is perhaps unreasonable to expect closer numerical agreement. The successful explanation of all the qualitative experimental results and the approximate quantitative agreement between theory and experiment establishes the general adequacy of the treatment of the problem.

The authors would like to express their gratitude in particular to Mr A. Marriage, Mr E. W. H. Selwyn and Mr A. K. Soper of these laboratories, who, in preliminary discussion on this problem, helped to suggest possible physical explanations of the observed phenomena, one of which was developed to form the basis of the account in this paper. Their support has been most encouraging.

Next, the authors are indebted to Sir Geoffrey Taylor, who discussed the problem at length and made available unpublished work bearing on it. His criticism has been very helpful and stimulating.

Finally, Dr J. R. A. Pearson discussed his problem with us and kindly made available his publication while in draft form, for which we should like to express our acknowledgements.

This paper is Communication No. 2143 H from the Kodak Research Laboratories.

REFERENCES

BANKS, W. H. & MILL, C. C. 1954 *Proc. Roy. Soc.* A, **223**, 414.
HOPKINS, M. R. 1957 *Brit. J. Appl. Phys.* **8**, 442.
PEARSON, J. R. A. 1960 *J. Fluid Mech.* **7**, 481.

Appendix

We require an approximate solution of equation (3.11). Let us introduce the variable ξ defined by equation (2.1) and put

$$G = H\sigma^{\frac{1}{2}}. \tag{A. 1}$$

Then substitution in equation (3.11), together with the definition of σ from equation (2.4), gives

$$\frac{d^2H}{d\xi^2} = H\left[3\left(\frac{1}{\sigma}-\frac{1}{2\sigma^2}\right)+N\right], \tag{A. 2}$$

where N is defined in equation (3.15). An approximate solution of equation (A. 2) may be obtained by replacing the term in square brackets by its value at the nose of the meniscus. The result may then easily be improved by successive approximations.

We shall therefore consider

$$\frac{d^2H}{d\xi^2} = \rho^2 H, \tag{A. 3}$$

where

$$\rho^2 = N+3\left(\frac{1}{\sigma_0}-\frac{1}{2\sigma_0^2}\right), \tag{A. 4}$$

and measure ξ from the point where the meniscus cuts the axis of symmetry. The perturbation must vanish as the nip is approached, i.e. as ξ tends to $-\infty$, so the solution of equation (A. 3) may be written

$$H = Be^{\rho\xi}. \tag{A. 5}$$

The condition in equation (3.14) gives the values of B immediately, and substitution in equation (3.18) results in the inequality

$$\frac{d\lambda}{d\xi} < \frac{\sigma_0^3}{3\sigma_1^2}\left[3\left(\frac{\sigma_1}{\sigma_0}\right)^2\left(1-\frac{\lambda}{\sigma_0}\right)-\left(\frac{\sigma_1-1}{2k}\right)^{\frac{1}{2}}\Theta^{-1}-\sigma_1^2\Theta^{-2}N\right]\left[\rho-\frac{3(\sigma_0-1)^{\frac{1}{2}}}{2^{\frac{1}{2}}\sigma_0}\right]. \tag{A. 6}$$

Since by definition

$$\sigma_1 = (1+\beta)\,\sigma_0, \tag{A. 7}$$

then

$$\frac{d\lambda}{d\xi} = 2^{\frac{1}{2}}(1+\beta)\,(\sigma_0-1)^{\frac{1}{2}}\frac{d\lambda}{d\sigma_1}, \tag{A. 8}$$

and the condition for instability may be written

$$4\cdot24(1+\beta)^4\frac{(\sigma_0-1)^{\frac{1}{2}}}{\sigma_1}\frac{d\lambda}{d\sigma_1} < \left[3\left(\frac{\sigma_1}{\sigma_0}\right)^2\left(1-\frac{\lambda}{\sigma_0}\right)-\left(\frac{\sigma_1-1}{2k}\right)^{\frac{1}{2}}\Theta^{-1}-\sigma_1^2\Theta^{-2}N\right]\left[\rho-\frac{3(\sigma_0-1)^{\frac{1}{2}}}{2^{\frac{1}{2}}\sigma_0}\right]. \tag{A. 9}$$

By developing the right-hand side of equation (A. 2) as a power series in ξ further approximations may readily be derived. We shall omit them here, since their effect on the expression (A. 6) is quite small, and moreover equation (A. 2) in any case is only valid in the immediate vicinity of the perturbed meniscus, so that extra terms are of very doubtful significance.

Stewartson's compressibility correlation in three dimensions

By J. C. COOKE
Royal Aircraft Establishment, Farnborough

(Received 16 January 1961)

On the assumption of (*a*) zero heat transfer, (*b*) unit Prandtl number, (*c*) linear viscosity temperature relation, and (*d*) small cross-flow, a correlation between a compressible laminar boundary-layer flow and an incompressible flow with different external conditions is established.

The correlation is applied to a known approximate method of solution for incompressible flow. For flow over a slender wing it is found that, so far as the effect on limiting streamlines—and hence on separation—is concerned, the fluid behaves as though it were incompressible but with pressure gradients multiplied by $1+\frac{1}{2}(\gamma-1)M_0^2$ approximately, where M_0 is the Mach number, supposed to be moderate in value. The effect on drag is also estimated.

An attempt is made to assess the effect of variable Prandtl number Pr, and it is found that the above multiplying factor must be replaced by

$$1+\tfrac{1}{2}Pr^{\frac{1}{2}}(\gamma-1)M_0^2,$$

but that variations in Prandtl number have little effect on the previous estimate of drag.

1. Introduction

Stewartson (1949) showed that if it is assumed in two-dimensional flow that (*a*) the surface is thermally insulating, (*b*) viscosity varies as the absolute temperature, and (*c*) the Prandtl number is unity, it is possible to transform the co-ordinates so that the boundary-layer equations for a compressible fluid with a given main-stream velocity become identical with those for an incompressible fluid with a different main-stream velocity. The particular transformation used by Stewartson was also used by Illingworth (1949), and is closely allied to one due to Howarth (1948).

In general three-dimensional flow it does not seem possible to find a transformation to correlate compressible and incompressible boundary layers in this way. However, there is one case which is amenable, namely the case of small cross-flow which has been fairly extensively studied for incompressible fluids. Here it is assumed that the velocity in the boundary layer normal to the external streamlines and certain of its derivatives are small. A general discussion of this case was given by Cooke (1959*a*) who derived the equations of motion in a 'streamline' co-ordinate system in which the co-ordinate curves were the

projections on to the surface of the external streamlines and their orthogonal trajectories in the surface.

We show in this paper that the same transformation, simply extended, will correlate the compressible boundary layer associated with a given external flow with an incompressible boundary layer associated with a different external flow, in the case where Stewartson's conditions (*a*), (*b*) and (*c*) hold, together with the small cross-flow condition. In the present state of knowledge the latter restriction does not trouble us unduly, since it is found in most approximate methods for incompressible flow.

The correlation having been established, a study is made of the flow over a conically cambered delta wing for which an incompressible-flow calculation has already been made. The effect is best seen by examining the angle β between streamlines and limiting streamlines as shown in figure 1. This angle is considerably increased by compressibility, and this leads to an earlier separation. It will be found that a useful guide to the effect on β is to assume the flow to be the same as it would be with incompressible fluid, but with all pressure gradients multiplied by $1+\frac{1}{2}(\gamma-1)M_0^2$, where M_0 is the Mach number. In the case studied, M_0 is equal to 2 and γ equal to 1·4, so that this multiplier is equal to 1·8.

An approximate allowance can be made for a Prandtl number Pr not equal to unity. A modified transformation, due to Rott (1953), is used. This causes minor modifications all through; in particular it is found that the factor mentioned above is changed to $1+\frac{1}{2}Pr^{\frac{1}{2}}(\gamma-1)M_0^2$ approximately, so that the multiplier 1·8 is reduced to 1·68 when M_0 is equal to 2. The other effects of the change in Prandtl number are very small for moderate Mach numbers.

2. The equations of motion

Taking streamline co-ordinates, we may define the length element dl by the relation

$$dl^2 = h_1^2 d\xi^2 + h_2^2 d\eta^2 + d\zeta^2, \tag{1}$$

where ζ is distance normal to the surface, while the curves $\eta = \text{const.}$, $\zeta = 0$ are the projections of the external streamlines on to the surface, and $\xi = \text{const.}$, $\zeta = 0$ are their orthogonal trajectories. As usual, h_1 and h_2 are taken to be independent of ζ. u, v and w are velocity components in the co-ordinate directions.

Cooke (1959*a*) wrote $h_2 = r$ and let ds be the length element along the curve $\eta = \text{const.}$, $\zeta = 0$; that is $ds = h_1 d\xi$. Assuming small cross-flow, Cooke obtained equations of motion which, when the thermal conductivity k was replaced by $c_p\mu$ (for unit Prandtl number), became

$$\rho\left(u\frac{\partial u}{\partial s} + w\frac{\partial u}{\partial \zeta}\right) = \rho_e u_e \frac{\partial u_e}{\partial s} + \frac{\partial}{\partial \zeta}\left(\mu\frac{\partial u}{\partial \zeta}\right), \tag{2}$$

$$\rho\left(u\frac{\partial v}{\partial s} + w\frac{\partial v}{\partial \zeta} + \frac{uv}{r}\frac{\partial r}{\partial s}\right) = \kappa(\rho_e u_e^2 - \rho u^2) + \frac{\partial}{\partial \zeta}\left(\mu\frac{\partial v}{\partial \zeta}\right), \tag{3}$$

$$\rho c_p\left(u\frac{\partial T}{\partial s} + w\frac{\partial T}{\partial \zeta}\right) = -\rho_e u u_e \frac{\partial u_e}{\partial s} + \frac{\partial}{\partial \zeta}\left(c_p\mu\frac{\partial T}{\partial \zeta}\right) + \mu\left(\frac{\partial u}{\partial \zeta}\right)^2, \tag{4}$$

$$\frac{\partial}{\partial s}(\rho r u) + \frac{\partial}{\partial \zeta}(\rho r w) = 0, \tag{5}$$

where $$\kappa = -\frac{1}{h_1 r}\frac{\partial h_1}{\partial \eta}.$$

We take the suffix e to denote values just outside the boundary layer, and the suffix 0 to denote values at some isentropic reference position.

Stewartson (1949) used the relation

$$\mu/\mu_0 = T/T_0;$$

but, following Chapman & Rubesin (1949), we may replace this by

$$\mu/\mu_0 = C(T/T_0). \tag{6}$$

In the special case of zero heat transfer and unit Prandtl number, a solution (Moore, 1951) of the energy equation is Crocco's temperature relation

$$\frac{T}{T_e} = 1 + \frac{\gamma-1}{2a_e^2}(u_e^2 - u^2 - v^2), \tag{7}$$

where a_e is the velocity of sound just outside the boundary layer. As v is small, we may neglect v^2 in equation (7).

3. The transformation

Modifying Stewartson's transformation slightly, we write

$$Z = \frac{a_e}{a_0}\int_0^\zeta \frac{\rho}{\rho_0}\,d\zeta, \tag{8}$$

$$S = C\int^s \left(\frac{a_e}{a_0}\right)^{(3\gamma-1)/(\gamma-1)} ds. \tag{9}$$

We write also

$$U_e = a_0 u_e/a_e, \tag{10}$$

$$V = v, \tag{11}$$

$$K = \frac{\kappa}{C}\left(\frac{a_0}{a_e}\right)^{(4\gamma-1)/(\gamma-1)} q, \tag{12}$$

$$q = 1 + \tfrac{1}{2}(\gamma-1)M_0^2. \tag{13}$$

We omit the details of the analysis, which are given in the Appendix. It is shown there that equations (2) and (3) become

$$U\frac{\partial U}{\partial S} + W\frac{\partial U}{\partial Z} = U_e\frac{\partial U_e}{\partial S} + \nu_0\frac{\partial^2 U}{\partial Z^2}, \tag{14}$$

$$U\frac{\partial V}{\partial S} + W\frac{\partial V}{\partial Z} + \frac{UV}{r}\frac{\partial r}{\partial S} = K(U_e^2 - U^2) + \nu_0\frac{\partial^2 V}{\partial Z^2}, \tag{15}$$

where W satisfies

$$\frac{\partial}{\partial S}(rU) + \frac{\partial}{\partial Z}(rW) = 0. \tag{16}$$

These equations are the same in form as equations (2), (3) and (5), with ρ and μ constant and $\nu_0 = \mu/\rho$. The boundary conditions $u = v = w = 0$ when $\zeta = 0$, and $u = u_e$, $v = 0$ when $\zeta = \infty$ become $U = V = W = 0$ when $Z = 0$ and $U = U_e$, $V = 0$ when $Z = \infty$.

Thus we have reduced the compressible equations with small cross-flow to incompressible equations with small cross-flow, and there is a complete correlation. Note that, although the co-ordinates are changed, r is not changed.

4. Arbitrary surface temperature

Stewartson (1949) extended the use of his transformation to the case where the boundary condition on the surface is arbitrary. This does not yield a correlation, but the transformation greatly simplifies the equations. We include this case for completeness.

Stewartson wrote

$$\frac{T}{T_e} = \left\{1 + \frac{\gamma - 1}{2a_e^2}(u_e^2 - u^2)\right\} + \frac{T_0}{T_e}\{1 + \tfrac{1}{2}(\gamma - 1)M_{0\infty}^2\}A, \tag{17}$$

where A is the temperature function. Note that we must have $A = 0$ when $\zeta = \infty$; when $\zeta = 0$, A is determined by the specified surface temperature T_w. Exactly as in Stewartson's paper, this leads to

$$U\frac{\partial U}{\partial S} + \tilde{W}\frac{\partial U}{\partial Z} = U_e\frac{\partial U_e}{\partial S}(1 + A) + \nu_0\frac{\partial^2 U}{\partial Z^2},$$

in place of equation (14).

Now, equation (17) may be written

$$\frac{T}{T_e} = B + \frac{T_0}{T_e}qA,$$

where B satisfies the energy equation (4), as is clear from equation (7) with v^2 neglected. It is now quite straightforward to show that A satisfies the equation

$$U\frac{\partial A}{\partial S} + W\frac{\partial A}{\partial Z} = \nu_0\frac{\partial^2 A}{\partial Z^2}, \tag{18}$$

with boundary conditions $A = 0$ when $Z = \infty$ and A given by the specified surface temperature when $Z = 0$.

Finally, equation (15) is changed to

$$U\frac{\partial V}{\partial S} + W\frac{\partial V}{\partial Z} + \frac{UV}{r}\frac{\partial r}{\partial S} = K\{U_e^2(1 + A) - U^2\} + \nu_0\frac{\partial^2 V}{\partial Z^2}.$$

5. Application of incompressible approximate methods

We now apply the transformation procedure to the methods of Zaat (1956, 1957) and Cooke (1959*b*). In these the length element is defined by

$$dl^2 = \frac{d\phi^2}{u_e^2} + \frac{d\psi^2}{\bar{\rho}u_e^2},$$

and this we will now suppose to be transformed into

$$dL^2 = \frac{d\Phi^2}{U_e^2} + \frac{d\Psi^2}{\bar{P}U_e^2}.$$

Since r is unchanged in the transformation, we have

$$\frac{1}{\bar{\rho}u_e^2} = r^2 = \frac{1}{\bar{P}U_e^2},$$

and so

$$\bar{P} = \bar{\rho}(a_e^2/a_0^2). \tag{19}$$

We also note that

$$\kappa = \rho^{\frac{1}{2}}\,\partial u_e/\partial\psi.$$

The streamwise length element is transformed by equation (9). Hence, when ψ or Ψ are constant, we have

$$\frac{d\Phi}{U_e} = C\left(\frac{a_e}{a_0}\right)^{(3\gamma-1)/(\gamma-1)}\frac{d\phi}{u_e}$$

or, by equation (10),

$$d\Phi = C\left(\frac{a_e}{a_0}\right)^{2\gamma/(\gamma-1)} d\phi. \tag{20}$$

The transformation of κ in equation (12) is used to find how ψ is transformed. It leads to

$$d\Psi = C\left(\frac{a_e}{a_0}\right)^{2\gamma/(\gamma-1)} d\psi, \tag{21}$$

when ϕ or Φ are constant. To verify this, we have, noting that $U_e(\partial U_e/\partial\Psi)$ is given by equation (A 5) with $\bar{S}$ replaced by Ψ,

$$\begin{aligned} K &= \bar{P}^{\frac{1}{2}}\frac{\partial U_e}{\partial\Psi} = \frac{\bar{\rho}^{\frac{1}{2}}}{C}\left(\frac{a_0}{a_e}\right)^{(4\gamma-2)/(\gamma-1)}\frac{\partial u_e}{\partial\psi}q \\ &= \frac{\kappa}{C}\left(\frac{a_0}{a_e}\right)^{(4\gamma-2)/(\gamma-1)} q. \end{aligned}$$

This, by equation (12), is the right form for K, and thus the relation (21) is verified.

We may therefore follow Zaat's or Cooke's methods using the new variables according to the above rules. We shall only go into details in connexion with the latter method. It is, however, just as easy to apply the transformation to Zaat's method.

In the transformed (incompressible) flow, we shall denote all variables by capital letters, and shall call them 'transformed variables', as distinct from 'true variables' in the compressible flow, which are denoted in general by the corresponding small letters.

Cooke's equations in transformed variables are

$$\frac{\partial}{\partial\Phi}\left(\frac{U_e^4\Sigma}{\bar{P}}\right) = 5{\cdot}08\,\frac{U_e^2}{\bar{P}}, \tag{22}$$

$$\bar{P}\Sigma^{\frac{1}{2}}\frac{\partial}{\partial\Phi}\left(\frac{\Sigma^{\frac{1}{2}}\Theta_{21}}{\bar{P}}\right) = \frac{1}{U_e^2}\{\Pi^* + M^*(0{\cdot}067\Lambda^* - 0{\cdot}669)\}, \tag{23}$$

where

$$\Theta_{21} = -(0{\cdot}295 + 0{\cdot}022\Lambda^*)\,\Pi^* - (0{\cdot}030 + 0{\cdot}004\Lambda^*)\,M^*, \tag{24}$$

$$\Lambda^* = \Sigma U_e(\partial U_e/\partial\Phi), \tag{25}$$

$$M^* = \bar{P}^{\frac{1}{2}}\Sigma U_e(\partial U_e/\partial\Psi). \tag{26}$$

In these equations, Π^* is a boundary-layer velocity-profile parameter, Σ is a variable proportional to the square of the boundary-layer thickness, Λ^* and M^* are proportional to the streamwise and crosswise pressure gradients, and Θ_{21} is a mixed 'momentum thickness'. [In Cooke (1959*b*) what we would here denote by λ^*, μ^*, π^* were written Λ, M and Π, and Θ_{21} had a different meaning. Nevertheless, the capital-letter notation is so convenient that we shall continue to use it. This should cause no confusion in practice.]

Introducing true variables (except for Σ) and putting $\gamma = 1{\cdot}4$, we find by equations (10), (19) and (20) that equation (22) becomes

$$\frac{\partial}{\partial\phi}\left\{\left(\frac{a_0}{a_e}\right)^6 \frac{u_e^4}{\overline{\rho}}\left(\frac{\Sigma}{C}\right)\right\} = 5{\cdot}08\left(\frac{a_e}{a_0}\right)^3 \frac{u_e^2}{\overline{\rho}}, \tag{27}$$

which thus determines Σ/C as a function of the true co-ordinates.

Equations (25) and (26) become, using equations (10), (19), (20) and (21) and putting $\gamma = 1{\cdot}4$,

$$\Lambda^* = \left(\frac{\Sigma}{C}\right)\left(\frac{a_0}{a_e}\right)^{11} u_e \frac{\partial u_e}{\partial\phi} q, \tag{28}$$

$$M^* = \overline{\rho}^{\frac{1}{2}}\left(\frac{\Sigma}{C}\right)\left(\frac{a_0}{a_e}\right)^{10} u_e \frac{\partial u_e}{\partial\psi} q. \tag{29}$$

Thus, Λ^* and M^* are determined as functions of the true co-ordinates, since Σ/C is known by equation (27).

Equation (23) may be written

$$\overline{\rho}\left(\frac{\Sigma}{C}\right)^{\frac{1}{2}}\left(\frac{a_0}{a_e}\right)^7 \frac{\partial}{\partial\phi}\left\{\frac{(\Sigma/C)^{\frac{1}{2}}\Theta_{21}}{\overline{\rho}}\frac{a_0^2}{a_e^2}\right\} = \frac{1}{u_e^2}\{\Pi^* + M^*(0{\cdot}067\Lambda^* - 0{\cdot}669)\}; \tag{30}$$

and hence, with the aid of equation (24), Π^* and Θ_{21} can be found as functions of the true co-ordinates. The method of solution is exactly the same as that outlined by Cooke (1959*b*).

For the skin friction we have

$$\tau_{01} = \mu_w\left(\frac{\partial u}{\partial\zeta}\right)_0;$$

hence, using the relations

$$T_w/T_e = \rho_e/\rho_w, \quad u/u_e = U/U_e,$$

and the isentropic relations

$$\rho_e/\rho_0 = (a_e/a_0)^5, \quad T_e/T_0 = (a_e/a_0)^2,$$

we obtain, following Cooke (1959*b*),

$$\tau_{01} = C\mu_0 \frac{u_e}{(\Sigma\nu_0)^{\frac{1}{2}}}\left(\frac{a_e}{a_0}\right)^8 \frac{2}{3\pi^{\frac{1}{2}}}(2+\Lambda^*). \tag{31}$$

We find in a similar way

$$\tau_{02} = C\mu_0 \frac{u_e}{(\Sigma\nu_0)^{\frac{1}{2}}}\left(\frac{a_e}{a_0}\right)^7 \frac{2}{3\pi^{\frac{1}{2}}}\left(\frac{3\pi^{\frac{1}{2}}}{2}\Pi^* + M^*\right). \tag{32}$$

If β is the angle between streamlines and limiting streamlines, we have

$$\tan\beta = \frac{\tau_{02}}{\tau_{01}} = \frac{(3\pi^{\frac{1}{2}}/2)\,\Pi^* + M^*}{2+\Lambda^*}\left(\frac{a_0}{a_e}\right). \tag{33}$$

6. Effect of arbitrary Prandtl number

Rott (1953) has suggested that, if the Prandtl number Pr is not unity, equation (7) may be replaced by

$$\frac{T}{T_e} = 1 + \bar{r}\left(\frac{\gamma-1}{2a_e^2}\right)(u_e^2 - u^2 - v^2), \tag{34}$$

where $\bar{r}$ is the recovery factor, which is a function of Prandtl number only. For values of σ not too far from unity, the approximate value $\bar{r} = Pr^{\frac{1}{2}}$ is usually taken.

Equation (34) is exact for $Pr = 1$. When $Pr \neq 1$, it still satisfies the boundary conditions at the wall and at the edge of the boundary layer. Consequently, equation (34) is probably a reasonable approximate solution of the energy equation (4).

Rott (1953) pointed out that in two dimensions a correlation can still be found by modifying Stewartson's transformation. In the present notation the new transformation is

$$Z = \left(\frac{a_e}{a_0}\right)^{\bar{r}} \int_0^{\xi} \frac{\rho}{\rho_0}\, d\xi,$$

$$S = C\int^{s} \left(\frac{a_e}{a_0}\right)^{2\gamma/(\gamma-1)+\bar{r}} ds,$$

$$U_e = (a_0/a_e)^{\bar{r}}\, u_e.$$

This reduces to the earlier transformation when $\bar{r} = 1$.

It is quite easy to show that the correlation in the V equation will still hold if, in addition to the above changes, equation (12) and (13) are replaced by

$$K = \frac{\kappa}{C}\left(\frac{a_0}{a_e}\right)^{(4\gamma-1)/(\gamma-1)} Q,$$

$$Q = 1 + \tfrac{1}{2}\bar{r}(\gamma-1)\, M_0^2 + (1-\bar{r})\{(a_e/a_0)^2 - 1\}. \tag{35}$$

This causes minor modifications to the approximate equations of § 5. These are given in table 1. We omit the details of the calculations.

7. An example and discussion

We consider the flow past the upper surface of a thin conically cambered delta wing with attached flow at the leading edges, as described by Brebner (1957). This wing (see figure 1) is flat inboard of the shoulders, which are straight lines through the apex, their equations in the notation of figure 1 being $y/Kx = \pm 0{\cdot}6$. They are shown dotted in the figure. Outboard of the shoulders the wing is drooped in such a way as to make the downwash distribution parabolic. The design lift coefficient chosen is 0·1; this will be achieved at a certain angle of incidence which will give attached flow along the leading edges. The fact that the calculated separation line is $y/Kx = 0{\cdot}63$ shows that the flow is unable to go right round the shoulder; hence, unless the flow quickly re-attaches after separating, the boundary-layer solution and the external flow cannot match, since the external velocity components used in the solution were calculated on the basis

of unseparated flow. Nevertheless, the example will illustrate the method (even though the external flow used is not that over the wing specified) and will show the general effect of compressibility.

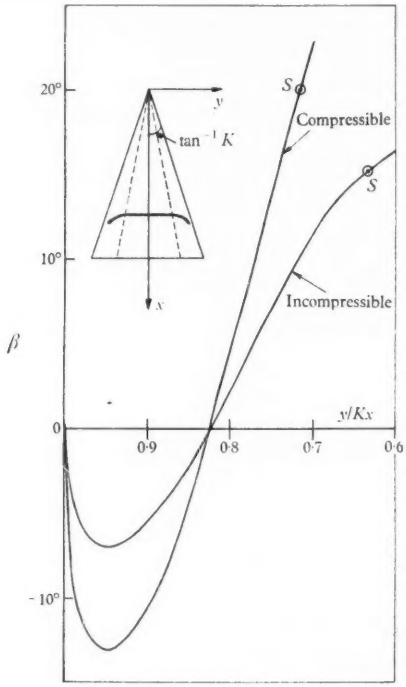

FIGURE 1. Angle between streamlines and limiting streamlines. Mach 2. ⊙ *S*, points of separation.

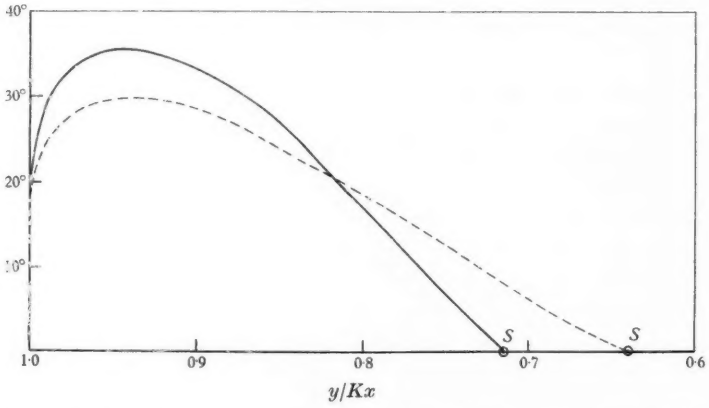

FIGURE 2. Angle between limiting streamlines and rays. ——, Compressible; – – – –, incompressible; ⊙ *S*, points of separation.

The boundary layer over this wing was the subject of an incompressible-flow calculation by Cooke (1959*b*). This has now been recalculated, using the same external flow but with $M_0 = 2$, the suffix 0 referring to conditions at infinity. The flow is conical, so that calculations along one streamline are sufficient to determine the flow over the whole wing as far as the separation line.

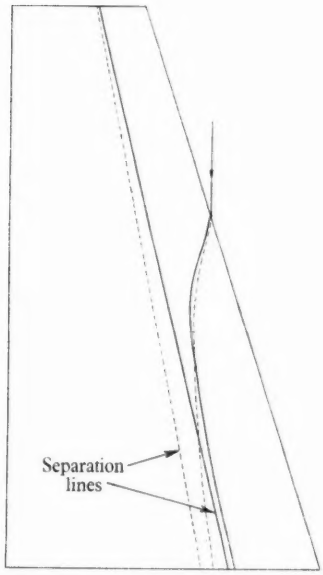

FIGURE 3. Limiting streamlines and separation lines. ——, Compressible; – – – –, incompressible.

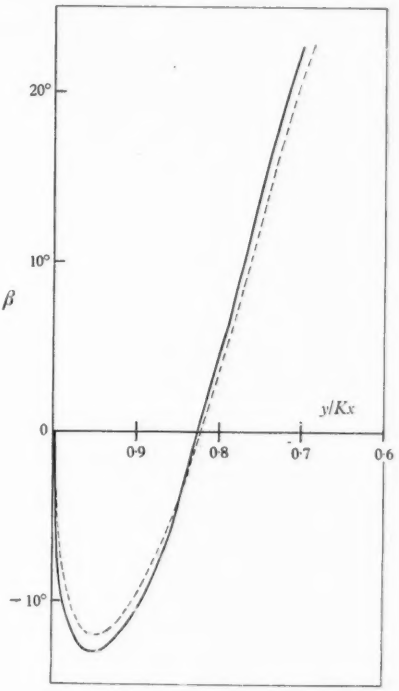

FIGURE 4. Angle between streamlines and limiting streamlines. ——, Full; – – – –, simplified.

The effect of compressibility is best seen by plotting the angle β between streamlines and limiting streamlines, as in figure 1. The effect is clearly seen to be an increase in this angle at all positions. Figure 2 shows the angle between limiting streamlines and rays. Separation takes place when this angle vanishes. It is earlier than in the incompressible case. In figure 3 an attempt is made to draw part of a limiting streamline and a separation line for the two cases.

It we are dealing with moderate Mach numbers, such as $M_0 = 2$, the ratio a_0/a_e is not far from unity. If it were constantly equal to unity, then Σ/C, obtained from equation (27), would have the same value as σ calculated on the assumption of incompressibility. Λ^* and M^* would then take their incompressible values multiplied by q, as can be seen from equations (28) and (29). Moreover, if we could assume $a_0/a_e = 1$ and Λ^* not too large, we should find from equations (23) and (24) that Π^* would also take its incompressible value multiplied by q.

Figures 4 and 5 shows curves for the compressible case marked 'full' and 'simplified'. The former are obtained by the full use of equations (27), (30), (31), (32) and (33). The latter are obtained from incompressible calculations followed by the multiplication of Λ^*, M^* and Π^* by $q\{= 1+\frac{1}{2}(\gamma-1)M_0^2\}$ and then by the use of equations (31), (32) and (33). It will be seen that the simplified method gives results of fair accuracy. Moreover, the simplified method shows that, as far as limiting streamline direction is concerned, compressible flow is like incompressible flow with pressure gradients multiplied by $1+\frac{1}{2}(\gamma-1)M_0^2$, at any rate for moderate Mach numbers. This effect is large; for example the pressure gradients would be doubled for $M_0 = \sqrt{5}$.

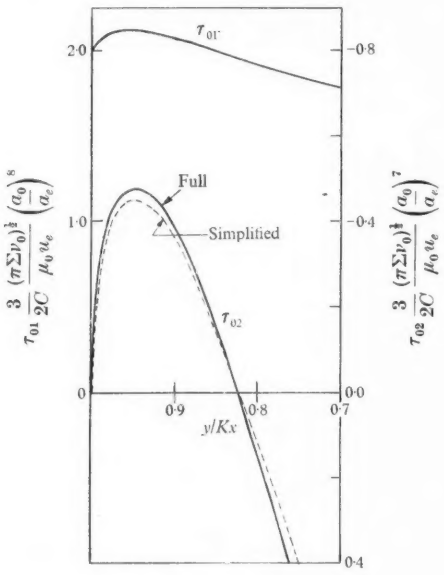

FIGURE 5

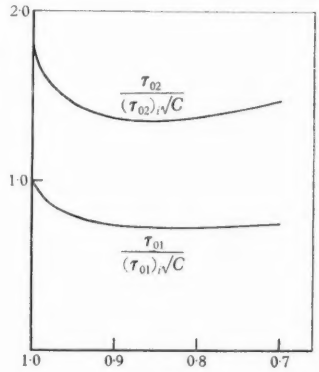

FIGURE 6

FIGURE 5. Values of streamwise and crosswise skin friction, τ_{01} and τ_{02}. Compressible, upper surface. ——, Full; – – –, simplified. (In the curve for τ_{01}, the results for the full and simplified methods are indistinguishable.)

FIGURE 6. Ratios of compressible to incompressible skin friction components. Upper surface.

The effect of compressibility on drag comes mainly from the term $(a_e/a_0)^8$ in equation (31), while the factor q multiplying the pressure gradient has only a small effect. Figure 6 shows that the streamwise shear stress τ_{01} is reduced, and that in this example one would expect the over-all drag of the upper surface of the wing to be about three-quarters of the incompressible value. The drag will, however, be increased over the lower surface. The crosswise shear stress τ_{02} on the upper surface is increased to nearly 1·5 times the incompressible value; this figure will be more than 2 over much of the lower surface.

The values just given are for $C = 1$ and $Pr = 1$. For an aeroplane flying in the stratosphere at Mach 2 with zero heat transfer, the value of C is about 0·89; on the other hand, C may have a value a little greater than unity under conditions experienced in a supersonic wind tunnel (Chapman & Rubesin 1949). These values will not affect the general nature of our conclusions.

Equation	Replace		by
(20)	—	Unchanged	—
(21)	—	Unchanged	—
(27)	Index 6	—	$6\bar{r}$
	Index 3	—	$7-4\bar{r}$
(28)	Index 11	—	$9+2\bar{r}$
	q	—	Q
(29)	Index 10	—	$9+\bar{r}$
	q	—	Q
(30)	a_0^2/a_e^2	—	$(a_0/a_e)^{2\bar{r}}$
(31)	Index 8	—	$7+\bar{r}$
(32)	—	Unchanged	—
(33)	a_0/a_e	—	$(a_0/a_e)^{\bar{r}}$

TABLE 1. Effect of non-unit Prandtl number

The effect of Prandtl number may be roughly assessed by consideration of the alterations made in § 6. We take $Pr = 0{\cdot}72$ and so $\bar{r} = 0{\cdot}85$. We have already seen that at moderate Mach numbers the ratio a_e/a_0 is near to unity; indeed, figures 4 and 5 show that the effect of putting this ratio equal to unity is very small. Hence the small changes in the powers to which a_e/a_0 is raised, as listed in table 1, will have little effect, and the main change will come from the change in q.

Since $\bar{r} = 0{\cdot}85$ and a_e/a_0 is near to 1, the last term in equation (35) is small, but the alteration in the second term may be significant. Thus, at $M_0 = 2$, q will change from 1·80 to 1·68, so that the apparent increase in pressure gradient due to compressibility is not quite so large as appeared for $Pr = 1$, and the risk of separation is reduced a little.

It also follows from § 6 that the change in Prandtl number has little effect on τ_{01} and so on the over-all drag, but that the crosswise skin friction τ_{02} and the angle β are not as large as had previously been estimated.

8. Conclusions

It is possible in the case of small cross-flow, unit Prandtl number and zero heat transfer to correlate a compressible three-dimensional laminar boundary layer with an incompressible three-dimensional laminar boundary layer. This makes it possible to make use of the approximate methods which have been developed for incompressible flow with small cross-flow.

The general effect of compressibility at moderate Mach numbers on the directions of the limiting streamlines and so on separation is approximately the same as if the pressure gradients had been multiplied by $1+\frac{1}{2}(\gamma-1)M_0^2$. Alternatively we may say that if in an incompressible flow the pressure gradients must be less than a certain figure in order to avoid separation, this figure must be

divided by $1+\frac{1}{2}(\gamma-1)M_0^2$ in order to avoid separation in compressible flow. Since for $M_0 = 2$ this factor is equal to 1·80, it can be seen that the effect may be severe.

Compressibility causes a reduced drag on the upper surface of a wing of the type considered here, but an increased drag on the lower surface. The crosswise skin friction is in general increased on both surfaces of the wing.

The limitation to unit Prandtl number has only a small effect on the drag, but it changes the factor $1+\frac{1}{2}(\gamma-1)M_0^2$ given above to $1+\frac{1}{2}Pr^{\frac{1}{2}}(\gamma-1)M_0^2$, and this minimizes the severity of the apparent increase in pressure gradients due to compressibility. For instance, it reduces the factor 1·80 above to 1·68.

Appendix

Details of the transformation

Equation (5) shows that there exists a stream function ψ such that

$$r\rho u = \rho_0 \frac{\partial\psi}{\partial\zeta}, \quad r\rho w = -\rho_0 \frac{\partial\psi}{\partial s}.$$

We first make the transformation

$$Z = \frac{a_e}{a_0}\int_0^\zeta \frac{\rho}{\rho_0}\,d\zeta, \quad \bar{S} = s,$$

the notation $\bar{S}$ being introduced to avoid confusion. $\psi(s,\zeta)$ transforms into $\psi(\bar{S},Z)$, and we note that $\partial\psi/\partial s$ is *not* the same as $\partial\psi/\partial\bar{S}$.

We have
$$u = \frac{a_e}{a_0 r}\frac{\partial\psi}{\partial Z}, \quad w = -\frac{\rho_0}{\rho r}\left(\frac{\partial\psi}{\partial\bar{S}} + \frac{\partial\psi}{\partial Z}\frac{\partial Z}{\partial s}\right). \tag{A 1}$$

Denoting $\partial\psi/\partial Z$ by ψ_Z, etc., we have

$$\frac{\partial u}{\partial s} = \frac{1}{a_0 r}\psi_Z\frac{\partial a_e}{\partial\bar{S}} + \frac{a_e}{a_0 r}\psi_{Z\bar{S}} + \frac{a_e}{a_0 r}\frac{\partial Z}{\partial s}\psi_{ZZ} - \frac{a_e}{a_0 r^2}\frac{\partial r}{\partial\bar{S}}\psi_Z,$$

$$\frac{\partial u}{\partial\zeta} = \frac{a_e^2\rho}{a_0^2\rho_0 r}\psi_{ZZ}.$$

We also have
$$\mu\frac{\partial u}{\partial\zeta} = C\frac{\mu_0}{r}\frac{T}{T_0}\frac{a_e^2\rho}{a_0^2\rho_0}\psi_{ZZ} = \frac{Cpa_e^2\mu_0}{p_0 a_0^2 r}\psi_{ZZ},$$

using the relation (6) and the equation $p = R\rho T$.

Hence, assuming as usual that p is independent of ζ or Z, we obtain

$$\frac{\partial}{\partial\zeta}\left(\mu\frac{\partial\mu}{\partial\zeta}\right) = \frac{Cp}{p_0}\frac{a_e^3}{a_0^3}\frac{\mu_0\rho}{\rho_0 r}\psi_{ZZZ} = \nu_0\frac{Cp}{p_0}\frac{a_e^3\rho}{a_0^3 r}\psi_{ZZZ}.$$

In the external isentropic flow, we also have Bernoulli's equation

$$a_e^2 + \tfrac{1}{2}(\gamma-1)u_e^2 = \text{const.} = a_0^2 + \tfrac{1}{2}(\gamma-1)u_0^2, \tag{A 2}$$

since $v_e = 0$ in the main stream.

Hence
$$a_e\frac{\partial a_e}{\partial\bar{S}} = -\tfrac{1}{2}(\gamma-1)u_e\frac{\partial u_e}{\partial\bar{S}}. \tag{A 3}$$

Since the pressure in the boundary layer is constant at a given station, we have

$$\frac{\rho_e}{\rho} = \frac{T}{T_e} = 1 + \frac{\gamma-1}{2a_e^2}(u_e^2 - u^2)$$

by equation (7), neglecting v^2.

Substituting in the equation of motion (2), we obtain

$$\frac{1}{r^2}\left\{\psi_Z \psi_{Z\bar{S}} - \frac{1}{r}\frac{\partial r}{\partial \bar{S}}\psi_Z^2 - \psi_{\bar{S}}\psi_{ZZ}\right\} = \frac{a_0^2}{a_e^2}u_e\frac{\partial u_e}{\partial \bar{S}}\left\{1 + \frac{\gamma-1}{2a_e^2}u_e^2\right\} + \frac{\nu_0 a_e}{a_0 r}\frac{Cp}{p_0}\psi_{ZZZ}. \quad \text{(A 4)}$$

If we use equations (10) and (A 3), we find

$$U_e\frac{\partial U_e}{\partial \bar{S}} = \frac{a_0^2}{a_e^2}u_e\frac{\partial u_e}{\partial \bar{S}}\left\{1 + \frac{\gamma-1}{2a_e^2}u_e^2\right\}. \quad \text{(A 5)}$$

Further, if we note that $$\frac{p}{p_0} = \left(\frac{a_e}{a_0}\right)^{2\gamma/(\gamma-1)},$$

and write $$S = C\int\left(\frac{a_e}{a_0}\right)^{(3\gamma-1)/(\gamma-1)} d\bar{S},$$

and also use (A 5), we find that equation (A 4) becomes

$$\frac{1}{r^2}\left\{\psi_Z\psi_{ZS} - \frac{1}{r}\frac{\partial r}{\partial S}\psi_Z^2 - \psi_S\psi_{ZZ}\right\} = U_e\frac{\partial U_e}{\partial S} + \frac{\nu_0}{r}\psi_{ZZZ}.$$

Finally, we write in this equation

$$U = \frac{1}{r}\psi_Z, \quad W = -\frac{1}{r}\psi_S, \quad \text{(A 6)}$$

thus satisfying an equation of the same form as (5) with constant ρ. We obtain

$$U\frac{\partial U}{\partial S} + W\frac{\partial U}{\partial Z} = U_e\frac{\partial U_e}{\partial S} + \nu_0\frac{\partial^2 U}{\partial Z^2}. \quad \text{(A 7)}$$

The above procedure is almost identical with that of Stewartson (1949).

We now substitute in equation (3), writing

$$V = v,$$

$$q = 1 + \tfrac{1}{2}(\gamma-1)M_0^2 = \frac{1}{a_0^2}\{a_0^2 + \tfrac{1}{2}(\gamma-1)u_0^2\} = \frac{1}{a_0^2}\{a_e^2 + \tfrac{1}{2}(\gamma-1)u_e^2\}$$

by equation (A 2). The result is

$$\frac{1}{r}\psi_Z V_S - \frac{1}{r}V_Z\psi_S + \frac{1}{r^2}\psi_Z\frac{\partial r}{\partial S}V = \frac{\kappa}{C}\left(\frac{a_0}{a_e}\right)^{(4\gamma-2)/(\gamma-1)}\left(U_e^2 - \frac{1}{r^2}\psi_Z^2\right)q + \nu_0 V_{ZZ}.$$

Using equations (12) and (A 6), we find

$$U\frac{\partial V}{\partial S} + W\frac{\partial V}{\partial Z} + \frac{UV}{r}\frac{\partial r}{\partial S} = K(U_e^2 - U^2) + \nu_0\frac{\partial^2 V}{\partial Z^2}.$$

Note that, by equations (A 1) and (A 6), we have $u = (a_e/a_0)U$, so that when $u = u_e$ we have $U = U_e$ by equation (10).

REFERENCES

BREBNER, G. G. 1957 *Aero. Res. Coun., Lond., Curr. Pap.* no. 428.

CHAPMAN, D. R. & RUBESIN, M. W. 1949 *J. Aero. Sci.* **16**, 547.

COOKE, J. C. 1959*a* *Aero. Res. Coun., Lond., Rep. & Mem.* no. 3200.

COOKE, J. C. 1959*b* *Aero. Res. Coun., Lond., Rep. & Mem.* no. 3201.

HOWARTH, L. 1948 *Proc. Roy. Soc.* A, **194**, 16.

ILLINGWORTH, C. R. 1949 *Proc. Roy. Soc.* A, **199**, 533.

MOORE, F. K. 1951 *Nat. Adv. Com. Aero., Wash., Tech. Note* 2279.

ROTT, N. 1953 *J. Aero. Sci.* **20**, 67.

STEWARTSON, K. 1949 *Proc. Roy. Soc.* A, **200**, 84.

ZAAT, J. A. 1956 *National Luchvaartlaboratorium, Amsterdam Rep.* no. F184.

ZAAT, J. A. 1957 *National Luchvaartlaboratorium, Amsterdam Bericht Tr.* no. F202.

Measurement of interfacial structure for co-current air–water flow

By LEMBIT U. LILLELEHT† AND THOMAS J. HANRATTY

Department of Chemistry and Chemical Engineering, University of Illinois, Urbana, Illinois

(Received 19 January 1961)

A method for measuring the interfacial structure between a co-current air–water flow using the absorption of light is described. Measurements of the root-mean-squared displacement and the frequency spectrum are presented. The use of a Gaussian model to describe the interface is explored.

1. Introduction

An understanding of the interaction between an air stream and a flowing liquid film is important to many engineering processes. A rectangular channel having an aspect ratio of 12 to 1 has been used in this laboratory to study the interaction. The liquid is injected through the bottom of the channel, and the air flows co-currently over the liquid surface. If a long enough channel is used, a fully developed condition is attained downstream in which there is no further change in the flow condition of the gas or the liquid. Pressure taps in the top of the channel allow measurement of the pressure gradient, which is the same in both the gas and the liquid. A total-head tube entering through the top wall is used to measure the velocity profile in the gas. The average shear stress at the interface between the air and the liquid can be calculated from the location of the maximum in the gas velocity and the pressure gradient.

Five types of interfacial structures have been described by Hanratty & Engen (1957) for air–water flow. For a fixed flow rate of the liquid, the following sequence of flow régimes is noted as the gas flow is increased: (1) smooth, (2) two-dimensional waves, (3) three-dimensional waves, (4) roll-waves, and (5) dispersed flow. At low enough gas flows no waves are visible to the eye, even though the air flow might be turbulent. The first disturbance which appears on the surface as the gas flow increases are low-amplitude two-dimensional waves extending over the whole width of the channel. They are nearly 0·4 in. apart and travel with a velocity of 0·75 to 1 ft./sec. If the gas velocity is increased only slightly above the transition condition for two-dimensional waves, a pebbled three-dimensional wave structure appears. The wavelength is 0·2–0·4 in. and the wave breadth is approximately equal to the length. The three-dimensional wave structure is stable over a wide range of gas flows. Eventually, however, roll waves appear at the interface. These are two-dimensional disturbances of large

† Now at the University of Alberta, Edmonton, Alberta, Canada.

wavelength with a steep front and long sloping back, which move over the three-dimensional structure and which resemble waves rolling in on a beach. At sufficiently high flow rates, droplets are torn from the liquid surface and the liquid becomes dispersed in the gas phase.

The transitions to these different flow régimes has been studied using a highly disturbed liquid entry (Hanratty & Engen 1957; Hershman 1960; Oosterhout 1958), and a theory explaining the roll-wave transition has been developed by Hanratty & Hershman (1960). The wave structures at the interface cause an increase in the interfacial shear stress over what would exist for a smooth surface in much the same way as roughness elements on solid surfaces (cf. Ellis 1959; Ellison 1956; Hanratty & Engen 1957; van Rossum 1959). The description of the liquid interfacial structure in the papers mentioned above has been based on visual observations. An understanding of the relation of the interfacial structure and of the increase of interfacial stress to system variables depends on a more exact definition of the waves. A technique for measuring the instantaneous height of the liquid has been developed for this purpose (Lilleleht 1961). The present paper has been written to describe the technique and to present the results of some of the initial measurements of the interfacial structure. The relation of interfacial structure to the interfacial shear stress is described in another paper (Lilleleht & Hanratty 1960).

A fine beam of light is passed through the top of the channel and the liquid film and is impinged on a photomultiplier tube. If methylene-blue dye is dissolved in the liquid, a large portion of the light will be absorbed by the liquid, and variations in the height of the liquid film will cause variations in the output signal from the photomultiplier tube. During the period of the development of the above technique in this laboratory, we became aware of similar work which had been done at the Purdue University Jet Propulsion Center by Greenberg (1956) and Charvonia (1959). However, although the basic techniques are the same, there are sufficient differences in the design of the experiments to justify the detailed description of the measurements given in this paper.

The numerical techniques used in this paper to characterize the wave structure are the same as those that have been used for the surface of large bodies of water (Hicks & Whittenbury 1956; Pierson 1955; Putz 1954). The height of the liquid film is defined as the sum of an average height and a fluctuating component. The fluctuating component is described in terms of the variance, the distribution functions describing liquid height and crest height, the frequency spectrum, and the number of crossings at a fixed height. Average film heights for horizontal air–liquid flows have been determined by Hershman (1960) and by van Rossum (1959) using conductance measurements, and by McManus (1959) using an electrical contacting method with a gauge connected to a micrometer screw Average height measurements have been made by Greenberg (1956) and by Charvonia (1959) using a photoelectric method for the co-current flow of air and water inside a vertical pipe. Charvonia has also presented measurements of wave-height distributions for his vertical flow system, and McManus has determined maximum wave heights for air–water flow inside a horizontal pipe.

2. Theory

If the instantaneous height of the liquid film is designated by h then a time average height $\bar{h}$ may be defined as

$$\bar{h} = \lim_{T\to\infty} \frac{1}{T}\int_0^T h\,dt, \tag{2.1}$$

and a fluctuating height h' may be defined by

$$h = \bar{h} + h'. \tag{2.2}$$

The variance of the height, designated by $\Delta(h')$, is the root-mean-squared value of h': thus

$$\Delta(h') = (\overline{h'^2})^{\frac{1}{2}} = \left[\lim_{T\to\infty} \frac{1}{T}\int_0^T h'^2 dT\right]^{\frac{1}{2}}. \tag{2.3}$$

A probability function may be defined by

$$P(h)\,dh = \text{fraction of the time the film height has a value between } h \text{ and } h+dh; \tag{2.4}$$

and if this probability function is Gaussian, we have

$$P(h) = \left(\frac{1}{2\pi}\right)^{\frac{1}{2}} \frac{1}{\Delta(h')} \exp\left\{-\frac{(h-\bar{h})^2}{2[\Delta(h')]^2}\right\}. \tag{2.5}$$

Measurements by Putz (1954) on a large body of water are described quite well by (2.5).

The average number $N(h)$ of times that the function describing h crosses a given value of h in a long period of time is a conveniently measured property, and can be related to the wave structure of the interface. If a wave crest is a maximum and a wave trough is a minimum in h, then $N(h)$ equals twice the difference of the number of crests from the number of troughs at heights greater than h. The difference of $N(h)$ at two values of h is related to the number of maxima and minima in that interval by

$$\tfrac{1}{2}\{N(h_2) - N(h_1)\} = \text{the average number of maxima minus the number of minima in the height interval } h_2 - h_1. \tag{2.6}$$

The above function was measured by Charvonia (1959) in his experiments on air–water flow in a vertical pipe. If, according to Pierson (1955), a wave is defined as the complete cycle during which h passes from $\bar{h}$ up to a crest, then falls through $\bar{h}$ down to a trough and finally passes up through $\bar{h}$ again, then the number of waves per second equals $\frac{1}{2}N(\bar{h})$.

As has been shown by Rice (1944, 1945), a frequency spectrum for the fluctuating height h' can be described as follows:

$$w(f)\,df = \text{fraction of } \overline{h'^2} \text{ contributed by frequencies between } f \text{ and } f+df, \tag{2.7}$$

$$\overline{h'^2} = \int_0^\infty w(f)\,df. \tag{2.8}$$

The frequency spectrum is defined in terms of the Fourier transform of the curve representing h' by the following equations:

$$w(f) = \lim_{T\to\infty} \frac{2\,|S(f)|^2}{T}, \tag{2.9}$$

$$S(f) = \int_0^T h(t)\, e^{-i2\pi ft}\, dt. \tag{2.10}$$

For cases in which both h' and dh'/dt are normally distributed and are statistically independent, $N(h)$ may be related to the frequency spectrum. Rice gave the results

$$N(\bar{h}) = 2\left[\int_0^\infty f^2 w(f)\, df \Big/ \int_0^\infty w(f)\, df\right]^{\frac{1}{2}}, \tag{2.11}$$

$$N(h) = \exp\left[-(h-\bar{h})^2/2\overline{h'^2}\right] \tfrac{1}{2} N(\bar{h}), \tag{2.12}$$

on the condition that the integrals converge. The expected number of maxima per second is

$$N(h_m) = \left[\int_0^\infty f^4 w(f)\, df \Big/ \int_0^\infty f^2 w(f)\, df\right]^{\frac{1}{2}}. \tag{2.13}$$

Rice also has calculated, on the basis of the Gaussian model, the fraction of the crests with heights greater than h. This result is presented in figure 4 of his paper.

The wave structure under different flow conditions are compared in this paper by means of the functions $w(f)$ and $\Delta(h')$. It will be assumed that the effect of the gas flow over the liquid surface can be described solely by the friction velocity u^*. For the cases considered in this paper, average velocity in a given liquid is fixed for fixed values of u^* and $\bar{h}$. Therefore,

$$\Delta(h') = F(h, u^*, g, \sigma/\rho, \rho, \mu/\rho), \tag{2.14}$$

where σ is the interfacial tension, μ is the liquid viscosity, ρ is the liquid density and g is the acceleration of gravity. If σ/ρ, μ/ρ and ρ are unimportant in so far as they directly affect $\Delta(h')$, then

$$\frac{g\Delta(h')}{u^{*2}} = F\left(\frac{g\bar{h}}{u^{*2}}\right). \tag{2.15}$$

For very deep bodies of water, $\Delta h'$ is independent of $\bar{h}$, and we have

$$\frac{g\Delta(h')}{u^{*2}} = \text{const.} \tag{2.16}$$

Analogous to (2.14), the following expression can be written for the frequency spectrum:

$$w = F(f, h, u^*, g, \sigma/\rho, \rho, \mu/\rho). \tag{2.17}$$

If σ/ρ, μ/ρ, and ρ are unimportant, then

$$\frac{wg^3}{u^{*5}} = F\left[\left(\frac{fu^*}{g}\right), \left(\frac{g\bar{h}}{u^{*2}}\right)\right]. \tag{2.18}$$

By using arguments similar to those used to explain the form of the energy spectrum obtained in turbulence measurements, Phillips (1958) has suggested that

w should be independent of u^* at large frequencies. If for the flows considered it is also independent of $\overline{h}$, then

$$\frac{wf^5}{g^2} = \text{const.} \tag{2.19}$$

Phillips showed that the high-frequency end of the spectrum measured in a reservoir could be represented by the equation

$$\frac{wf^5}{g^2} = 9{\cdot}5 \times 10^{-6}. \tag{2.20}$$

3. Flow system

The design of the flow system used in the experiments described in this paper is similar to that used by Hanratty & Engen (1957) and by Hershman (1960). The 'Plexiglass' channel was 1·020 in. high, 12 in. wide and 21 ft. long. The entry was quite different from that used in previous work in this laboratory. The air and the liquid were brought together at the inlet of the Plexiglass channel. The liquid was introduced into the channel from an entry box fastened to the channel bottom through 60 holes of 0·1540 in. diameter, which were slanted 45° in the direction of liquid flow and which were spaced in a scattered fashion. The liquid-entry area containing the holes was covered with a 6×12 in. piece of 200-mesh copper screen to prevent any possible jetting effects at high rates of liquid flow. This design gave a much smoother entry condition of the liquid film than the one used by Hanratty & Engen. The liquid discharging from the channel was collected in a reservoir and recirculated. Liquid-height measurements were made at a position 11 ft. 8 in. from the channel inlet. A $2\frac{5}{16}$ in. diameter hole was cut in the bottom of the channel at this position and a $\frac{1}{4}$ in. thick circular disk of Plexiglass was inserted into the hole. The top of the channel at the test section consisted of a $3\frac{1}{2}$ in. piece of Plexiglass that could be slid into place. Both the top and bottom pieces at the test section were easily removable to facilitate cleaning, and replacement if they became scratched. The top could also be replaced by the total-head tube assembly for gas phase velocity-profile measurements. Pressure taps on the top of the channel were located 6 ft. 2 in., 12 ft. 8 in. and 15 ft. 2 in. from the entry. A total-head tube mounted on a micrometer screw at a distance 15 ft. 2 in. was used in conjunction with a static pressure tap on the top of the channel to measure the velocity distribution in the air stream. All pressures were measured with a Wahlen manometer (Engen 1956).

4. Measurement of liquid heights

The equipment used to measure the average and instantaneous liquid height is sketched in figure 1. A chopped beam of light is passed through a filter and a lens system, and is focused at the interface between the gas and the liquid as a beam about 1 mm in diameter. It passed through the water containing methylene-blue dye and through the bottom of the channel on to a diffuser screen. The light beam on the diffuser screen was picked up by a photomultiplier tube. The signal from the photomultiplier tube was amplified, clipped, and demodulated to give an electrical signal corresponding to the wave-form.

The light source was chopped in order to eliminate the effect of background light and to simplify the problem of amplifying the signal from the photomultiplier tube. This signal consisted of a DC portion, which was a measure of the background light, and an AC portion whose amplitude varied with the height of the liquid in the channel. By using an AC amplifier, only the AC portion was transmitted to the recording device. A mechanical chopper was used consisting of an aluminium disk with forty $\frac{5}{16}$ in. holes drilled on a 4 in. circle. Each revolution

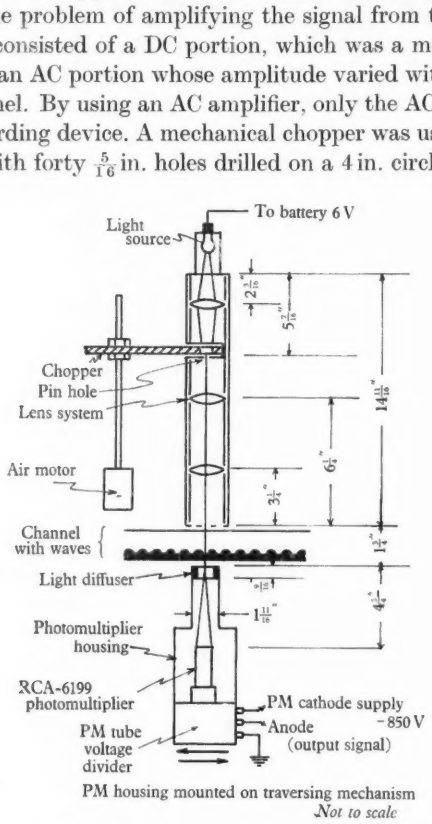

FIGURE 1. Diagram of the lens and photomultiplier arrangement.

of the chopper produced forty rectangular pulses of light. In order to minimize 60-cyc. AC pick-up, the disk was driven by an air motor at a speed of about 40 rev./sec. This produced a light beam of 1600 pulses/sec, or 100 pulses for each cycle of a 16 c/s sine wave. The lens system for focusing the light beam was mounted in a $2\frac{3}{4}$ in. brass tube, plastic spacers being used to locate them in the proper position. The inside of the assembly was painted with a matt black paint to prevent internal reflexions. Several filters were placed in the brass tube to provide a beam approximately 530 mμ in wavelength, such as is strongly absorbed by methylene blue.

An RCA type 6199 photomultiplier tube housed in a $3\frac{1}{2}$ in. cylindrical brass tube was used. It had a 1·24 in. diameter flat face with semi-transparent cathode. In testing the tube it was found that the photocathode was not of uniform sensitivity. Owing to refraction at the liquid–gas interface, the light beam emerged from the gas–liquid interface at different angles from the vertical and, therefore, was aimed at different positions on the cathode surface. Consequently, the non-

uniformity of the photocathode could lead to serious error. A diffuser disk was placed between the bottom of the channel and the photomultiplier tube to diffuse the light uniformly in all directions. The photomultiplier tube was placed approximately 5 in. from the diffuser, so that small movements of the light spot on the diffuser would not affect the solid angle intercepted by the photomultiplier tube. A Beckman 'heliopot' precision potentiometer was used as a load resistor for the photomultiplier tube to take varying fractions of the total output signal for amplification and analysis. The anode was at ground potential and the cathode

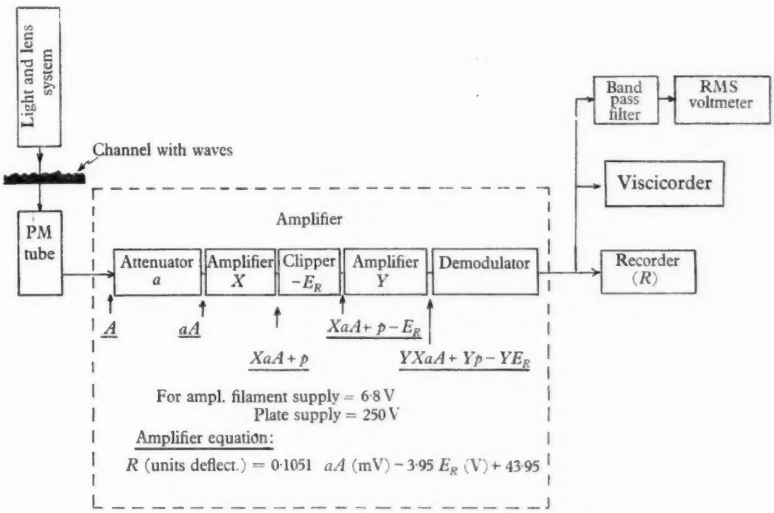

FIGURE 2. Block diagram of electronic equipment.

was at -850 V. Electrostatic shielding of the photomultiplier tube was provided by a closely fitted copper foil covering the uncoated area of the tube and connected through a 12 MΩ resistor to the cathode supply.

A block diagram of the amplifier circuit is shown in figure 2, and the detailed design is shown in figure 3. The signal A from the photomultiplier tube is reduced to a fraction a by the precision potentiometer load resistor. The DC part of the signal is filtered out, and the AC part is amplified by a factor X and put on a pedestal p in the first stage of amplification. The amplifier output is clipped by an amount E_R in order to accentuate the fluctuations of the pulse heights, and to cut the pulse heights below the maximum allowable input signal that the next stage of amplification could tolerate without distortion. In the second stage of amplification, the clipped signal is amplified by a factor Y. The signal from the second stage of amplification is fed to a cathode follower. The cathode-follower output is passed through a capacitor to remove its DC pedestal and is clamped to ground potential. A diode demodulator produces a signal which is a measure of the fluctuations of the water-film thickness. The demodulator circuit is provided with a limiter to protect the measuring instruments against being

overdriven. If there were indications that the limiter was conducting, the input signal was decreased by adjusting the potentiometer. The signal was recorded either on a Honeywell Model 906 Viscicorder or on a General Electric CE Photoelectric Recorder. The Viscicorder had a wide frequency response (flat over a 0–270 c/s range) and was used to record fluctuations in the height. The General Electric recorder was used to record average heights. A Flow Corporation Model TBM r.m.s.-voltmeter was used to measure the power of the AC portion of the signal. A Krohn–Hite Model 330-A ultra-low-frequency band-pass filter was used in the spectral analysis of the AC signal. It has a range of 0·02–2000 c/s.

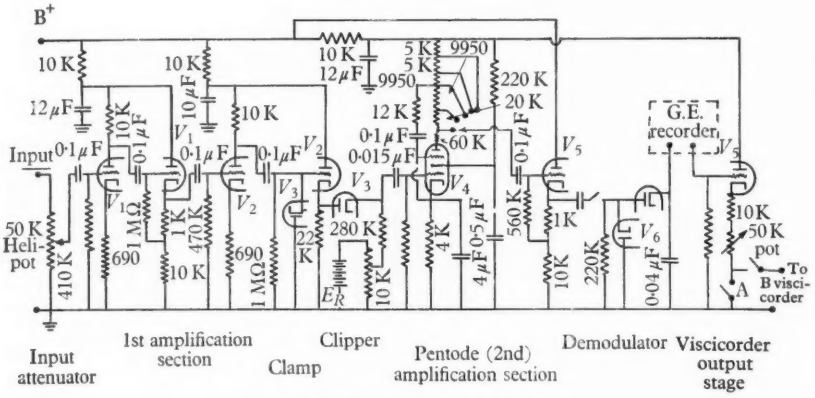

FIGURE 3. Amplifier circuit diagram.

Tubes: V_1, 6SN7; V_2, 6SN7; V_3, 6H6; V_4, 6SJ7; V_5, 6SN7; V_6, 6H6.

The battery supplies were maintained at constant voltages during all runs. The relation between the signal coming from the demodulator and the signal coming from the photomultiplier tube could be varied by changing the potentiometer setting a and the clipping level. The equation describing this relation is

$$R = YXaA + Yp - YE_R. \tag{4.1}$$

The constants Y, X, and p were evaluated by sending a 2 kc/s square wave of known amplitude through the circuit. The circuit was found to behave linearly except at very small attenuator setting a, or at very large clipping levels. The equipment was operated only in the region of linearity.

Equation (4.1) was used to calculate the photomultiplier output A for a given value of the signal R, and for given circuit settings. Since A was directly proportional to the intensity of the light I impinging on the photomultiplier tube, we could write

$$A = k_1 I. \tag{4.2}$$

The intensity I can be related to liquid height h by Lambert's law (Prutton & Maron 1944)

$$I = I_0 e^{-k_2 h}, \tag{4.3}$$

where I_0 is the intensity of the light signal without any liquid in the path and k_2 is a constant which depends on the concentration of methylene-blue dye in the water. Making use of (4.2) and (4.3), we get

$$\frac{I}{I_0} = \frac{A}{A_0} = e^{-k_2 h}. \tag{4.4}$$

The constant k_2 in the above equation was measured for various dye concentrations in the specially constructed cell shown in figure 4. The cell was machined out of Plexiglass, and the flat surfaces were highly polished to remove any scratches. A number of spacers of uniform and known thickness were inserted

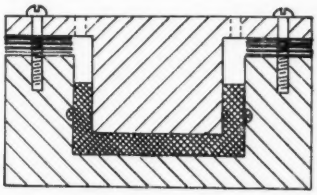

FIGURE 4. Calibration cell (not to scale).

between the bottom and the top part of the cell to vary the liquid-layer thickness in the gap. The effect of the liquid-film thickness on the light transmission for various concentrations of dye in deionized water was measured using the calibrating cell in place of the disk at the bottom of the channel at the test section. The zero level of the photomultiplier output A_0 was measured by removing the cell from the light path. The zero level was inclined to vary, so that during operation it was measured at frequent intervals. Likewise, during extended periods of operation, the effective dye concentration in the test solution varied. Therefore, the effective concentration of dye in the test solution was measured before and after each run.

When power spectral measurements were made, the power passing through the filter for a particular setting of the upper f_2 and the lower f_1 cut-off frequencies was measured with the random-signal voltmeter.

5. Accuracy of height measurements

The chief sources of error in the measurements of the film height were the reflexion and the refraction of light rays at the air–liquid interface. The percentage of the light reflected from the interface of two transparent media depends on the angle of incidence and the refractive index between the media. The percentage of 589 mμ wavelength light reflected from an air–water interface remains constant at about 2 % for low angles of incidence. For light passing from water to air, a significant increase in the amount reflected occurs at angles of incidence larger than about 30°. For light passing from air to water a marked increase occurs at angles of incidence of about 45°. Therefore, height measurements were made using the second mode of operation. However, this choice had the disadvantage that light beams refracted at the surface had a path of travel through the liquid whose length might depend on the angle of inclination of the interface.

This error was calculated to be less than 1 % of the film thickness at angles of incidence less than 30°, and approximately 2 % at an angle of incidence of 40°. These considerations indicate that the method is limited to interfacial slopes of less than about 40°. Of course, the limitations would be more severe for waves whose heights are a very small percentage of the average film height. All of the data reported in this paper, with the exception of the roll wave data, were taken on systems for which the slope of the interface was 40° or less.

Some runs were conducted with no dye in the liquid film. The fluctuation of the signal coming from the height measuring equipment was significant (about 6·3 % fluctuations) only when roll waves were present. These runs indicated that reflexion of light from the interface was not affecting the data appreciably, and that the diffuser plate was operating satisfactorily.

No method was available for comparing directly the photometric wave-height measurements with an independent set of measurements. The depth of the liquid film at the wave crests was estimated with a pointer that could be moved in a direction perpendicular to the channel bottom. The point of contact was determined visually. A reasonable comparison was obtained between these measurements and the sum of the average height and the root-mean-square wave height obtained photometrically.

6. Treatment of data

Average film heights were calculated from the photomultiplier output by (4.4). A fluctuation δh in the film height from the average height is related to a corresponding fluctuation in the photomultiplier output as follows:

$$\delta h = \frac{1}{k_2} \ln \left(\frac{\bar{A} + \delta A}{\bar{A}} \right). \tag{6.1}$$

It should be noted that measurements of fluctuating heights do not depend on the transmission A_0 in the absence of a film. If the fluctuations are small compared with the average amount of light transmitted $\bar{A}$, the following approximation can be used for the wave height:

$$\delta h = \frac{\delta A}{2{\cdot}303 \bar{A} k_2}. \tag{6.2}$$

The error due to this approximation in all the data taken was less than one part in 500.

The transfer function $Y(f; f_1; f_2)$ of the band-pass filter was given by the manufacturer as

$$Y(f; f_1; f_2) = \frac{(f/f_1)^4}{[1 + 2jB(f/f_1) - (f/f_1)^2]^2 [1 + 2jB(f/f_2) - (f/f_2)^2]^2}, \tag{6.3}$$

where B is the peaking factor, equal to 0·6. The frequency spectrum of the waves is related to power from the band-pass filter through the equation

$$\text{Mean power} = \int_0^\infty |Y(f; f_1; f_2)|^2 w(f)\, df. \tag{6.4}$$

A power transfer function can be defined as

$$H(f; f_1; f_2) = |Y(f; f_1; f_2)|^2. \tag{6.5}$$

If the equivalent width of the band-pass window is narrow enough so that the spectral density within the window can be considered as constant and equal to that at the mid-band frequency $f_M = \sqrt{(f_1 f_2)}$, then

$$\text{Mean power} = Kw(f_M), \tag{6.6}$$

$$K = \int_0^\infty H(f; f_1; f_2)\, df. \tag{6.7}$$

The parameter K varies with f_1 and f_2. The spectral density $w(f_M)$ calculated from (6.7) is approximate in that it is based on the assumption of constant power spectrum within the window width. This assumption becomes less objectionable for narrow pass-bands and for spectra varying slowly with frequency. The narrowest pass-band for the filter without undue attenuation is obtained by setting the lower and the upper cut-off frequencies equal. This setting was used in all the measurements reported. The stability of the output signal at this narrowest window setting was not a serious problem because of the large time constant (16 sec) of the random-signal voltmeter used to measure the power.

The assumption of a constant spectral density within the window was checked by comparing the measured total power in the 0·2–60 c/s range with the area under the frequency spectrum curve over the same frequency range. The integral of the frequency spectrum curve yielded 0–10 % lower values. A wider spectral window in which the upper and the lower cut-off frequencies were separated by a factor of 1·75 showed much poorer agreement between the directly measured power and that calculated from the frequency spectrum.

An attempt was made in run *G*, where a 10 % error was noted in power calculated from the spectrum, to obtain a second approximation for the frequency spectrum by applying a linear correction based on the slope of the first approximation to the spectral density curve. The correction has the tendency to lower the spectral-density function in the region of positive slope, and increase it in the high-frequency end of negative slope. The total power of 370×10^{-6} in.^{2} obtained by integrating the corrected frequency spectrum is to be compared with a value of 372×10^{-6} in.^{2} obtained by direct measurement. However, none of the frequency-spectrum results reported in this paper were corrected by this technique.

7. Results

The same type of interfacial structures that were observed by Hanratty & Engen (1957) and by Hershman (1960) with a highly disturbed entry were observed using the specially designed liquid entry described in this paper. The transition to roll waves appeared to be independent of the entry design. However, transition from a smooth surface to one with two-dimensional waves occurred at somewhat higher gas rates with the undisturbed entry. A Visicorder record of the surface structure when three-dimensional waves are present was shown in a previous paper (Lilleleht & Hanratty 1960) for a single flow condition.

Twice the root-mean-square of the fluctuating liquid height, $2\Delta(h')$, is a measure of the wave heights. Figure 5 presents measured values of $\Delta(h')$ as a

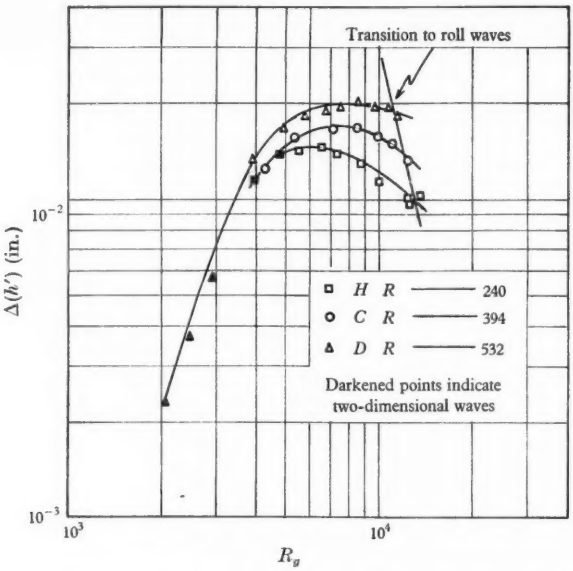

FIGURE 5. Measurements of the root-mean-squared surface displacement.

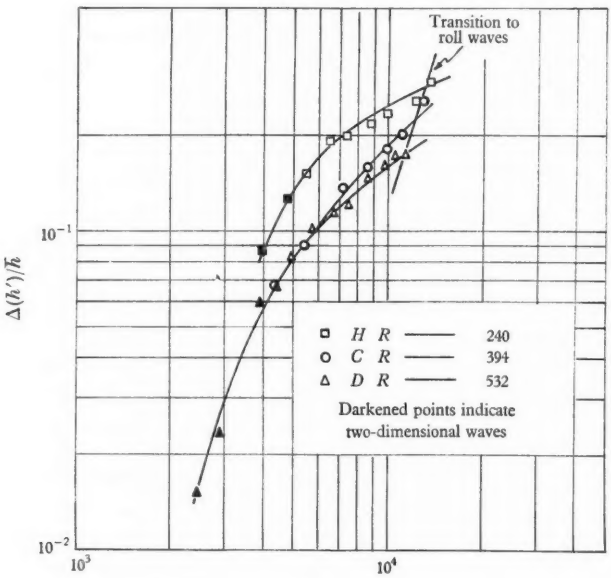

FIGURE 6. Measurements of the root-mean-squared surface displacement, plotted as $\Delta(h')/\bar{h}$.

function of the gas Reynolds number R_g with liquid Reynolds number R as a parameter. The Reynolds numbers are defined in terms of the time-average thicknesses and the mixed average velocities of the air and water layers. The wave height in the region of two-dimensional waves increases markedly with increasing gas Reynolds number. However, in the region of three-dimensional waves, the wave height does not change as rapidly with increasing gas Reynolds number. Measurements of $\Delta(h')/\bar{h}$ are presented in figure 6. For fixed rate of liquid flow (fixed R), the average liquid height $\bar{h}$ decreases with increasing gas

Run	$\bar{h}$ (in.)	$\Delta(h')$ (in.)	R	R_g	u^* (ft./sec)
A†	0·1110	0·0109	239	4,700	0·714
B	0·0743	0·0111	227	8,420	1·285
C	0·1886	0·0126	394	4,350	0·709
D	0·200	0·0166	532	4,930	0·889
E	0·1608	0·0193	532	7,420	1·313
F	0·1129	0·0194	532	10,560	1·820
G	0·1344	0·0193	581	7,300	1·329
H	0·0378	0·0096	240	12,280	1·866

† Two-dimensional waves. All the other runs had a three-dimensional wave structure.

TABLE 1. Run conditions.

Reynolds number R_g, and, therefore, the quantity $\Delta(h')/\bar{h}$ increases with increasing gas Reynolds number. It is to be noted that at high R_g the wave heights approach the magnitude of the average liquid height. Velocity profiles were measured for a number of runs, and friction velocities were calculated. These calculated friction velocities, presented in table 1, were used to correlate measurements of $\Delta(h')$ as shown in figure 7. Spectral measurements are shown in figure 8 for some of the runs summarized in table 1. At small frequencies the spectral function is dependent on the height of the liquid film. However, the high-frequency end of the spectrum for the three-dimensional waves appears to be independent of liquid height since all of the spectral measurements appear to come into a single envelope. A line of slope such that w varies as f^{-5} is shown for reference purposes. Although the high-frequency end of the envelope appears to be described approximately by such a relation, insufficient data have been obtained to say whether any appreciable portion of the envelope obeys this relation and, therefore, is independent of u^*. In run F, a sharp maximum was indicated by the data as at a value of fu^*/g of about 0·035 (0·6 c/s). This run was carried out just below the gas velocity at which roll waves were observed visually. It is possible that this maximum could be due to incipient roll waves. These data have not been presented since it is intended to check them more thoroughly before publication. Values of $(fu^*/g)_{\max}$ and $(wg^3/u^{*5})_{\max}$ are presented as functions of gh/u^{*2} in table 2. The data for $(fu^*/g)_{\max}$ may be represented by the equation

$$(fu^*/g)_{\max} = 0{\cdot}207(g\bar{h}/u^{*2})^{-\frac{1}{2}}. \tag{7.1}$$

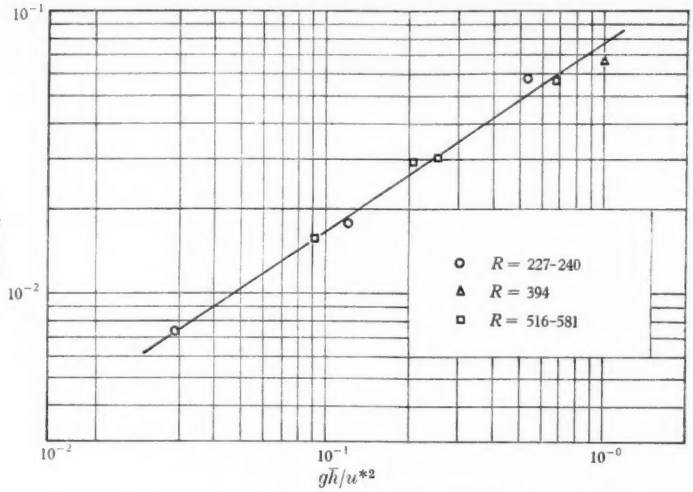

FIGURE 7. Correlation of interfacial displacement measurements.

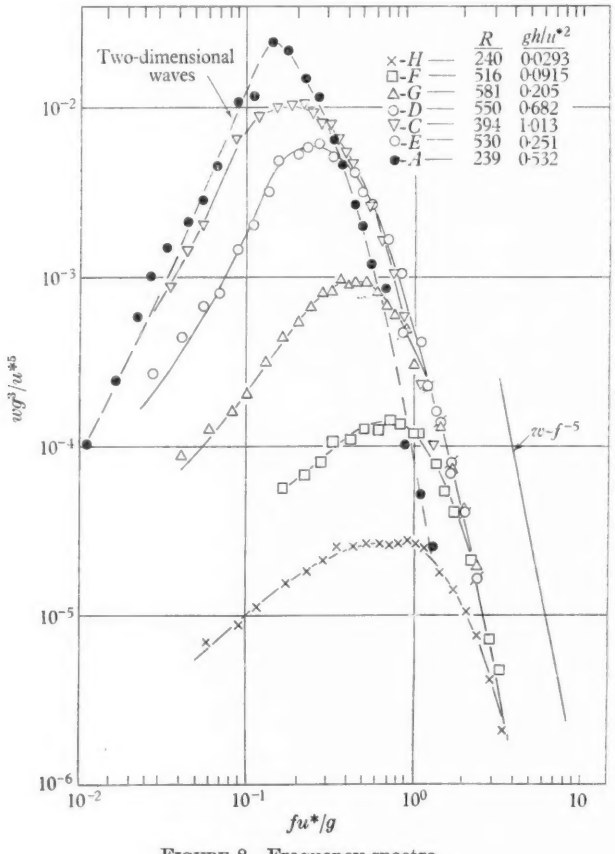

FIGURE 8. Frequency spectra.

This equation indicates that for waves which are affected by the liquid depth, the value of f_{max} is independent of u^* and can be represented by the relation

$$f_{max} = 0{\cdot}207\sqrt{(g/\bar{h})}. \tag{7.2}$$

If the definition of a wave cycle given by Pierson is used (cf. § 2), then $\frac{1}{2}N(\bar{h})$ is the number of waves per second. Values of this parameter measured from Viscicorder wave records are compared with the values of frequency at the

Run	$\frac{g\bar{h}}{u^{*2}}$	$\left(\frac{fu^*}{g}\right)_{max}$	$\left(\frac{wg^3}{u^{*5}}\right)_{max} \times 10^5$	f_{max} (sec^{-1})	$\frac{1}{2}N(\bar{h})$ (sec^{-1})
H	0·0293	0·8	2·7	14	—
F	0·0915	0·7	14	12	26·4
B	0·120	0·52	44	13	—
G	0·205	0·46	95	11	21·2
E	0·251	0·40	120	9·7	22·2
A†	0·532	0·14	2500	6·4	—
D	0·682	0·25	600	9·2	21·9
C	1·013	0·18	1020	8·0	—

† Two-dimensional waves.

TABLE 2. Maxima from the spectral density data.

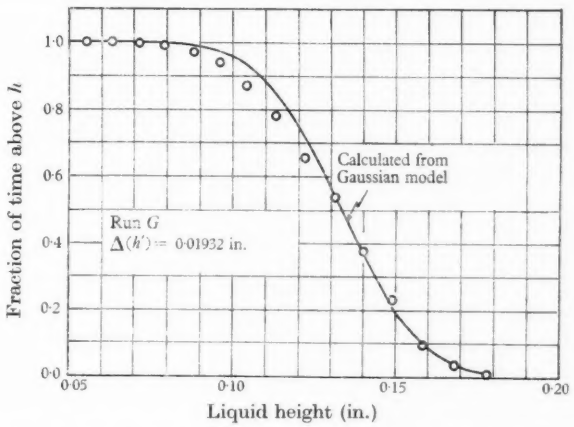

FIGURE 9. Comparison of the wave record with the Gaussian model.

maxima of the spectral density in table 2. It is noted that the maxima are about one half the number of waves per second. As can be seen from figures 7 and 8 and table 2, the measurements of $\Delta(h')$ and of $w(f)$ for three-dimensional waves are correlated quite well by dimensionless groups obtained on neglecting the direct effect of liquid density and viscosity and of interfacial tension. The agreement does not mean that these parameters are not important. The range of physical variables investigated was not sufficient to define the respective roles of fluid properties.

A very long Viscicorder record was analysed for run G to examine the applicability of Gaussian model to the three-dimensional waves observed. Data on

the fraction of the time the fluid is below a given height are presented in figure 9. The curve was calculated from (2.5) by use of the value of $\Delta(h')$ measured with the r.m.s.-voltmeter. In figure 10, measured values of $N(h)/N(\bar{h})$ are compared with those calculated from (2.12). Figure 11 compares the fraction of the crests above a certain value of h, or the fraction of the troughs below h, with curves

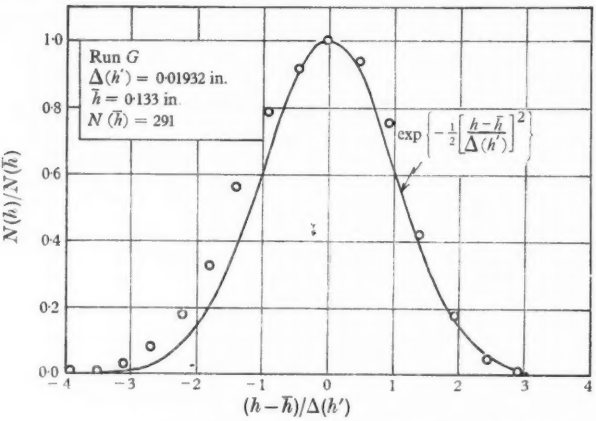

FIGURE 10. Comparison of the measured number of crossings with the Gaussian model.

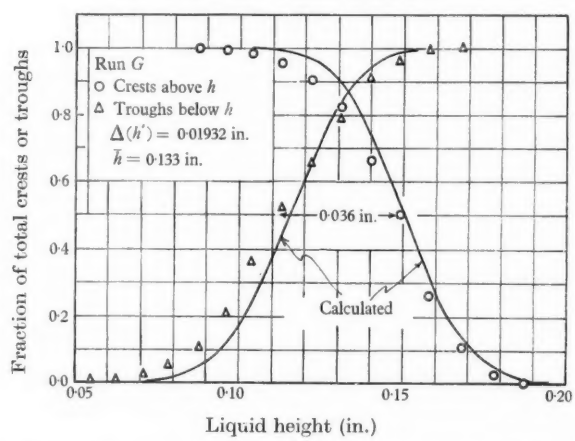

FIGURE 11 Comparison of the measured distribution of crests and troughs with the Gaussian model.

calculated by Rice (1944, 1945) on the basis of the Gaussian model. The measurements in figures 9–11 are approximately described by the Gaussian model. However, the wave structure below $\bar{h}$ appears to be slightly different from the wave structure above $\bar{h}$. It is not certain whether the differences from the Gaussian model are real, or whether they are due to limitations in the experimental technique such as might be caused by refraction effects. This will be explored in future work in this laboratory. The number of zero crossings per

second, $N(\bar{h})$, and the number of maxima per second measured for run G and for three other wave records are presented in table 3. Values of $N(\bar{h})$ calculated from the spectral measurements by use of (2.11) are in very good agreement with

Run	$N(\bar{h})$ (sec^{-1}) Measured	$N(\bar{h})$ (sec^{-1}) Equation (11)	$N(h_m)$ (sec^{-1}) measured
G	42·5	45	33·8
D	43·8	40	59·0
E	44·5	43	68·8
F	52·8	47	82·6

TABLE 3. Number of zero crossings per second and number of maxima per second.

measured values of $N(\bar{h})$. The spectral measurements did not converge to zero rapidly enough at large frequencies to calculate the number of maxima per second from (2.13).

The authors are grateful to the American Oil Company and E. I. duPont deNemours and Company for support.

REFERENCES

CHARVONIA, D. A. 1959 A study of the mean thickness of the liquid film and the characteristics of the interfacial surface in annular two-phase flow in a vertical pipe. *Jet Propulsion Center, Purdue University, Rep.* no. I–59–1.

ELLIS, S. R. M. & GAY, B. 1959 *Trans. Instn Chem. Engrs, Lond.*, **37**, 206.

ELLISON, T. H. 1956 Article in *Surveys in Mechanics*. Cambridge University Press.

ENGEN, J. M. 1956 M.S. Thesis, Dep. Chem. and Chem. Eng., University of Illinois.

GREENBERG, A. B. 1956 Ph.D. Thesis, Purdue University.

HANRATTY, T. J. & ENGEN, J. M. 1957 *J. Amer. Instn Chem. Engrs*, **3**, 299.

HANRATTY, T. J. & HERSHMAN, A. 1960 Initiation of roll waves. Paper presented at Annual Meeting of Amer. Instn Chem. Engrs, Washington, D.C. (December); to be published in *J. Amer. Instn Chem. Engrs.*

HERSHMAN, A. 1960 Ph.D. Thesis, Dep. Chem. and Chem. Eng., University of Illinois.

HICKS, B. L. & WHITTENBURY, C. G. 1956 Wind waves on the water. *Control Systems Lab., University of Illinois, Rep. R-83.*

LILLELEHT, L. U. 1961 Ph.D. Thesis, Dep. Chem. and Chem. Eng., University of Illinois.

LILLELEHT, L. U. & HANRATTY, T. J. 1960 Paper submitted for publication in *J. Amer. Instn Chem. Engrs.*

MCMANUS, H. N. 1959 *Proc. 6th Ann. Conf. on Fluid Mech., University of Texas (September).*

OOSTERHOUT, K. C. 1958 M.S. Thesis, Dep. Chem. and Chem. Eng., University of Illinois.

PHILLIPS, O. M. 1958 *J. Fluid Mech.* **4**, 426.

PIERSON, W. J. 1955 *Advances in Geophysics.* II. New York: Academic Press.

PRUTTON, C. F. & MARON, S. H. 1944 *Fundamental Principles of Physical Chemistry*, p. 756. London: Macmillan.

VAN ROSSUM, J. J. 1959 *Chem. Engng Sci.* **11**, 35.

PUTZ, R. R. 1954 *Proc. 4th Conf. on Coastal Eng., Coun. of Wave Res., Univ. Calif., Berkeley*, p. 13.

RICE, S. O. 1944 *Bell System Tech. J.* **23**, 282; (1945), *ibid.* **24**, 46.

Linearized slip flow past a semi-infinite flat plate

By J. A. LAURMANN

National Aeronautics and Space Administration, Ames Research Centre
Moffett Field, California

(Received 4 October 1960 and in revised form 21 February 1961)

Incompressible slip flow past a semi-infinite flat plate at zero incidence is treated in terms of the linearized viscous flow equations. A formal solution is obtained using Fourier transforms and the Wiener–Hopf technique. Explicit inversion of the transform is not possible, but asymptotic expansions are discussed. These reveal the inadequacy of boundary-layer theory in predicting the nature of the solution, even at the plate surface. For example, the local shear forces on the plate are significantly different from boundary-layer values, even far downstream, where slip effects are small. The boundary-layer limit is approached as the Reynolds number based on the mean free path or, equivalently, the free-stream Mach number tends to infinity.

1. Introduction

The first estimate for the effect of slip on the flow over a flat plate was made in 1949 by Donaldson. Since then numerous refinements and extensions, of which the present paper is one, have been made. Unfortunately, from the point of view of the theoretician working on the subject, experimental confirmation of the predictions of these analyses has not been forthcoming. Thus, it appears today that in the most important cases of practical interest, namely, in hypersonic low-density flows, slip effects are masked by shock-wave–boundary-layer interactions effects and it is even claimed (Probstein 1960) that slip effects may never be significant in such cases. In spite of this, the more academic interest in the phenomenon of slip flow persists and it seems desirable to be able to treat the low-speed incompressible case more carefully, for it is in this régime that conclusive comparisons of theory and experiment can be made.

The present analysis, therefore, is an attempt to solve completely the slip-flow problem for incompressible flow over a flat plate. No restriction is placed on the magnitude of the slip velocity

$$u' = a_1 \lambda \left| \frac{\partial u}{\partial y} \right|$$

at the plate surface, $y = 0$. Here $\partial u/\partial y$ is the normal velocity gradient, λ is the mean free path and a_1 is a constant. This boundary condition on the surface velocity, as derived from kinetic theory, holds strictly only for small departures from continuum flow, i.e. for small values of the slip velocity u', and most work has been restricted to the study of small perturbations about zero-slip boundary-layer solutions (Schaaf & Chambré 1957). The possibility exists, however, that

the slip condition has an extended range of validity (Laurmann 1958; Sherman & Talbot 1958; Yang & Lees 1956), holding not only for small values of the mean free path λ, but also for arbitrary large departures from no-slip flow, and it is this viewpoint that provides the interest in the type of solution considered here. Indeed, the need for the more general approach is demonstrated by the result, derived below, that the low-speed case cannot be handled correctly in terms of boundary-layer theory, even far downstream where slip effects become relatively small.

In view of these observations it would clearly be desirable to analyse the slip-flow problem using the full Navier–Stokes equations. However, since these equations have not yet been solved even for the simpler zero-slip case, we will be satisfied here to treat the problem in terms of the linearized Oseen model, which we anticipate will contain most of the essential features of the full solution.

2. Formulation of the problem

We consider the two-dimensional incompressible Oseen equations

$$U\Delta\frac{\partial u}{\partial x} = \nu\Delta^2 u, \quad U\Delta\frac{\partial v}{\partial y} = \nu\Delta^2 v, \quad \frac{\partial u}{\partial x}+\frac{\partial v}{\partial y} = 0 \tag{2.1}$$

in which Δ is the Laplacian operator $(\partial^2/\partial x^2)+(\partial^2/\partial y^2)$; U is the free-stream velocity, directed along the x-axis; u and v are perturbations from this velocity in the x- and y-directions, respectively; and ν is the kinematic viscosity. The boundary conditions are taken as

$$u, v \to 0, \quad y \to \infty,$$

and

$$\left.\begin{aligned} u+U &= a_1\lambda\left|\frac{\partial u}{\partial y}\right|, && x>0,\\ \frac{\partial u}{\partial y} &= 0, && x<0,\\ v &= 0, \end{aligned}\right\} \quad y = 0, \tag{2.2}$$

where λ is the mean free path and the coefficient a_1 in the slip-boundary condition is a numerical constant whose value depends on the plate reflexion coefficient σ:

$$a_1 = (2-\sigma)/\sigma, \tag{2.3}$$

so that, for perfectly diffuse reflexion, $a_1 = 1$.

To solve the system of equations (2.1), under boundary conditions (2.2), we construct the general solution in terms of an integral of the fundamental solution† of (2.1). A detailed discussion of the fundamental solution of the linearized flow equations has been given by Lagerstrom, Cole & Trilling (1949). They find that it can be expressed as the sum of three terms,

$$\mathbf{v}_0 = \mathbf{v}_1+\mathbf{v}_2+\mathbf{v}_2^*. \tag{2.4}$$

† Given a differential form $L[u] \equiv \Sigma A_{ij}(\partial^2 u/\partial x_j \partial x_i)$, the function $K(x, y; \xi, \eta)$ such that $L[K(x, y; \xi, \eta)] = \delta(x-\xi, y-\eta)$, where δ is the Dirac delta function, is called the *fundamental solution* of $L[u]$.

where, in the incompressible case,

$$\left.\begin{aligned} \mathbf{v}_1 &= \frac{1}{2\pi U}\begin{pmatrix}\partial/\partial x\\ \partial/\partial y\end{pmatrix}\ln r, \quad \mathbf{v}_2 = -\frac{1}{2\pi\nu}\exp\left(\frac{Ux}{2\nu}\right)K_0\left(\frac{Ur}{2\nu}\right)\begin{pmatrix}1\\0\end{pmatrix},\\ \mathbf{v}_2^* &= \frac{1}{2\pi U}\begin{pmatrix}\partial/\partial x\\ \partial/\partial y\end{pmatrix}\left[\exp\left(\frac{Ux}{2\nu}\right)K_0\left(\frac{Ur}{2\nu}\right)\right]. \end{aligned}\right\} \tag{2.5}$$

Here $r = (x^2+y^2)^{\frac{1}{2}}$ and K_0 is the modified Bessel function of zero order; $\mathbf{v}_1$ is the velocity of the so-called longitudinal wave and satisfies Laplace's equation. In the sense of Lagerstrom & Cole (1955), it is the 'outer' solution for the flow. The 'inner' part, equal to $\mathbf{v}_2+\mathbf{v}_2^*$, is the solenoidal 'transverse wave' and includes all the viscous effects. However, as shown by Lagerstrom *et al.* (1949), $\mathbf{v}_2^*$ is irrotational and the vorticity is given entirely by $\mathbf{v}_2$. Thus the latter component corresponds to the boundary layer, or at least to the vorticity boundary layer. However, in general, and in particular for our problem near or at the leading edge, significant contributions to $\mathbf{v}_0$ are made by all three components and it is not possible to represent the flow field close to the body by only the transverse wave or a part of it.

We now propose as the general solution

$$\mathbf{v} = \int_0^\infty \mathbf{v}_0(x-t, y)f(t)\,dt, \tag{2.6}$$

where $f(t)$ is an unknown distribution function. For convenience we define

$$F(t) = \exp(-Ut/2\nu)f(t). \tag{2.7}$$

From the properties of fundamental solutions, it follows that, when $y = 0$,

$$v = 0, \qquad \frac{\partial u}{\partial y} = 0 \quad (x < 0), \qquad \frac{\partial u}{\partial y} = \pm\frac{U}{2\nu}f(x) \quad (x > 0); \tag{2.8}$$

in the last equation the positive sign holds for $y \to 0$ from above and the negative sign for $y \to 0$ from below. Comparing (2.2) and (2.8) we see that all the boundary conditions are satisfied automatically by (2.6), except for the slip condition, which requires that

$$u + U = a_1(\lambda U/2\nu)f(x) \quad (y = 0). \tag{2.9}$$

If we now combine (2.6) and (2.9), we obtain

$$U + \frac{1}{2\pi}\exp\left(\frac{Ux}{2\nu}\right)\int_0^\infty F(t)\left[\frac{1}{x-t}\exp\left\{-\frac{U(x-t)}{2\nu}\right\} - \frac{U}{2\nu}K_0\left(\frac{U|x-t|}{2\nu}\right)\right.$$
$$\left. - \operatorname{sgn}(x-t)\frac{U}{2\nu}K_1\left(\frac{U|x-t|}{2\nu}\right)\right]dt = a_1\frac{\lambda U}{2\nu}F(x)\exp\left(\frac{Ux}{2\nu}\right) \quad (x > 0), \tag{2.10}$$

which is an integral equation for the determination of $F(t)$.

3. Transformation of the integral equation

In §2 the problem was reduced to the solution of the integral equation (2.10). This equation is of the Wiener–Hopf type and there are standard methods of solution based on the use of the Fourier transform (Noble 1958).

Study of the equation shows that, in order to obtain existence of the Fourier transforms in a finite strip of the transformed w-plane, we need to introduce a convergence factor $\exp(-\alpha|x-t|)$, α constant, in the first (potential) term of

the integral. After the nature of the solution in the w-plane has been studied, we can let $\alpha \to 0$. Thus, we write

$$U\exp\left(-\frac{Ux}{2\nu}\right)+\frac{1}{2\pi}\int_0^\infty F(t)\left[\frac{1}{x-t}\exp\left\{-\frac{U(x-t)}{2\nu}-\alpha|x-t|\right\}\right.$$
$$\left.-\frac{U}{2\nu}K_0\left(\frac{U|x-t|}{2\nu}\right)-\frac{U}{2\nu}\operatorname{sgn}(x-t)\,K_1\left(\frac{U|x-t|}{2\nu}\right)\right]dt=\frac{a_1\lambda U}{2\nu}F(x)\quad(x>0). \tag{3.1}$$

In order to be able to use the convolution theorem for Fourier transforms, we must modify (3.1) to hold for all x. Hence we introduce

$$u_-(x)=\begin{cases}u(x)\exp\left(\dfrac{Ux}{2\nu}\right) & (x<0);\\ 0 & (x>0);\end{cases} \tag{3.2}$$

and define

$$F_+(x)=\begin{cases}F(x) & (x>0);\\ 0 & (x<0);\end{cases}\qquad U_+(x)=\begin{cases}U & (x>0);\\ 0 & (x<0).\end{cases} \tag{3.3}$$

Then (3.1) becomes

$$U_+\exp\left(-\frac{Ux}{2\nu}\right)+\frac{1}{2\pi}\int_{-\infty}^\infty F_+(t)\left[\frac{1}{x-t}\exp\left\{-\frac{U(x-t)}{2\nu}-\alpha|x-t|\right\}\right.$$
$$\left.-\frac{U}{2\nu}K_0\left(\frac{U|x-t|}{2\nu}\right)-\frac{U}{2\nu}\operatorname{sgn}(x-t)\,K_1\left(\frac{U|x-t|}{2\nu}\right)\right]dt=\frac{a_1\lambda U}{2\nu}F_+(x)+u_-(x)$$
$$\text{for all } x. \tag{3.4}$$

Equation (3.4) is in the form needed for application of the Fourier transform.

We define

$$\mathrm{F}[g(x)]=\bar{g}(w)=\frac{1}{(2\pi)^{\frac{1}{2}}}\int_{-\infty}^\infty e^{ixw}g(x)\,dx, \tag{3.5}$$

and in general $\bar{g}(w)$ will be regular in some interval $\tau_-<\tau<\tau_+$, where $w=\sigma+i\tau$. Applying (3.5) to the integral equation (3.4), and using the convolution theorem

$$\int_{-\infty}^\infty e^{-ixw}\bar{f}(w)\,\bar{g}(w)\,dw=\int_{-\infty}^\infty f(t)\,g(x-t)\,dt,$$

we get

$$\frac{1}{(2\pi)^{\frac{1}{2}}}\int_{-\infty}^\infty U_+\exp\left\{-\frac{Ux}{2\nu}+ixw\right\}dx+\frac{1}{(2\pi)^{\frac{1}{2}}}\bar{F}_+(w)\,\mathrm{F}\left[\frac{1}{x}\exp\left\{-\frac{Ux}{2\nu}-\alpha|x|\right\}\right.$$
$$\left.-\frac{U}{2\nu}K_0\left(\frac{U|x|}{2\nu}\right)-\operatorname{sgn}(x)\frac{U}{2\nu}K_1\left(\frac{U|x|}{2\nu}\right)\right]=\frac{a_1\lambda U}{2\nu}\bar{F}_+(w)+\bar{u}_-(w). \tag{3.6}$$

The values of the various transforms involved in (3.6) and their ranges of existence are as follows:

$$\frac{1}{(2\pi)^{\frac{1}{2}}}\int_{-\infty}^\infty U\exp\left\{-\frac{Ux}{2\nu}+ixw\right\}dx=-\frac{U}{(2\pi)^{\frac{1}{2}}}\left(iw-\frac{U}{2\nu}\right)^{-1}\quad\left(\tau>-\frac{U}{2\nu}\right); \tag{3.7}$$

$$\frac{1}{2\pi}\int_{-\infty}^{\infty}\frac{1}{x}\exp\left\{x\left(iw-\frac{U}{2\nu}\right)-\alpha|x|\right\}dx=\frac{i}{\pi}\tan^{-1}\left\{\left(w+\frac{iU}{2\nu}\right)\Big/\alpha\right\}\quad(\alpha>0)$$

$$\left(\alpha>\tau+\frac{U}{2\nu}>-\alpha\right);\qquad(3.8)$$

$$-\frac{1}{2\pi}\int_{-\infty}^{\infty}\frac{U}{2\nu}K_0\left(\frac{U|x|}{2\nu}\right)e^{ixw}dx=-\frac{1}{2}\frac{U}{2\nu}\left[\left(\frac{U}{2\nu}\right)^2+w^2\right]^{-\frac{1}{2}}\quad\left(\frac{U}{2\nu}>\tau>-\frac{U}{2\nu}\right);\qquad(3.9)$$

$$-\frac{1}{2\pi}\int_{-\infty}^{\infty}\operatorname{sgn}(x)\frac{U}{2\nu}K_1\left(\frac{U|x|}{2\nu}\right)e^{ixw}dx=-\tfrac{1}{2}iw\left[\left(\frac{U}{2\nu}\right)^2+w^2\right]^{-\frac{1}{2}}\quad\left(\frac{U}{2\nu}>\tau>-\frac{U}{2\nu}\right).\qquad(3.10)$$

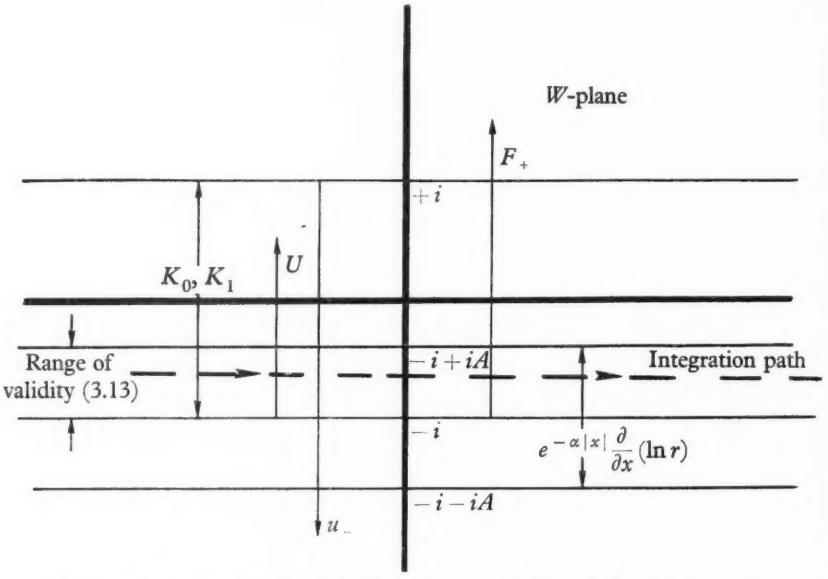

FIGURE 1. Regions of analyticity of the terms of the transformed equation.

Substituting these results into (3.6) we get

$$\bar{F}_+(w)\left[\frac{2}{\pi}\tan^{-1}\left\{\left(w+\frac{iU}{2\nu}\right)\Big/\alpha\right\}+i\frac{a_1\lambda U}{\nu}-\left\{\left(w-\frac{iU}{2\nu}\right)\Big/\left(w+\frac{iU}{2\nu}\right)\right\}^{\frac{1}{2}}\right]$$

$$=\sqrt{\frac{2}{\pi}}U\left(w+\frac{iU}{2\nu}\right)^{-1}-2i\bar{u}_-(w).\qquad(3.11)$$

Finally, if we put†

$$W=\frac{2\nu}{U}w,\quad\Lambda=a_1\frac{U\lambda}{\nu},\quad A=\frac{U\alpha}{2\nu},\qquad(3.12)$$

then

$$\bar{F}_+(W)\left[\frac{2}{\pi}\tan^{-1}\frac{W+i}{A}+i\Lambda-\left(\frac{W-i}{W+i}\right)^{\frac{1}{2}}\right]=\sqrt{\frac{2}{\pi}}\frac{2\nu}{W+i}-2i\bar{u}_-(W),\qquad(3.13)$$

and this equation is to be solved for $\bar{F}_+(W)$.

† Note that Λ is proportional to both the Reynolds number based on the mean free path and, since $\lambda=(\pi\gamma/2)^{\frac{1}{2}}\nu/a$, to the Mach number $M=U/a$, where a is the velocity of sound and γ the ratio of the specific heats.

The ranges of existence of the various terms in (3.13) are indicated in figure 1. It is assumed that $f(x)$ is bounded for $x \to \infty$, so that $F_+(x) \sim e^{-Ux/2\nu}$ and $\overline{F}_+(w)$ exists for $\tau > -iU/2\nu$. Clearly $u \to 0$ as $x \to -\infty$, so that $u_- \sim e^{Ux/2\nu}$, $x \to -\infty$, and hence $\overline{u}_-(w)$ converges for $\tau < iU/2\nu$. The former assumption is based on the fact that $f(x)$ is proportional to the shearing stress on the plate (equation (2.8)), and since the slip solution must reduce to the zero-slip case far downstream, it follows that $f(x) \to 0$ as $x \to \infty$. We use $\mathscr{I}(W)$ for imaginary part of W and from the ranges of validity of the terms of equation (3.13), as depicted in figure 1, we see that the transformed equation holds where

$$-1+A > \mathscr{I}(W) > -1. \tag{3.14}$$

4. Resolution of the transformed equation

To solve (3.13) for $\overline{F}_+(W)$ it is necessary to write it as the sum of terms analytic in the upper and lower half planes. To this end we need to write

$$K(W) = \frac{2}{\pi}\tan^{-1}\frac{W+i}{A} + i\Lambda - \left(\frac{W-i}{W+i}\right)^{\frac{1}{2}} \tag{4.1}$$

as

$$K(W) = \frac{K_+(W)}{K_-(W)}, \tag{4.2}$$

where $K_+(W)$ is analytic for $\mathscr{I}(W) > -1$ and $K_-(W)$ is analytic for

$$\mathscr{I}(W) < -1+A.$$

There is a standard method for performing this factorization (see Noble 1958, p. 21). Thus we must consider

$$\begin{aligned} h(W) = \frac{d}{dW}[\ln K(W)] &= \frac{d}{dW}\ln K_+(W) - \frac{d}{dW}\ln K_-(W) \\ &= \frac{(2/\pi)\{A/W'^2 + A^2)\} - i(W'-2i)^{-\frac{1}{2}}W'^{-\frac{3}{2}}}{(2/\pi)\tan^{-1}(W'/A) - i\Lambda - (W'-2i)^{\frac{1}{2}}W'^{-\frac{1}{2}}}, \end{aligned} \tag{4.3}$$

where $W' = W+i$. Application of Cauchy's theorem to a rectangular region lying within the strip of regularity of $h(W)$, $a > \mathscr{I}(W) > b$, yields

$$h(W) = \frac{1}{2\pi i}\int_{-\infty+ib}^{\infty+ib}\frac{h(s)}{s-W}\,ds - \frac{1}{2\pi i}\int_{-\infty+ia}^{\infty+ia}\frac{h(s)}{s-W}\,ds,$$

where the first and second members of the right-hand side are regular in $\mathscr{I}(W) > b$, $\mathscr{I}(W) < a$, respectively. Hence we have

$$\frac{d}{dW}\ln K_+(W) = \frac{1}{2\pi i}\int_{-\infty+ib}^{\infty+ib}\frac{h(s)}{s-W}\,ds, \quad \frac{d}{dW}\ln K_-(W) = \frac{1}{2\pi i}\int_{-\infty+ia}^{\infty+ia}\frac{h(s)}{s-W}\,ds. \tag{4.4}$$

The strip of regularity of $h(W)$, $b < \mathscr{I}(W) < a$, in fact coincides with the region of analyticity of $K(W)$, $-1 < \mathscr{I}(W) < -1+A$, since by suitable choice of the branches of $(W+i)^{\frac{1}{2}}$ and $(W-i)^{\frac{1}{2}}$ we can ensure that the denominator of $h(W)$ in equation (4.3) is non-zero everywhere.

The singular points of $h(W)$ are at $W' = \pm iA$, $2i$, 0, and the paths of integration for the integrals in (4.4) lie between $W' = 0$ and $W' = iA$, as seen in figure 1. The contour integral for $(d/dW')\ln K_+(W')$ can be deformed into a path along the cut from $W' = 0$ to $\mathscr{I}(W') = -\infty$, figure 2. After reduction in the limit $A \to 0$, this integral becomes

$$\frac{d}{dW}\{\ln K_+(W)\} = -\frac{1}{2(W+i)} + \frac{\Lambda}{\pi}\int_1^\infty \frac{2(r^2-1)^{\frac{1}{2}} + (2+\Lambda^2)\,r - \Lambda^2}{\Lambda^2(\Lambda^2+4)\,r^2 - 2(2+\Lambda^2)\,\Lambda^2 r + 4 + \Lambda^4}\,\frac{dr}{(r^2-1)^{\frac{1}{2}}(ir+W)}. \tag{4.5}$$

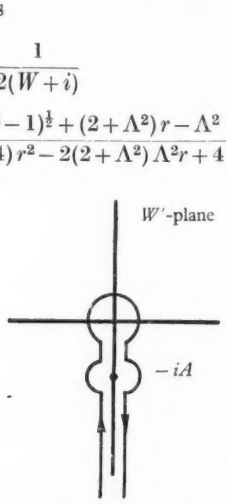

FIGURE 2. Contour integral for resolution of the transformed equation.

The roots of the quadratic form in the denominator of the integrand are given by

$$\alpha_1, \alpha_2 = \frac{2+\Lambda^2}{4+\Lambda^2} \pm \frac{4i}{\Lambda(4+\Lambda^2)}, \tag{4.6}$$

and in terms of these parameters we find that (4.5) yields

$$\frac{d}{dW}\{\ln K_+(W)\} = -\frac{1}{2(W+i)} + \frac{1}{4\pi i}\,\frac{1}{(W+i\alpha_1)(W+i\alpha_2)}\left[\frac{8}{\Lambda(4+\Lambda^2)}\ln\{\tfrac{1}{2}\Lambda^2(1-iW)\}\right.$$
$$\left. + 2\pi\left(iW - \frac{2+\Lambda^2}{4+\Lambda^2}\right) - \frac{4i}{\Lambda(4+\Lambda^2)}\,\frac{(2+\Lambda^2)\,iW - \Lambda^2}{(1+W^2)^{\frac{1}{2}}}\ln\{-[iW + i(1+W^2)^{\frac{1}{2}}]\}\right]. \tag{4.7}$$

The integrated form of (4.7) is

$$K_+(W) = (1-iW)^{-\frac{1}{2}}\exp\left[-\frac{1}{\pi}\,\frac{2}{\Lambda(4+\Lambda^2)}\int_{-1}^{-iW}\frac{\ln\frac{1}{2}\Lambda^2(1+t)}{(t+\alpha_1)(t+\alpha_2)}\,dt\right]$$
$$\times[-\Lambda^2(4+\Lambda^2)\,W^2 - 2i\Lambda^2(2+\Lambda^2)\,W + 4 + \Lambda^4]^{\frac{1}{4}}$$
$$\times\exp\left[-\frac{1}{\pi}\,\frac{1}{\Lambda(4+\Lambda^2)}\int_{i\pi}^{\cosh^{-1}-iW}\frac{(2+\Lambda^2)\cosh\theta + \Lambda^2}{(\cosh\theta+\alpha_1)(\cosh\theta+\alpha_2)}\,d\theta\right]. \tag{4.8}$$

A similar integration can be carried out to find $K_-(W)$, or more simply, it can be found using the relation

$$K_-(W) = \frac{K_+(W)}{K(W)}.$$

Once $K(W)$ has been resolved into parts regular in the upper and lower half planes, we can write the transformed equation (3.13) as

$$\overline{F}_+(W)\,K_+(W)-\sqrt{\frac{2}{\pi}}\,2\nu\frac{K_-(-i)}{W+i}=\sqrt{\frac{2}{\pi}}\,2\nu\frac{K_-(W)-K_-(-i)}{W+i}-2i\overline{u}_-(W)\,K_-(W), \tag{4.9}$$

in which the left-hand side is regular for $\mathscr{I}(W)>-1$ and the right-hand side is regular for $\mathscr{I}(W)<-1+A$. Hence, both sides having the common region of validity, $-1<\mathscr{I}(W)<-1+A$, each must be equal to the same entire function of W. Moreover, $K_-(W)\to$ constant as $W\to\infty$, and, since $u_-(x)$ approaches a constant value as $x\to 0$, $\overline{u}_-(W)\sim 1/W$ for $W\to\infty$; hence the right-hand side of (4.9) approaches zero algebraically as $W\to\infty$, and the entire function represented by (4.9) must in fact be zero. Thus finally we have

$$\overline{F}_+(W)=\sqrt{\frac{2}{\pi}}\,2\nu\frac{K_-(-i)}{(W+i)\,K_+(W)} \tag{4.10}$$

and

$$\begin{aligned}F_+(x)&=\frac{U}{\pi}K_-(-i)\int_{-\infty}^{\infty}\frac{\exp(-iUxW/2\nu)}{(W+i)\,K_+(W)}\,dW\\&=\frac{U}{\pi}\left[-\left(\frac{W+i}{-2i}\right)^{\frac{1}{2}}K_+(W)\right]_{W=-i}\int_{-\infty}^{\infty}\frac{\exp(-iUxW/2\nu)}{(W+i)\,K_+(W)}\,dW,\end{aligned} \tag{4.11}$$

since, from (4.1) and (4.2),

$$K_-(-i)=\lim_{W\to -i}\left[-K_+(W)\left(\frac{W+i}{-2i}\right)^{\frac{1}{2}}\right].$$

Equation (4.11) represents the full solution of the integral equation and hence of the problem. However the integration indicated in (4.11) cannot, in general, be carried out, and therefore it becomes necessary to study approximate forms of the solution for particular ranges of the variables. Thus, it is possible to obtain expressions valid for small and large values of x, using Tauberian theorems that relate a function and its transform for large and small values of its argument.

5. Asymptotic forms of the solution

We obtain an approximation to $F_+(x)$ for large positive x by studying the expansion of $\overline{F}_+(W)$ about its singularity with largest imaginary part (cf. Carslaw & Jaeger 1947, p. 279). This is at $W=-i$, i.e. at $W'=0$. From the solution (4.8) for $K_+(W)$, we can derive the expansion

$$\begin{aligned}\frac{1}{W'K_+(W')}&=\frac{1}{\sqrt{2}}(-iW')^{-\frac{1}{2}}\\&\quad\times\left[1-\frac{\Lambda}{\sqrt{2}}(-iW')^{\frac{1}{2}}-\frac{\Lambda}{2\pi}iW'\ln(-\tfrac{1}{2}\Lambda^2iW')-\tfrac{1}{2}\Lambda^2iW'+\ldots\right]\end{aligned} \tag{5.1}$$

for small W'. So, from (4.11), we get

$$F_+(x)=-\frac{U}{\pi}e^{-Ux/2\nu}\int_{-\infty}^{\infty}\frac{\exp(-iUxW'/2\nu)}{W'K_+(W')}\,dW'. \tag{5.2}$$

There are a number of Tauberian theorems that relate a transformed expansion to its original (see Doetsch 1937, p. 265), but because of the mixed nature of the terms in (5.1) none of these theorems applies directly. However, they can be used formally, and the result is

$$F_+(x) \sim \frac{2U}{\sqrt{\pi}}\left(\frac{Ux}{\nu}\right)^{-\frac{1}{4}} e^{-Ux/2\nu}\left[1-\frac{\Lambda^2}{2}\left(\frac{\nu}{Ux}\right)+\frac{\Lambda}{2\pi}\left(\ln\frac{Ux}{2\nu}-2+2\ln 2+C\right)\frac{\nu}{Ux}+\ldots\right], \tag{5.3}$$

where C = Euler's constant = 0·577 ..., for $x \to \infty$. That (5.3) is indeed the correct expansion can be proved directly from (5.2) (Carlsaw & Jaeger 1947, p. 280). The procedure is to integrate along a contour of the type indicated in figure 3, in which the horizontal path is a distance $\epsilon_1 < \Lambda$ above the real axis, and we choose the radius of the circular path about the singularity at $W' = 0$ to be ϵ_2/x. In the limit $x \to \infty$, the integrals along the horizontal portions and about the circle vanish asymptotically and the vertical path yields the contribution written in (5.3). This method may be applied to obtain any further number of terms in the asymptotic expansion for large x.

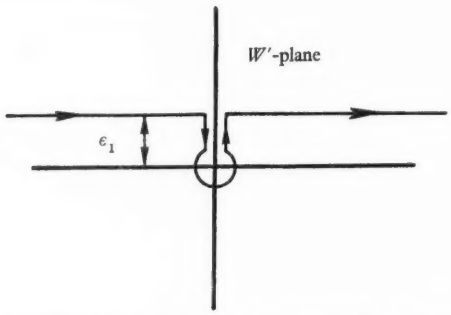

FIGURE 3. Integration path for the asymptotically large x expansion.

The other expansion required is for small positive x and this we obtain by investigating the transformed function for large W. We will evaluate the leading term only.† From (4.8) we get, for $|W| \to \infty$, $\mathscr{I}(W) > 0$,

$$K_+(W) \sim \frac{1}{i}[\Lambda^2(4+\Lambda^2)]^{\frac{1}{4}} \exp\left[-\frac{1}{\pi}\frac{2}{\Lambda(4+\Lambda^2)}\int_{-1}^{\infty}\frac{\ln\frac{1}{2}\Lambda^2(1+t)}{(t+\alpha_1)(t+\alpha_2)}\,dt\right]$$
$$\times \exp\left[-\frac{1}{\pi}\frac{1}{\Lambda(4+\Lambda^2)}\int_{i\pi}^{\infty}\frac{(2+\Lambda^2)\cosh\theta+\Lambda^2}{(\cosh\theta+\alpha_1)(\cosh\theta+\alpha_2)}\,d\theta\right]. \tag{5.4}$$

Moreover, we find on integration that

$$\exp\left[-\frac{1}{\pi}\frac{2}{\Lambda(4+\Lambda^2)}\int_{-1}^{\infty}\frac{\ln\frac{1}{2}\Lambda^2(1+t)}{(t+\alpha_1)(t+\alpha_2)}\,dt\right] \sim \left\{\frac{\Lambda}{(4+\Lambda^2)^{\frac{1}{2}}}\right\}^{[\tan^{-1}(2/\Lambda)-\pi]/2\pi}$$

† Closer study shows that difficulties may occur in obtaining further terms of the series if Λ is large (the boundary-layer limit), due to non-uniformities when $W \to \infty$, $\Lambda \to \infty$.

and

$$\exp\left[-\frac{1}{\pi}\frac{1}{\Lambda(4+\Lambda^2)}\int_{i\pi}^{\infty}\frac{(2+\Lambda^2)\cosh\theta+\Lambda^2}{(\cosh\theta+\alpha_1)(\cosh\theta+\alpha_2)}\,d\theta\right]$$
$$\sim\left\{\frac{\Lambda}{(4+\Lambda^2)^{\frac{1}{2}}}\right\}^{[\pi-\tan^{-1}(2/\Lambda)]/2\pi}\exp\left\{\frac{1}{2\pi i}\left[L_2\left(\frac{\Lambda}{\Lambda+2i}\right)-L_2\left(\frac{\Lambda}{\Lambda-2i}\right)\right]\right\}$$
$$=\left\{\frac{\Lambda}{(4+\Lambda^2)^{\frac{1}{2}}}\right\}^{[\pi-\tan^{-1}(2/\Lambda)]/2\pi}\exp\left[\frac{1}{\pi}\sum_{n=1}^{\infty}\frac{1}{n^2}\left\{\frac{\Lambda}{(4+\Lambda^2)^{\frac{1}{2}}}\right\}^n\sin\left(n\tan^{-1}\frac{2}{\Lambda}\right)\right],$$

where $L_2(z)$ is the dilogarithmic function

$$L_2(z)=\int_0^z\frac{\ln s}{1-s}\,ds.$$

Hence, altogether, in the limit $|W|\to\infty$, we have

$$K_+(W)\sim -i\Lambda\left\{\frac{\Lambda}{(4+\Lambda^2)^{\frac{1}{2}}}\right\}^{-\frac{1}{2}}\exp\left[-\frac{1}{\pi}\sum_{n=1}^{\infty}\frac{1}{n^2}\left\{\frac{\Lambda}{(4+\Lambda^2)^{\frac{1}{2}}}\right\}^n\sin\left(n\tan^{-1}\frac{2}{\Lambda}\right)\right]. \quad (5.5)$$

Using the inversion formula (5.2) and the appropriate Tauberian theorem (Doetsch 1937, p. 269), (5.5) yields the result†

$$F_+(0)=2U\Lambda^{-1}\left\{\frac{\Lambda}{(4+\Lambda^2)^{\frac{1}{2}}}\right\}^{\frac{1}{2}}\exp\left[-\frac{1}{\pi}\sum_{n=1}^{\infty}\frac{1}{n^2}\left\{\frac{\Lambda}{(4+\Lambda^2)^{\frac{1}{2}}}\right\}^n\sin\left(n\tan^{-1}\frac{2}{\Lambda}\right)\right]. \quad (5.6)$$

Finally, we can obtain an expansion of $F_+(x)$ valid for small values of Λ. Thus, from (4.8), we obtain the following expression for $\Lambda\to 0$,

$$K_+(W)\simeq(2\Lambda)^{\frac{1}{2}}\frac{\{(1/\Lambda^2)-W^2\}^{\frac{1}{4}}}{(1-iW)^{\frac{1}{2}}}\exp\left\{\frac{1}{8\pi}\int_0^{-4\tan^{-1}i\Lambda W}\ln(2\sin\tfrac{1}{2}\theta)\,d\theta\right\}.$$

Substituting into (5.2) this gives

$$F_+(x)\simeq\frac{U}{\pi}\frac{1}{(2\Lambda)^{\frac{1}{2}}}\int_{-i\infty}^{i\infty}\frac{i\exp\left[\dfrac{Ux\xi}{2\nu}-\dfrac{1}{8\pi}\displaystyle\int_0^{4\tan^{-1}\Lambda\xi}\ln(2\sin\tfrac{1}{2}\theta)\,d\theta\right]}{\xi^{\frac{1}{2}}\{\xi^2+(1/\Lambda^2)\}^{\frac{1}{4}}}\,d\xi \quad (5.7)$$

approximately, where $\xi=iW$. The path of integration lies to the right of the singularity of the integrand at $\xi=0$. Numerical integration of (5.7) has been carried out for a series of values of the relevant parameter $Ux/2\nu\Lambda=x/(a_1\lambda)$, and the results will be discussed in the next section.

6. Shearing force and slip velocity

The approximate expressions developed in §5 enable us to find the plate shearing stress (and hence the slip velocity) directly without further integration, using the result given in §2; namely that

$$\left|\frac{\partial u}{\partial y}\right|=\frac{U}{2\nu}F(x)\,e^{Ux/2\nu}\quad(y=0,x>0). \quad (6.1)$$

† We remark here that the exponential term in (5.6) is never far from unity, and, to within approximately 5%, $F_+(0)=2U\Lambda^{-1}\{\Lambda/(4+\Lambda^2)^{\frac{1}{2}}\}^{\frac{1}{2}}$.

First, for $x \to \infty$, we get from (5.3)

$$\left|\frac{\partial u}{\partial y}\right| \sim \frac{U^2}{\sqrt{\pi\nu}}\left(\frac{Ux}{\nu}\right)^{-\frac{1}{2}}\left[1-\frac{a_1^2}{2}\left(\frac{U\lambda^2}{\nu x}\right)+\frac{a_1\lambda}{2\pi x}\left(\ln\frac{Ux}{2\nu}-0{\cdot}04\right)+\ldots\right], \tag{6.2}$$

in which we have replaced Λ by $a_1(U\lambda/\nu)$, and have evaluated the numerical coefficient in the last term. Defining

$$c_f = \frac{\nu\,|\partial u/\partial y|}{\frac{1}{2}U^2},$$

we get

$$c_f \sim \frac{2}{\sqrt{\pi}}\left(\frac{\nu}{Ux}\right)^{\frac{1}{2}}\left[1-\frac{a_1^2}{2}\left(\frac{U\lambda^2}{\nu x}\right)+\frac{a_1\lambda}{2\pi x}\left(\ln\frac{Ux}{2\nu}-0{\cdot}04\right)+\ldots\right]. \tag{6.3}$$

Slip boundary-layer theory gives the following expression for the skin-friction coefficient (Mirels 1952)

$$c_{fbl} = \frac{2}{\sqrt{\pi}}\left(\frac{\nu}{Ux}\right)^{\frac{1}{2}}\left[1-\frac{a_1^2}{2}\left(\frac{U\lambda^2}{\nu x}\right)+O\left(\frac{U\lambda^2}{\nu x}\right)^2\right], \tag{6.4}$$

so that the full Oseen equations yield a correction to the zero-slip skin-friction coefficient of the first order in λ, whereas the lowest-order term in the boundary-layer result is of order λ^2. In fact the former term is dominant for $U\lambda/\nu \ll 1$, but becomes negligible for $U\lambda/\nu \to \infty$. Since $\lambda \propto M/(U/\nu)$, where M is the Mach number of the free-stream flow, an alternative statement is that the additional terms arising from use of the full equations of motion are important in estimating the plate shearing stress for small Mach numbers, while for $M \to \infty$ boundary-layer theory gives the correct value.† Within the range of applicability of the present analysis, since we are treating the incompressible case (low Mach number), it therefore follows that boundary-layer analysis does not give a satisfactory estimate of the shearing stress, even far downstream, where slip effects are small (but not negligible). Since the slip condition is $u' = \lambda(\partial u/\partial y)$, $y = 0$, similar statements apply to values of the velocity at the plate surface.

For $x \to 0$ we have the result (equations (5.6) and (6.1))

$$u+U = a_1\lambda\left|\frac{\partial u}{\partial y}\right| \to U\left\{\frac{\Lambda}{(4+\Lambda^2)^{\frac{1}{2}}}\right\}^{\frac{1}{2}}\exp\left[-\frac{1}{\pi}\sum_{n=1}^{\infty}\frac{1}{n^2}\left\{\frac{\Lambda}{(4+\Lambda^2)^{\frac{1}{2}}}\right\}^n\sin\left(n\tan^{-1}\frac{2}{\Lambda}\right)\right] \tag{6.5}$$

and

$$c_f \to \frac{2}{\Lambda}\left\{\frac{\Lambda}{(4+\Lambda^2)^{\frac{1}{2}}}\right\}^{\frac{1}{2}}\exp\left[-\frac{1}{\pi}\sum_{n=1}^{\infty}\frac{1}{n^2}\left\{\frac{\Lambda}{(4+\Lambda^2)^{\frac{1}{2}}}\right\}^n\sin\left(n\tan^{-1}\frac{2}{\Lambda}\right)\right]. \tag{6.6}$$

For $\Lambda \to \infty$, (6.5) yields

$$U+u = U$$

in agreement with boundary-layer theory (Mirels 1952), and for $\Lambda \to 0$

$$U+u \to U(\tfrac{1}{2}\Lambda)^{\frac{1}{2}}, \quad c_f \to U(\tfrac{1}{2}\Lambda)^{-\frac{1}{2}}, \tag{6.7}$$

so that in the limit of zero slip we regain the normal result, namely $c_f \to \infty$ as $x \to 0$.

† The general conclusion, that with a slip-boundary condition the boundary-layer equations become valid in the limit M or $U\lambda/\nu \to \infty$, can in fact be deduced from the complete Oseen equations (2.1).

For small Λ (i.e. for small values of the Mach number M) we can present results valid for all x. Thus from (5.7), using (6.1), we obtain the approximate expression for c_f:

$$c_f = \frac{1}{\pi(2\Lambda)^{\frac{1}{2}}}\int_{-i\infty}^{i\infty} \frac{i\exp\left\{-\frac{1}{8\pi}\int_0^{4\tan^{-1}\Lambda\xi} \ln(2\sin\tfrac{1}{2}\theta)\,d\theta\right\}}{\xi^{\frac{1}{2}}\{\xi^2+(1/\Lambda^2)\}^{\frac{1}{4}}} \exp\left(-\frac{Ux\xi}{2\nu}\right) d\xi. \quad (6.8)$$

The relationship (6.8) between $\pi(\frac{1}{2}\Lambda)^{\frac{1}{2}}c_f$ and $Ux/2\nu\Lambda = x/2a_1\lambda$ evaluated by means of a high-speed electronic computer is plotted in figure 4. Shown also is the zero-slip result, for which $\pi(\frac{1}{2}\Lambda)^{\frac{1}{2}}c_f = \sqrt{\pi(x/2a_1\lambda)^{-\frac{1}{2}}}$. Increase of the shear above the zero-slip value for $x/2a_1\lambda$ greater than about 0·3 should be interpreted as a result of viscous interaction effects of order higher than included in boundary-layer theory rather than as a direct consequence of slip. The boundary-layer result is approached as we let Λ (or the Mach number) approach infinity, and in this limit the shear force is always less than the no-slip shear.

7. Displacement thickness

The total displacement thickness

$$\delta^* = -\int_0^\infty \frac{u}{U}\,dy \quad (7.1)$$

is infinite in the case of any semi-infinite body. However, we can find the displacement thickness corresponding to the transverse wave part of the solution $\mathbf{v}_2+\mathbf{v}_2^*$ (equation (2.5)), and in fact this gives a boundary-layer profile, the potential flow about which yields the longitudinal wave $\mathbf{v}_1$. We should make it clear that the boundary layer calculated in this way is not a line of demarcation between potential and rotational viscous flow, since at the leading edge, near or on the plate, neither potential nor vorticity waves dominate. Moreover, as will be shown, this displacement thickness is zero ahead of the plate, while in fact there is a spreading of vorticity upstream of the plate, as indicated by the fundamental solution $\mathbf{v}_2$ for the vorticity (equation (2.5)).

From (2.5) and (2.6) we have for the displacement thickness defined in this way

$$\delta^* = \frac{e^{Ux/2\nu}}{2\pi U}\int_0^\infty F(t)\int_0^\infty \left[\frac{U}{2\nu}K_0\left(\frac{Ur_t}{2\nu}\right) - \frac{U}{2\nu}\frac{x-t}{r_t}K_1\left(\frac{Ur_t}{2\nu}\right)\right] dy\,dt, \quad (7.2)$$

where $$r_t = \{(x-t)^2+y^2\}^{\frac{1}{2}},$$

or
$$\delta^* = \frac{e^{Ux/2\nu}}{2\pi U}\int_0^\infty F(t)\left\{\frac{U}{2\nu}\left[\left(\frac{\nu|x-t|}{U}\right)^{\frac{1}{2}}\Gamma(\tfrac{1}{2})K_{-\frac{1}{2}}\left(\frac{U|x-t|}{2\nu}\right)\right.\right.$$
$$\left.\left. + (x-t)\left(\frac{\nu}{U|x-t|}\right)^{\frac{1}{2}}\Gamma(\tfrac{1}{2})K_{\frac{1}{2}}\left(\frac{U|x-t|}{2\nu}\right)\right]\right\} dt$$
$$= \frac{e^{Ux/2\nu}}{4U}\int_0^\infty F(t)\left[\exp\left\{-\frac{U|x-t|}{2\nu}\right\} + \operatorname{sgn}(x-t)\exp\left\{-\frac{U|x-t|}{2\nu}\right\}\right] dt. \quad (7.3)$$

For $x < 0$ this is zero, while for $x > 0$ we have

$$\delta^* = \frac{1}{4U}\int_0^x F(t)\,e^{Ut/2\nu}\,dt. \quad (7.4)$$

Asymptotic forms of δ^* for $x \to \infty$ and $x \to 0$ can be obtained using the results derived in §5. For $x \to \infty$ care has to be exercised in evaluating the integral, and to avoid convergence difficulties, we write

$$\begin{aligned}\int_0^x F(t)\, e^{Ut/2\nu}\, dt &= \int_0^x F(\infty)\, e^{Ut/2\nu}\, dt \\ &\quad + \int_0^\infty [F(t) - F(\infty)]\, e^{Ut/2\nu}\, dt - \int_x^\infty [F(t) - F(\infty)]\, e^{Ut/2\nu}\, dt \\ &= \int_0^x F(\infty)\, e^{Ut/2\nu}\, dt - \int_x^\infty [F(t) - F(\infty)]\, e^{Ut/2\nu}\, dt \\ &\quad + \lim_{w \to -iU/2\nu} \left[(2\pi)^{\frac{1}{2}} \overline{F}(w) - \int_0^\infty F(\infty)\, e^{itw}\, dt \right]. \end{aligned} \tag{7.5}$$

Using the expansion (5.3) this yields

$$\begin{aligned}\delta^*(x) \sim -a_1\lambda + \sqrt{\frac{2}{\pi}\frac{2\nu}{U}} \left(\frac{Ux}{2\nu}\right)^{\frac{1}{2}} \\ \times \left\{ 1 + \frac{a_1^2}{2}\left(\frac{U\lambda^2}{\nu x}\right) - \frac{a_1\lambda}{2\pi x}\left(\ln\frac{Ux}{2\nu} - 0{\cdot}04\right) + \ldots \right\} \quad (x \to \infty), \end{aligned} \tag{7.6}$$

and far enough downstream this gives the usual boundary-layer result (Schaaf & Chambré 1957), namely that the boundary-layer thickness is a mean free path thinner than the zero-slip value.

The expansion for δ^* near $x = 0$ is obtained directly from (5.6):

$$\begin{aligned}\delta^* &\simeq \frac{1}{2U}\int_0^x 2U\Lambda^{-1} \left\{ \frac{\Lambda}{(4+\Lambda^2)^{\frac{1}{2}}} \right\}^{\frac{1}{2}} \exp\left[\frac{1}{\pi} \sum_{n=1}^{\infty} \frac{1}{n^2} \left\{ \frac{\Lambda}{(4+\Lambda^2)^{\frac{1}{2}}} \right\}^n \sin\left(n \tan^{-1}\frac{2}{\Lambda} \right) \right] dt \\ &= \frac{x}{\Lambda} \left\{ \frac{\Lambda}{(4+\Lambda^2)^{\frac{1}{2}}} \right\}^{\frac{1}{2}} \exp\left[\frac{1}{\pi} \sum_{n=1}^{\infty} \frac{1}{n^2} \left\{ \frac{\Lambda}{(4+\Lambda^2)^{\frac{1}{2}}} \right\}^n \sin\left(n \tan^{-1}\frac{2}{\Lambda} \right) \right], \end{aligned} \tag{7.7}$$

again agreeing with boundary-layer theory as $\Lambda \to \infty$ (Schaaf & Chambré 1957).

8. Experimental evidence

As has been discussed in §1, it appears essential that experimental checks on slip-flow analyses be carried out under low subsonic incompressible-flow conditions. Moreover, the present theory has been shown to give results essentially different from past work, based on boundary-layer approximations, in the low Mach number range.

Unfortunately, very little experimental work has been carried out in this régime and to the author's knowledge the only relevant study is that carried out by Sherman (1952) in measurements of the drag of flat plates in a low-density subsonic airstream. To be able to compare our results with such experiments, an integration of the expression for the shearing stress on the plate has to be made. Such an integration has been carried out graphically for the case Λ small (low Mach number) from figure 4. The results are shown in figure 5 in terms of a

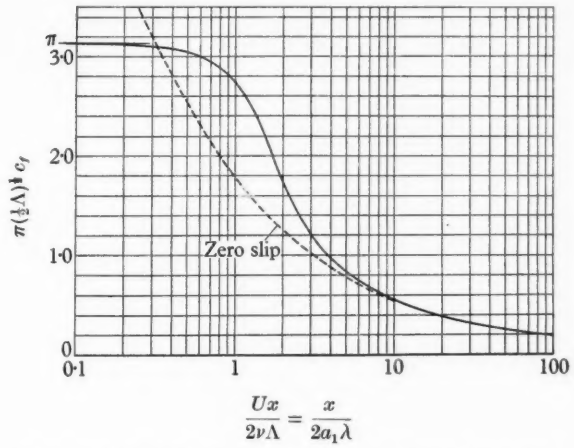

FIGURE 4. Skin-friction coefficient distribution for Λ small.

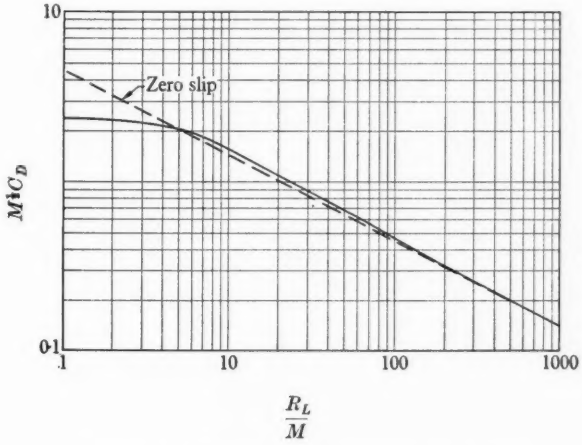

FIGURE 5. Drag coefficient variation for Λ small.

Reynolds number R_L based on an integration length from $x = 0$ to $x = L$ along the plate and a drag coefficient defined by

$$C_D = \frac{2}{L}\int_0^L c_f \, dx.$$

It will be seen from the figure that significant departures from the no-slip cases are not predicted until $R_L/M < 4$ approximately. In Sherman's experimental work the smallest value of R_L/M was 6 and thus marked effects of slip should not be visible in his low-speed data. In view of experimental errors, the corrections necessary to allow for compressibility and for the finite length of the plates (Kuo 1953) and for the approximations of linearized theory (Lewis & Carrier

1949), no observations as to the validity of this analysis or those of other slip-flow theories can be made. It is desirable and probably essential not only that experiments at lower Reynolds numbers be made, but that experiments on the local modifications of the flow due to slip (such as the change in plate shearing stress c_f) be undertaken in order that a definite conclusion be reached.

REFERENCES

Carslaw, H. S. & Jaeger, J. C. 1947 *Operational Methods in Applied Mathematics.* Oxford University Press.

Doetsch, G. 1937 *Theorie und Anwendung der Laplace-Transformation.* Berlin: Springer.

Donaldson, C. du P. 1949 An approximate method of estimating the incompressible laminar boundary-layer characteristics in slipping flow. *NACA RM* no. L9602.

Kuo, Y. H. 1953 On the flow of an incompressible viscous fluid past a flat plate at moderate Reynolds numbers. *J. Math. Phys.* **32**, 83.

Lagerstrom, P. A. & Cole, J. D. 1955 Examples illustrating expansion procedures for the Navier–Stokes equations. *J. Rat. Mech. Anal.* **4**, 817.

Lagerstrom, P. A., Cole, J. D. & Trilling, L. 1949 Problems in the theory of viscous compressible fluids. *GALCIT report.*

Laurmann, J. A. 1958 Slip flow over a short flat plate. *First International Symposium on Rarefied Gas Dynamics, Nice.* (Published by Pergamon Press, 1960.)

Lewis, J. A. & Carrier, G. F. 1949 Some remarks on the flat plate boundary-layer. *Quart. Appl. Math.* **7**, 228.

Mirels, H. 1952 Estimate of slip effects on compressible laminar boundary-layer skin friction. *NACA TN* 2609.

Noble, B. 1958 *Methods Based on the Wiener-Hopf Technique.* London: Pergamon Press.

Probstein, R. F. 1960 Shock-wave and flow field development in hypersonic re-entry. *Amer. Rocket Soc. Semi-Annual Meeting, Los Angeles, May.*

Schaaf, S. A. & Chambré, P. 1957 Flow of rarefied gases. *High Speed Aerodynamics and Jet Propulsion*, vol. III, sect. 8. Princeton University Press.

Sherman, F. S. 1952 Skin friction in subsonic low density gas flow. *Univ. Calif. Inst. Engng Res. Rep.* no. He-150-105 (1952). Also *J. Aero. Sci.* **21** (1954), 85.

Sherman, F. S. & Talbot, L. 1958 Experiment versus kinetic theory for rarefied gases. *First International Symposium on Rarefied Gas Dynamics, Nice.* (Published by Pergamon Press, 1960.)

Yang, H. & Lees, L. 1956 Rayleigh's problem at low Mach numbers according to the kinetic theory of gases. *J. Math. Phys.* **35**, 195.

Equilibrium layers and wall turbulence

By A. A. TOWNSEND
Emmanuel College, Cambridge

(Received 5 December 1960)

In turbulent flow past rigid boundaries, there can be distinguished regions close to the wall in which the local rates of energy production and dissipation are so large that aspects of the turbulent motion concerned with these processes are determined almost solely by the distribution of shear stress within the region and are independent of conditions outside it. These regions are here called equilibrium layers because of the equilibrium existing between local rates of energy production and dissipation. Three kinds of equilibrium layer have been studied experimentally, the constant-stress layer, the transpiration layer and the zero-stress layer, but there are other possible forms. One that is of importance in the theory of self-preserving flow in boundary layers and in diffusers is the 'linear-stress' layer in which the stress increases linearly with distance from the wall. The properties of these various equilibrium layers are considered and the distributions of mean velocity are derived from the equation for the turbulent kinetic energy and certain assumptions of flow similarity.

The theory of self-preserving wall flow, usually expressed as a combination of the law of the wall and the defect law, assumes compatibility between the outer flow and the equilibrium layer, and the course of development depends on the kind of equilibrium layer. Earlier work by the author, which assumed the defect law, is only valid if the whole of the equilibrium layer is a constant-stress layer and this is not true in strong adverse pressure gradients. A consistent theory is developed for these flows by assuming a 'linear-stress' layer, and the solutions show the relation between flows of finite stress and of zero stress and provide a plausible explanation of the phenomenon of downstream instability observed by Clauser. Self-preserving flow in wedges is treated on similar lines.

1. Introduction

So much has been written about the defects of the mixing-length theories of turbulent flow that it can be forgotten that the momentum-transfer form of this theory provides a simple and accurate description of the mean flow near a rigid boundary, but the usefulness of this limited success depends on establishing the conditions for its validity. The more fundamental objections to the general validity of the mixing-length approximation concern not so much the crudity of the assumed mixing process as the dependence of mixing length and eddy transport on local conditions in the flow, and they are supported by observations that the turbulent kinetic energy at a point may depend as much on transport processes from remote parts of the flow as on local production and

dissipation. These objections that a turbulent flow is an integrated whole and not an assembly of quasi-independent flows do not apply to important aspects of the flow near a rigid boundary where the balance of turbulent kinetic energy is virtually unaffected by the nature of the flow in adjacent regions. Layers in which these conditions are satisfied to an acceptable approximation will be called equilibrium layers and it will be assumed that they possess an essential universality of structure which shows itself as a simple dependence of mean velocity gradient on Reynolds stress and distance from the boundary, i.e. apparent validity of the momentum-transfer theory. The best-known example is the constant-stress layer whose structure has been studied in great detail by Laufer (1955), Klebanoff (1956) and many others; other forms are the 'zero-stress' layer (Stratford 1959*a*, *b*) and the equilibrium layers on porous walls with transpiration (e.g. Dorrance & Dore 1954; Black & Sarnecki 1958), but this does not exhaust the possibilities. The purpose of this paper is to set out the necessary conditions for the existence of an equilibrium layer and to derive a slightly more general relation between velocity gradient and shear stress than the mixing-length relation. With this, a unified description of the layers is possible and this description is applied to correct and extend the theory of the development of self-preserving boundary layers in adverse pressure gradients (Townsend 1956*a*, *b*). A similar theory may be developed for self-preserving flow in conical or wedge-shaped diffusers.

2. Notation

Two-dimensional mean flows are described in terms of rectangular co-ordinates with the direction of mean flow in the xOy plane and with the Ox axis either parallel to the wall (in a boundary layer) or in the plane of symmetry (in wedge flow). Axisymmetric mean flow is described in polar co-ordinates with Ox the axis of symmetry. Then

$U, V, 0$ are the components of the mean velocity,
u, v, w are the components of the velocity fluctuation,
$q^2 = u^2 + v^2 + w^2$,
p is the fluctuation from the mean pressure P,
ν is the kinematic viscosity,
ϵ is the local rate of destruction of turbulent energy by viscous forces,
τ is the local Reynolds stress,
K is the Kármán constant,
B is a diffusion constant, and
K_0 is a constant characteristic of zero-stress layers.

Kinematic stresses and pressures are used, i.e. the mechanical quantities divided by the fluid density. Values at the rigid boundary are distinguished by the suffix 0 and in the free stream or on the axis of symmetry by the suffix 1.

3. Energy equilibrium in wall turbulence

In the momentum-transfer form of the mixing-length theory, velocity gradient and Reynolds stress are related by

$$\tau = -\overline{uv} = l^2 \frac{\partial U}{\partial y}\left|\frac{\partial U}{\partial y}\right|, \tag{3.1}$$

where l is a length whose magnitude must be inferred by dimensional or other considerations, and it is fairly well known that an equivalent relation may be derived from the equation for the kinetic energy of the velocity fluctuations assuming local energy and structural equilibrium (Rotta 1953). The equation is, to the usual boundary-layer approximation,

$$U\frac{\partial(\frac{1}{2}\overline{q^2})}{\partial x} + V\frac{\partial(\frac{1}{2}\overline{q^2})}{\partial y} + \overline{uv}\frac{\partial U}{\partial y} + \frac{\partial}{\partial y}(\tfrac{1}{2}\overline{q^2 v} + \overline{pv}) + \epsilon' = 0 \tag{3.2}$$

and $\epsilon' = -\nu[\overline{u\nabla^2 u} + \overline{v\nabla^2 v} + \overline{w\nabla^2 w}]$ is almost identical with the local rate of conversion of turbulent energy to heat, ϵ, in the fully turbulent part of the flow. The first two terms represent the net effect of advection of turbulent energy by the mean flow, and the *first* requirement for an equilibrium layer is that they should be negligible compared with the rate of generation of turbulent energy, $-\overline{uv}(\partial U/\partial y)$. The fourth term is the net rate of energy loss by turbulent diffusive movements and by working against turbulent pressure gradients. If this term is also negligible (the magnitude of this term and its effect on the energy balance is discussed below), the energy equation becomes

$$-\overline{uv}\frac{\partial U}{\partial y} = \epsilon, \tag{3.3}$$

indicating local equilibrium between the production and dissipation of turbulent energy.

Dissipation of energy in turbulent flow depends on working against viscous forces caused by intense velocity gradients of very small scale, and these gradients are maintained by a continuous process of stretching vortex-lines by diffusive movements. Much theoretical and experimental work shows that the rate is independent of the viscosity of the fluid and is determined by the components of the motion that contribute most to the turbulent energy and to the Reynolds stress (Batchelor 1953). Another characteristic of turbulent flow is that prolonged unidirectional shear leads to the attainment of a condition of structural similarity in which velocity fluctuations at different points in the flow are statistically similar.* If this is true, the local motion is specified by a scale of velocity and a scale of length, and it follows from dimensional considerations that

$$\epsilon = (\overline{q^2})^{\frac{3}{2}} L_\epsilon^{-1} \tag{3.4}$$

and that

$$|-\overline{uv}| = a_1 \overline{q^2}, \tag{3.5}$$

* The experimental evidence for structural similarity is derived mostly from measurements of free turbulence or of pipe and channel turbulence outside the equilibrium layers (Townsend 1956*a*, pp. 77, 152, 179, 204, 212, 253), and direct evidence for its existence in equilibrium layers is very incomplete. Some of the difficulties are mentioned in §8.

using $(\overline{q^2})^{\frac{1}{2}}$ as the scale of velocity and L_ϵ as the scale of length. Combining equations (3.3) to (3.5), we get

$$\frac{\partial U}{\partial y} = (a_1^{\frac{3}{2}} L_\epsilon)^{-1} (-\overline{uv})^{\frac{1}{2}}, \tag{3.6}$$

which is equivalent to the mixing-length result if $l = a_1^{\frac{3}{2}} L_\epsilon$.

The relation (3.6) between gradient of mean velocity and Reynolds stress becomes useful if the dissipation length L_ϵ can be inferred as a function of position in the flow, and it is usual to assume that

$$l = a_1^{\frac{3}{2}} L_\epsilon = Ky, \tag{3.7}$$

where $K \approx 0{\cdot}41$ is the Kármán constant. Dimensional reasoning confirms this assumption if (i) the scale of the motion is unaffected by the width of the whole flow, and if (ii) the scale of motion is unaffected by length scales characteristic of the stress distribution in the equilibrium layer. The first of these conditions may be satisfied by requiring that the equilibrium layer occupies only a small fraction of the total width of the flow (a *second* condition for an equilibrium layer), but the second can only be a working hypothesis justified by results. In physical terms, this condition could be satisfied if the Reynolds stress at any point were caused mostly by contributions from eddies whose scales are comparable with distance of the point from the wall since they all extend to the wall and are, in a sense, attached to it. Further, the distribution of Reynolds stress must be such that it can be produced by a possible size distribution of these eddies, and the only layer for which this is obviously possible is one of constant stress.

So far, the effects of lateral transport of turbulent energy, represented by the term $\partial(\frac{1}{2}\overline{q^2 v} + \overline{pv})/\partial y$, have been neglected, but the hypothesis of structural equilibrium indicates that

$$\tfrac{1}{2}\overline{q^2 v} + \overline{pv} = -a_2 (\overline{q^2})^{\frac{3}{2}} \operatorname{sgn}(\partial \overline{q^2}/\partial y), \tag{3.8}$$

where a_2 is a constant of order one, and the sign of $\partial \overline{q^2}/\partial y$ has been introduced to ensure that the net energy flux is down the gradient of turbulent intensity. Substituting in the energy equation and omitting the advection terms, we obtain

$$\frac{\partial U}{\partial y} = \frac{\tau^{\frac{1}{2}}}{Ky}\left(1 - B\frac{y}{\tau}\left|\frac{\partial \tau}{\partial y}\right|\right), \tag{3.9}$$

where $B = \frac{3}{2} K a_2 a_1^{-\frac{3}{2}}$. This equation should be valid in the fully turbulent part of an equilibrium layer, i.e. in a region defined by the conditions

$$\left.\begin{aligned} &\text{(i)} \quad \left|U\frac{\partial(\frac{1}{2}\overline{q^2})}{\partial x} + V\frac{\partial(\frac{1}{2}\overline{q^2})}{\partial y}\right| \ll -\overline{uv}\frac{\partial U}{\partial y}, \\ \text{or} \quad &\tfrac{1}{2}a_1\left|U\frac{\partial \tau}{\partial x} + V\frac{\partial \tau}{\partial y}\right| \ll \tau\frac{\partial U}{\partial y} \\ \text{and} \quad &\text{(ii)} \quad y \ll D, \text{ where } D \text{ is the total width of the flow.} \end{aligned}\right\} \tag{3.10}$$

If these conditions are satisfied, no restrictions need be imposed on the magnitudes of the mean flow acceleration and of the longitudinal pressure gradient.*

* If $B(y/\tau)|\partial\tau/\partial y| > 1$, equation (3.9) is meaningless and no equilibrium layer is possible. This is most unlikely to occur in unidirectional flow.

4. Distributions of mean velocity in equilibrium layers

Within the region determined by the conditions (3.10), mean velocity distributions are obtained by substitution of the stress distribution in equation (3.9). Near an impermeable boundary, the stress distribution may be approximated by

$$\tau = \tau_0 + \alpha y, \tag{4.1}$$

and then integration of the equation (3.9) with this stress distribution leads to

$$U = \frac{\tau_0^{\frac{1}{2}}}{K}\left[\log\frac{(\tau_0+\alpha y)^{\frac{1}{2}}-\tau_0^{\frac{1}{2}}}{(\tau_0+\alpha y)^{\frac{1}{2}}+\tau_0^{\frac{1}{2}}}\right]+\frac{2(1-B\operatorname{sgn}\alpha)}{K}(\tau_0+\alpha y)^{\frac{1}{2}}+U_l. \tag{4.2}$$

The constant of integration, U_l, may be regarded as a slip velocity or velocity of translation that has no effect on the motion in the fully turbulent flow and its magnitude may be expected to depend on the nature of the surface and on τ_0, α and ν. If the surface is smooth and at rest and if the layer is fully turbulent at distances from the wall small compared with τ_0/α, the velocity distribution (4.2) must be identical with the ordinary logarithmic distribution for constant stress

$$U = \frac{\tau_0^{\frac{1}{2}}}{K}\left[\log\frac{\tau_0^{\frac{1}{2}}y}{\nu}+A\right] \tag{4.3}$$

for small values of $\alpha y/\tau_0$. For these small values, (4.2) may be written

$$U = \frac{\tau_0^{\frac{1}{2}}}{K}\left[\log\frac{\alpha y}{4\tau_0}+2(1-B\operatorname{sgn}\alpha)\right]+U_l,$$

and so

$$U_l = \frac{\tau_0^{\frac{1}{2}}}{K}\left[\log\frac{4\tau_0^{\frac{3}{2}}}{\alpha\nu}+A-2(1-B\operatorname{sgn}\alpha)\right]$$

and

$$U = \frac{\tau_0^{\frac{1}{2}}}{K}\left[\log\left(\frac{4\tau_0^{\frac{3}{2}}}{\alpha\nu}\frac{(\tau_0+\alpha y)^{\frac{1}{2}}-\tau_0^{\frac{1}{2}}}{(\tau_0+\alpha y)^{\frac{1}{2}}+\tau_0^{\frac{1}{2}}}\right)+A-2(1-B\operatorname{sgn}\alpha)\right]+\frac{2(1-B\operatorname{sgn}\alpha)}{K}(\tau_0+\alpha y)^{\frac{1}{2}}. \tag{4.4}$$

The condition that the layer is fully turbulent at a distance from the wall small compared with τ_0/α is met if $\alpha y \ll \tau_0$ at the inner edge of the turbulent flow, i.e. at $y = 20\nu/\tau_0^{\frac{1}{2}}$, the requirement being that $\tau_0^{\frac{3}{2}}(\alpha\nu)^{-1} \gg 20$.

The best-known equilibrium layer of this class, the constant-stress layer, has been studied in great detail, especially by Laufer (1955)* and by Klebanoff (1956), and there is little doubt that in it the basic requirements of energy equilibrium and universality of structure are nearly satisfied so far as the motions responsible for momentum and heat transfer are concerned. In most flows along solid walls, a constant-stress layer may be distinguished in which the mean velocity varies in the way given by equation (4.3) but, if the flow is opposed by a strong adverse pressure gradient, the constant-stress region forms only a small part of the total equilibrium layer defined by the conditions (3.10). Even though the

* In a pipe or channel, the stress variation is linear, but the thickness of the equilibrium layer is small compared with the channel width, and, to the same approximation, the stress variation is negligible.

stress gradient depends on the varying flow acceleration as well as the constant (with y) longitudinal pressure gradient, (4.1) is often a satisfactory approximation to the stress distribution and the distribution of mean velocity is given by equation (4.4). This equation takes a more convenient form if $\alpha y \gg \tau_0$ (α necessarily positive):

$$U = \frac{2(1-B)}{K}(\alpha y)^{\frac{1}{2}} + \frac{\tau_0^{\frac{1}{2}}}{K}\left[\log\frac{4\tau_0^{\frac{3}{2}}}{\alpha\nu} + A - 2(1-B)\right], \tag{4.5}$$

which differs from the velocity distribution in a layer of zero wall stress,

$$U = \frac{2}{K_0}(\alpha y)^{\frac{1}{2}} + C(\alpha\nu)^{\frac{1}{3}} \tag{4.6}$$

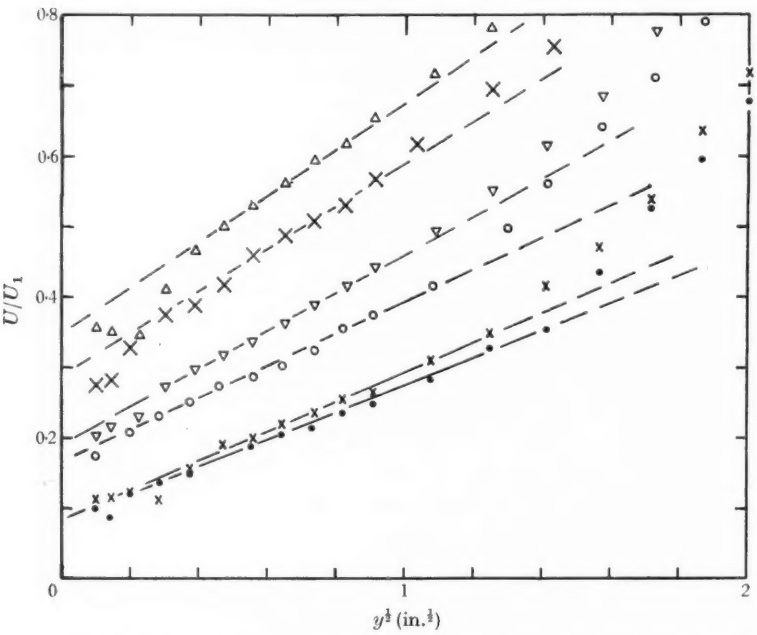

FIGURE 1. Distributions of mean velocity in a turbulent boundary layer near separation (from Schubauer & Klebanoff 1951). ●, $x = 25{\cdot}4$ ft.; ×, $x = 25{\cdot}0$ ft.; ○, $x = 24{\cdot}5$ ft.; ▽, $x = 24{\cdot}0$ ft.; ×, $x = 23{\cdot}0$ ft.; △, $x = 22{\cdot}0$ ft. N.B. Separation occurs between $x = 25{\cdot}5$ ft. and $x = 26{\cdot}0$ ft. Reynolds number $= 10^6$ ft.$^{-1}$ Dashed curves indicate limits to validity of approximations.

(Stratford 1959*a*; Ellison 1960), only in the additive constant which represents a 'slip' velocity at the edge of the layer. Because of the condition $\tau_0^{\frac{3}{2}}(\alpha\nu)^{-1} \gg 20$, equation (4.5) does not hold for very small values of τ_0, and its limiting form as τ_0 approaches zero is slightly different from (4.6). Notice that if the viscosity is very small, i.e. the Reynolds number is large, $\log(4\tau_0^{\frac{3}{2}}/\alpha\nu)$ becomes large and a comparatively small wall stress may produce a large slip velocity.

Experimental evidence of the occurrence of velocity distributions of the form (4.5) can be found in the measurements by Schubauer & Klebanoff (1951) of

flow in a turbulent boundary layer immediately upstream of the position of separation of flow from the surface. In figure 1, some of their measurements of mean velocity are plotted against the square root of distance from the surface, and extensive linear regions are found for the positions, $x = 24{\cdot}5$, $25{\cdot}0$, $25{\cdot}4$ ft., and less extensive ones at positions further upstream. The region of validity of the logarithmic distribution (4.3) does not extend beyond $y = 0{\cdot}08$ in. although the total thickness of the layer is between 6 and 7 in. These measurements may be used to estimate the 'zero-stress' constant K_0, but uncertainty in the magnitudes of the flow accelerations makes the calculation difficult.* Using smoothed values of the acceleration at the wall-end of the linear regions and the measured slopes, it is found that

$$K_0 = 0{\cdot}48 \pm 0{\cdot}03,$$

which may be compared with the value of $0{\cdot}50$ (Townsend 1960) based on measurements by Stratford (1959*b*) in a self-preserving flow of zero wall stress. Since $K_0 = K/(1-B)$, the diffusion constant B is about $0{\cdot}2$ and is of the expected sign.

Another kind of equilibrium layer is found on a porous wall though which fluid is moving with an average velocity V_0. If the longitudinal pressure gradient is not too large, the acceleration of the mean flow will also be small and the momentum equation reduces to

$$V_0 \frac{\partial U}{\partial y} = \frac{\partial \tau}{\partial y},$$

which integrates to

$$\tau - UV_0 = \tau_0, \tag{4.7}$$

showing that the total flux of momentum from the wall is independent of y. Substituting in the basic equation (3.9) and integrating, we obtain

$$\frac{2K}{V_0}[(\tau_0 + UV_0)^{\frac{1}{2}} - \tau_0^{\frac{1}{2}}] + B \operatorname{sgn} V_0 \log\left(1 + \frac{UV_0}{\tau_0}\right) = \log y + \text{const.}, \tag{4.8}$$

where the constant of integration is expected to depend on the nature of the surface and on V_0, τ_0 and ν. For small values of UV_0/τ_0, the distribution must become identical with the logarithmic distribution, and so

$$\frac{2K}{V_0}[(\tau_0 + UV_0)^{\frac{1}{2}} - \tau_0^{\frac{1}{2}}] + B \operatorname{sgn} V_0 \log\left(1 + \frac{UV_0}{\tau_0}\right) = \log \frac{\tau_0^{\frac{1}{2}} y}{\nu} + A. \tag{4.9}$$

Except for the term $B \log\{1 + (UV_0/\tau_0)\} \operatorname{sgn} V_0$, which is usually small, this equation is that derived from the mixing-length theory by Dorrance & Dore (1954) and by others, and it has been confirmed by measurements of velocity distributions in boundary layers with suction and blowing (Black & Sarnecki 1958).

5. Equilibrium layers and self-preserving flow

A turbulent flow is self-preserving in structure if the motions at different sections of the flow differ only in scales of velocity and length, and are dynamically similar in those aspects of the motion that control the distributions of mean

* The flow accelerations are negative and equal to about one-third of the longitudinal pressure gradient.

velocity and Reynolds stress. The importance of self-preserving flows in the theory of turbulence is that the governing equations become ordinary differential equations and that predictions of growth and of friction are then possible, but only a few types of flow can be exactly self-preserving. A greater number can develop in a nearly self-preserving way and it is useful to distinguish two ways in which this is possible. An example of the first kind is the wake of a cylinder in a uniform stream in which the distribution of mean velocity is of the form

$$\left.\begin{aligned} U &= U_1 - u_0 f(y/l_0) \\ \text{and the Reynolds stress} \quad \overline{uv} &= u_0^2 g(y/l_0), \end{aligned}\right\} \tag{5.1}$$

where l_0 and u_0 are scales of length and velocity depending only on x, and the functions $f(\eta)$ and $g(\eta)$ are characteristic of the whole flow. Substitution in the equation of mean motion leads to an ordinary differential equation with solutions satisfying the condition of constant momentum flux only if $l_0 \propto (x-x_0)^{\frac{1}{2}}$ and $u_0 \propto (x-x_0)^{-\frac{1}{2}}$.* In this kind of self-preserving flow, eddy structures and mean velocity distributions develop in a natural and unforced way from similar forms further upstream, and the advection terms in the momentum and energy equations are of the same order of magnitude as those representing local effects such as stress gradient or rate of energy production. The other kind of self-preserving development is one of nearly absolute equilibrium and would occur in flow in a channel whose width changed very slowly. Then the flow at each section would adjust itself to the local width and, conforming to the principle of Reynolds number similarity would have velocity and stress distributions of the self-preserving form (5.1). The condition for this kind of flow is that advection terms should be negligible in the energy equation.

Considered as a whole, but independently of its outer flow, an equilibrium layer with the linear stress distribution (4.1) is self-preserving with length scale τ_0/α and velocity scale $\tau_0^{\frac{1}{2}}$, and the whole of the flow may be self-preserving if these same scales are suitable for self-preserving development of the outer flow. This requirement is very restrictive in boundary-layer flow unless either τ_0 or α is negligibly small. If these conditions can be satisfied, exactly or approximately, the course of development may be obtained from the equation of mean motion in terms of the velocity distribution function. This function has the form given by the similarity arguments in the equilibrium layer and a good approximation to it in the outer flow may be obtained by assuming

(i) that the Reynolds stress is related to velocity gradient by a coefficient of eddy viscosity depending on x alone, i.e.

$$-\overline{uv} = \nu_T \frac{\partial U}{\partial y}, \tag{5.2}$$

(ii) that its magnitude is determined by the condition

$$\frac{1}{\nu_T} \int (U_1 - U)\, dy = R_s, \tag{5.3}$$

where R_s is a constant characteristic of the kind of flow (boundary layer, channel, pipe, etc.),

* Exactly true only if $U_1 - U \ll U_1$.

(iii) that the velocity distribution in the outer layer joins smoothly the velocity distribution in the inner layer. Clauser (1956) and Townsend (1956*a*, *b*, 1960) describe some experimental measurements that confirm these assumptions.

6. Boundary layers in adverse pressure gradients

To the usual boundary-layer approximation, the equation of mean motion for a boundary layer is

$$U\frac{\partial U}{\partial x}+V\frac{\partial U}{\partial y}+\frac{\partial \overline{uv}}{\partial y}=U_1\frac{dU_1}{dx}, \tag{6.1}$$

where U_1 is the velocity in the free stream and two-dimensional mean flow is assumed. Substitution of the self-preserving forms for the distribution of mean velocity and Reynolds stress (5.1) gives

$$-\frac{d(u_0U_1)}{dx}f+\frac{u_0}{l_0}\frac{d(U_1l_0)}{dx}\eta f'+u_0\frac{du_0}{dx}f^2-\frac{u_0}{l_0}\frac{d(u_0l_0)}{dx}f'\int_0 f\,d\eta+\frac{u_0^2}{l_0}g'=0, \tag{6.2}$$

which is an ordinary differential equation with independent variable $\eta=y/l_0$ if the coefficients are in constant ratio. It follows that $dl_0/dx=$ constant, $u_0/U_1=$ constant, $(l_0/u_0)(du_0/dx)=$ constant, but the scales so defined must be compatible with the scales of the equilibrium layer, $u_0=\tau_0^{\frac{1}{2}}$, $l_0=\tau_0/\alpha$, which is only possible either

(*a*) if $U_1\propto(x_0-x)^{-1}\propto\tau_0^{\frac{1}{2}}$, $l_0\propto(x_0-x)$ (Townsend 1956*a*),

or (*b*) if $\tau_0=0$, $U_1\propto(x-x_0)^{-0\cdot23}$, $l_0\propto(x-x_0)$ (Stratford 1959*a*, *b*; Townsend 1960).

The first is an accelerating flow in a converging wedge and the second a zero-stress flow in an adverse pressure gradient.

The converging flow may be regarded as the prototype of a family of approximately self-preserving layers which share two of its characteristics, an equilibrium layer of nearly constant stress and an outer layer with small velocity defects $[(U_1-U)\ll U_1]$ at high Reynolds numbers. If the distribution of velocity in the equilibrium layer is given by the logarithmic equation (4.3), the velocity defect always becomes small at sufficiently large Reynolds numbers and self-preserving flow in the pressure distribution defined by $U_1\propto(x-x_0)^a$ is possible if $a>-\frac{1}{3}(x>x_0)$. For values of a close to $-\frac{1}{3}$ the wall stress is very small and the pressure gradient large so that a large variation of stress in the equilibrium layer is inevitable (Dunn 1956).

Flows in these strong adverse pressure gradients must resemble more closely the zero-stress self-preserving flow, and we now consider nearly self-preserving flows with equilibrium layers whose stress distribution is nearly linear with a characteristic length τ_0/α small compared with the thickness and a velocity distribution given by equation (4.5). The distribution of free stream velocity is assumed to be $U_1\propto(x-x_0)^a$ and, as in the zero-stress layer, the scales of velocity and length are the free stream velocity U_1 and $(x-x_0)$. Substituting these scales in equation (6.2) yields

$$2af-(a+1)\eta f'-af^2+(a+1)f'\int_0 f\,d\eta-g'=0, \tag{6.3}$$

which has a self-preserving solution if the inner boundary condition can be expressed in a form independent of x. Within the equilibrium layer and not too close to the wall, the velocity distribution function is

$$f(\eta) = \zeta + \frac{2}{K_0}\left[\frac{\alpha(x-x_0)}{U_1^2}\eta\right]^{\frac{1}{2}}, \tag{6.4}$$

where

$$\zeta = \frac{\tau_0^{\frac{1}{2}}}{KU_1}\left[\log\frac{4\tau_0^{\frac{3}{2}}}{\alpha\nu} + A - 2(1-B)\right], \tag{6.5}$$

and the flow is self-preserving if ζ and $\alpha(x-x_0)/U_1^2$ are constant. It will be seen that this can not be exactly true but the variation of ζ is very slow and it is reasonable to suppose that the flow adjusts itself to the local value of ζ and resembles the hypothetical self-preserving flow of constant ζ over moderate ranges of x.

The wall stress is related to the velocity distribution and the pressure gradient by the equation for the momentum integral,

$$\frac{d}{dx}\int_0^\infty U(U_1-U)\,dy + \frac{dU_1}{dx}\int_0^\infty (U_1-U)\,dy = \tau_0, \tag{6.6}$$

or in terms of the function $f(\eta)$,

$$(2a+1)(I_a - I_b) + aI_a = \tau_0/U_1^2, \tag{6.7}$$

where

$$I_a = \int_0^\infty f(\eta)\,d\eta, \quad I_b = \int_0^\infty [f(\eta)]^2\,d\eta.$$

This relation is consistent with the assumption of self-preserving flow if the variation of τ_0/U_1^2 is small compared with $-aI_a$.

The velocity distribution function is now obtained using the eddy-viscosity assumptions of the last section. Making use of equations (5.2) and (5.3), the distribution function in the outer layer satisfies

$$2af - (a+1)\eta f' - af^2 + (a+1)f'\int_0 f\,d\eta + I_a f''/R_s = 0, \tag{6.8}$$

a form of the Falkner–Skan equation. For flows in strong adverse pressure gradients, the wall stress is small compared with the pressure force on the layer, i.e. $\tau_0/U_1^2 \ll -aI_a$, and may be neglected except in so far as it determines ζ. An approximate solution of (6.8) satisfying the boundary conditions

$$f(0) = C, \quad f'(0) = 0, \quad f''(0) = R_s Ca(2-C)/I_a$$

is

$$f(\eta) = C\exp(-\tfrac{1}{2}R^2\eta^2), \tag{6.9}$$

where

$$I_a R^2 = -aR_s(2-C). \tag{6.10}$$

For a smooth junction with the velocity distribution in the equilibrium layer at $\eta = \eta_1$,

$$1 - C\exp(-\tfrac{1}{2}R^2\eta_1^2) = \zeta + 2K_0^{-1}(\alpha_0\eta_1)^{\frac{1}{2}},$$
$$CR^2\eta_1\exp(-\tfrac{1}{2}R^2\eta_1^2) = K_0^{-1}(\alpha_0/\eta_1)^{\frac{1}{2}}, \tag{6.11}$$

where $\alpha_0 = -a(1-\zeta^2)$ very nearly (see Appendix). Approximately, if $R^2\eta_1^2$ is not too large,

$$I_a = (\tfrac{1}{2}\pi)^{\frac{1}{2}}CR^{-1} + 2\alpha_0/3K_0^2R^2,$$

$$I_b = \tfrac{1}{2}\pi^{\frac{1}{2}}C^2R^{-1} + \frac{4\alpha_0}{3K_0^2R^2} + \frac{2\alpha_0}{3K_0^2}\frac{\alpha_0^{\frac{3}{2}}}{(K_0CR^2)^{\frac{1}{2}}}. \tag{6.12}$$

The solutions of these equations are conveniently presented by plotting the friction coefficient τ_0/U_1^2 as a function of ζ for various values of the exponent a (from equations (6.7), (6.10), (6.11) and (6.12)) and as a function of ζ for various values of $-3aR_x$ (substituting values of ζ obtained from equations (6.10), (6.11) and (6.12) in equation (6.5)). This has been done to slide-rule accuracy in figure 2, in which possible self-preserving flows are represented by intersections of the two families of curves, e.g. in the pressure gradient defined by $a = -0{\cdot}24$, the friction coefficient is nearly $\tau_0/U_1^2 = 9{\cdot}6 \times 10^{-4}$ at a Reynolds number of 10^6. The two bounding curves indicate the limits of validity of the approximations used, the left-hand curve imposing the condition that the constant-stress part of the equilibrium layer is fully turbulent and the right-hand one that the wall friction plays a small part in the momentum balance.*

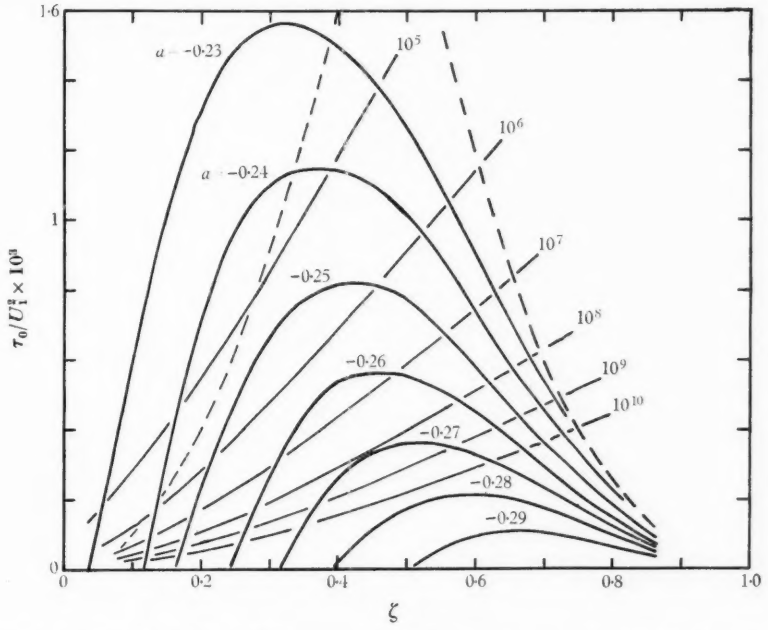

FIGURE 2. Boundary-layer development with a 'linear-stress' equilibrium layer. The numbers on the 'upper' family of curves refer to values of the exponent a, and on the lower family to values of $-3aR_x$ which is not much different from R_x.

The most interesting feature of these solutions is that two different layers are possible, one with comparatively large wall stress and small velocity defect and another with low stress and large defect, but this is only consistent with the known existence of a zero-stress layer for $a \approx -0{\cdot}23$ (Stratford 1959*b*) and of finite-stress layers for this and more negative exponents (Clauser 1956). In figure 3, the friction coefficient is shown as a function of Reynolds number for

* Conditions for internal consistency of the 'linear-stress' approximation are derived in the Appendix. It turns out that they are satisfied if $\tau_0/U_1^2 \ll -3aI_a$.

flows of constant exponent and it is seen that, although flow at infinite Reynolds number is possible with exponents as negative as $-\frac{1}{3}$, the limiting value at ordinary Reynolds numbers is very much less, changing from $-0{\cdot}25$ near $R_x = 3\times10^5$ to $-0{\cdot}28$ near $R_x = 10^{11}$. It is interesting to compare this variation of the friction coefficient with the dependence in a flow constrained by a continuous, slight adjustment of the pressure gradient to obey the defect law

$$U = U_1 - \tau_0^{\frac{1}{2}} F(y/\delta) \tag{6.13}$$

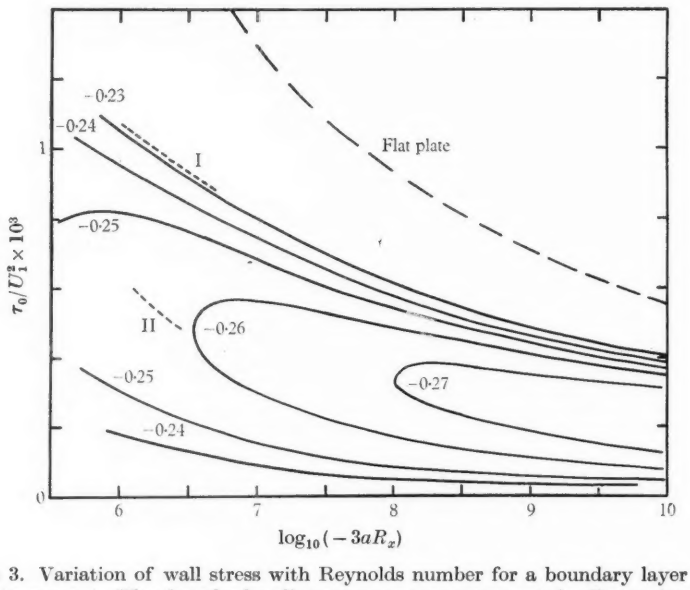

FIGURE 3. Variation of wall stress with Reynolds number for a boundary layer with a constant exponent. (The short broken lines represent measurements by Clauser in pressure distributions I and II.)

in the outer flow (figure 4). If development takes place along the upper branch of the friction curve, the necessary adjustment is small and development with constant exponent might be indistinguishable experimentally from development with constant velocity-defect ratio, but along the lower branch this is not true. On this branch, the defect constant C approaches a constant value as the Reynolds number increases and the wall stress tends to zero comparatively rapidly.

Some comparisons of these theoretical predictions with the measurements of Clauser (1954, 1956) are given in table 1. If it is remembered that uncertainty in the position of the flow origin leads to considerable uncertainty in the appropriate values of R_x and a, the agreement is quite satisfactory. Lines showing the observed variation of friction with Reynolds number have been drawn on figure 3 and it is clear that flow I is developing along the upper branch. Flow II is in a region of ambiguous development and its observed development is not described by this theory. However, Clauser adjusted the pressure gradient so that the outer

flow obeyed the defect law (6.13) which, in this region, requires an 'unnatural' course of development, and it is not surprising that the maintenance of this development was difficult and that, unlike most self-preserving flows, small deviations tended to grow rather than to disappear. Some remarks of Stratford (1959*b*) suggest that flow on the lower branch is stable in this sense and so this

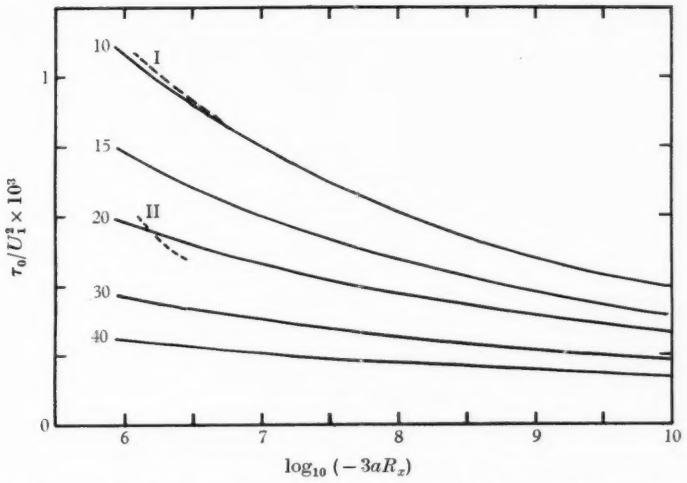

FIGURE 4. Variation of wall stress with Reynolds number for constant velocity-defect ratio, $U_1 C/\tau_0^{\frac{1}{2}}$, in the outer layer. The numbers near the curves are the corresponding values of the ratio. (N.B. The measured defect ratio for distribution I is 12, for distribution II, 24.)

	Observed				Theory		
Flow	τ_0/U_1^2	$\frac{\delta^*}{\tau_0}\frac{dP_1}{dx}$	$-3aI_a$	C	τ_0/U_1^2	a	C
I	$9{\cdot}5\times10^{-4}$	2	$5{\cdot}7\times10^{-3}$	0·39	$9{\cdot}6\times10^{-4}$	−0·24	0·374
					8·5	−0·245	0·374
II	5·0	7	10·5	0·53	6·0	−0·256	0·491
					5·3	−0·258	0·491

N.B. The theoretical values refer to two values of Reynolds number, 0·75 and $1{\cdot}5\times10^6$, and the observed values of $-3aI_a$.

TABLE 1

explanation of this phenomenon of downstream instability has the virtue that self-preserving development remains a stable asymptotic state for turbulent flow.

The calculations that are presented in the diagrams have assumed that $K = 0{\cdot}41$, $K_0 = 0{\cdot}50$, $B = 0{\cdot}2$, $R_s = 75$, values which have been found to describe flow in a zero-stress layer (Townsend 1960). The value of R_s also agrees closely with the value necessary to describe boundary-layer development in zero pressure gradient by the procedure of § 5.

7. Self-preserving flow between diverging planes

The Reynolds number of two-dimensional mean flow between converging or diverging plane boundaries, based on local velocity and channel width, has the same value everywhere and so it is possible that the motion is dynamically similar at all sections of the flow and that the flow is self-preserving. We consider flow in a wedge of semi-angle θ, with the Oz axis the apex of the wedge and the xOz plane the central plane of symmetry. To the boundary-layer approximation, applicable if the angle θ is small, the equation of mean motion may be written

$$-f^2+g' = -\mathscr{P}+\nu M^{-1}f'', \tag{7.1}$$

self-preserving flow being implied by the use of the distribution functions, f and g and the pressure recovery coefficient, $\mathscr{P}$, defined by

$$\left.\begin{aligned} U = Mf(\eta)/x, \quad V = M\eta f(\eta)/x, \quad \eta = y/x, \\ \overline{uv} = M^2x^{-2}g(\eta), \quad \mathscr{P} = \frac{x^3}{M^2}\frac{dP_1}{dx}. \end{aligned}\right\} \tag{7.2}$$

It is convenient to define M so that $f(0) = 1$, i.e. $M/x = U_1$, the mean velocity in the central plane at distance x from the apex. The Reynolds number of the flow is

$$R_x = U_1x/\nu = M/\nu.$$

Integrating equation (7.1) from the centre line to the wall,

$$\int_0^\theta f^2 d\eta = \mathscr{P}\theta+\frac{\tau_0}{U_1^2}, \tag{7.3}$$

where τ_0 is the shear stress on the walls of the diffuser.

For sufficiently large Reynolds numbers, the converging flow takes the form of two boundary layers separated by a central region of negligible Reynolds stress,* but a diverging flow must be turbulent over the whole width of the channel. We now apply to the diverging flow the same procedure that has been used in § 6 to obtain the mean-flow properties of self-preserving boundary layers. Outside the equilibrium layers, the mean velocity distribution is found by assuming a constant coefficient of eddy viscosity, given by

$$R_s = \frac{1}{\nu_T}\int_0^{\theta x}(U_1-U)\,dy = \frac{U_1x}{\nu_T}I_a, \tag{7.4}$$

where R_s is a constant characteristic of fully developed flow between plane boundaries. Measurements by Laufer (1951) of pressure flow between parallel planes indicate that $R_s = 28\pm3$. Within the central flow then, we have

$$f^2+(I_a/R_s)f'' = \mathscr{P}, \tag{7.5}$$

and the solution of this equation for the boundary conditions $f(0) = 1$, $f'(0) = 0$ is

$$\eta = \left[\frac{2I_a}{R_s(1-\mathscr{P})}\right]^{\frac{1}{2}}\beta_1\int_0^{X/\beta_1}\frac{dt}{[(1-t^2)(1-k^2t^2)]^{\frac{1}{2}}}, \tag{7.6}$$

* In a rapidly accelerating flow, the only strong sources of vorticity are the walls and so boundary layers develop.

where β_1^2, β_2^2 are the roots of $x^2-3x+3(1-\mathscr{P})=0$, and

$$k=\beta_1/\beta_2 \quad (\beta_1<\beta_2) \quad \text{and} \quad X^2=1-f(\eta).$$

The integral in (7.6) is tabulated as the elliptic integral of the first kind,

$$F(x)=\int_0^x \frac{dt}{[(1-t^2)(1-k^2t^2)]^{\frac{1}{2}}}$$

and its inverse function, sn, is defined by

$$\mathrm{sn}\,[F(x)]=x.$$

The velocity distribution function is

$$f(\eta)=1-\beta_1^2\,\mathrm{sn}^2\left[\left\{\frac{R_s(1-\mathscr{P})}{2I_a}\right\}^{\frac{1}{2}}\frac{\eta}{\beta_1}\right], \tag{7.7}$$

and a good approximation to the flow integral I_a is

$$\begin{aligned} I_a &= \int_0^\theta \{1-f(\eta)\}\,d\eta = \left[\frac{2I_a}{R_s(1-\mathscr{P})}\right]^{\frac{1}{2}}\beta_1^3\int_0^{u_1}\mathrm{sn}^2 u\,du \\ &= \left[\frac{2I_a}{R_s(1-\mathscr{P})}\right]^{\frac{1}{2}}\beta_1^3 k^{-2}(F-E), \end{aligned} \tag{7.8}$$

where F, E are the elliptic integrals of the first and second kinds evaluated at $X(\theta)/\beta_1$ and

$$u_1=\left[\frac{R_s(1-\mathscr{P})}{2I_a}\right]^{\frac{1}{2}}\frac{\theta}{\beta_1}.$$

Using the relations between β_1, $\mathscr{P}$ and k implied by the definition of β_1, i.e.

$$\beta_1^2=\frac{3k^2}{1+k^2}, \quad 1-\mathscr{P}=\frac{3k^2}{(1+k^2)^2},$$

it follows that

$$R_sI_a=\frac{18}{1+k^2}(F-E)^2 \tag{7.9}$$

and the wall stress is given by

$$\frac{\tau_0}{U_1^2}=-\frac{I_a}{R_s}f'(\theta)=\frac{18}{R_s}\frac{k^2}{(1+k^2)^2}(F-E)\,\mathrm{sn}\,u_1\,\mathrm{cn}\,u_1\,\mathrm{dn}\,u_1. \tag{7.10}$$

Both these relations depend on the approximation that the difference between the true value of the flow integral, I_a, and the value found by assuming the central velocity distribution (7.7) to extend all the way to the wall is negligible. These equations relate $\mathscr{P}$ and τ_0 if θ and R_s are known, and their values are found by imposing conditions for a smooth junction of the central velocity distribution with the velocity distribution in the equilibrium layer.

For a linear variation of stress in the equilibrium layer, $\tau=\tau_0+\alpha y$ where $\alpha y \gg \tau_0$ for most of the layer, and

$$f(\eta)=\zeta+2K_0^{-1}[(\mathscr{P}-\zeta^2)(\theta-\eta)]^{\frac{1}{2}}, \tag{7.11}$$

since the stress gradient in the layer is nearly $(\mathscr{P}-\zeta^2)U_1^2x^{-1}$ (see Appendix). The conditions for a smooth junction are that

$$\left.\begin{aligned} &\zeta+2K_0^{-1}[(\mathscr{P}-\zeta^2)(\theta-\eta_1)]^{\frac{1}{2}}=1-\beta_1^2\,\mathrm{sn}^2\,u_1, \\ \text{and that}\quad &\frac{1}{K_0}\left(\frac{\mathscr{P}-\zeta^2}{\theta-\eta_1}\right)^{\frac{1}{2}}=\frac{R_s}{I_a}(\mathscr{P}-\zeta^2)(\theta-\eta_1)+\frac{R_s}{I_a}\frac{\tau_0}{U_1^2}. \end{aligned}\right\} \tag{7.12}$$

The assumption of linear stress implies that $\mathrm{sn}\, u_1 = 1$ and that

$$(\mathscr{P}-\zeta^2)(\theta-\eta_1) \gg \tau_0/U_1^2,$$

so, eliminating $\theta-\eta_1$, we have

$$\zeta+\frac{2}{K_0}\left[\frac{I_a}{R_s K_0}(\mathscr{P}-\zeta^2)\right]^{\frac{1}{3}} = 1-\beta_1^2, \tag{7.13}$$

essentially a relation between ζ and $\mathscr{P}$. Now ζ is related to the wall stress by

$$\zeta = \frac{\tau_0^{\frac{1}{2}}}{KU_1}\left[\log\left(\frac{4\tau_0^{\frac{3}{2}}}{U_1^3}\frac{R_x}{\mathscr{P}-\zeta^2}\right)+A-2(1-B)\right], \tag{7.14}$$

and the condition $\mathrm{sn}\, u_1 = 1$ can be expressed as

$$R_s\theta = 6K(K-E), \tag{7.15}$$

so that the wall stress can be calculated as a function of flow Reynolds number and angle of divergence. The results of these calculations are shown in figure 5 with an indication of the limit of validity of the approximation that $\tau_0 \ll \alpha y_1$. Validity of the approximation that the stress distribution is substantially linear can be expressed by the condition

$$10\theta^{\frac{2}{3}}\zeta \ll 1$$

(see (A. 20) in the Appendix). $10\theta^{\frac{2}{3}}\zeta$ is about 0·30 for $\theta = 0{\cdot}05$, and so the results of this treatment are only applicable for larger values of θ.

A special case of some interest is the flow with zero wall stress and with $\zeta = 0$, which occurs at a critical angle of divergence θ_0. This angle depends on the values of K_0 and R_s, but the pressure recovery and $R_s\theta_0$ are functions of $K_0 R_s^{\frac{1}{2}}$ and a few values are tabulated in table 2.

Assuming $K_0 = 0{\cdot}50$, $R_s = 28$, we find $\theta_0 = 0{\cdot}075$ rad. $= 4{\cdot}3$ deg., $\mathscr{P} = 0{\cdot}53$. Milliat (1957) has reported steady diffuser flow for a semi-angle of three degrees which is not much less than this calculated value. It should be emphasized that secondary flow is very likely to occur in these flows and will cause separation of flow from the walls at smaller angles of divergence than the critical value for truly two-dimensional flow. An interesting point about the critical flow is that the pressure-recovery coefficient is less than for flows in wedges of smaller angle.

If the stress in the equilibrium layer is nearly constant,

$$f(\eta) = \frac{\tau_0^{\frac{1}{2}}}{KU_1}\left[\log\left\{\frac{\tau_0^{\frac{1}{2}}}{U_1}R_x(\theta-\eta)\right\}+A\right] \tag{7.16}$$

and the conditions for a smooth junction are

$$\left.\begin{aligned} \frac{\tau_0^{\frac{1}{2}}}{KU_1}\left[\log\left\{\frac{\tau_0^{\frac{1}{2}}}{U_1}R_x(\theta-\eta_1)\right\}+A-1\right] &= 1-\beta_1^2\,\mathrm{sn}^2 u_1 \\ \text{and} \qquad \frac{\tau_0^{\frac{1}{2}}}{KU_1}\frac{1}{\theta-\eta_1} &= \frac{R_s}{I_a}\frac{\tau_0}{U_1^2}, \end{aligned}\right\} \tag{7.17}$$

or, eliminating $\theta-\eta_1$,

$$\frac{\tau_0^{\frac{1}{2}}}{KU_1}\left[\log R_x+\log\frac{I_a}{KR_s}+A-1\right] = 1-\beta_1^2\,\mathrm{sn}^2 u_1. \tag{7.18}$$

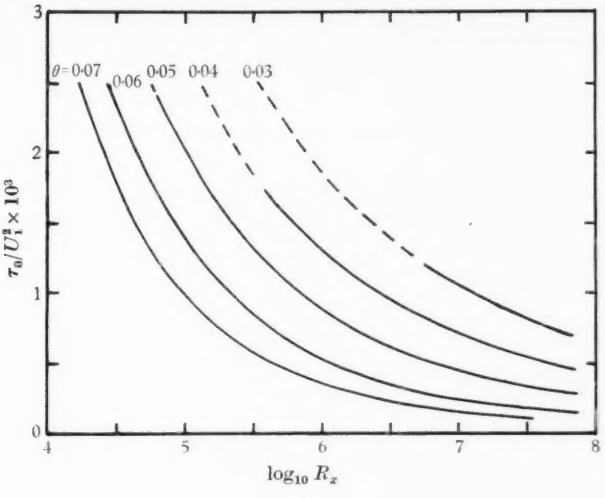

(*a*)

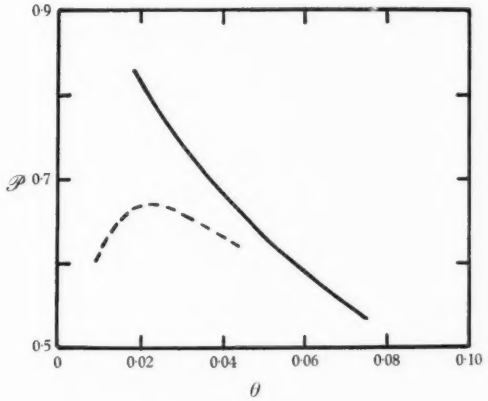

(*b*)

FIGURE 5. Self-preserving flow in a wedge with a 'linear-stress' equilibrium layer. (*a*) Variation of wall stress with Reynolds number for various angles of divergence. (The broken portions of the curves are outside the range of validity of the linear-stress approximation.) (*b*) Variation of pressure-recovery coefficient with angle of divergence. (The dashed curve shows, for comparison, the variation for $\theta R_x = 3 \times 10^4$ if the equilibrium layer is of nearly constant stress.)

$K_0 R_x^{\frac{1}{2}}$	$\mathscr{P}$	$\theta_0 R_x$
1·64	0·718	0·935
2·12	0·614	1·492
2·83	0·520	2·21
4·26	0·441	3·11

TABLE 2

This equation and equations (7.9) and (7.10) determine τ_0/U_1^2 and $\mathscr{P}$ as functions of R_x for a given θ, and the results of solving these equations are shown graphically in figure 6. The approximation of constant stress is valid if the corresponding velocity distribution could be maintained with a small variation of stress in the equilibrium layer and the condition for this, derived in the Appendix, is

$$\tau_0/U_1^2 > 0{\cdot}2\theta^{\frac{1}{4}}.$$

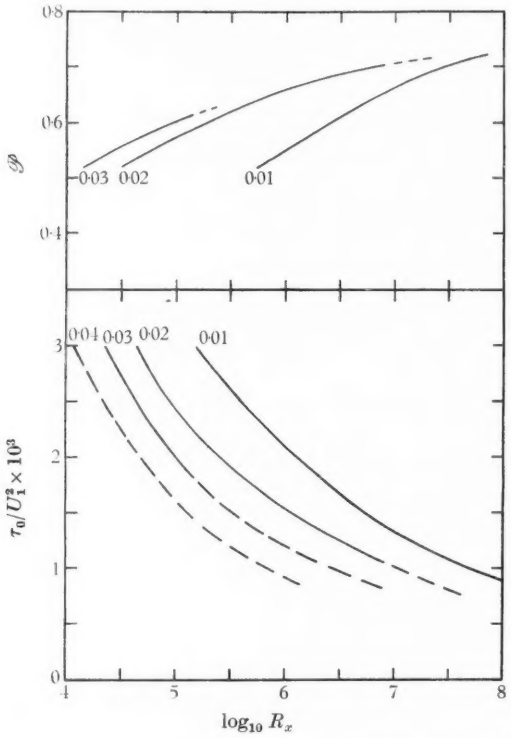

FIGURE 6. Self-preserving flow in a wedge with a 'constant-stress' equilibrium layer. (The broken portions of the curves are outside the range of validity of the constant-stress approximation.)

It follows that the constant-stress approximation will fail at very high Reynolds numbers however small the angle of divergence, and that the increase in pressure-recovery coefficient with Reynolds number has a limit.

Ruetenik (1954, see also Ruetenik & Corrsin 1955) and Craya & Milliat (1955) have made studies of the self-preserving turbulent flow in a wedge of semi-angle one degree, each at a Reynolds number of nearly $1{\cdot}8 \times 10^6$. Reference to figure 6 shows that these conditions are within the range of validity of the constant-stress approximation, and that the theory predicts a friction coefficient $\tau_0/U_1^2 = 15 \times 10^{-4}$, and a pressure coefficient $\mathscr{P} = 0{\cdot}67$. The two sets of measurements are in good general agreement but Ruetenik gives rather more detail. He finds that

$\tau_0/U_1^2 = 13 \pm 1{\cdot}3 \times 10^{-4}$, and $\mathscr{P} = 0{\cdot}57$ and his measured distributions of mean velocity and of Reynolds stress are compared with the theoretical distributions in figure 7. Excepting the large difference between the observed and predicted values of $\mathscr{P}$, general agreement is found and the discrepancies can be attributed to uncertainty in the value of the flow constant R_s. A considerable part of the error

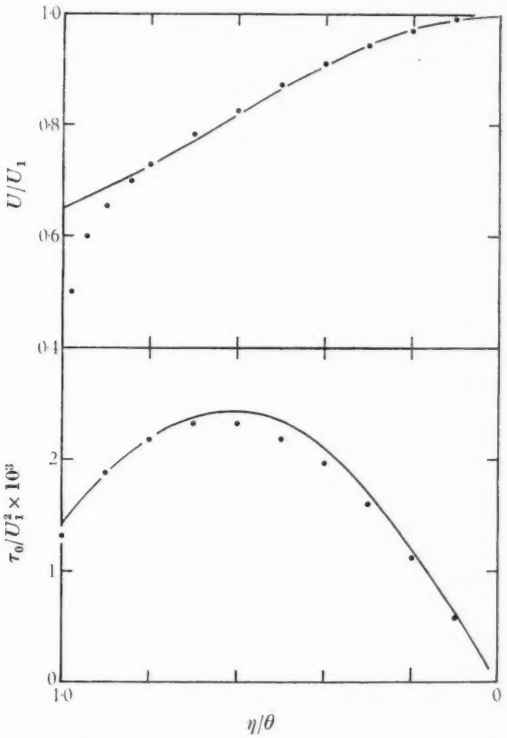

FIGURE 7. Comparison of theoretical predictions with measurements by Ruetenik (1954) of velocity and stress distributions in a diverging wedge of semi-angle one degree. (Experimental results ●, theory ——.)

in $\mathscr{P}$ is due to assuming that integrals over the whole flow can be approximated by replacing the composite velocity distribution by the velocity distribution for the central flow extrapolated to the walls. This procedure underestimates I_a and overestimates the integral $\int_0^\theta f^2(\eta)\,d\eta$ by about 10%. Since

$$\mathscr{P}\theta = \int_0^\theta f^2\,d\eta - \frac{\tau_0}{U_1^2},$$

the overestimate is reflected in the value of $\mathscr{P}$. The necessary modification of the equations is straightforward but their solution becomes even more tiresome.

8. Discussion

The essential property of an equilibrium layer is local and absolute equilibrium between energy supply and dissipation, and definition by this property rather than by stress equilibrium extends considerably the applicability of similarity arguments. If we are interested only in the mean-velocity distribution inside the equilibrium layer, the only gain over simple acceptance of the momentum-transfer theory is a plausible explanation of the difference between the Kármán constant and the corresponding constant for zero-stress flow, but the requirement of energy equilibrium sets clear limits to the extent of the layer which are not provided by the mixing-length theory. It is interesting that the energy equilibrium is of the same kind as that assumed in the theory of local similarity, the difference being that one is localized in physical space and the other in wave-number space. Unlike the motion described by the theory of local similarity, the motion in an equilibrium layer has an influence on all parts of the flow, and the second half of this paper is an attempt to develop a method for solving the mean-flow problem in wall flows with different kinds of equilibrium layers. The origin of the method is an observation of Clauser (1956) that the velocity distribution in the outer part of self-preserving boundary layers is nearly that produced by an eddy viscosity of constant ratio to the integrated velocity defect at the particular section. Although the final results are not very sensitive to this assumption, comparison with experiment suggests that the eddy-viscosity hypothesis gives a good description of the mean-velocity distribution and that the constant ratio may depend only on the conformation of the bounding surfaces and not on the pressure gradient.

The hypothesis that the *turbulent* motion in an equilibrium layer is in a universal state determined by the stress distribution is not confirmed by numerous observations that turbulent intensities in constant-stress layers vary considerably between different flows of the same stress. This is in strong contrast with the universality of the distributions of mean velocity and it is difficult to reconcile these observations without supposing that the motion at any point consists of two components, an active component responsible for turbulent transfer and determined by the stress distribution and an inactive component which does not transfer momentum or interact with the universal component. This does not mean that the eddy structures contributing to the inactive component at a particular point can not form part of the active component at points further from the wall, and it seems likely that the inactive motion is a meandering or swirling motion made up from attached eddies of large size which contribute to the Reynolds stress much further from the wall than the point of observation. If this is true, the ratio of turbulent intensity to Reynolds stress would increase with total thickness of the constant-stress layer, and comparison of the ratios in the very thick boundary layer on the earth's surface and in laboratory boundary layers confirms this.

REFERENCES

BATCHELOR, G. K. 1953 *Homogeneous Turbulence.* Cambridge University Press.

BLACK, T. J. & SARNECKI, A. J. 1958 *Aero. Res. Counc., Lond.*, Rep. no. 20,501.

CLAUSER, F. H. 1954 *J. Aero. Sci.* **21**, 91.

CLAUSER, F. H. 1956 *Advanc. App. Mech.* **4**, 1.

CRAYA, A. & MILLIAT, J.-P. 1955 *C.R. Acad. Sci., Paris*, **241**, 542.

DORRANCE, W. H. & DORE, F. J. 1954 *J. Aero. Sci.* **21**, 404.

DUNN, J. W. 1956 *Math. Rev.* **17**, 1249.

ELLISON, T. H. 1960 *J. Fluid Mech.* **8**, 33.

JEFFREYS, H. & JEFFREYS, B. S. 1950 *Methods of Mathematical Physics.* Cambridge University Press.

KLEBANOFF, P. S. 1956 *Nat. Adv. Comm. Aero., Wash.*, Rep. no. 1247.

LAUFER, J. 1951 *Nat. Adv. Comm. Aero., Wash.*, Rep. no. 1033.

LAUFER, J. 1955 *Nat. Adv. Comm. Aero., Wash.*, Rep. no. 1174.

MILLIAT, J.-P. 1957 *9me. Congrès intern. Mécan. appl., Univ. Bruxelles*, **3**, 419.

ROTTA, J. 1953 *Ing.-Arch.* **19**, 31.

RUETENIK, J. R. 1954 *Johns Hopk. Univ., Inst. Co-op. Res.*, Rep. no. 1–19.

RUETENIK, J. R. & CORRSIN, S. 1955 *50 Jahre Grenzschichtforschung*, p. 446. (Ed. H. Görtler and W. Tollmien.) Vieweg: Braunschweig.

SCHUBAUER, G. B. & KLEBANOFF, P. S. 1951 *Nat. Adv. Comm. Aero., Wash.*, Rep. no. 1030.

STRATFORD, B. S. 1959*a* *J. Fluid Mech.* **5**, 1.

STRATFORD, B. S. 1959*b* *J. Fluid Mech.* **5**, 17.

TOWNSEND, A. A. 1956*a* *Structure of Turbulent Shear Flow.* Cambridge University Press.

TOWNSEND, A. A. 1956*b* *J. Fluid Mech.* **1**, 561.

TOWNSEND, A. A. 1960 *J. Fluid Mech.* **8**, 143.

Appendix: stress distributions in equilibrium layers

The procedure described in § 5 gives good results only if the simplified distribution of stress in the equilibrium layer, assumed for mathematical convenience, bears some resemblance to the real distribution. Close resemblance requires that the stress distribution computed from the assumed velocity distribution and the inferred rate of development of the layer should be nearly the same as the assumed stress distribution. If the stress variation in the equilibrium layer is assumed to be small, the velocity distribution is given by the logarithmic profile, and it is easy to show that the distribution of stress must be

$$\tau - \tau_0 = \frac{dP_1}{dx} y + \frac{1}{2K^2} \frac{d\tau_0}{dx} y \left[\left(\log \frac{\tau_0^{\frac{1}{2}} y}{\nu} + A - 1 \right)^2 + 1 \right] \tag{A. 1}$$

within the equilibrium layer. The original assumption of constant stress is only valid if $\tau - \tau_0$ so computed is small compared with τ_0.

If a self-preserving boundary layer has an equilibrium layer of nearly constant stress, the velocity defect outside the equilibrium layer is small at sufficiently large Reynolds numbers, and wall stress and Reynolds number are related by

$$R_x = (1 + 3a) K^{-3} I_1 \gamma^{-2} \exp(\gamma^{-1} - A), \tag{A. 2}$$

where

$$\gamma = \tau_0^{\frac{1}{2}} / (K U_1), \quad I_1 = \int_0^\infty K \frac{U_1 - U}{\tau_0^{\frac{1}{2}}} d\eta,$$

and $$\eta = \frac{\tau_0^{\frac{1}{2}} y}{\nu} \exp(A - \gamma^{-1}).$$

Assuming a constant eddy viscosity in the outer layer, the velocity distribution function is

$$f(\eta) = K(U_1 - U)/\tau_0^{\frac{1}{2}} = CHh_n(R\eta), \tag{A. 3}$$

where $$R = \frac{KR_s^{\frac{1}{2}}}{I_1}\left(\frac{1+a}{1+3a}\right)^{\frac{1}{2}}, \quad n = \frac{2a}{1+a}$$

and the function Hh_n is defined by

$$Hh_n(x) = \int_0^\infty \frac{t^n}{n!} \exp[-\tfrac{1}{2}(t+x)^2]\, dt, \quad \frac{d}{dx} Hh_n(x) = -Hh_{n-1}(x) \tag{A. 4}$$

(Jeffreys & Jeffreys 1950, p. 622). In the constant-stress equilibrium layer, $f(\eta) = -\log \eta$ and the integral I_1 is nearly

$$I_1 = CR^{-1} Hh_{n+1}(0) + \eta_1, \tag{A. 5}$$

where η_1 specifies the junction of the two layers. The conditions for a smooth junction are approximately

$$1 - CHh_n(0) = \log \eta_1, \quad CRHh_{n-1}(0) = \eta_1^{-1}, \tag{A. 6}$$

so that $$I_1 CR = KR_s^{\frac{1}{2}}\left(\frac{1+a}{1+3a}\right)^{\frac{1}{2}} C = \frac{\pi^{\frac{1}{2}} C^2}{2^{\frac{1}{2}n+1}(\frac{1}{2}n + \frac{1}{2})!} + \pi^{-\frac{1}{2}} 2^{\frac{1}{2}n}(\tfrac{1}{2}n - \tfrac{1}{2})!. \tag{A. 7}$$

The three equations (A. 5), (A. 6) and (A. 7) determine C, R and I_1 as functions of the exponent a. From the friction equation (A. 2), we have

$$\frac{d\tau_0}{dx} = K^2 \gamma^2 \frac{dU_1^2}{dx}[1 + O(\gamma)] \tag{A. 8}$$

and, to the approximation that $\gamma \ll 1$,

$$\frac{\tau - \tau_0}{\tau_0} = \frac{2a}{3a+1} \frac{\eta_1(\log \eta_1 - 1)}{I_1}. \tag{A. 9}$$

Using the values of η_1 and I_1 given by equations (A. 6) and (A. 7), we find

$$\frac{\tau - \tau_0}{\tau_0} = \frac{-2a}{[2(1+a)(1+3a)]^{\frac{1}{2}}} \frac{1}{KR_s^{\frac{1}{2}}} \frac{(\frac{1}{2}n - \frac{1}{2})!}{(\frac{1}{2}n)!}, \tag{A. 10}$$

omitting the small second term on the right of (A. 7). This shows that the stress variation in the equilibrium layer must become very large as a approaches the critical value of $-\frac{1}{3}$, whatever the Reynolds number. For $a = -0{\cdot}2$, the ratio is nearly 0·4, and so the assumption of constant stress in the equilibrium layer must fail for more negative values of a.

A similar calculation of the stress variation in the equilibrium layer of self-preserving wedge flow leads to

$$\frac{\tau - \tau_0}{\tau_0} = \frac{I_a}{KR_s} \frac{U_1^3}{\tau_0^{\frac{3}{2}}} \left[\mathscr{P} - (1 - \beta_1^2 \operatorname{sn}^2 u_1)^2 - \frac{\tau_0}{K^2 U_1^2}\right], \tag{A. 11}$$

and substitution of values of I_a, τ_0, $\mathscr{P}$, β_1 and u_1 would show whether the constant-stress approximation is permissible in any particular flow. The condition for

this may be expressed more compactly and with sufficient accuracy by observing that

$$\frac{I_a}{KR_s} = \frac{\theta^2}{2K}\frac{1}{(1+k^2)F^2}$$

(equations (7.9) and (7.10)) and that $\mathscr{P}-(1-\beta_1^2\operatorname{sn}^2 u_1)^2 = 0{\cdot}25$, $1+k^2 = 1{\cdot}25$, $F^2 = 1{\cdot}5$ very roughly for all the points calculated in figure 4. Substituting these approximate values and allowing a 50 % variation of stress in the equilibrium layer, the condition for an equilibrium layer of nearly constant stress is that

$$\tau_0/U_1^2 > 0{\cdot}2\theta^{\frac{1}{3}}. \tag{A. 12}$$

The contrasting approximation is that the stress variation is linear, i.e. $\tau = \tau_0 + \alpha y$ with $\alpha y \gg \tau_0$ for most of the equilibrium layer, when the velocity distribution is (equation (4.5))

$$U = U_l + 2K_0^{-1}(\alpha y)^{\frac{1}{2}}, \tag{A. 13}$$

where

$$U_l = \frac{\tau_0^{\frac{1}{2}}}{K}\left[\log\frac{4\tau_0^{\frac{3}{2}}}{\alpha\nu} + A - 2(1-B)\right].$$

The stress distribution necessary to maintain this velocity distribution is

$$\tau-\tau_0 = \left(\frac{dP_1}{dx}+U_l\frac{dU_l}{dx}\right)y + \frac{2}{3K_0\alpha^{\frac{1}{2}}}\frac{d(\alpha U_l)}{dx}y^{\frac{3}{2}} + \frac{2}{3K_0^2}\frac{d\alpha}{dx}y^2, \tag{A. 14}$$

and the linear stress distribution is a good approximation to this distribution if

$$\alpha = \frac{dP_1}{dx}+U_l\frac{dU_l}{dx} \tag{A. 15}$$

and if the last two terms on the right-hand side are small compared with the first. In a boundary layer, $dP_1/dx = -U_1\,dU_1/dx$, and $\zeta = U_l/U_1$ varies much more slowly than U_1, so the conditions for smallness become

$$\frac{2}{3K_0}\frac{1-3a}{(-a)^{\frac{1}{2}}}\frac{\zeta}{(1-\zeta^2)^{\frac{1}{2}}}\left(\frac{y_1}{x}\right)^{\frac{1}{2}} \ll 1 \quad \text{and} \quad \frac{2}{3K_0^2}(1-2a)\frac{y_1}{x} \ll 1. \tag{A. 16}$$

Substituting in the first condition the value of $\eta_1 = y_1/x$ implied by equations (6.10), (6.11) and (6.12), we obtain the condition for development with an equilibrium layer of nearly linear stress distribution

$$\frac{2(1-3a)}{-3a}\left(\frac{\pi}{2}\right)^{\frac{1}{3}}(K_0R_s^2)^{-\frac{2}{3}}\frac{\zeta}{1+\zeta} \ll 1. \tag{A. 17}$$

This condition is satisfied if the exponent defining the pressure gradient is more negative than the value for zero-stress development, $\alpha = -0{\cdot}23$. The second condition of (A. 16) imposes no additional restriction. A last requirement is that $\alpha y_1 \gg \tau_0$, necessary for validity of the velocity distribution (A. 13). Using the approximate forms of equations (6.10), (6.11) and (6.12),

$$CR = -a(2/\pi)^{\frac{1}{2}}R_s(2-C), \quad \zeta = 1-C,$$

we find that the requirement is satisfied if

$$\left(\frac{\pi}{2K_0R_s^2}\right)^{\frac{2}{3}}(1-\zeta)^2 \geqslant \tau_0/U_1^2. \tag{A. 18}$$

In self-preserving wedge flow, the conditions for smallness of the last two terms in (A. 14) become

$$\frac{8}{3K_0}\frac{\zeta}{(\mathscr{P}-\zeta^2)^{\frac{1}{2}}}(\theta-\eta_1)^{\frac{1}{2}} \ll 1, \quad \frac{2}{K_0^2}(\theta-\eta) \ll 1. \tag{A. 19}$$

Substituting the value of $(\alpha-\eta_1)$ given by the conditions for a smooth junction (7.12), we obtain

$$\frac{8}{3K_0}\frac{\zeta}{(\mathscr{P}-\zeta^2)^{\frac{1}{2}}}\left(\frac{I_a}{R_sK_0}\right)^{\frac{1}{3}} \ll 1,$$

and, using the typical values of the slowly varying quantities $\mathscr{P}-\zeta^2$, $(1+k^2)$ and F previously listed, we find that the condition is

$$10\theta^{\frac{2}{3}}\zeta \ll 1. \tag{A. 20}$$

The condition that $\alpha y_1 \geqslant \tau_0$ may be obtained in a similar way as

$$\left[\frac{\theta^2}{2K_0F^2(1+k^2)}(\mathscr{P}-\zeta^2)\right]^{\frac{2}{3}} \geqslant \tau_0/U_1^2,$$

or, using the typical values,

$$0{\cdot}26\theta^{\frac{4}{3}} \geqslant \tau_0/U_1^2. \tag{A. 21}$$

End effects in inviscid flow in a magnetohydrodynamic channel

By G. W. SUTTON AND A. W. CARLSON*

Space Sciences Laboratory, General Electric Company, Philadelphia

(Received 16 January 1961)

The flow of an inviscid, incompressible electrical conducting fluid in a channel of constant rectangular cross-section is considered, when the flow enters a region which contains a magnetic field transverse to the flow and electrodes on opposite sides of the channel. This geometry is typical of a d.c. induction pump or magnetohydrodynamic generator. The conducting fluid external to the magnetic field acts as a shunt and produces a non-uniform electric potential field and hence a non-uniform Lorenz force on the fluid, and causes the fluid velocity profile to be distorted. These effects are calculated theoretically for small magnetic Reynolds number and small magnetic interaction parameter. It is found that the velocity at the centre-line of the channel is retarded and at the walls the velocity is accelerated. The fractional change of velocity at the wall is equal to approximately 0·44 times a modified magnetic interaction parameter.

1. Introduction

In a magnetohydrodynamic electrical power generator, an electrically conducting fluid flows through a channel, in which a transverse magnetic field is applied. The magnetic field interacts with the fluid flow to induce an e.m.f. in the direction perpendicular to the magnetic field and to the direction of the fluid flow. Electrodes are inserted into the channel walls parallel to the magnetic field. If the electrodes are connected to an external load, electrical power can be extracted from the magnetohydrodynamic generator, since the induced e.m.f. produces a voltage difference between the electrodes (figure 1). Alternatively, if the electrodes are connected to a current supply, the channel will act as an induction pump.

The electric current in the fluid is composed of two parts: one due to the induced e.m.f., and the other due to the electric field caused by the voltage difference between the two electrodes. The latter current flows from the positive to the negative electrode and opposes the current caused by the induced e.m.f. (figure 2). At the entrance and exit regions of the channel, that is, near the ends of the electrodes, electric field is not uniform, causing the current density to vary in magnitude and direction in the entrance and exit regions.

The Lorentz force due to the induced e.m.f. opposes the flow and is constant, but the Lorentz force due to the voltage differences between the electrodes

* Now at Princeton University.

varies in magnitude and direction in the entrance and exit regions. The variation of the Lorentz force causes the velocity profile of the fluid to change in the en-

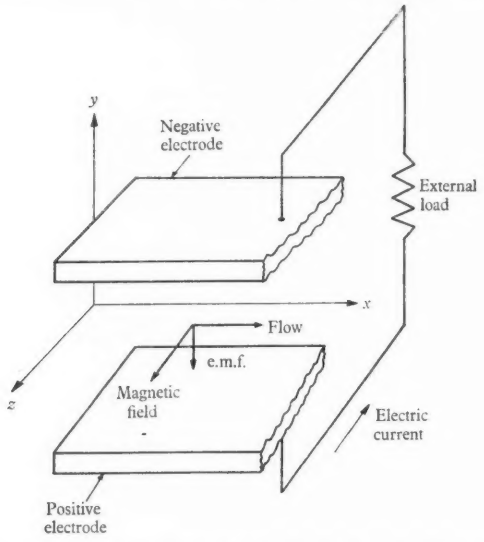

FIGURE 1. Schematic diagram of a magnetohydrodynamic channel.

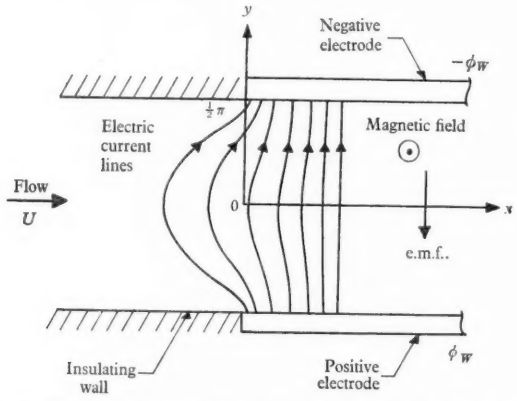

FIGURE 2. Electric current lines due to electric fields in the entrance region of the channel.

trance region and then to assume an asymptotic shape throughout the channel. The Lorentz forces in the exit region will be identical to the Lorentz forces in the entrance region, and will cause further distortion to the flow.

In this investigation, the fluid dynamic effects of the Lorentz forces in the entrance region are determined. Analytical expressions are found which show the manner in which the fluid velocity is altered by the Lorentz forces. The results are illustrated by a set of velocity profiles and a diagram of the streamline pattern.

In order to obtain a solution to the problem, several simplifying assumptions and idealized boundary conditions have been used. The fluid dynamic assumptions are as follows: (1) The flow is steady. (2) The density of the fluid is constant. (3) The viscosity is negligible. (4) The flow is two-dimensional; that is, all gradients in the direction of the magnetic field are zero. (5) The velocity perturbations are small, hence the flow equations may be linearized.

The magnetohydrodynamic assumptions are as follows: (1) The electrical conductivity of the fluid is constant. (2) The Hall effects are negligible. (3) The magnetic Reynolds number is assumed very small so that the applied magnetic field is not altered by the presence of electric currents in the fluid. (4) The magnetic interaction parameter is assumed to be small.

The idealized boundary conditions are as follows: (1) The channel walls, including the electrodes, are parallel. (2) The electrodes are infinitely long, $0 < x < \infty$. (3) The voltage of each electrode is constant, $\pm \phi_W$. (4) The walls, except for the electrodes, are perfect electrical insulators. (5) The magnetic field is zero upstream from the electrodes and has a constant value between the electrodes. It is directed perpendicular to the diagram in figure 2. (6) The velocity far upstream from the electrodes is constant across the channel.

2. Equations

Since the velocity perturbations are assumed small, the axial and transverse velocities can be written as

$$u = U + u', \quad v = v', \tag{1}$$

where u' and v' are small compared to U. Thus, the fluid dynamic equations may be linearized as follows, the continuity equation becoming

$$(\partial u'/\partial x) + (\partial v'/\partial y) = 0, \tag{2}$$

and the momentum equations becoming

$$\rho U(\partial u'/\partial x) + (\partial p/\partial x) = j_y B, \tag{3}$$

and

$$\rho U(\partial v'/\partial x) + (\partial p/\partial y) = -j_x B. \tag{4}$$

Differentiation of equation (3) with respect to y and equation (4) with respect to x and subtraction of the resulting equations gives

$$\rho U(\partial \zeta/\partial x) = -[j_y(\partial B/\partial y) + B(\partial j_y/\partial y) + j_x(\partial B/\partial x) + B(\partial j_x/\partial x)], \tag{5}$$

where the vorticity ζ is given by

$$\zeta = (\partial v'/\partial x) - (\partial u'/\partial x). \tag{6}$$

The first term on the right of equation (5) is zero. From the continuity equation of electricity, the second and fourth terms on the right are also zero. Thus equation (5) becomes

$$\rho U(\partial \zeta/\partial x) = -j_x(\partial B/\partial x). \tag{7}$$

The magnetic field, B, is zero or constant everywhere except at $x = 0$. Therefore, for $x < 0$, the vorticity is a function of y alone and for $x > 0$, it is another function

of y alone. Since the flow is initially irrotational, it remains irrotational up to $x = 0$. At $x = 0$, there is a vorticity jump which is given by

$$\rho U \Delta\zeta = -(j_x)_{x=0} \Delta B, \tag{8}$$

where $(j_x)_{x=0}$ is a function of y only. Thus

$$\left.\begin{aligned} &\zeta = 0 && \text{for} \quad x < 0, \\ \text{and} \quad &\zeta = -(B/\rho U)(j_x)_{x=0} && \text{for} \quad x > 0. \end{aligned}\right\} \tag{9}$$

If the longitudinal component of the electric current density at $x = 0$ is known, the vorticity can be found anywhere in the channel. The vorticity may be expressed in terms of the stream function by

$$u' = \partial\psi/\partial y, \quad v' = -\partial\psi/\partial x. \tag{10}$$

The vorticity is then given by

$$\zeta = -(\partial^2\psi/\partial x^2) - (\partial^2\psi/\partial y^2) = -\nabla^2\psi,$$

so that equation (9) becomes

$$\left.\begin{aligned} &\nabla^2\psi = 0 && (x < 0); \\ &\nabla^2\psi = (B/\rho U)(j_x)_{x=0} && (x > 0). \end{aligned}\right\} \tag{11}$$

Equation (11) is the required fluid dynamical equation. The electric field equation is obtained from conservation of electricity. Neglecting the Hall effect, the generalized Ohm's law is taken as

$$\mathbf{j} = \sigma(\mathbf{E} + \mathbf{q} \times \mathbf{B}). \tag{12}$$

Since the problem is steady, $\nabla \times \mathbf{E} = 0$, and therefore $\mathbf{E}$ may be considered to be the negative gradient of electric potential

$$\mathbf{E} = -\nabla\phi. \tag{13}$$

The divergence of the electric current is zero; for constant σ equation (12) then becomes

$$\nabla^2\phi = \mathbf{B}.(\nabla \times \mathbf{q}) - \mathbf{q}.(\nabla \times \mathbf{B}). \tag{14}$$

Since $\nabla \times \mathbf{q} = \zeta\mathbf{k}$, $\mathbf{B} = B\mathbf{k}$, equation (14) becomes

$$\nabla^2\phi = B\zeta - v(\partial B/\partial x). \tag{15}$$

For $x \neq 0$, $(\partial B/\partial x) = 0$, and the vorticity is obtained from equation (9), so that equation (15) becomes

$$\left.\begin{aligned} &\nabla^2\phi = 0 && (x < 0); \\ &\nabla^2\phi = -(B^2/\rho U)(j_x)_{x=0} && (x > 0). \end{aligned}\right\} \tag{16}$$

The electric current is obtained from equation (12) as

$$j_x = \sigma(E_x + vB) \tag{17}$$

or

$$j_x = -\sigma[(\partial\phi/\partial x) + B(\partial\psi/\partial x)]. \tag{18}$$

Thus equations (11) and (16) become

$$\nabla^2\phi = \nabla^2\psi = 0 \quad (x < 0); \tag{19a}$$

$$\nabla^2\psi = -\frac{\sigma B}{\rho U}\left(\frac{\partial\phi}{\partial x} + B\frac{\partial\psi}{\partial x}\right)_{x=0} \quad (x > 0); \tag{19b}$$

$$\nabla^2\phi = \frac{\sigma B^2}{\rho U}\left(\frac{\partial\phi}{\partial x} + B\frac{\partial\psi}{\partial x}\right)_{x=0} \quad (x > 0). \tag{19c}$$

The boundary conditions are

$$\phi = \pm\phi_W, \quad y = \mp\tfrac{1}{2}\pi \quad (x > 0); \tag{20a}$$

$$\partial\phi/\partial y = 0, \quad y = \pm\tfrac{1}{2}\pi \quad (x < 0); \tag{20b}$$

$$\psi = \pm U\tfrac{1}{2}\pi, \quad y = \pm\tfrac{1}{2}\pi \quad (-\infty < x < \infty). \tag{20c}$$

Equations (19) may be made dimensionless by use of the following new variables

$$\psi = Uh\Psi, \quad \phi = UBh\Phi, \quad x = h\xi, \quad y = h\xi', \tag{21}$$

where h is the channel width.

With the use of equations (21), equations (19*b*) and (19*c*) become

$$\nabla^2\Phi = I(\partial/\partial\xi)(\Phi + \Psi), \tag{22a}$$

and

$$\nabla^2\Psi = I(\partial/\partial\xi)(\Phi + \Psi), \tag{22b}$$

where I is the magnetic interaction parameter, $\sigma B^2 h/\rho U$. To solve equations (22*a*) and (22*b*) for small I, Φ and Ψ are expressed in terms of series whose coefficients are powers of I

$$\Phi = \Phi_0 + I\Phi_1 + \ldots, \tag{23a}$$

$$\Psi = \Psi_0 + I\Psi_1 + \ldots. \tag{23b}$$

These are then substituted into equations (22*a*) and (22*b*), and the terms having common powers of I are equated, to give

$$\nabla^2\Phi_0 = 0 \quad (-\infty < x < \infty); \tag{24a}$$

$$\nabla^2\Psi_0 = 0 \quad (-\infty < x < \infty); \tag{24b}$$

$$\nabla^2\Phi_1 = 0 \quad (x < 0); \tag{24c}$$

$$\nabla^2\Phi_1 = (\partial/\partial\xi)(\Phi_0 + \Psi_0) \quad (x > 0); \tag{24d}$$

$$\nabla^2\Psi_1 = 0 \quad (x < 0); \tag{24e}$$

$$\nabla^2\Psi_1 = (\partial/\partial\xi)(\Phi_0 + \Psi_0) \quad (x > 0). \tag{24f}$$

The boundary conditions then become, in terms of the dimensional variables,

$$\phi_0 = \pm\phi_W, \quad y = \mp\tfrac{1}{2}\pi \quad (x > 0); \tag{25a}$$

$$\partial\phi_0/\partial y = 0, \quad y = \pm\tfrac{1}{2}\pi \quad (x < 0); \tag{25b}$$

$$\phi_1 = 0, \quad y = \pm\tfrac{1}{2}\pi \quad (x > 0); \tag{25c}$$

$$\partial\phi_1/\partial y = 0, \quad y = \pm\tfrac{1}{2}\pi \quad (x < 0); \tag{25d}$$

$$\psi_0 = \pm\tfrac{1}{2}\pi U, \quad y = \pm\tfrac{1}{2}\pi \quad (-\infty < x < \infty); \tag{25e}$$

$$\psi_1 = 0, \quad y = \pm\tfrac{1}{2}\pi \quad (-\infty < x < \infty). \tag{25f}$$

3. Solution to the electric potential equations

It is convenient to make the transformation

$$\eta = y + \tfrac{1}{2}\pi \tag{26}$$

to shift the origin of the co-ordinate system to the lower wall, see figure 2. To solve equation (24*a*) with the boundary conditions of equations (25*a*, *b*), the original region is mapped conformally by means of the following transform (see figure 3),

$$e^z = \sin z', \tag{27}$$

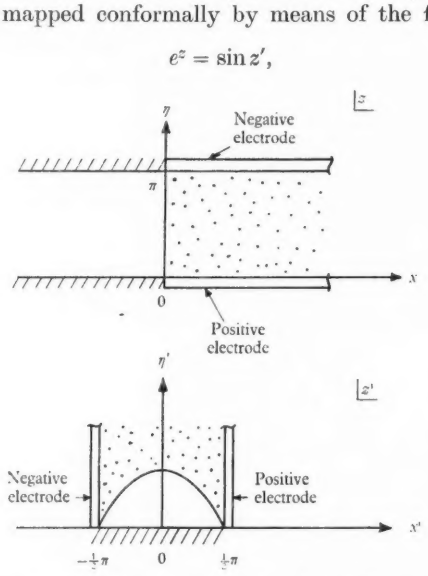

FIGURE 3. Complex planes showing the regions mapped.

where $z = x + i\eta$, $z' = x' + i\eta'$. In the z'-plane, the boundary conditions are

$$\phi_0 = \pm\phi_W, \quad x' = \pm\tfrac{1}{2}\pi; \quad \partial\phi_0/\partial\eta' = 0 \quad (\eta' = 0). \tag{28}$$

The solution is obviously

$$\phi_0 = 2\phi_W x'/\pi. \tag{29}$$

Thus, in the z'-plane lines of constant η' are flux lines, while lines of constant x' are equipotential lines. These are shown in figure 4.

The electric current to the electrodes between $x = 0$ and x may be calculated next from

$$J_0 = \int_0^x j_y\,dx = -\sigma\int_0^x [(\partial\phi_0/\partial y) + UB]\,dx = \sigma\left[\int_0^{\eta'} (\partial\phi_0/\partial x')\,d\eta' - UBx\right]$$

or

$$J_0 = 2\pi^{-1}\sigma\phi_W\eta' - \sigma UBx. \tag{30}$$

For large η' along $x' = \frac{1}{2}\pi$, the transformation of equation (27) becomes $e^x = \frac{1}{2}e^{\eta'}$, so that

$$\eta' = x + \ln 2, \tag{31}$$

and when substituted into equation (30) this yields

$$J_0 = \sigma(2\pi^{-1}\phi_W - UB)\,x + 2\pi^{-1}\sigma\phi_W \ln 2. \tag{32}$$

Thus, there is a current loss of $2\pi^{-1}\sigma\phi_W \ln 2$ associated with the inlet, and a similar loss at the exit. If the channel length is L, the total current to the electrodes, per unit height in the direction of the magnetic field, is

$$J_L = \sigma[(2\phi_W/h) - UB]\,L + 4\pi^{-1}\sigma\phi_W \ln 2, \tag{33}$$

where h is the channel width and the voltage across the electrodes is $2\phi_W$; thus the last term represents the inlet and exit losses. The power consumed or produced is $P = -2\phi_W J_L$, and, in the case of a magnetohydrodynamic generator, the external resistance is given by $-2\phi_W/J_L$.

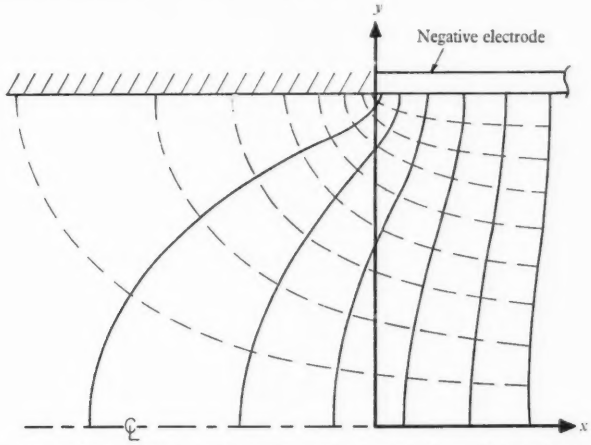

FIGURE 4. Electric flux lines (solid) and equipotential lines (dashed) in the upper half of the channel.

The change in total average pressure may be calculated from

$$\Delta p = 2\pi^{-1} \int_{-\infty}^{\infty} (\mathbf{j} \times \mathbf{B})_x \, dx\, dy. \tag{34}$$

Substitution for the current from the generalized Ohm's laws and integration yields

$$\Delta p = \sigma BL[2\phi_W h^{-1} - UB]. \tag{35}$$

It is interesting to note that there is no term representing the end loss in equation (35).

A pump or generator efficiency, ϵ_p or ϵ_g, may be defined in terms of the flow work $(\Delta p)\,Uh$ and the power P by

$$\epsilon_p = \epsilon_g^{-1} = \frac{\Delta p Uh}{P} = \frac{BLUh[2\phi_W h^{-1} - UB]}{2\phi_W\{L[2\phi_W h^{-1} - UB] + 4\pi^{-1}\phi_W \ln 2\}}. \tag{36}$$

Finally, if $L \to \infty$, the end losses become negligible, and the efficiencies become

$$\epsilon_p = \epsilon_g^{-1} = UBh/2\phi_W. \tag{37}$$

Thus for efficient operation, the electrode voltage should be close to the induced voltage. It should be noted that this analysis applies to finite length electrodes with an error of less than 1 % if $L/h > 1$.

The equation for ϕ_0, equation (25a), has also been solved for constant magnetic field extensions by Fishman (1959) and for exponentially decreasing magnetic fields by Sutton, Hurwitz & Poritsky (1959), for which efficiencies have also been calculated. In addition, Hurwitz, Kilb & Sutton (1961) have also considered the Hall effect. However the influence on the fluid motion was not considered. In addition, the electric fields associated with extensions to the magnetic fields complicate the calculation of ψ_1, but do not materially alter the main effect. Therefore, in the remainder, extensions to the magnetic field will not be considered.

The solution to equations (24c, d) for ϕ_1 are also not simple to obtain because of the inhomogeneous term and the boundary conditions for ϕ_1 but this is not required in obtaining the solution for ψ_0 or ψ_1. However, the expression for $\partial\phi_0/\partial x$ is required. In terms of the transformed coordinates, this is given by

$$(\partial\phi_0/\partial x)_{x=0} = 2\pi^{-1}\phi_W(\partial x'/\partial x)_{x=0}. \tag{38}$$

Use of equation (27) to determine (dx'/dx) yields

$$(\partial\phi_0/\partial x)_{x=0} = \pi^{-1}\phi_W[(1\pm\sin\eta)/\sin\eta]^{\frac{1}{2}}. \tag{39}$$

4. Solution to the flow equations

The solution to equation (24b) with boundary conditions (25e) is

$$\psi_0 = Uy. \tag{40}$$

With equations (40), (39) and (24e), the equation for ψ_1 then becomes

$$\nabla^2\psi_1 = f(y), \tag{41}$$

where $f(y) = 0$ when $x < 0$

and $f(y) = -(\sigma B\phi_W/\pi\rho U)[(1-\cos y)/\cos y]^{\frac{1}{2}}$ when $x > 0$. } (42)

Since $f(y)$ is a forcing function, the solution for ψ_1 may be obtained by means of a Green's function as

$$\psi_1 = \int_0^\infty G(x-\xi, y)\,d\xi, \tag{43}$$

where $$\nabla^2 G_{1,2}(x-\xi, y) = \delta(\xi)f(y) \tag{44}$$

and δ is the Dirac delta function. By means of separation of variables, the following solution is obtained for G,

$$G_1 = \sum_{n=1}^{\infty} a_n \sin(2ny)\, e^{2n(x-\xi)} \quad \text{when} \quad x < \xi, \tag{45a}$$

and $$G_2 = \sum_{n=1}^{\infty} a_n \sin(2ny)\, e^{-2n(x-\xi)} \quad \text{when} \quad x > \xi. \tag{45b}$$

The coefficients a_n are the same in equations (45a, b) since $G_1 = G_2$ at $x = \xi$. Substitution of equations (45a, b) in equation (44) and integration from $x = \xi - \epsilon$ to $x = \xi + \epsilon$ yields

$$-4\sum_{n=1}^{\infty} n a_n \sin(2ny) = f(y), \tag{46}$$

so that $$a_n = \frac{1}{n\pi}\int_{-\frac{1}{2}\pi}^{0} f(y)\sin(2ny)\,dy. \tag{47}$$

Use of equation (42) for $f(y)$ and a change of variable to η by equation (26) yields

$$a_n = \frac{(-1)^n}{n\pi}\left(\frac{B\phi_W}{\pi\rho U}\right)\int_0^{\frac{1}{2}\pi} \sin(2n\eta)\left[\frac{1-\sin\eta}{\sin\eta}\right]^{\frac{1}{2}} d\eta. \tag{48}$$

The integral in equation (48) is the imaginary part of

$$\int_0^{\frac{1}{2}\pi} e^{2in\theta}\left[\frac{1-\sin\theta}{\sin\theta}\right]^{\frac{1}{2}} d\theta. \tag{49}$$

The integral may be taken in the complex plane from $Z = 1$ to $Z = i$, where

$$Z = e^{i\theta}, \quad d\theta = dZ/iZ \quad \text{and} \quad \sin\theta = (Z^2-1)/2iZ. \tag{50}$$

Substitution of equation (50) into (49) yields the integral

$$\int_1^i \frac{Z^{2n}(1+iZ)}{Z(1-Z^2)^{\frac{1}{2}}} dZ. \tag{51}$$

Since there are no singularities in the quadrant concerned, the path of integration may be taken from 1 to 0, then 0 to i. The integral (51) then becomes

$$\int_0^1 \frac{x^{2n}(1+ix)}{x[1-x^2]^{\frac{1}{2}}} dx + \int_0^1 \frac{(iy)^{2n}(1-y)\,i\,dy}{iy(1-y^2]^{\frac{1}{2}}}. \tag{52}$$

The only imaginary part is the second term of the first integral. Upon letting $x^2 = \beta$, it becomes

$$-\frac{1}{2}\int_0^1 \frac{\beta^{n-\frac{1}{2}}}{(1-\beta)^{\frac{1}{2}}} d\beta = -\frac{1}{2}\frac{\Gamma(n+\frac{1}{2})\,\Gamma(\frac{1}{2})}{\Gamma(n+1)}.$$

Thus, the coefficients a_n are given by

$$a_n = \frac{\sigma B\phi_W}{\pi\rho U}\left\{\frac{(-1)^n}{2n}\frac{1.3.5\ldots(2n-1)}{2.4.6\ldots(2n)}\right\}. \tag{53}$$

Values of a_n are shown in table 1. The stream function is obtained by substitution of equation (45) into equation (43) and integration. The result is

$$\psi_1 = \int_0^\infty G_1 d\xi = \sum_{n=1}^\infty \frac{a_n}{2n}\sin(2ny)\,e^{2nx} \quad \text{for} \quad x < 0;$$

$$\psi_1 = \int_0^x G_2 d\xi + \int_x^\infty G_1 d\xi = \sum_{n=1}^\infty \frac{a_n}{2n}\sin(2ny)\,(2-e^{-2nx}) \quad \text{for} \quad x > 0. \tag{54}$$

The solution is shown graphically by the streamline pattern in figure 5.

The velocity perturbation is then given by differentiation of equation (54), and substitution of a_n from equation (53). Hence

$$u' = \frac{\sigma B\phi_W}{2\pi\rho U}\sum_{n=1}^\infty \frac{(-1)^n}{n}\frac{1.3.5\ldots(2n-1)}{2.4.6\ldots(2n)}\cos(2ny)\,[1 \mp (1-e^{\pm 2nx})], \tag{55}$$

$$v' = -\frac{\sigma B\phi_W}{2\pi\rho U}\sum_{n=1}^\infty \frac{(-1)^n}{n}\frac{1.3.5\ldots(2n-1)}{2.4.6\ldots(2n)}\sin(2ny)\,e^{\pm 2nx}.$$

For $x < 0$, the upper sign, and for $x > 0$, the lower sign is to be used. It is obvious that the change in axial velocity at $x = 0$ is one-half of that at $x = \infty$. When the

n	$\pi\rho U a_n/\sigma B\phi_W$	n	$\pi\rho U a_n/\sigma B\phi_W$
1	−0·250000	11	−0·007645
2	0·092500	12	0·006716
3	−0·052080	13	−0·005961
4	0·034180	14	0·005337
5	−0·024610	15	−0·004815
6	0·018800	16	0·004373
7	−0·014960	17	−0·003995
8	0·012270	18	0·003668
9	−0·010300	19	−0·003384
10	0·008809	20	0·003134

TABLE 1. Values of the Fourier coefficients a_n.

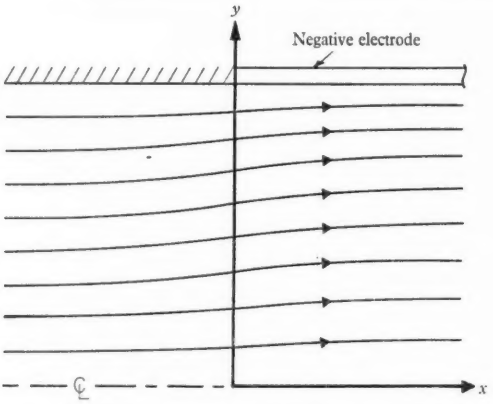

FIGURE 5. Streamline pattern in the upper half of the channel.

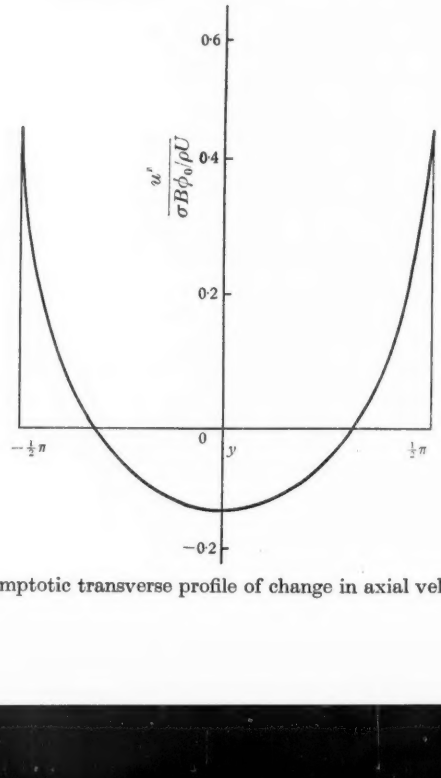

FIGURE 6. Asymptotic transverse profile of change in axial velocity, as $x \to \infty$.

fluid leaves the magnetic field, the effects are exactly doubled and the velocity change is also doubled.

It can be seen from the form of the solution that the changes in velocity are linearly dependent on a modified magnetic interaction parameter $I' = \sigma B\phi_W/\rho U^2$, or in terms of I,

$$I' = (\phi_W/BUh)\,I. \tag{56}$$

The maximum value of u' occurs at the wall; this is given by $u'/U = 0{\cdot}44I'$ as $x \to \infty$. Thus, the linearization of the flow is consistent with the assumption of small magnetic interaction parameter. Also, if the two electrodes are at the same potential, the $u' = v' = 0$. The axial velocity perturbation profile for $x \to \infty$ is shown in figure 6 and the development is shown in figure 7.

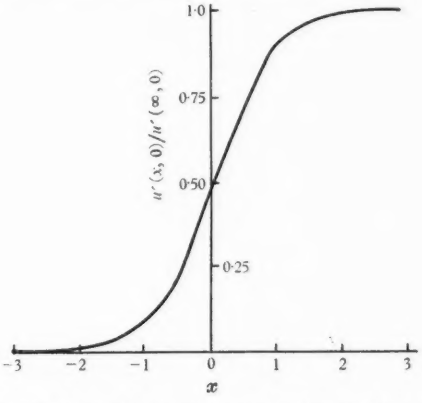

FIGURE 7. Axial variation of change in axial velocity along axis of channel.

5. Asymptotic velocity profile

In the region of the channel far downstream from the entrance the velocity can be calculated directly, without first finding the solution throughout the entire channel.

As x becomes very large, the vertical component of the velocity becomes very small. Therefore, the vorticity is

$$\zeta = -\partial u/\partial y \tag{57}$$

so that

$$u = -\int \zeta\, dy. \tag{58}$$

From equation (9), the vorticity is given by

$$\zeta = \frac{\sigma B\phi_W}{\pi\rho U}\left[\frac{1-\sin\eta}{\sin\eta}\right]^{\frac{1}{2}}, \tag{59}$$

and integration of the radical with respect to η yields

$$2\sinh^{-1}(\sin\eta)^{\frac{1}{2}} + \text{const.} \tag{60}$$

Since the average velocity must be U, the constant may be evaluated, from which it is found that

$$u' = \frac{2\sigma B\phi_W}{\pi\rho U}\left[\ln 2 - \sinh^{-1}(\cos y)^{\frac{1}{2}}\right]. \tag{61}$$

Thus $$u'/U = -0{\cdot}118\,\sigma B\phi_W/\rho U^2 \quad \text{at} \quad y = 0 \tag{62}$$

and $$u'/U = 0{\cdot}442\,\sigma B\phi_W/\rho U^2 \quad \text{at the walls.} \tag{63}$$

For $I' = \frac{1}{4}$, the velocity variation at the wall is about 10 % of the initial velocity. For larger values of the parameter, the assumption of small velocity perturbations is no longer valid.

This solution is qualitatively similar to that found by Shercliff (1956) for the flow distortion at the inlet to a flowmeter; however, equation (18) predicts that the flow disturbance would be about 50 % greater than that for the flowmeter problem. Also, Shercliff gives only the asymptotic velocity profile and not the development of the perturbation, as given by equation (55).

6. Discussion

Measurements of the flow distortion have recently been made in copper sulphate solutions by Rossow, Jones & Huerta (1961). The mean flow velocity was 4·22 in./sec, taken at the point where $u' = 0$ from the theory, which corresponds to 1·17 in. from the centre-line. The value of $u'(0)$ was then 0·83 in./sec. Using a magnetic field of 4000 G, equation (62) predicts that $u' = 1{\cdot}15$ in./sec., which is higher by about 28 %. This is good agreement, considering that viscosity was neglected, and that the magnetic field does not abruptly decrease to zero at $x = 0$.

This work was supported by the United States Air Force Office of Scientific Research, under contract 49(638)–914. The authors gratefully acknowledge the helpful suggestions of Dr H. Hurwitz, Jr.

REFERENCES

Fishman, F. 1959 End effects in magnetohydrodynamic flow. *AVCO-Everett Res. Rep.* 78.

Hurwitz, H., Kilb, R. W. & Sutton, G. W. 1961 Influence of tensor conductivity on current distribution in an MHD generator. *J. Appl. Phys.* **32**, 205.

Rossow, V., Jones, W. P. & Huerta, R. 1961 On the induced flow of an electrically conducting liquid in a rectangular duct by electric and magnetic fields of finite extent. *Nat. Adv. Comm. Aero., Wash., Tech. Note* no. D-349.

Shercliff, J. A. 1956 Edge effects in electromagnetic flowmeters. *J. Nuclear Energy*, **3**, 305.

Sutton, G. W., Hurwitz, H. & Poritsky, H. 1959 Electrical and pressure losses in a magnetohydrodynamic channel due to end current loops. *General Electric Co., TIS Rep.* R59SD431.

The force on a sphere moving through a conducting fluid in the presence of a magnetic field

By J. R. REITZ AND L. L. FOLDY
Case Institute of Technology, Cleveland, Ohio

(Received 8 July 1960 and in revised form 16 January 1961)

The force on a sphere moving through an inviscid, conducting fluid in the presence of a uniform magnetic field $\mathbf{B}_0$ is calculated for the low-conductivity case where the hydrodynamic motion deviates only slightly from potential flow. The magnetic Reynolds number is assumed small. The force on the sphere is found to consist of both a drag and a deflective component which tends to orient its motion parallel to a magnetic field line; if the sphere's velocity is $\mathbf{V}$, the force may be written

$$\mathbf{R} = -AB_0^2\mathbf{V} + C(\mathbf{V}.\mathbf{B}_0)\,\mathbf{B}_0,$$

where the coefficients A and C depend on the conductivities of both sphere and fluid. The coefficients are evaluated by calculating the Joule dissipation for particular orientations of $\mathbf{V}$ relative to $\mathbf{B}_0$. In one case the force is also calculated directly from the perturbed pressure distribution in the fluid. In an analogous way, a spinning sphere in a conducting fluid experiences both resistive and gyroscopic torques.

1. Introduction

An uncharged, non-magnetic body moving through an inviscid conducting fluid or plasma in the presence of a magnetic field should experience a resistive drag force or torque due to the Joule dissipation of energy caused by induced currents in the conducting system. We call this *induction drag*. Accompanying such drag forces are generally deflective forces or torques of similar magnitude at right angles to the velocity or angular velocity of the body, which might be called induction deflexion. The problem in the case of a strong magnetic field has been studied in some detail by Stewartson (1956). For the case of a weak magnetic field, calculations of the induction drag for a sphere have been made by Chopra (1956, 1957) and by Chopra & Singer (1958), but the expressions they obtain are incorrect as is evident from the fact that their drag force does not vanish when the conductivity of the fluid goes to zero, a result in conflict with the Special Theory of Relativity. Their error appears to arise, among other things, from a failure to observe that a concomitant of such motion is the induction of charges on the surface of a sphere (and in the case of a spinning sphere, induced volume charge density in the sphere itself) producing electric fields of comparable magnitude to those produced by induction (dynamo effect). There are additional effects if the body is charged or magnetized, but such cases are not considered in this paper.

It is the purpose of the present paper to provide correct expressions for induction drag and deflective forces for a sphere moving with constant velocity, and expressions for induction drag and deflective torques for a spinning sphere, on the assumption that the induced magnetic field is small and that the hydrodynamic motion differs only slightly from the situation of potential flow. Such situations should exist when the magnetic field is sufficiently weak or the conductivity of the fluid is sufficiently small. In obtaining drag and deflective forces it is tacitly assumed that the fluid motion is steady in the system of co-ordinates in which the sphere is at rest. We have not been able to show that our solution to the problem is unique or even that a steady-state solution of the magnetohydrodynamic equations exists in all cases of this type. However, for the case of motion of the sphere parallel to the magnetic lines of induction, we demonstrate that the drag force obtained from Joule losses is the same as that computed from the perturbed pressure distribution in the fluid to first order in the fluid conductivity.† The assumption that the zero-order magnetic field can be taken to be a uniform field in these cases also requires examination, since Ludford & Murray (1960) have shown that for a similar geometry, the perturbation expansion of the magnetic field in the fluid conductivity is not regular.

In §2 we carry out in a straightforward manner the calculation of the forces by the use of the Joule-loss method for several cases of interest. In §3, we examine in more detail the assumptions and approximations made in the special case of a sphere moving parallel to the magnetic field and verify that a complete first-order calculation yields the same result for the drag force as does the Joule-loss calculation.

2. Force and torque from Joule losses

Consider a homogeneous spherical body of radius a and electrical conductivity σ' moving with velocity $-\mathbf{V}$ (or spinning with angular velocity $\boldsymbol{\omega}$) in an inviscid, incompressible fluid of conductivity σ in the presence of a uniform magnetic field $\mathbf{B}_0$. The Joule losses resulting from the induced currents in the sphere-fluid system will be calculated and equated to the rate at which mechanical energy is dissipated by the sphere, $\mathbf{R}.\mathbf{V}$ (or $\mathbf{D}.\boldsymbol{\omega}$). These calculations enable us to obtain the drag force, $\mathbf{R}$, or the drag torque, $\mathbf{D}$, respectively.

In calculating the induced currents, the magnetic field is taken to be the zero-order uniform field, and the fluid velocity is taken to be that which would exist if the conductivity of the system were zero. The first of these statements requires that the magnetic Reynolds number, $R_M = \sigma\mu Va$, be small and that the perturbation expansion of the magnetic field in terms of this parameter, although irregular at large distances, does not change the uniform field in the current-carrying region. The second statement requires that the parameter $\beta R_M = \sigma a B_0^2/\rho V$ be small and that the perturbation expansion for the fluid velocity be sufficiently regular in the same sense. These remarks will be amplified in §§3.2 and 3.3. Here ρ is the density of the fluid.

† After completion of this work, our attention has been directed to a paper by Ludford (1960) who also makes the point that, for flow at low magnetic Reynolds number, the induction drag can be computed directly from the undisturbed potential flow and magnetic field.

No restrictions will be placed on the conductivity σ' of the translating sphere,† although for the rotating sphere it will be necessary to assume that R'_M (defined using σ' and μ') is small also. We shall take the permeabilities of sphere and fluid equal to each other so that induced dipole effects may be neglected.

2.1. *Force on a moving sphere from Joule losses*

The basic equations of the electromagnetic field under steady conditions are:

$$(a)\ \operatorname{div}\mathbf{B}=0,\quad (b)\operatorname{curl}\mathbf{E}=0,\quad (c)\operatorname{curl}\mathbf{B}=\mu\mathbf{j},\quad (d)\ \operatorname{div}\mathbf{E}=\rho/\epsilon,$$
$$(e)\operatorname{div}\mathbf{j}=0,\quad (f)\ \mathbf{j}=\sigma\mathscr{E}, \tag{1}$$

where, for convenience, we have defined $\mathscr{E}$ by

$$\mathscr{E}=\mathbf{E}+\mathbf{v}\times\mathbf{B}, \tag{2}$$

and will refer to it as the 'effective electric field'. The Joule energy dissipation per unit volume is then $\sigma\mathscr{E}^2$. In this paper we use rationalized electromagnetic units. Equation (1*c*) will not be used in this section since it serves to generate the perturbation expansion for $\mathbf{B}$. Instead we take $\mathbf{B}=\mathbf{B}_0$.

The Joule losses will be calculated in the system of co-ordinates at rest in the sphere, where the hydrodynamic motion is steady. As discussed earlier, the velocity in the fluid is described by potential flow; thus, we write

$$\mathbf{v}=\mathbf{V}+\tfrac{1}{2}a^3\nabla(\mathbf{V}.\mathbf{r}/r^3) \tag{3}$$

relative to an origin at the centre of the sphere.

It is expedient to break up the problem into several parts and discuss first the case where $\mathbf{V}$ is parallel to $\mathbf{B}_0$. Next, the case where $\mathbf{V}$ is perpendicular to $\mathbf{B}_0$ is considered. Finally, the general case where $\mathbf{V}$ makes an oblique angle with $\mathbf{B}_0$ may be described simply in terms of the other two fundamental solutions.

(*a*) *Case* 1: $\mathbf{V}$ *parallel to* $\mathbf{B}_0$. In this case there is no induction term inside the sphere; furthermore, since $\mathbf{v}\times\mathbf{B}_0$ in the fluid has no component perpendicular to the spherical surface, it is evident that there is no surface electric charge. In fact, there is no electrostatic field at all since both $\operatorname{div}(\mathbf{v}\times\mathbf{B}_0)=0$ and $\operatorname{div}\mathbf{j}=0$. This implies that $\operatorname{div}\mathbf{E}_s=0$ and, hence, no volume charge. Thus, inside the sphere the effective electric field is given by

$$\mathscr{E}'=0, \tag{4}$$

and in the fluid by

$$\mathscr{E}=\mathbf{v}\times\mathbf{B}_0=(3VB_0a^3/2r^3)\,[0,0,\cos\theta\sin\theta]. \tag{5}$$

Here we use spherical polar co-ordinates (r,θ,ϕ) with $\mathbf{V}$ taken as the direction of the polar axis.

The total rate of Joule energy dissipation is obtained by integrating $\sigma\mathscr{E}^2$ over the fluid volume. If this is equated to R_1V one obtains for the drag force

$$R_1=\tfrac{2}{5}\pi a^3\sigma B_0^2\,V. \tag{6}$$

For this geometry there is pure drag, i.e. no deflexion, as may be readily verified by symmetry arguments.

† The conductivity of the sphere may be arbitrarily large; if the conductivity is infinite, however, the results of the calculation may have to be modified, depending on the magnitude and orientation of the magnetic field initially frozen into the sphere.

(*b*) *Case* 2: $\mathbf{V}$ *perpendicular to* $\mathbf{B}_0$. When the sphere is moving perpendicular to the magntic field, the effective electric field inside the sphere is just the electric field $\mathbf{E}'$, or

$$\mathscr{E}' = \mathbf{E}'. \tag{7}$$

In the fluid the effective electric field is given by the sum of two terms, namely

$$\mathscr{E} = \mathbf{v} \times \mathbf{B}_0 + \mathbf{E}, \tag{8}$$

or

$$\mathscr{E} = -(VB_0 a^3/2r^3)\,[-\sin\theta\sin\phi, 2\cos\theta\sin\phi, \cos\phi(3\cos^2\theta - 1)] + \mathbf{V} \times \mathbf{B}_0 + \mathbf{E}. \tag{8a}$$

Here $\mathbf{V}$ is taken as the polar direction and B_0 in the $\phi = 0$ plane. $\mathscr{E}$ must vanish at infinity; the second term in (8*a*) does not vanish there so it must be cancelled by a part of $\mathbf{E}$. Now $\operatorname{div}(\sigma'\mathscr{E}') = 0$ and $\operatorname{div}(\sigma\mathscr{E}) = 0$; since the induction term in (8*a*) is itself divergence-free, we have

$$\operatorname{div}\mathbf{E} = 0, \quad \operatorname{div}\mathbf{E}' = 0.$$

This result combined with (1*b*) allows us to write formal series expansions for $\mathbf{E}$ and $\mathbf{E}'$ in terms of tesseral harmonics, $Z_j(\theta, \phi)$. Thus we write

$$\mathbf{E} = -\mathbf{V} \times \mathbf{B} - \nabla \sum_{j=0}^{\infty} b_j Z_j(\theta, \phi)\, a^{2j+1}/r^{j+1}, \tag{9}$$

$$\mathbf{E}' = -\mathbf{V} \times \mathbf{B} - \nabla \sum_{j=0}^{\infty} b'_j Z_j(\theta, \phi)\, r^j, \tag{10}$$

with the b_j and b'_j as yet undetermined constants. The boundary conditions to be satisfied are continuity of the tangential component of electric field and continuity of the normal component of current density on the spherical surface. The first of these conditions leads immediately to the result $b_j = b'_j$.

The boundary condition on the current density shows that all $b_j = 0$ except for the tesseral harmonic involving $\sin\theta\sin\phi$ for which

$$b = -\tfrac{1}{2}VB_0(\sigma + 2\sigma')/(2\sigma + \sigma').$$

Incorporation of these results into the formal series expansions, (9) and (10), leads to

$$\mathbf{E}' = -\tfrac{1}{2}VB_0[3\sigma/(2\sigma + \sigma')]\,\nabla(r\sin\theta\sin\phi), \tag{11}$$

i.e. a uniform field, and

$$\mathbf{E} + \mathbf{V} \times \mathbf{B}_0 = -\tfrac{1}{2}VB_0[(\sigma + 2\sigma')/(2\sigma + \sigma')]\,\nabla(a^3\sin\theta\sin\phi/r^2). \tag{12}$$

The total rate of energy dissipation is obtained by integrating $\sigma' E'^2$ over the volume of the sphere and adding the result to the integral of $\sigma\mathscr{E}^2$ over the external region. Equating this to the rate of mechanical energy dissipation, $R_2 V$ (where R_2 is the drag force), we obtain

$$R_2 = \tfrac{3}{5}\pi a^3 B_0^2 V\sigma(\sigma + 3\sigma')/(2\sigma + \sigma'). \tag{13}$$

For this geometry there is again pure drag as may be readily verified by symmetry arguments. The current lines (lines of effective electric field) in the fluid are shown in figure 1 for the case in which $\sigma' = 0$.

(*c*) *Case* 3: *oblique angle*. When the magnetic field $\mathbf{B}_0$ makes an oblique angle with the velocity $\mathbf{V}$, the sphere experiences both deflective and drag forces. That a deflective force exists may be readily verified by considering the $\mathbf{j} \times \mathbf{B}_0$ contribution from the sphere itself. Now a vector force proportional to $B_0^2 V$ can be constructed from a linear combination of $\mathbf{B}_0 \times (\mathbf{V} \times \mathbf{B}_0)$ and $\mathbf{B}_0(\mathbf{V} . \mathbf{B}_0)$ terms, or equivalently, from a combination of $B_0^2\mathbf{V}$ and $\mathbf{B}_0(\mathbf{V} . \mathbf{B}_0)$ terms. Thus, the

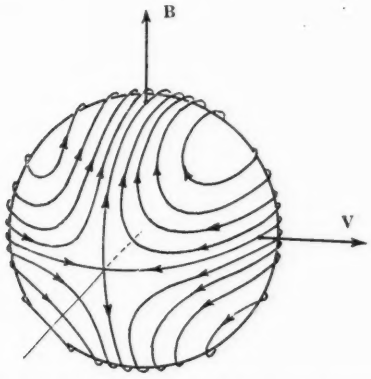

FIGURE 1. Current lines in a conducting fluid for a non-conducting sphere moving with velocity $\mathbf{V}$ at right angles to a uniform magnetic field $\mathbf{B}$.

force on the sphere (here we let $\mathbf{V}$ stand for the sphere's actual velocity in the stationary fluid) can be written

$$\mathbf{R} = -AB_0^2\mathbf{V} + C(\mathbf{V} . \mathbf{B}_0)\,\mathbf{B}_0. \tag{14}$$

The coefficients A and C may be evaluated from equations (6) and (13). We find

$$A = \tfrac{2}{5}\pi a^3[\sigma(\sigma + 3\sigma')/(2\sigma + \sigma')], \tag{14a}$$

$$C = \tfrac{1}{5}\pi a^3[\sigma(7\sigma' - \sigma)/(2\sigma + \sigma')]. \tag{14b}$$

A moving sphere thus experiences, in general, a deflective force which tends to orient its motion parallel to a magnetic field line. Such forces may have a measurable effect on the orbital motion of earth satellites, although it must be emphasized that the hydrodynamic model of the fluid assumed here is quite different from that of an atmospheric plasma with its long free-path for charged particles.

2.2. *Discussion*

There are several points regarding equation (14) worth commenting upon. First, the induction drag and deflexion vanish when the conductivity of the fluid is zero. For finite σ but vanishing σ', on the other hand, there is a drag and in general a deflective force also. This result is due to the presence of complete eddy-current paths in the fluid, an example of which is shown in figure 1. Finally, it should be mentioned that a calculation of the direct electromagnetic force on the sphere, obtained from the Maxwell stress-tensor, does not give the total force $\mathbf{R}$. The integral of the normal component of the stress tensor over the surface

of the sphere is equivalent in cases 1 and 2 to integrating the body force, $\mathbf{j} \times \mathbf{B}_0$, over the spherical volume; for case 1 this gives zero, while for case 2 one obtains $2\pi a^3 B_0^2 V \sigma\sigma'/(2\sigma + \sigma')$. Thus, equations (6), (13) and (14) include mechanical forces which are transmitted by the fluid. This point will be discussed further in §3 of the paper.

2.3. *Torque on a spinning sphere from Joule losses*

The torque on a sphere spinning about its axis with angular velocity $\boldsymbol{\omega}$ in the presence of a magnetic field $\mathbf{B}_0$ can be calculated by the procedure of §2.1. If the fluid is inviscid, there is no fluid motion and hence no induction field in the fluid. Here we shall have to make the additional restriction that the magnetic Reynolds number in the sphere, $R'_M = \sigma'\mu'\omega a^2$, is small in order that the magnetic field shall not deviate appreciably from $\mathbf{B}_0$. This is necessary because of the presence of complete eddy-current paths within the sphere itself for certain orientations.

We shall only summarize the results because the basic solutions for the electric fields are encompassed in the work of Bullard (1949) who determined the form of the electric and magnetic fields in a rotating conducting sphere of *arbitrary* magnetic Reynolds number, surrounded by a stationary shell of the same electrical conductivity. In Bullard's solutions the radial dependence is given in terms of spherical Bessel functions of the complex argument $(iR'_M)^{\frac{1}{2}} r/a$, but by making the appropriate small argument expansion of the Bessel functions, his solutions reduce to ours in lowest order.

(*a*) *Case* 4: $\boldsymbol{\omega}$ *parallel to* $\mathbf{B}_0$. The induction field inside the sphere may be written as

$$\mathbf{E}_{\text{induc}} = \tfrac{1}{2}\omega B_0 \nabla(r^2 \sin^2\theta), \tag{15}$$

where, for convenience, $\boldsymbol{\omega}$ is taken as the direction of the polar axis. Although the divergence of this field does not vanish, its curl does. Thus the divergence may be cancelled by an appropriate electrostatic field. For steady conduction the effective electric field must be divergence-free. We find that all boundary conditions can be satisfied by taking the effective electric field inside the sphere to be

$$\mathscr{E}' = -[\tfrac{1}{2}\sigma\omega B_0/(3\sigma + 2\sigma')]\nabla[r^2(3\cos^2\theta - 1)], \tag{16}$$

and the electric field in the fluid to be

$$\mathbf{E} = [\sigma'\omega B_0/(3\sigma + 2\sigma')]\nabla[(3\cos^2\theta - 1)\, a^5/3r^3]. \tag{17}$$

By equating the rate of Joule energy dissipation to $D_1\omega$, we obtain, for the drag torque,

$$D_1 = \tfrac{8}{15}\pi a^5 \omega B_0^2 \sigma\sigma'/(3\sigma + 2\sigma'). \tag{18}$$

If we let $\sigma = \sigma'$, this result reduces to that found by Bullard (see, for example, his equation (29)].

(*b*) *Case* 5: $\boldsymbol{\omega}$ *perpendicular to* $\mathbf{B}_0$. When $\boldsymbol{\omega}$ is oriented perpendicular to $\mathbf{B}_0$, the effective electric field inside the sphere may be written as

$$\mathscr{E}' = -\boldsymbol{\omega} B_0 r \sin\theta\cos\phi + \mathbf{E}' \tag{19}$$

if $\boldsymbol{\omega}$ is taken as the polar direction and $\mathbf{B}_0$ is in the $\phi = 0$ plane. In the fluid,

$$\mathscr{E} = \mathbf{E}. \tag{20}$$

The boundary conditions are satisfied by taking

$$\mathbf{E}' = [\sigma'\omega B_0/(3\sigma+2\sigma')]\,\nabla(r^2\cos\theta\sin\theta\cos\phi) \tag{21}$$

and

$$\mathbf{E} = [\sigma'\omega B_0 a^5/(3\sigma+2\sigma')]\,\nabla(\cos\theta\sin\theta\cos\phi/r^3). \tag{22}$$

From the energy dissipation, we readily obtain

$$D_2 = \tfrac{4}{5}\pi a^5\omega B_0^2\sigma'(\sigma+\tfrac{1}{3}\sigma')/(3\sigma+2\sigma'). \tag{23}$$

In this case there is drag torque on a conducting sphere even when the conductivity σ of the fluid vanishes. This results from eddy currents wholly inside the sphere. The torque can be calculated alternatively by integrating $\mathbf{r}\times(\mathbf{j}\times\mathbf{B}_0)$ over the sphere; in both cases, (4) and (5), the total torque is in the direction $-\boldsymbol{\omega}$.

(*c*) *Case* 6: *oblique angle*. By analogy with case 3, the vector torque on a spinning sphere may be written as

$$\mathbf{D} = -\alpha B_0^2\boldsymbol{\omega} + \gamma\mathbf{B}_0(\mathbf{B}_0.\boldsymbol{\omega}). \tag{24}$$

Comparison with equations (20) and (25) yields the relations

$$\alpha = \tfrac{4}{15}\pi a^5\sigma'(3\sigma+\sigma')/(3\sigma+2\sigma'), \tag{24a}$$

$$\gamma = \tfrac{4}{15}\pi a^5\sigma'(\sigma+\sigma')/(3\sigma+2\sigma'). \tag{24b}$$

3. More detailed mathematical analysis

In calculating the resistive force on a translating sphere by the Joule-loss method, we found that part of the force had to be transmitted via mechanical forces in the fluid. It is of interest, therefore, to see what can be said about the perturbed hydrodynamic flow.

3.1. *Fundamental equations*

We shall work in the system of co-ordinates in which the sphere is at rest, and look for a steady solution to the hydrodynamic equations. The equations governing the steady motion of an incompressible, inviscid, electrically conducting fluid are

$$\left.\begin{aligned} &(a)\ \operatorname{div}\mathbf{v} = 0, \\ &(b)\ \operatorname{curl}\mathbf{v}\times\mathbf{v} = -\nabla[(p/\rho)+\tfrac{1}{2}v^2] + (1/\rho\mu)\operatorname{curl}\mathbf{B}\times\mathbf{B}, \end{aligned}\right\} \tag{25}$$

together with the equations for the electromagnetic field, equations (1). The velocity, pressure, and magnetic field can be developed in perturbation series in powers of an expansion parameter proportional to B_0^2/V^2 (Ludford & Murray 1960). The zero-order magnetic field can also be expanded in powers of the magnetic Reynolds number, R_M (see §3.2).

Writing $\mathbf{v} = \mathbf{v}_0 + \mathbf{v}_1$, with

$$\mathbf{v}_0 = \mathbf{V} + \tfrac{1}{2}a^3\nabla(\mathbf{V}.\mathbf{r}/r^3) \tag{26}$$

the unperturbed velocity, and $\mathbf{v}_1$ the perturbed velocity of the fluid, writing the pressure $p = p_0 + p_1$, and $\mathbf{B} = \mathbf{B}(0) + \mathbf{B}_1$, we obtain the linearized equations

for $\mathbf{v}_1$ (here we have written $\mathbf{B}(0)$ for the zero-order field since $\mathbf{B}_0$ has been used to denote the uniform field) in the form

$$\left.\begin{aligned} &(a)\ \operatorname{div}\mathbf{v}_1 = 0, \\ &(b)\ (\operatorname{curl}\mathbf{v}_1)\times\mathbf{v}_0 = -\nabla(\mathbf{v}_0\cdot\mathbf{v}_1 + p_1/\rho) + (1/\rho\mu)\operatorname{curl}\mathbf{B}(0)\times\mathbf{B}(0). \end{aligned}\right\} \tag{27}$$

If equation (27*b*) is put in dimensionless form by writing all velocities in units of V, all pressures in units of ρV^2, and all distances in units of a, then it is seen that the magnetic body force is of order

$$\xi = \beta R_M, \tag{28}$$

where $$\beta = B_0^2/\mu\rho V^2, \quad R_M = \sigma\mu V a.$$

Not only must ξ be small in order to treat $\mathbf{v}_1$ as a perturbation, but the magnetic Reynolds number R_M must also be small in order that the magnetic field shall not deviate appreciably from $\mathbf{B}_0$ in the current-carrying region.

If the sphere's velocity $\mathbf{V}$ is too small, then (28) shows that the magnetic force cannot be treated as a perturbation. Thus it is not immediately clear that a solution to equation (27) is appropriate when the sphere is brought to a steady velocity after starting from rest. However, when the sphere is moving very slowly the effect of viscosity cannot be neglected. Chester (1957) has studied the effect of a magnetic field on Stokes's flow in a conducting fluid and has found a steady solution of the hydrodynamic equations which does not diverge as $\mathbf{V}$ approaches zero.

3.2. *Expansion of* $\mathbf{B}(0)$ *in terms of the magnetic Reynolds number*

The use in § 1 of the uniform field $\mathbf{B}_0$ for the zero-order field (with reference to an expansion in powers of R_M) requires some justification, particularly since Ludford & Murray found that such a perturbation expansion is irregular. The magnetic field $\mathbf{B}(0)$, or for brevity $\mathbf{B}$, in the fluid must satisfy the equations

$$\operatorname{curl}\mathbf{B} = \sigma\mu[\mathbf{E} + \mathbf{v}_0\times\mathbf{B}], \tag{29}$$

$$\operatorname{div}\mathbf{B} = 0. \tag{30}$$

We consider only case 1 geometry. Here there is no electric field. For the remainder of the paper we shall make $\mathbf{v}$, $\mathbf{r}$, and $\mathbf{B}$ dimensionless by referring them to the velocity at infinity $\mathbf{V}$, the radius of the sphere a, and the uniform magnetic field B_0, respectively. Let us write

$$\mathbf{B} = \mathbf{v}_0 + \mathbf{b}. \tag{31}$$

The first term, $\mathbf{v}_0$, satisfies both equations (29) and (30) and gives the correct asymptotic form to the field at infinity. Thus we need consider only $\mathbf{b}$. If we satisfy (30) by means of

$$b_r = \frac{1}{r^2\sin\theta}\frac{\partial A}{\partial\theta}, \quad b_\theta = -\frac{1}{r\sin\theta}\frac{\partial A}{\partial r}, \quad (b_\phi = 0), \tag{32}$$

with $A = A(r,\theta)$, then in the fluid, (29) becomes

$$\frac{\partial^2 A}{\partial r^2} + \frac{\sin\theta}{r^2}\frac{\partial}{\partial\theta}\left(\frac{1}{\sin\theta}\frac{\partial A}{\partial\theta}\right) = R_M\left[(1-r^{-3})\cos\theta\frac{\partial A}{\partial r} - \frac{1}{r}(1+\tfrac{1}{2}r^{-3})\sin\theta\frac{\partial A}{\partial\theta}\right]. \tag{33}$$

For small values of R_M, the appropriate solution to (33) may be found by a perturbation expansion. We require a solution with dipole character to cancel approximately the dipole behaviour in $\mathbf{v}_0$. This is just the solution, which has been discussed by Ludford & Murray (1960),

$$A = \exp[-\tfrac{1}{2}R_M r(1-\cos\theta)]\{(\kappa/r)\sin^2\theta + R_M[\tfrac{1}{2}\kappa + (\lambda/r^2)\cos\theta]\sin^2\theta\} + O(R_M^2). \tag{34}$$

Inside the sphere, the total magnetic field may be derived from

$$A' = (kr^2 + R_M l r^3\cos\theta)\sin^2\theta. \tag{35}$$

Continuity of the normal component of $\mathbf{B}$ and the tangential component of magnetic intensity across the sphere boundary gives

$$\kappa = k = \frac{3\mu'}{2(\mu'+2\mu)}, \quad \lambda = -\frac{9\mu\mu'}{4(\mu'+2\mu)(3\mu+2\mu')}, \quad l = -\frac{2\mu'}{3\mu}\lambda,$$

where μ and μ' are the permeabilities of fluid and sphere, respectively. For our problem $\mu = \mu'$; thus

$$\kappa = k = \tfrac{1}{2}, \quad \lambda = -\tfrac{3}{20}, \quad l = \tfrac{1}{10}.$$

To zero order in R_M, the magnetic field is given by

$$\mathbf{B} = \mathbf{v}_0 + \exp[-\tfrac{1}{2}R_M r(1-\cos\theta)]\left\{\frac{\cos\theta}{r^3}, \frac{\sin\theta}{2r^3}, 0\right\}, \tag{36}$$

and $\mathbf{v}_0 \times \mathbf{B}$ is found to be

$$\mathbf{v}_0 \times \mathbf{B} = (\tfrac{3}{2}r^{-3})\exp[-\tfrac{1}{2}R_M r(1-\cos\theta)]\{0, 0, \sin\theta\cos\theta\}.$$

The Joule-loss density is thus

$$\sigma\mathscr{E}^2 = \tfrac{9}{4}\rho V^3 a^2 \beta R_M r^{-6}\cos^2\theta\sin^2\theta\exp[-R_M r(1-\cos\theta)],$$

which differs from the result found in § 2.1 only by the presence of the exponential factor. When this loss density is integrated over the volume of the fluid, the total Joule loss is the same as before to the lowest order, $[O(R_M)]$.

3.3. *Drag force from the perturbed velocity (case 1)*

We have not been able to establish the existence of a solution to equation (27) for each of the cases discussed in § 2.1. But Ludford & Murray have discussed the method of solution for equation (27) when the magnetic field $\mathbf{B}$ has axial symmetry about the direction $\mathbf{V}$ and hence their results may be applied directly to our case 1. The essence of their method is to take the curl of (27*b*), giving

$$\operatorname{curl}[\boldsymbol{\omega}\times\mathbf{v}_0] = \beta R_M \operatorname{curl}[(\mathbf{v}_0\times\mathbf{B})\times\mathbf{B}], \tag{37}$$

where $\boldsymbol{\omega} = \operatorname{curl}\mathbf{v}_1$ is the vorticity. Since this equation and $\boldsymbol{\omega}$ each have but a single component for case 1 geometry, the resulting equation for ω is relatively simple and may be solved by means of a series expansion,†

$$\omega = \sum_{n=1}^{\infty} \omega_n(r)\sin\theta\, P_n'(\cos\theta).$$

† For the necessity of this form of expansion the reader is referred to Ludford & Murray, p. 524.

Ludford & Murray show for this geometry that the drag force due to the pressure is $R = \rho V^2 a^2 D_p$, where

$$D_p = \pi\beta \int_1^\infty \int_0^\pi (F_\theta \sin\theta + 2F_r \cos\theta) \sin\theta \, d\theta \frac{dr}{r}. \tag{38}$$

Here $\mathbf{F} = \{F_r, F_\theta, 0\}$ is defined as $\mathbf{F} = R_M(\mathbf{v}_0 \times \mathbf{B}) \times \mathbf{B}$. Using equation (36) for the magnetic field, it is readily seen that

$$F_\theta \sin\theta + 2F_r \cos\theta = \tfrac{9}{2} R_M \exp[-\tfrac{1}{2} R_M r(1-\cos\theta)] r^{-3} \sin^2\theta \cos^2\theta + O(R_M^2).$$

In evaluating D_p we may set $R_M = 0$ in this last exponential since this leads only to an error of $O(R_M^2)$. The result is

$$D_p = \tfrac{2}{5}\pi\beta R_M, \tag{38a}$$

which agrees with (6).

In our problem (case 1), this is the total drag force since the Maxwell stress-tensor gives no contribution to this order.

The authors would like to thank Dr F. Winterberg, and particularly Dr G. Kuerti, for several stimulating discussions concerning this problem. They would also like to thank the referee for calling their attention to the irregular nature of the perturbation expansion of the magnetic field, and for referring them to the work of Bullard.

The work was supported in part by the National Carbon Company, a division of Union Carbide Corporation, and by the United States Atomic Energy Commission

REFERENCES

Bullard, E. C. 1949 Electromagnetic induction in a rotating sphere. *Proc. Roy. Soc.* A, **199**, 413.

Chester, W. 1957 The effect of a magnetic field on Stokes flow in a conducting fluid. *J. Fluid Mech.* **3**, 304.

Chopra, K. P. 1956 *Indian J. Phys.* **30**, 605.

Chopra, K. P. 1957 Note on induction drag. *J. Geophys. Res.* **62**, 143.

Chopra, K. P. & Singer, S. F. 1958 Drag of a sphere moving in a conducting fluid in the presence of a magnetic fluid. *Heat Transfer and Fluid Mechanics Institute, Berkeley*, p. 155. Stanford University Press.

Ludford, G. S. S. 1960 Inviscid flow past a body at low magnetic Reynolds number. *Rev. Mod. Phys.* **32**, 1000.

Ludford, G. S. S. & Murray, J. D. 1960 On the flow of a conducting fluid past a magnetized sphere. *J. Fluid Mech.* **7**, 516.

Stewartson, K. 1956 Motion of a sphere through a conducting fluid in the presence of a strong magnetic field. *Proc. Camb. Phil. Soc.* **52**, 301.

On the dynamics of unsteady gravity waves of finite amplitude

Part 2. Local properties of a random wave field

By O. M. PHILLIPS

Mechanics Department, The Johns Hopkins University, Baltimore, Maryland*

(Received 16 January 1961)

Expressions in closed form are derived for a number of local properties of a random, irrotational wave field. They are: (i) the mean potential and kinetic energies per unit projected area; (ii) the energy balance among the processes of energy input from the surface pressure fluctuations, rate of growth of potential and kinetic energy and horizontal energy flux; and (iii) the partition between potential and kinetic energy. These expressions are mainly in terms of quantities measured at the free surface, which are therefore functions of only two spatial variables (x, y) and of time t.

Approximations for these expressions can be found simply by subsequent expansion methods; the fourth order being the highest for which the assumption of irrotational motion is appropriate in a real fluid. It is shown that the mean product of any three first-order quantities is of fourth or higher order in the root-mean-square wave slope, and this result is applied in estimating the magnitude of some higher order effects. In particular, the skewness of the surface displacement is of the order of the root-mean-square surface slope, which has been confirmed observationally by Kinsman (1960).

1. Introduction

This paper is concerned with the specification of properties of a random wave field of finite amplitude that are associated with a single point in the horizontal plane, and with the interrelations among them. The problem of the dynamical interactions among the various wave components is a complex one; the object of this paper is to derive a number of simple basic expressions and results from which a more detailed analysis can be developed. The usual method of approach to such problems involves *ab initio* an expansion about the equilibrium free surface and an investigation of successively higher order terms This was the technique used in Part 1 of this sequence (Phillips 1960*a*), concerned with the elementary wave interactions, where it was shown that continuing energy transfer from one Fourier component of the wave field to another was possible through a certain type of resonant third-order interaction. As the order of the approximation increases, however, so does the algebraic complexity—very rapidly indeed—so that it is very desirable to carry the analysis in closed form as far as

* Present address: St John's College, Cambridge.

possible. This is accomplished in the present paper by expressing properties of the three-dimensional wave motion in terms of quantities measured on the free surface at a fixed horizontal location, which are functions of only two spatial variables (x, y) and of time. Typical quantities of this kind are the surface displacement $\xi(x, y, t)$ itself, and, say, the velocity potential at the free surface

$$[\phi(x, y, z, t)]_{z=\xi(x, y, t)}.$$

Clearly, the specification of quantities in this way differs from both an Eulerian and a Lagrangian description, since the horizontal co-ordinates are fixed but the vertical co-ordinate moves up and down with the free surface.

A number of expressions of a type somewhat similar to those derived in this paper have been given by Starr (1947). He considered periodic or solitary waves and was concerned with finding relations among the wave energy, phase velocity, wave momentum, etc. These relations, however, cannot be generalized to the case of a random wave field, nor are Starr's methods capable of treating the multi-point properties that occur in the full dynamical problem.

The technique to be developed here results in higher order effects (i.e. those that do not appear in the infinitesimal wave theory) presenting themselves frequently as mean products of three or more first-order quantities. To obtain a first approximation for these higher-order effects, only the infinitesimal wave solution is required, and a considerable gain in simplicity is achieved. An elementary application of this technique was made in a recent paper (Phillips 1960*b*) where the drift velocity and mean surface velocity in an irrotational wave field were found very readily. In cases where these effects are represented by the mean product of three first-order terms, the theorem derived in § 5 shows that they are quite generally of the fourth order, not the third as might at first appear. This theorem is used to estimate the orders of magnitude of the skewness of the surface displacement and of the difference between the kinetic and potential energies per unit area of the wave field.

Although the results given by this approach are in closed form and 'exact' within the context of potential theory, it is well known (Longuet-Higgins 1953) that in a real fluid, the motion is not truly irrotational. A mean vorticity field, of second order, diffuses inwards from the free surface (and also perhaps from the bottom), ultimately affecting the whole fluid. This results in, for example, a mass transport velocity in a two-dimensional motion that is different from the value found by Stokes for potential motion, even when the fluid viscosity is vanishingly small. Also, in oceanographical contexts where the water motion is three-dimensional, one must expect the vorticity field to become distorted or convoluted, resulting in a turbulent motion that is maintained by the rate of strain associated with the wave field. This turbulent layer near the surface has been shown (Phillips 1961) to influence the momentum equation for potential motion at the third order, and results in a slow attenuation of the waves. In the energy equation (discussed in some detail in § 3), which is formed by multiplying the momentum equation by the first-order surface velocity $\dot{\xi}$, the influence is thus of the fourth order. As a consequence, the exactness implied by the closed form of the expressions given below is partly illusory, and the energy relations

cannot be expected to be physically reliable beyond the fourth order. However, their concise form makes them convenient for subsequent approximation to this order.

2. The basic equations for finite amplitude irrotational waves

Consider a field of gravity waves on the surface of an incompressible liquid in which the depth is large compared with any wavelengths involved.† It will be supposed that the motion is irrotational, keeping in mind the conclusions of the previous section. A Cartesian reference frame will be used, with the z-axis vertically upwards and the plane $z = 0$ corresponding to the equilibrium free surface. Let $\mathbf{q}$ represent the velocity of the fluid at an interior point $\mathbf{x} = (x, y, z)$ so that

$$\left.\begin{aligned} \mathbf{q} &= \left(\frac{\partial\phi}{\partial x}, \frac{\partial\phi}{\partial y}, \frac{\partial\phi}{\partial z}\right), \\ \text{and} \quad \frac{\partial^2\phi}{\partial x^2} + \frac{\partial^2\phi}{\partial y^2} + \frac{\partial^2\phi}{\partial z^2} &= 0. \end{aligned}\right\} \tag{2.1}$$

The pressure at any point in the fluid is given by Bernoulli's equation

$$\frac{p}{\rho} + \frac{\partial\phi}{\partial t} + \tfrac{1}{2}q^2 + gz = 0. \tag{2.2}$$

If surface tension is neglected, the pressure is continuous across the free surface $z = \xi(x, y, t)$, so that from equation (2.2) we obtain the dynamical surface boundary condition

$$-\frac{p}{\rho} = \left(\frac{\partial\phi}{\partial t}\right)_\xi + \tfrac{1}{2}q_\xi^2 + g\xi, \tag{2.3}$$

where $p(x, y, t)$ now represents the departure of the atmospheric surface pressure from its mean value, ρ the water density and the subscript ξ indicates that a quantity is to be measured at the free surface. There is, in addition, a kinematical boundary condition

$$\begin{aligned} \left(\frac{\partial\phi}{\partial z}\right)_\xi &= \frac{D\xi}{Dt} \\ &= \frac{\partial\xi}{\partial t} + (\nabla\phi)_\xi . \nabla\xi, \end{aligned} \tag{2.4}$$

where, here and for the remainder of this paper the two-dimensional operator $\nabla \equiv (\partial/\partial x, \partial/\partial y)$. If $\mathbf{u} = \nabla\phi$, the horizontal (vectorial) component of the fluid velocity $\mathbf{q}$ and $w = \partial\phi/\partial z$, the vertical component of $\mathbf{q}$, equation (2.4) can be expressed as

$$w_\xi = \dot{\xi} + \mathbf{u}_\xi . \nabla\xi. \tag{2.5}$$

Two further differential relations will be used frequently in the following analysis. If

$$f_\xi \equiv [f(x, y, z, t)]_{z=\xi(x,y,t)} \tag{2.6}$$

† Cases of finite (even variable) depth can be considered formally in a manner similar to that given here, but the influence of the vorticity field may be more serious.

represents some function measured at the free surface, then by the rules of partial differentiation,

$$\left.\begin{aligned} \frac{\partial}{\partial t}(f_\xi) &= \left(\frac{\partial f}{\partial t}\right)_\xi + \left(\frac{\partial f}{\partial z}\right)_\xi \frac{\partial \xi}{\partial t}, \\ \nabla(f_\xi) &= (\nabla f)_\xi + \left(\frac{\partial f}{\partial z}\right)_\xi \nabla\xi. \end{aligned}\right\} \tag{2.7}$$

Clearly, the operations $(\ )_\xi$ and differentiation do not commute; a little care is sometimes necessary as a result. Important special cases of (2.7) are given when $f = \phi$, the velocity potential

$$\left.\begin{aligned} \frac{\partial}{\partial t}(\phi_\xi) &= \dot{\phi}_\xi + w_\xi \dot{\xi}, \\ \nabla(\phi_\xi) &= \mathbf{u}_\xi + w_\xi \nabla\xi. \end{aligned}\right\} \tag{2.8}$$

Also, by differentiation of (2.5), we have, with the aid of (2.7),

$$\dot{w}_\xi = \ddot{\xi} + \dot{\mathbf{u}}_\xi . \nabla\xi + \nabla . (\dot{\xi}\mathbf{u}_\xi), \tag{2.9}$$

concerning the acceleration of the free surface.

3. Single point analysis–energy relations

(i) *Potential and kinetic energy densities*

The potential energy per unit horizontal area, taking as a datum the equilibrium plane $z = 0$, is simply

$$\mathscr{V} = \tfrac{1}{2}\rho g \xi^2, \tag{3.1}$$

and the mean potential energy per unit projected area, or the potential energy density, is

$$V = \tfrac{1}{2}\rho g \overline{\xi^2}, \tag{3.2}$$

where the bar denotes a probability or ensemble average. If the wave field is statistically stationary in time (as, for example, when a steady wind blows for a long time over a finite fetch) this average is equal to the usual time average. Similarly, if the wave field is spatially homogeneous, the probability average is equal to the space average. The expression (3.2) is valid quite generally, with the appropriate interpretation of the averaging process.

The kinetic energy of the wave motion per unit projected area is given by

$$\mathscr{T} = \tfrac{1}{2}\rho \int_{-\infty}^{\xi} q^2 dz. \tag{3.3}$$

From (3.3),

$$\begin{aligned} \frac{2}{\rho}\mathscr{T} &= \int_{-\infty}^{\xi} \left\{ (\nabla\phi)^2 + \left(\frac{\partial\phi}{\partial z}\right)^2 \right\} dz, \\ &= \int_{-\infty}^{\xi} \left\{ \nabla . (\phi\nabla\phi) - \phi\nabla^2\phi + \frac{\partial}{\partial z}\left(\phi\frac{\partial\phi}{\partial z}\right) - \phi\frac{\partial^2\phi}{\partial z^2} \right\} dz, \\ &= \phi_\xi w_\xi + \int_{-\infty}^{\xi} \nabla . (\phi\nabla\phi)\, dz, \end{aligned}$$

since

$$\nabla^2\phi + \frac{\partial^2\phi}{\partial z^2} = 0.$$

Furthermore, $$\nabla.\int_{-\infty}^{\xi}\phi\nabla\phi dz = \nabla\xi.(\nabla\phi)_\xi\phi_\xi + \int_{-\infty}^{\xi}\nabla.(\phi\nabla\phi)dz,$$

so that
$$\frac{2}{\rho}\mathscr{T} = \phi_\xi\{w_\xi - \mathbf{u}_\xi.\nabla\xi\} + \nabla.\int_{-\infty}^{\xi}\phi\nabla\phi dz,$$
$$= \phi_\xi\dot{\xi} + \nabla.\int_{-\infty}^{\xi}\phi\mathbf{u}dz, \tag{3.4}$$

in virtue of (2.5). The mean kinetic energy density of the wave field is thus

$$T = \tfrac{1}{2}\rho\overline{\phi_\xi\dot{\xi}} + \tfrac{1}{2}\rho\nabla.\overline{\int_{-\infty}^{\xi}\phi\mathbf{u}dz}. \tag{3.5}$$

If the wave field is spatially homogeneous, the mean value of the integral is independent of position, and the previous expression becomes

$$T = \tfrac{1}{2}\rho\overline{\phi_\xi\dot{\xi}}. \tag{3.6}$$

These expressions can be obtained alternatively by using the relation

$$\mathscr{T} = \tfrac{1}{2}\rho\int\phi\frac{\partial\phi}{\partial n}dS,$$

where the integral is over the surface of a vertical prism of unit cross-sectional area terminating at the moving free surface $z = \xi(x, y, t)$.

(ii) *Rate of change of kinetic energy density*

The time rate of change of the mean kinetic energy per unit projected area can be expressed in a number of alternative and equivalent ways. One such form is obtained as follows:

$$\frac{2}{\rho}\frac{\partial\mathscr{T}}{\partial t} = \frac{\partial}{\partial t}\int_{-\infty}^{\xi}q^2dz,$$
$$= \dot{\xi}q_\xi^2 + 2\int_{-\infty}^{\xi}\mathbf{q}.\dot{\mathbf{q}}dz. \tag{3.7}$$

But
$$\int_{-\infty}^{\xi}\mathbf{q}.\dot{\mathbf{q}}dz = \int_{-\infty}^{\xi}\left\{\nabla\dot{\phi}.\nabla\phi + \frac{\partial\dot{\phi}}{\partial z}\frac{\partial\phi}{\partial z}\right\}dz$$
$$= \int_{-\infty}^{\xi}\left\{\nabla.(\dot{\phi}\nabla\phi) - \dot{\phi}\nabla^2\phi + \frac{\partial}{\partial z}\left(\dot{\phi}\frac{\partial\phi}{\partial z}\right) - \dot{\phi}\frac{\partial^2\phi}{\partial z^2}\right\}dz$$
$$= \dot{\phi}_\xi w_\xi + \int_{-\infty}^{\xi}\nabla.(\dot{\phi}\nabla\phi)dz$$
$$= \dot{\phi}_\xi w_\xi + \nabla.\int_{-\infty}^{\xi}\dot{\phi}\nabla\phi dz - \dot{\phi}_\xi\nabla\xi.(\nabla\phi)_\xi$$
$$= \dot{\phi}_\xi\dot{\xi} + \nabla.\int_{-\infty}^{\xi}\dot{\phi}\mathbf{u}dz \tag{3.8}$$

from (2.5). Thus
$$\dot{\mathscr{T}} = \rho\dot{\phi}_\xi\dot{\xi} + \tfrac{1}{2}\rho q_\xi^2\dot{\xi} + \nabla.\int_{-\infty}^{\xi}\rho\dot{\phi}\mathbf{u}dz. \tag{3.9}$$

If the wave field is spatially homogeneous, the average of equation (3.9) yields

$$\dot{T} = \rho\overline{\dot{\phi}_\xi\dot{\xi}} + \tfrac{1}{2}\rho\overline{q_\xi^2\dot{\xi}}, \tag{3.10}$$

since the mean of the integral is independent of position (x, y), whereas for a field statistically steady in time, $\dot{T} = 0$ and

$$-\nabla . \overline{\int_{-\infty}^{\xi} \rho \phi \mathbf{u} dz} = \rho \overline{\phi_\xi \xi} + \tfrac{1}{2} \rho \overline{q_\xi^2 \xi}. \tag{3.11}$$

These particular forms lead to simple physical interpretations that are of some interest. Equation (3.10), say, gives the mean rate of change of the kinetic energy in a column of fluid of unit cross-sectional area as the sum of two terms. The first arises from the rate of change of q^2 in the column and the second from the rate of change of length (and so mass) of the column. These are exactly equivalent to the two terms arising in

$$\frac{\partial}{\partial t}(\tfrac{1}{2} m q^2) = m \mathbf{q} . \dot{\mathbf{q}} + \tfrac{1}{2} \dot{m} q^2.$$

The integral in equation (3.9) can be shown to represent the negative flux of energy per unit horizontal length, or minus the energy flux across a vertical surface of unit width and infinite depth. To demonstrate this, we must add the rate of working by pressure forces across this surface to the rate of convection of kinetic energy across the surface by the motion. Consider, then, a vertical strip cutting the equilibrium free surface in the line element $d\mathbf{s}$. The difference between the pressure at any point and the undisturbed hydrostatic pressure is $(p + \rho g z)$, so that the rate at which work is done by pressure forces acting across the strip is

$$d\mathbf{s} . \int_{-\infty}^{\xi} (p + \rho g z) \mathbf{u} dz.$$

The rate at which kinetic energy is convected across the strip is

$$d\mathbf{s} . \int_{-\infty}^{\xi} \tfrac{1}{2} \rho q^2 \mathbf{u} dz.$$

The total flux energy across the strip is thus

$$d\mathbf{s} . \int_{-\infty}^{\xi} (p + \tfrac{1}{2} \rho q^2 + \rho g z) \mathbf{u} dz = -d\mathbf{s} . \int_{-\infty}^{\xi} \rho \frac{\partial \phi}{\partial t} \mathbf{u} dz,$$

from Bernoulli's equation (2.2). The instantaneous energy flux vector is thus

$$-\int_{-\infty}^{\xi} \rho \phi \mathbf{u} dz, \tag{3.12}$$

and the mean energy flux is

$$\mathbf{F} = -\overline{\int_{-\infty}^{\xi} \rho \phi \mathbf{u} dz}. \tag{3.13}$$

It appears, then, that the left-hand side of equation (3.11) can be interpreted as the horizontal divergence of the mean energy-flux vector $\mathbf{F}$. A more general expression, valid for a non-stationary, non-homogeneous wave field is obtained by taking the probability average of equation (3.9),

$$\dot{T} + \nabla . \mathbf{F} = \rho \overline{\phi_\xi \xi} + \tfrac{1}{2} \rho \overline{q_\xi^2 \xi}. \tag{3.14}$$

An alternative expression for $\dot{T}$ can be found by returning to (3.7) and (3.8).

$$\begin{aligned}\int_{-\infty}^{\xi} \mathbf{q}.\dot{\mathbf{q}}\,dz &= \int_{-\infty}^{\xi} \left\{\nabla.(\phi\nabla\dot{\phi}) - \phi\nabla^2\dot{\phi} + \frac{\partial}{\partial z}\left(\phi\frac{\partial\dot{\phi}}{\partial z}\right) - \phi\frac{\partial^2\dot{\phi}}{\partial z^2}\right\} dz \\ &= \phi_\xi\left(\frac{\partial\dot{\phi}}{\partial z}\right)_\xi - \phi_\xi\nabla\xi.(\nabla\dot{\phi})_\xi + \nabla.\int_{-\infty}^{\xi}\phi\nabla\dot{\phi}\,dz \\ &= \phi_\xi(\dot{w}_\xi - \dot{\mathbf{u}}_\xi.\nabla\xi) + \nabla.\int_{-\infty}^{\xi}\phi\dot{\mathbf{u}}\,dz.\end{aligned}$$

The use of (2.9) immediately, and then of (2.8) and (2.5) leads to

$$\int_{-\infty}^{\xi}\mathbf{q}.\dot{\mathbf{q}}\,dz = \phi_\xi\dot{\xi} - \dot{\xi}q_\xi^2 + w_\xi\dot{\xi}^2 + \nabla.\{\phi_\xi\dot{\xi}\mathbf{u}_\xi\} + \nabla.\int_{-\infty}^{\xi}\phi\dot{\mathbf{u}}\,dz,$$

which, after addition of $\frac{1}{2}\dot{\xi}q_\xi^2$, represents $\rho^{-1}\mathscr{T}$, as (3.7) indicates. In a homogeneous wave field, the mean value of this expression simplifies since both of the divergence terms vanish, and we find that

$$\dot{T} = \rho\overline{\phi_\xi\dot{\xi}} + \rho\overline{(w_\xi\dot{\xi} - \tfrac{1}{2}q_\xi^2)\dot{\xi}}. \tag{3.15}$$

Adding this result to the expression (3.10), previously obtained, we have

$$\dot{T} = \tfrac{1}{2}\rho\{\overline{\phi_\xi\dot{\xi}} + \overline{\phi_\xi\dot{\xi}} + \overline{w_\xi\dot{\xi}^2}\}, \tag{3.16}$$

which, as the reader may verify, can be obtained more readily by direct differentiation of (3.6).

(iii) *The energy balance*

If we multiply the dynamic free surface condition (2.3) by $\dot{\xi}$ and take the probability average of the result, we obtain

$$-\overline{p\dot{\xi}} = \rho\overline{\phi_\xi\dot{\xi}} + \tfrac{1}{2}\rho\overline{q_\xi^2\dot{\xi}} + \rho g\overline{\xi\dot{\xi}}, \tag{3.17}$$

which can be interpreted as the equation for the mean energy balance for a field of gravity waves without restriction to stationarity in time or homogeneity in space. The term $-\overline{p\dot{\xi}}$ represents the rate at which energy is supplied to the waves per unit projected area by the atmospheric pressure fluctuations. The first and second terms on the right-hand side together represent, from equation (3.14), $\dot{T} + \nabla.\mathbf{F}$, the rate of change of the mean kinetic energy per unit projected area plus the horizontal divergence of the mean energy flux vector. The last term clearly represents $\dot{V}$, the rate of change of mean potential energy per unit projected area. Equation (3.17) can therefore be written

$$-\overline{p\dot{\xi}} = \dot{T} + \dot{V} + \nabla.\mathbf{F}. \tag{3.18}$$

If the wave field is homogeneous, $\mathbf{F}$ is constant,

$$-\overline{p\dot{\xi}} = \dot{T} + \dot{V}, \tag{3.19}$$

and if it is statistically steady

$$-\overline{p\dot{\xi}} = \nabla.\mathbf{F}. \tag{3.20}$$

(iv) *Energy partitions in a homogeneous wave field*

In a homogeneous wave field of infinitesimal amplitude, the total energy per unit projected area is divided equally between potential and kinetic energy. For finite amplitude waves, this is in general not so, though the difference is small. The determination of $T-V$ has certain intrinsic interest [Starr (1947) and Mack (1958) having considered certain special cases], but our object here is simply to devise a method of eliminating the kinetic energy density from our dynamical considerations.

The required expression is obtained by multiplying the dynamical surface boundary condition (2.3) by the surface displacement $\xi(x,y,t)$:

$$\begin{aligned}\rho^{-1}p\xi+\tfrac{1}{2}q_\xi^2\xi+g\xi^2 &= -\xi\left(\frac{\partial\phi}{\partial t}\right)_\xi\\ &= -\xi\frac{\partial}{\partial t}(\phi_\xi)+w_\xi\dot{\xi}\xi\\ &= -\frac{\partial}{\partial t}(\xi\phi_\xi)+\dot{\xi}\phi_\xi+w_\xi\dot{\xi}\xi.\end{aligned}$$

Rearranging the terms and averaging the whole equation, we find that, for a homogeneous wave field,

$$V = T+\tfrac{1}{2}\rho\,\overline{\xi(w_\xi\dot{\xi}-\tfrac{1}{2}q_\xi^2)}-\tfrac{1}{2}\overline{p\xi}-\tfrac{1}{2}\rho\frac{\partial}{\partial t}(\overline{\xi\phi_\xi}). \tag{3.21}$$

Under most physical circumstances, the last two terms can be neglected. The term $\frac{1}{2}\overline{p\xi}$ is clearly the contribution to V from the air pressure fluctuations acting hydrostatically. Some recent unpublished observations by Dr M. S. Longuet-Higgins indicate that $(\overline{p^2})^{\frac{1}{2}}$ is of order $\rho_a g(\overline{\xi^2})^{\frac{1}{2}}$ under typical sea conditions, where ρ_a is the air density. The ratio of this term to V is then of order $\rho_a/\rho_w \sim 10^{-3}$, which we can neglect. The ratio of the last term to the kinetic energy term T is of order τ/θ where τ is a characteristic wave period and θ the time scale of growth of the wave field as a whole. Recent observational evidence indicates that this ratio is of order 10^{-3} for the shorter components of a wind-generated wave field (those which travel at a phase speed less than half the speed of the wind) and may be as small as 10^{-5} for the longer components. It appears then that the energy partition can be expressed to sufficient accuracy as

$$V = T+\tfrac{1}{2}\rho\,\overline{\xi(w_\xi\dot{\xi}-\tfrac{1}{2}q_\xi^2)}. \tag{3.22}$$

With this expression, the kinetic energy density can be eliminated from the energy balance in a homogeneous wave field, yielding

$$2\dot{V}-\tfrac{1}{2}\rho\frac{d}{dt}\{\overline{\xi(w_\xi\dot{\xi}-\tfrac{1}{2}q_\xi^2)}\} = -\overline{p\dot{\xi}}. \tag{3.23}$$

This equation gives the rate of growth of the potential energy density (the most accessible physical observable) directly in terms of the rate of energy supply and the small 'unbalance' term.

Another type of energy partition is perhaps worth noting in passing. In a homogeneous wave field, for any fixed point always below the water surface,

$$\overline{\mathbf{u}^2} = \overline{w^2} = \tfrac{1}{2}\overline{q^2}, \tag{3.24}$$

so that the kinetic energy per unit mass at such points is divided equally between the horizontal and vertical motions. This result was proved (Phillips 1955) in a rather different, but equivalent context.

4. The energy-flux vector

As an illustration of the use of these expressions in finding lowest-order approximations, let us relate the energy-flux vector **F** to the spectrum of surface displacements (or the potential energy spectrum, which differs only by the factor $\frac{1}{2}\rho g$).

The surface displacement $\xi(\mathbf{x}, t)$ can be represented quite generally by the generalized Fourier transform

$$\xi(\mathbf{x}, t) = \int_{\mathbf{k}} \int_{n} B(\mathbf{k}, n)\, e^{i(\mathbf{k}.\mathbf{x} - nt)}\, d\mathbf{k}\, dn, \tag{4.1}$$

where the integrations range over the entire wave-number plane and over all values of frequency n. A clear and concise account of the modern theory of generalized Fourier transforms is given by Lighthill (1958). In free infinitesimal wave theory, the generalized Fourier transform $B(\mathbf{k}, n)$ can be shown simply to be of the form

$$B(\mathbf{k}, n) = A(\mathbf{k})\, \delta(n - \omega), \tag{4.2}$$

where δ represents the Dirac delta function, $\omega = (gk)^{\frac{1}{2}}$ and we have adopted the convention that the direction of propagation of a wave is in the direction of **k**. The expression (4.2) is simply a statement of the fact that, in infinitesimal wave theory, a wave-number k has associated with it a unique frequency ω.

To the first order, then, the surface displacement is given from (4.1) and (4.2) by

$$\left.\begin{aligned} \xi(\mathbf{x}, t) &= \int_{\mathbf{k}} A(\mathbf{k})\, e^{i(\mathbf{k}.\mathbf{x} - \omega t)}\, d\mathbf{k} \\ &= \int_{\mathbf{k}} A^*(\mathbf{k})\, e^{-i(\mathbf{k}.\mathbf{x} - \omega t)}\, d\mathbf{k}, \end{aligned}\right\} \tag{4.3}$$

since ξ is real, where the asterisk represents the complex conjugate quantity. The associated velocity potential, correct to first order, is given by

$$\phi(\mathbf{x}, z, t) = -i \int \frac{\omega}{k} A(\mathbf{k})\, e^{kz}\, e^{i(\mathbf{k}.\mathbf{x} - \omega t)}\, d\mathbf{k}. \tag{4.4}$$

The relation between the surface displacement spectrum $\Phi(\mathbf{k})$ and the surface displacement covariance

$$\Xi(\mathbf{x}, \mathbf{r}; t, \tau) = \overline{\xi(\mathbf{x}, t)\, \xi(\mathbf{x} + \mathbf{r}, t + \tau)} \tag{4.5}$$

is constructed by multiplying (4.3) by a corresponding expression for $\xi(\mathbf{x} + \mathbf{r}, t + \tau)$. If the wave field approximates sufficiently to stationarity and homogeneity, we have from the theory of generalized functions

$$\overline{A^*(\mathbf{k})\, A(\mathbf{k}')} = \Phi(\mathbf{k})\, \delta(\mathbf{k} - \mathbf{k}'), \tag{4.6}$$

where $\delta(\mathbf{k}-\mathbf{k}')$ represents the product of the Dirac delta functions involving the two components of the vector argument. Thus

$$\Xi(\mathbf{r},\tau) = \int_{\mathbf{k}} \Phi(\mathbf{k})\, e^{i(\mathbf{k}.\mathbf{r}-\omega\tau)}\, d\mathbf{k}. \tag{4.7}$$

In particular, when the time interval $\tau = 0$,

$$\Xi(\mathbf{r},0) = \int_{\mathbf{k}} \Phi(\mathbf{k})\, e^{i\mathbf{k}.\mathbf{r}}\, d\mathbf{k}, \tag{4.8}$$

and when $\mathbf{r} = 0$, we have the frequency spectrum for the surface oscillations measured at a point

$$\Xi(0,\tau) = \int_{\mathbf{k}} \Phi(\mathbf{k})\, e^{-i\omega\tau}\, d\mathbf{k} = \int_0^\infty \int_0^{2\pi} \Phi(\mathbf{k})\, e^{-i\omega\tau}\, k\, dk\, d\theta,$$

where the integration is taken in polar co-ordinates. But, since $\omega^2 = gk$,

$$k\,dk = \frac{2\omega^3 d\omega}{g^2},$$

so that

$$\Xi(0,\tau) = \int_0^\infty \Psi(\omega)\, e^{i\omega\tau}\, d\omega, \tag{4.9}$$

where

$$\Psi(\omega) = \Psi^*(\omega) = \frac{2\omega^3}{g^2} \int_0^{2\pi} \Phi(\mathbf{k})\, d\theta \tag{4.10}$$

and $k = |\mathbf{k}| = \omega^2/g$. The spectrum $\Psi(\omega)$ is measured fairly readily using a conventional wave pole.

In a similar manner, we can construct an expression for the energy-flux vector $\mathbf{F}$ in terms of $\Phi(\mathbf{k})$. From (3.13),

$$\mathbf{F} = -\rho \overline{\int_{-\infty}^{\xi} \phi \mathbf{u}\, dz} = -\rho \int_{-\infty}^{0} \overline{\phi \mathbf{u}}\, dz,$$

correct to second order. From (4.4),

$$\mathbf{F} = \rho \int_{-\infty}^{0} dz \int_{\mathbf{k}} \int_{\mathbf{k}'} \frac{\omega^2}{k} \frac{\omega' \mathbf{k}'}{k'} \overline{A^*(\mathbf{k})\, A(\mathbf{k}')}\, e^{(k+k')z} \times \exp i\{(\mathbf{k}'-\mathbf{k}).\mathbf{x} - (\omega'-\omega)\, t\}\, d\mathbf{k}\, d\mathbf{k}',$$

where $\omega' = (gk')^{\frac{1}{2}}$ so that, in view of (4.6),

$$\mathbf{F} = \rho \int_{\mathbf{k}} \frac{\omega^3 \mathbf{k}}{k^2} \Phi(\mathbf{k}) \left\{ \int_{-\infty}^{0} e^{2kz}\, dz \right\} d\mathbf{k}$$

$$= \tfrac{1}{2}\rho g \int \mathbf{c}(k)\, \Phi(\mathbf{k})\, d\mathbf{k}, \tag{4.11}$$

where $\mathbf{c}(k) = \omega\mathbf{k}/k^2$ is the phase velocity of waves of wave-number $\mathbf{k}$. This is a simple generalization of the statement that, in a simple sinusoidal wave, the energy flux is equal to the potential energy density moving at the phase velocity, or to the total energy moving at half the phase velocity (the group velocity). The expression (4.11) is correct to second order; the next approximation could be found by substituting the next-order solutions for $\phi(\mathbf{x}, z, t)$ into (3.13).

5. Mean products of three first-order quantities

A number of the higher order quantities, such as the difference (3.22) between the potential and kinetic energy densities, presented themselves as the average product of three first-order terms. One would expect, in view of the observed closeness to which the surface displacement distribution approaches the Gaussian form, that third-order correlations (i.e. dimensionless covariances) would be numerically small. However, we can show that they are small in an order of magnitude sense, or, more precisely, that in a homogeneous stationary wave field *any mean triple product of first-order terms is of fourth (or higher) order.*

For the proof of this statement, we observe first that any first-order quantity can be represented (correct to this order) as a generalized Fourier integral involving $A(\mathbf{k})$ multiplied by algebraic factors whose nature depends on the particular quantity concerned. The expression (4.4) for $\phi(\mathbf{x}, z, t)$ is an illustration of this, and clearly $\phi_\xi(\mathbf{x}, t)$, $\mathbf{u}_\xi(\mathbf{x}, t)$, etc., are of the same form.

Let $f_1(\mathbf{x}, t)$, $f_2(\mathbf{x}+\mathbf{r}, t+\tau_2)$ and $f_3(\mathbf{x}+\mathbf{s}, t+\tau_3)$ represent three first-order quantities measured at positions $\mathbf{x}$, $\mathbf{x}+\mathbf{r}$, $\mathbf{x}+\mathbf{s}$ and times t, $t+\tau_2$, $t+\tau_3$ respectively. Then the mean triple product can be represented, correct to the third order, as

$$\begin{aligned}\overline{f_1 f_2 f_3} = \int_{\mathbf{k}_1}\int_{\mathbf{k}_2}\int_{\mathbf{k}_3} K(\mathbf{k}_1, \mathbf{k}_2, \mathbf{k}_3)\, \overline{A^*(\mathbf{k}_1) A(\mathbf{k}_2) A(\mathbf{k}_3)} \\ \times \exp -i\{(\mathbf{k}_1 - \mathbf{k}_2 - \mathbf{k}_3).\mathbf{x} - (\omega_1 - \omega_2 - \omega_3)t\} \\ \times \exp i\{\mathbf{k}_2.\mathbf{r} - \omega_2\tau_2\} \exp i\{\mathbf{k}_3.\mathbf{s} - \omega_3\tau_3\}\, d\mathbf{k}_1 d\mathbf{k}_2 d\mathbf{k}_3,\end{aligned}$$

where K is an algebraic function and $\omega_i = (gk_i)^{\frac{1}{2}}$ for $i = 1, 2, 3$. The simplest argument is as follows.† If the left-hand side of this expression is to be independent of position $\mathbf{x}$ and time origin t, then the only non-zero contributions to the integral can occur only when both

$$\mathbf{k}_1 - \mathbf{k}_2 - \mathbf{k}_3 = 0, \quad \omega_1 - \omega_2 - \omega_3 = 0. \tag{5.1}$$

From the second of these conditions,

$$k_1^{\frac{1}{2}} = k_2^{\frac{1}{2}} + k_3^{\frac{1}{2}},$$

or

$$\frac{k_1}{k_2 + k_3} = 1 + \frac{2(k_2 k_3)^{\frac{1}{2}}}{k_2 + k_3} > 1. \tag{5.2}$$

But from the first of the conditions (5.1), $-\mathbf{k}_1$, $\mathbf{k}_2$, $\mathbf{k}_3$ form a closed triangle, so that $k_1/(k_2+k_3) < 1$, which is incompatible with (5.2) except for the degenerate case when either k_2 or k_3 vanishes. This contingency can be excluded since it would imply the existence of covariances of the kind above that were independent of $\mathbf{r}$ or $\mathbf{s}$. The conclusion is that there are no non-zero contributions to the integral, and that any triple covariance of this kind is zero to the third order.

Two comments on this rather general result might be pertinent. The result depends crucially on the dispersive nature of the wave, where a wave-number $\mathbf{k}$ is associated with a unique frequency which depends on but is not proportional to $k = |\mathbf{k}|$. In a non-dispersive wave system where ω is proportional to k, the

† An alternative but slightly longer procedure involves inversion of this expression.

conditions (5.1) are satisfied by triads of parallel vectors. Also if the frequency is not a unique function of scalar wave-number, as in the *second* approximation to a gravity-wave field, we do not have the simple separation (3.2) and the result fails. Secondly, it might be noted that the reasons for this result are precisely the same as those for the absence of any continuing energy transfer from one wave-number to another in second-order gravity wave theory (Phillips 1960*a*). The conditions required for such a transfer are equivalent to (5.1) which are incapable of satisfaction.

An immediate consequence of this result is that the difference between the potential and kinetic energy density is of fourth order. Since T and V are themselves second-order quantities, the fractional difference is of order $(\overline{\nabla\xi})^2$ since $[(\overline{\nabla\xi})^2]^{\frac{1}{2}}$ is our representative first-order quantity. The energy partition is thus very nearly equal; even in a well-developed sea where $[(\overline{\nabla\xi})^2]^{\frac{1}{2}}$ is of order 0·15 the energy densities are equal to within a few per cent.

A second consequence is an interesting one that can be compared directly with observation, though it is not involved in the discussion of § 3. According to the above result, $\overline{\xi^3}$ is of fourth order or smaller, whereas $\overline{\xi^2}$ is clearly of second order. It follows that the skewness of the probability distribution of the surface displacement, namely

$$\overline{\xi^3}/[\overline{\xi^2}]^{\frac{3}{2}}, \tag{5.3}$$

is a first-order dimensionless quantity, and so is of order $[(\overline{\nabla\xi})^2]^{\frac{1}{2}}$. In other words,

$$\frac{\overline{\xi^3}}{[(\overline{\nabla\xi})^2]^{\frac{1}{2}}\,[\overline{\xi^2}]^{\frac{3}{2}}} \tag{5.4}$$

is of order unity or less. As $[(\overline{\nabla\xi})^2]^{\frac{1}{2}} \to 0$, the skewness (5.3) tends to zero also, in accord with the well known property that in the limit of infinitesimal wave slopes, the surface displacement has a symmetric probability distribution. As the root mean square slope increases, so does the skewness, reflecting the tendency of the waves to form sharper crests and shallower troughs. A direct calculation, using the second-order terms, confirms that the quantity (5.4) is of order unity, although the resulting expression, involving ratios of integrals involving the spectrum $\Phi(\mathbf{k})$ is too complicated to be of much value in a general case. A second direct calculation for a single train of finite amplitude waves shows that the quantity (5.4) is 3/8 plus a term of order (slope)^2, in agreement with our order-of-magnitude result.

The prediction that the quantity (5.4) is quite generally of order unity can be compared with some observations made by Kinsman (1960) on wind-generated waves in a branch of the Chesapeake Bay. He measured properties of the waves set up by a steady wind blowing over a fixed fetch. The conditions were chosen so that the wave field was stationary in time and the rate of growth with increasing fetch was slow, and so they approximated to the conditions envisaged in the theorem above. Kinsman measured the skewness for each of 24 sets of observations, and the root mean square slope was calculated approximately from his measured spectra. Table 1 gives the results of these calculations, and it is evident that the quantity (5.4) is indeed of order unity or less. The sets

numbered between 81 and 88 gave exceptionally low (even negative) values for the skewness, but in no case is the ratio (5·4) of order larger than unity, and the variation from one observation to another is no more than is to be expected from the widely differing properties of the wave field generated on the different occasions.

This work was sponsored by the Office of Naval Research under contract Nonr 248(56).

Observation number	Skewness	Skewness $\overline{[(\nabla\zeta)^2]^{\frac{1}{2}}}$
9	0·172	2·3
10	0·143	2·1
11	0·096	1·4
12	0·182	2·4
17	0·175	2·1
18	0·219	2·4
27	0·158	2·1
28	0·178	2·3
67	0·082	1·1
68	0·087	1·1
69	0·067	1·0
70	0·027	0·4
75	0·101	1·5
76	0·092	1·4
81	0·029	0·4
82	0·034	0·5
83	−0·002	0
84	0·044	0·7
85	−0·005	−0·1
86	0·011	0·2
87	0·005	0·1
88	−0·046	−0·7
93	0·144	2·1
94	0·136	2·1

TABLE 1

REFERENCES

KINSMAN, BLAIR 1960 *Chesapeake Bay Institute, Johns Hopk. Univ. Tech. Rep.* no. 19.

LIGHTHILL, M. J. 1958 *Fourier Analysis and Generalised Functions.* Cambridge University Press.

LONGUET-HIGGINS, M. S. 1953 *Phil. Trans.* A, **245**, 525–81.

MACK, L. R. 1958 Ph.D. Dissertation, University of Michigan.

PHILLIPS, O. M. 1955 *Proc. Camb. Phil. Soc.* **51**, 220–9.

PHILLIPS, O. M. 1960*a* *J. Fluid Mech.* **9**, 193–217.

PHILLIPS, O. M. 1960*b* *J. Geophys. Res.* **65**, 3473–6.

PHILLIPS, O. M. 1961 *J. Geophys. Res.* **66** (in the Press).

STARR, V. P. 1947 *J. Mar. Res.* **6**, 175–93.

REVIEWS

Advances in Applied Mechanics. Vol. VI. Edited by H. L. DRYDEN, TH. VON KARMAN and G. KUERTI. New York: Academic Press, 1960. 294 pp. $9.00.

This latest volume in the series includes five articles on a diversity of topics in the field of fluid mechanics. The first two of these are concerned with boundary layers, 'The theory of unsteady laminar boundary layers' written by K. Stewartson and 'Boundary layer theory with dissociation and ionization', by G. Ludwig and M. Heil. W. Chester discusses 'The propagation of shock waves along ducts of varying cross-section,' and K. Oswatitsch, in the longest of the five articles, deals with 'Similarity and equivalence in compressible flow'. The book concludes with a short account, by R. Wille, of some recent work under the heading of 'Karman vortex streets'.

After a short introduction, the first two chapters of Stewartson's article examine Rayleigh-type problems (in which the solid boundaries move parallel to themselves). The importance of the relatively simple analytical solutions, which can be obtained from studies of this kind, in helping to understand more complicated phenomena is emphasized. Of particular interest are the current attempts to tackle Rayleigh problems via kinetic theory. The discussion here centres mostly about the use of Grad's thirteen-moment equations, by Lees and Yang, but the pessimistic conclusions to this section would seem to be of satisfaction only to the most superstitious gas kineticist!

Schaaf's use of the Navier–Stokes equations with a simple slip velocity boundary condition is commented upon as a '. . . somewhat crude approximation'. This seems rather harsh comment in view of the fact that this approximation links both free-molecule behaviour at small times with continuum behaviour at large times, preserves some of the essential physics of the problem throughout, and does all this with considerable analytical simplicity; not very refined, perhaps, but not crude.

The remaining chapters are concerned with boundary layers proper. A discussion of the boundary-layer equations in incompressible flow brings out their mixed wave-like and diffusive character and leads to the distinction between two types of unsteady boundary layer. These are then examined separately under the headings 'Stagnation boundary layers' and 'Leading edge boundary layers'. Fluctuating boundary layers are treated next (e.g. a cylinder in a free stream whose velocity oscillates about a mean value) and the article concludes with a review of shock-tube boundary-layer theory.

The next article, by Ludwig and Heil, is rather misleadingly titled. In fact about 70% of their space is devoted to a discussion of the kinetic theory of a dissociating, ionizing and relaxing gas, without any special reference to boundary-layer problems as such. This is not in any way to be implied as a criticism of the article in general. Indeed this (necessarily brief in places) discourse on molecular encounters and the Boltzmann equation and its application to problems of modern continuum gas dynamics is most valuable. It should at the very least serve as a salutory warning to the gas dynamicist not to treat his

transport coefficients lightly and might even make some of the braver spirits reach for the nearest book on wave mechanics. One of the most stimulating aspects of present day gas dynamics lies in its close link with 'respectable' subjects like physics and physical chemistry.

The use of the binary collision approximation in Ludwig's and Heil's article restricts their treatment of the ionized gas problem to low degrees of ionization. Furthermore, the absence of sufficient data on the multitudinous cross-sections required by the formal kinetic theory is a little depressing. With current work under way on this question we may hope that it will not be too long before sound theoretical predictions of viscosities, conductivities, etc., can be made for the complicated gas mixtures of interest. There is a strong need to know how these quantities behave, especially in gases which are far removed from chemical and internal state equilibrium, but which are otherwise according to 'Navier–Stokes'.

The boundary-layer part of this article discusses first the usual Prandtl approximations applied to a dissociating gas flow, and then deals with similar and locally similar solutions for flat plates and stagnation point regions. The catalytic wall boundary condition is given incorrectly as 'dissociation fraction equals zero', the authors remarking simply, 'However, see also reference 59'. Reference 59, by Scala, presents the correct boundary condition, as does other work which was presumably available to the authors at the time of writing. The failure to present this quite important boundary condition properly must count as something of an omission in an article with the stamp of authority.

Chester's article returns to Utopia, in which γ is constant. After introducing the exact steady-state theory and its need for the presence of contact discontinuities, the majority of the remainder of the article is concerned with Chisnell's and Whitham's approximate theories (which are capable of handling the time dependent problem). Chisnell's theory is developed first via Chester's own linear theory results for the change of shock Mach number brought about by a small change in duct area.

Comparisons between the exact and approximate theories show up the way in which accumulated wave interactions behind the shock ultimately modify its strength.

The article concludes with some previously unpublished results, derived by the author using an extension of Chisnell's hypothesis. These refer to the case in which a steady flow exists in the duct before the advent of the shock wave. Of especial interest here is the suggestion that second-throat flow breakdown in wind tunnels may be associated with wave propagation effects as well as with those arising from the boundary layer.

The fourth article, by Oswatitsch, is a formidably comprehensive account of similarity and equivalence theory in inviscid gas dynamics. There is no limit to the Mach number range of this study, each of the four ranges of sub-, trans-, super- and hypersonic receiving its share of attention. The first twenty or so pages are devoted to basic considerations; for example, differential equations, shock equations, boundary conditions, and their simplification and linearization are all included here.

The linear theory and its resulting Prandtl–Glauert analogies is dealt with (both for wings and bodies) in the next chapter, followed by a short chapter on higher approximations. Transonic similarity is examined for wings and profiles at incidence and zero incidence. Bodies of revolution in this Mach number régime are also considered, a special section being devoted to the flow about right-circular cones. Hypersonic similarity comes next and unsteady flow is treated, mostly within the domain of the linearized two-dimensional equations. Flutter problems receive some attention also. A chapter on bodies of low aspect ratio, involving the equivalence laws and area rules, concludes the article.

The text is liberally supported by diagrams representing the results of theory and experiment. This compact and thorough account of an important topic is a valuable addition to the literature.

The final article in this volume comes as a suitable epilogue to what has been, largely, a discussion of theoretical fluid mechanics. Two remarks in particular caught the reviewer's eye. The opening sentence of the introduction reminds the reader that the phenomenon of periodic vortex shedding and the formation of vortex streets have been engaging the attentions of experimenters and theoreticians for the past 50 years. Then, in the summary, while commenting on the results of vortex street stability theory and their (not wholly encouraging) relation to observation, the author remarks, 'Whether this is a contradiction between theory and experiment, so often lightheartedly referred to, or whether theory and experiment actually refer to two entirely different subjects is worthy of clarification'. Truly, applied mechanics has advanced, but there remains a great deal of interesting mopping-up to be done.

JOHN F. CLARKE

Incompressible Aerodynamics. Edited by BRYAN THWAITES. Oxford University Press, 1960. 636 pp. 75*s*.

This is the first volume of a new series, the Fluid Motion Memoirs, sponsored by the Aeronautical Research Council. It is a comprehensive review of certain flows of incompressible fluid, which are of special importance to aeronautics. The central theme of the book is the up-to-date theoretical and experimental treatment of the uniform flow of air and other viscous fluids past two-dimensional aerofoils and three-dimensional wings. The motion is assumed to be steady, and the effect of compressibility is neglected. Two more volumes of Fluid Motion Memoirs, on laminar boundary layers and on turbulence, are in preparation, and the three volumes will cover in the main the same ground as the now classical *Modern Developments in Fluid Dynamics*, edited by Sydney Goldstein and published in 1938.

The editor of the present volume is Bryan Thwaites, and the book is a synthesis of original contributions by D. G. Ainley, L. F. Crabtree, M. B. Glauert, D. Küchemann, M. J. Lighthill, A. W. Mair, E. C. Maskell, T. R. F. Nonweiler, R. C. Pankhurst, J. H. Preston, A. G. Smith, D. A. Spence, B. Thwaites, J. Weber, L. G. Whitehead, L. C. Woods, with the assistance of

other well-known authorities. The result is a homogeneous work, not merely a collection of chapters by several authors.

The chapter headings are: (1) Some general principles (60 pages). (2) The calculation of the boundary layer (30 pages). (3) Theoretical models of real flows (20 pages). (4) Uniform inviscid flow past aerofoils (64 pages). (5) Uniform viscous flow past aerofoils (30 pages). (6) Boundary-layer control (49 pages). (7) The displacement effect of wings in uniform flow (36 pages). (8) The lifting effect of wings in uniform flow (78 pages). (9) Uniform flow past bodies of revolution (53 pages). (10) Uniform flow past joined bodies (41 pages). (11) Rotary flows (35 pages). (12) Some miscellaneous topics (75 pages). References (38 pages).

Chapter 1 on general principles gives a brief but readable account, touching on, for instance, the Navier–Stokes equation, boundary layers, inviscid flow, irrotational flow, free and forced transition to turbulence. Chapter 2 on boundary layers examines critically various formulae which have been proposed for laminar and turbulent boundary layers, under various conditions. Chapter 3 describes the decomposition of the field of flow into regions of inviscid flow, boundary layers, bubbles, cavities, etc., and discusses the appropriate flow models and the interaction of the various flow regions. These first three chapters lay the foundation for the later chapters.

Chapter 4 gives a detailed exposition of the inviscid model in two dimensions. Here it is necessary to distinguish between unmixed and mixed boundary conditions; the former are appropriate to unseparated flows and state that the velocity normal to a given boundary is zero, the latter are appropriate to separated flows bounded partly by the aerofoil (where the normal velocity is zero) and partly by a hypothetical line representing the edge of the separated region (where the velocity is regarded as known). For unmixed boundary conditions it is further necessary to distinguish between the direct problem where the shape and incidence of the aerofoil are given and the velocity distribution on the surface is required, and the inverse problem where the velocity distribution is prescribed and the shape of the aerofoil is required. The thorough treatment given in this substantial chapter is a fine example of applied mathematics. Chapter 5, concerned with viscous effects, is necessarily less elegant in its mathematical aspects. Important problems here are the determination of the drag and lift both for unseparated and for separated flows. Chapter 6 describes boundary-layer control by sucking and blowing, and introduces some challenging problems where more work is needed.

We now come to consider wings of finite span. Chapter 7 treats the effect of wing thickness in inviscid flow when there are no trailing vortices in the flow. The effect of the wing is approximated by a distribution of sources inside the wing, where an approximation to the source strength may be determined from a linearized theory. Difficulties arise near the wing tips and for wings of small aspect ratios; for the latter a slender-body theory is described. The discussion also includes swept wings, wing-tip effects, and wings of general planform.

Chapter 8 treats inviscid lifting-surface theory; here a sheet of trailing vorticity accompanies the thin wing and is associated with the lift and the

induced drag. Further approximations are appropriate when the wing is of large or small aspect ratio; the former case is by now classical, the latter has become important only recently. The present state of knowledge of both cases is presented in considerable detail in this chapter. Chapter 9 deals with the problem, not covered by previous chapters, of flow past bodies of revolution. For axially symmetric inviscid flows the body is replaced by distributions of sources, either on the axis or on the surface of the body, where the source strength must be found by numerical computation. Alternatively, a slender-body approximation may be used. These methods can all be extended to lateral flows without separation. Some very interesting numerical comparisons are given, and it is shown that in certain circumstances the agreement with experiment is also very close. The calculation of the boundary layer at incidence presents a difficult problem which is discussed at length.

So far the flows have been past simple geometrical configurations. The treatment for joined bodies, described in Chapter 10, is much more complicated and often much less exact, but is clearly of great practical importance. Chapter 11, on rotary flows, considers fluid flows such as are encountered in axial-flow compressors, and in particular the model of the actuator-disk on which the velocity vector and pressure are assumed discontinuous.

Chapters 4 to 11 give an up-to-date account of a number of well-defined classical topics of lasting importance; chapter 12 treats a number of more recent fringe topics which are likely to be of importance in the future. These include the analysis of a theoretical model of the jet flap; wings with non-planar vortex sheets; wings with bubble-type flow separation; non-planar lifting systems such as biplanes, annular aerofoils and cascades; and the effect of a non-uniform mainstream on bodies, from tail-planes behind wings to Pitot tubes in boundary layers.

This book presents a rational theoretical basis for an understanding of aerodynamical phenomena. Comparison of theory and experiment is one of the main themes of the work, and it is seen in many places how theories have been modified and generalized in the light of observations. The very good style, presentation, and printing make this book a pleasure to read. It is warmly recommended to all who take an interest in fluid mechanics, whether specialists or not. It is also recommended to workers in other branches of engineering where a more scientific approach might sometimes be used with profit.

F. URSELL

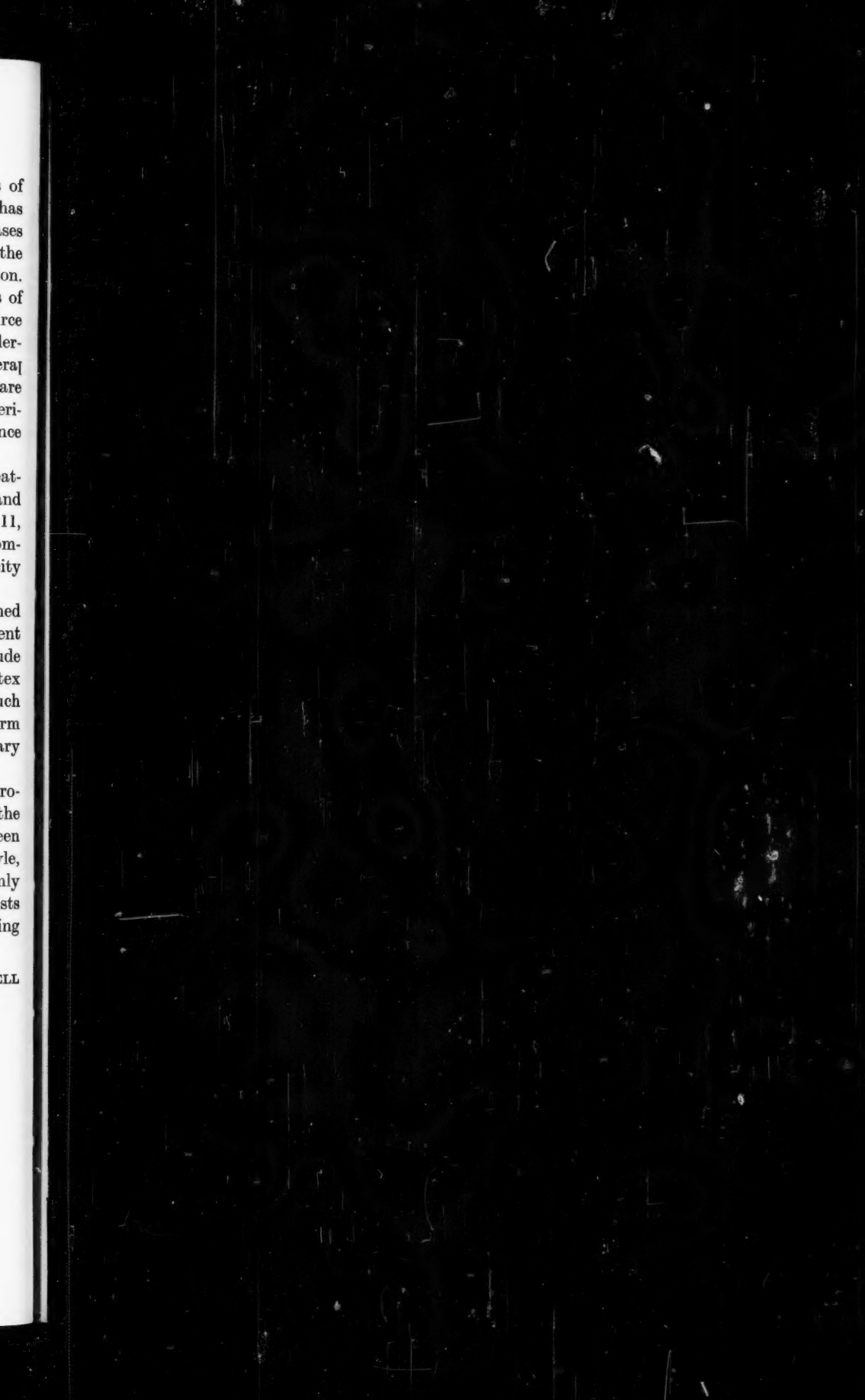

Hydraulics Research 1960

The Annual Report of the D.S.I.R.'s Hydraulics Research Station records the wide range of model studies and field investigations carried out there during the year. These include research into the effects of land reclamation in Hong Kong harbour, the influence on Thames shipping of the new £3 million underpass near Blackfriars Bridge, the measurement of littoral drift along beaches with and without groynes, and a study of the possibilities of using the Indian Ocean to generate electricity in Mauritius. It also gives an account of several investigations on which work has recently begun and recommends subjects for future research. **Price 5s. 6d.** (*post 6d.*)

HMSO

From the Government Bookshops or through any bookseller

The Theory of Subsonic Plane Flow

L. C. WOODS

A concise and systematic treatment of two-dimensional subsonic, inviscid fluid motion and its aeronautical applications. This is the first book to give an extensive account of mixed boundary-value problems and to treat examples of these problems occurring in ventilated wind-tunnel theory, jet-flap theory and unsteady Helmholtz motions. CAMBRIDGE AERONAUTICAL SERIES. 616 *pages.* £6 *net*

from all booksellers

CAMBRIDGE UNIVERSITY PRESS

JOURNAL OF FLUID MECHANICS

Volume 11, Part 1 August 1961

CONTENTS

A simplified analysis of spherical and cylindrical blast waves *page* 1
by MANFRED P. FRIEDMAN

Propagation of a solitary wave along a magnetic field in a cold collision-free plasma
by P. G. SAFFMAN 16

Measurements of entrainment by axisymmetrical turbulent jets
by F. P. RICOU and D. B. SPALDING 21

The flow of thin liquid films between rollers
by E. PITTS and J. GREILLER 33

Stewartson's compressibility correlation in three dimensions
by J. C. COOKE 51

Measurement of interfacial structure for co-current air-water flow
by LEMBIT U. LILLELEHT and THOMAS J. HANRATTY 65

Linearized slip flow past a semi-infinite flat plate
by J. A. LAURMANN 82

Equilibrium layers and wall turbulence
by A. A. TOWNSEND 97

End effects in inviscid flow in a magnetohydrodynamic channel
by G. W. SUTTON and A. W. CARLSON 121

The force on a sphere moving through a conducting fluid in the presence of a magnetic field
by J. R. REITZ and L. L. FOLDY 133

On the dynamics of unsteady gravity waves of finite amplitude. Part 2. Local properties of a random wave field
by O. M. PHILLIPS 143

REVIEWS
Advances in Applied Mechanics 156
Incompressible Aerodynamics 158

Printed in Great Britain at the University Press, Cambridge
(Brooke Crutchley, University Printer)